Process Intensification: Absorption and Desorption of Carbon Dioxide from Monoethanolamine Solutions Using Higee Technology

By

M. S. Jassim, MEng.

Thesis submitted for the Degree of Doctor of Philosophy in the Faculty of Engineering, University of Newcastle upon Tyne

February, 2002

Department of Chemical and Process Engineering

University of Newcastle upon Tyne

To my Parents

"It is Allah Who created you in a state of (helpless) weakness, then gave (you) strength after weakness, then, after strength, gave (you weakness and a hoary head: He creates as He wills, and it is He Who has all knowledge and power", The Quran (30:54)

"Knowledge is light", The Holy Prophet

- "There is no greater wealth than wisdom, no greater poverty than ignorance; no greater heritage than culture and no greater support than consultation", Imam Ali

Acknowledgements

I would like to express my gratitude and appreciation to my supervisor Professor Colin Ramshaw for his guidance and supervision throughout duration of this project.

Special thanks to Dr. Dag Eimer for his advice, suggestions, and keeping a close eye on my progress with his six months visits which accelerated my motivation to deliver goods.

I would like to express my gratitude to Mr. Erik Horsley, Department Superintendent, for the assistance with the procurement orders and his suggestions for the encountered problems. I extend my gratitude to Mr. Ian Strong, a skilful craftsman, who constructed the pilot rig and was always promptly available when needed to repair or change the rig configuration. My thanks to Mr. Paul Sterling, who assisted me in collecting gas samples during the experimental runs. Also, I would like to thank Brian Dourish, George, Rob, Stuart, Brian Grover, and Jimmy for their help.

I would like to thank my PIIC group-mates for enjoyable atmosphere in the group and good bond between its members. I would like to extend my gratitude to Dr. John Burns for his comments and advice.

Special recognition goes to my parents, brothers and sisters for their warm support throughout my career. Also, special thanks goes to Gulnur Coskuner for her care and encouragement.

Finally, I gratefully thank Norsk Hydro for their generous financial support to carry out this research.

Abstract

Process intensification (PI) technologies are challenging the traditional unit operations in a wide range of engineering processes. The Rotating Packed Bed (RPB) or the Higee is a compact mass transfer machine that could challenge the conventional absorption/desorption columns especially in the off-shore oil facilities where space and weight are of great importance. This counter-current mass transfer operation between the gas and the liquid phases occurs at high rotational speed and with a short residence time.

The objective of the project was to test the capability of the mass transfer machine (RPB) in gas sweetening field. Therefore, a RPB pilot plant facility was modified then experimentally tested for the chemical absorption of 4 vol.% CO_2/Air mixture using different concentrations of aqueous ethanolamine solutions (30, 55, 75, and 100 wt.%) at different temperatures (20°, and 40°C).

The hydraulic capacity or the flooding behaviour of the machine was initially investigated and then compared with Sherwood correlation. In addition, Wallis method was approached to correlate the flooding data. The analysis of the carbon dioxide concentration in the liquid and gas samples was carried out by a gas chromatograph. The mass transfer studies were carried out to identify the effect of temperature, rotor speed, liquid flowrate, and concentration on the HTU. The percentage recovery of carbon dioxide was 98.6, 92.8, 88.4 and 44.4% for 100, 75, 55, and 30 wt% MEA solutions.

In addition, the regeneration of the amine solution by steam was investigated at various (G/L) ratios and rotor speeds. It was observed the efficiency of the operation was highest when the ratio (kg steam/L solution) was greater than 0.4.

Key Words: Rotating packed bed, process intensification, Higee, gas sweetening, MEA, carbon dioxide, absorption, steam desorption, HTU.

Table of Contents

CHAPTER 1:INTRODUCTION 1

CHAPTER 2: LITERATURE REVIEW 5

2.1 REGENERABLE MASS TRANSFER PROCESSES 5

2.1.1 Introduction 5

2.1.2 Description of the Operation of A Conventional Gas Treating Plant ... 7

2.1.3 Operating Modes 8

2.1.4 Operating Variables 8

2.2 CHEMISTRY 11

2.2.1 Selection of Amine 11

2.2.2 Classification of Amine 12

2.2.3 Amine Concentration 13

2.2.4 Reaction Kinetics 15

2.2.5 The Rate Limiting Step 16

2.2.6 Kinetic Data 18

2.2.7 Properties of Monoethanolamine (MEA) 19

2.2.7.1 Physical Properties 19

2.2.7.2 Oxidation 19

2.2.7.3 Foaming 19

2.2.7.4 Diffusivity of CO_2 in Aqueous Solutions of Monoethanolamines .. 19

2.3 MASS TRANSFER PROCESSES 21

2.3.1 Physical Mass Transfer Processes 21

2.3.1.1 General Concepts 21

2.3.1.2 Mass Transfer Models 23

2.3.1.2.1 The Two film Theory 23

2.3.1.2.2 The Penetration Theory 24
2.3.1.2.3 Surface-Renewal Models 25
2.3.2 Mass Transfer Accompanied by Chemical Reaction 26
2.3.2.1 Introduction 26
2.3.2.2 Reasons for Higher Rate of Mass Transfer Using Chemical Solvents 26
2.3.2.2.1 Equilibrium considerations 26
2.3.2.2.2 Non-equilibrium considerations 27
2.3.2.3 Reaction Regimes 27
2.4 ROTATING PACKED BED (RPB) 29
2.4.1 Comparison Between the Classical Packed Tower and RPB 29
2.4.2 Background 29
2.4.3 Packed Bed Design 40
2.4.3.1 Mass Transfer Equations in RPB 40
CHAPTER 3: EXPERIMENTAL FACILITY 42
3.1 OBJECTIVE OF THE EXPERIMENTS 42
3.2 FLOWSHEET OF THE RIG 42
3.3 MATERIAL OF CONSTRUCTION 43
3.4 RIG SUPPORT FRAME 45
3.5 ROTOR 46
3.6 PACKING 50
3.7 LIQUID DISTRIBUTION TO THE RPB 51
3.8 CARBON DIOXIDE / AIR MIXTURE 53
3.9 DRY STEAM SYSTEM 55
3.10 LIQUID SAMPLING 56
3.11 GAS SAMPLING 56

CHAPTER 4: FLOODING BEHAVIOUR OF THE RPB 59

4.1 INTRODUCTION 59

4.2 LITERATURE REVIEW 59

4.2.1 Flooding in Packed Towers 59

4.2.2 Flooding in Rotating Packed Bed 63

4.3 VISUAL STUDY OF THE FLOODING BEHAVIOUR IN RPBS 65

4.3.1 Flooding Experimental Facility 65

4.3.2 The Procedure for the Determination of the Flooding Point 65

4.3.3 Flooding Point Results 66

4.3.3.1 Sherwood Correlation 66

4.3.3.2 Wallis Correlation 69

4.3.4 The Effective Wetted Area of the RPB. 72

CHAPTER 5: METHOD OF ANALYSIS AND SOLUBILITY EXPERIMENTS ... 73

5.1 INTRODUCTION 73

5.2 DETERMINATION OF THE CARBON DIOXIDE CONCENTRATION IN AN AQUEOUS ETHANOLAMINE SOLUTION 74

5.2.1 Titration and Analytical Methods 74

5.2.2 Indirect Methods 76

5.2.3 Gas Chromatography 78

5.3 ANALYSIS METHOD: GAS CHROMATOGRAPHY 80

5.3.1 Description of the Process 80

5.3.1.1 Analysis of the Liquid Sample. 80

5.3.1.2 Analysis of the Gas Sample. 81

Column 1 82

5.3.2 FID (Flame Ionization Detector) 83

5.3.3 The Carrier Gas 83

5.3.4 GC output *83*

5.4 SOLUBILITY EXPERIMENTS 85

5.4.1 Introduction *85*

5.4.2 Literature Review *85*

5.4.3 Solubility Experiments *89*

5.4.3.1 Materials and Equipment 89

5.4.3.2 Experimental Procedure 90

5.4.3.3 Results and Discussion 92

5.4.3.4 Correlation of Data 93

CHAPTER 6: TROUBLESHOOTING OF THE PILOT RIG 97

6.1 DRY RUNS EXPERIMENTS 97

6.1.1 Introduction *97*

6.1.2 Procedure of the Runs *97*

6.1.3 Results of the Dry Runs *98*

6.1.4 Discussion *99*

6.1.5 Troubleshooting of the Rig *100*

6.2 ABSORPTION RUNS 102

6.2.1 Introduction *102*

6.2.2 Mass Balance Across the Higee Rig *103*

6.2.2.1 Operational Procedure 103

6.2.2.2 Results and Discussions 104

CHAPTER 7: MASS TRANSFER STUDIES 109

7.1 INTRODUCTION 109

7.2 APPLICATION OF TWO-FILM THEORY IN ABSORPTION WITH CHEMICAL REACTION 109

7.2.1 Mass Transfer Control *110*

7.2.1.1 Fundamental Equations 110
7.2.1.2 Mathematical Limiting Behaviour 113
7.2.1.3 Plate Efficiency 113
7.3 TIME PARAMETERS IN THE HIGEE 114
7.3.1 Residence Time 114
7.3.2 Reaction Time 116
7.3.3 Diffusion Time and Film Thickness 117
7.3.4 The Enhancement Factor 118
7.4 ABSORPTION RUNS 119
7.4.1 Calculation of HTU 119
7.4.2 Effect of Varying the RPM 120
7.4.3 Effect of Varying the Temperature 124
7.4.4 Effect of Varying the Liquid Flow 127
7.4.5 Effect of Varying the Concentration of the Ethanolamine Solution .. 129
7.5 COMPARISON WITH OTHER MASS TRANSFER MACHINES 133
7.5.1 Rotating Beds 133
7.5.2 Conventional Column 133
7.6 DESORPTION RUNS 134
7.6.1 Calculation of HTU 134
7.6.2 Air 135
7.6.3 Steam 135
7.7 END EFFECTS 139
CHAPTER 8: CONCLUSIONS AND RECOMMENDATIONS 140
8.1 CONCLUSIONS 140
8.2 RECOMMENDATIONS 141

Nomenclature.....143

Bibliography.....148

Appendices

Appendix A: Properties of Monoethanolamine A1

Appendix B: Calibration Charts for Ethanolamine Solution and Air Flowmeters B1

Appendix C: Properties of the Rotating Packed Bed C1

Appendix D: Pressure Drop in 4-Arm Distributor D1

Appendix E: Heat Transfer Rate in CO_2 Heating System E1

Appendix F: Determination of the Flooding Point in RPB F1

Appendix G: Calibration of the Ethanolamine Solution G1

Appendix H: Calibration of Carbon Dioxide/ Air H1

Appendix I: Gas Chromatography Calibration Charts I1

Appendix J: Literature Solubility Data J1

Appendix K: Experimental Solubility Results K1

Appendix L: Dry Runs Results L1

Appendix M: Typical Mass Balance Calculation M1

Appendix N: Steam Desorption Runs N1

List of Figures

FIGURE 1.1	Schematic diagram of overall process for production of electricity and oil recovery.	3
FIGURE 1.2	The PI methodology courtesy of (Green, 1999)	4
FIGURE 2.1	Classification of the gas sweetening methods	5
FIGURE 2.2	Choice of solvent in gas treating (Tennyson and Schaaf, 1977)	6
FIGURE 2.3	Flowsheet of a typical amine plant	9
FIGURE 2.4	Position of the operating line in the absorber and desorber.	9
FIGURE 2.5	Share of MEA in amines global market (dupart et al., 1993a)	12
FIGURE 2.6	Classification of solvents	13
FIGURE 2.7	Vapour pressure of amines.	15
FIGURE 2.8	Vapour pressure of CO2 at different MEA concentration (Kohl and Nielsen, 1997).	15
FIGURE 2.9	Concentration profile of physical absorption using Two-film Theory	23
FIGURE 2.10	Asymptotic behaviour for I	28
FIGURE 2.11	Chamber's centrifugal absorber.	30
FIGURE 2.12	Podlbieiniak's deodrizner.	33
FIGURE 2.13	Singh's stripper	36
FIGURE 2.14	Sanilya's centrifugal contactor.	39
FIGURE 2.15	A section of counter-current mass transfer in RPB	40
FIGURE 3.1	Flowsheet of experimental facility	43
FIGURE 3.2	Phase equilibrium data for MEA solutions	44
FIGURE 3.3	Optimum and recommended amine strength	44
FIGURE 3.4	The Rig Support Frame	45
FIGURE 3.5	Comparison between the stroboscope results and the manual controller.	46

FIGURE 3.6	Cross sectional view of the Higee rig	48
FIGURE 3.7	Cross sectional view of the rotor	49
FIGURE 3.8	Details of the stainless steel disc	49
FIGURE 3.9	Irrigation of RPB with 4-arm distributor.	51
FIGURE 3.10	Flowsheet of CO2/Air system	54
FIGURE 3.11	Effect of time on the temperature of CO2/Air Stream	54
FIGURE 3.12	Flowsheet of steam delivery system	56
FIGURE 3.13	Positions of liquid sampling	57
FIGURE 3.14	Positions of gas sampling	58
FIGURE 4.1	Pressure Drop Regimes in a Packed Column.	60
FIGURE 4.2	Flooding Diagram by Sherwood	61
FIGURE 4.3	Discrepancies on (Lobo et al., 1945) Correlation	62
FIGURE 4.4	(Hassan-beck, 1997) visual flooding data on Sherwood plot.	65
FIGURE 4.5	Flooding behaviour at different liquid flowrates.	67
FIGURE 4.6	Flooding gas flowrate vs. RPM at varying liquid flowrate.	68
FIGURE 4.7	L/G vs. RPM at varying liquid flowrate	68
FIGURE 4.8	Flooding data using Wallis Plot	69
FIGURE 4.9	Variation of C with N_g	70
FIGURE 4.10	Sherwood-Wallis flooding plot.	71
FIGURE 4.11	Variation of the effective wetted area of the packing on the inside radius and the RPM	72
FIGURE 5.1	Mass balance across the Higee rig for absorption cycle.	73
FIGURE 5.2	Modified Knorr Method	75
FIGURE 5.3	Variation of pH with temperature for 20wt% MEA and DEA.	75
FIGURE 5.4	Variation of pH with temperature for 20wt% MEA and DEA.	75
FIGURE 5.5	Schematic diagram of the gas chromatography	80

FIGURE 5.6 Main components of the FID 83

FIGURE 5.7 A typical chromatogram for CO_2 and MEA peaks in liquid sample. 84

FIGURE 5.8 Solubility data for 30wt% MEA solution (Jou et al., 1995). 87

FIGURE 5.9 Comparison of solubility data of (Jou et al., 1995) against (Shen and Li, 1992) 88

FIGURE 5.10 Comparison of solubility data of (Jou et al., 1995) against (Mason and Dodge, 1936) and (Nasir and Mather, 1977). 88

FIGURE 5.11 Comparison of solubility data of (Jou et al., 1995) against (Murrieta-Guevara et al., 1993) 88

FIGURE 5.12 Comparison of solubility data of (Jou et al., 1995) against (Lee et al., 1974). 88

FIGURE 5.13 Loading of Carbon Dioxide into the Ethanolamine Solution in the Equilibrium Vessel 91

FIGURE 5.14 The increase of the carbon dioxide peak in the solution with time. 91

FIGURE 5.15 Percentage deviation between the solubility data and (Jou et al., 1995). 93

FIGURE 5.16 Carbon dioxide concentration vs. Time at 0.285 loading and @ 25°C. 94

FIGURE 5.17 Carbon dioxide concentration vs. Time at 0.248 loading and @ 25°C. 94

FIGURE 5.18 Comparison of solubility data with those of Jou et al (1995) @ 25°C. 95

FIGURE 5.19 Comparison of solubility data with those of Jou et al (1995) @ 40°C. 95

FIGURE 5.20 Comparison of solubility data with those of Jou et al (1995) @ 60°C. 96

FIGURE 5.21	Comparison of solubility data with those of Jou et al (1995) @ 80°C.	96
FIGURE 6.1	Sampling points: (A) eye; (B) periphery and positions of air leakage into the RPB	98
FIGURE 6.2	% error between inlet/outlet CO_2 concentrations at different sampling locations.	99
FIGURE 6.3	Air leakages blocked	100
FIGURE 6.4	% error between inlet/outlet CO_2 concentrations after initial modifications to the Higee rig.	101
FIGURE 6.5	The effect of a slight change of the loading on mass balance (Periphery Samples).	105
FIGURE 7.1	Concentration gradients of mass transfer accompanied by a chemical reaction	109
FIGURE 7.2	Residence time for different amine strengths at 40°C and 40 L/min.	115
FIGURE 7.3	Variation of liquid flowrate and temperature on the Residence time at 30 wt%.	116
FIGURE 7.4	Variation of HTU with rotor speed at constant temperature and liquid flowrate for 30wt% solution.	122
FIGURE 7.5	Variation of HTU with rotor speed at constant temperature and liquid flowrate for 55wt% solution.	122
FIGURE 7.6	Variation of HTU with rotor speed at constant temperature and liquid flowrate for 75wt% solution.	123
FIGURE 7.7	Variation of HTU with rotor speed at constant temperature and liquid flowrate for 100 wt% solution.	123
FIGURE 7.8	Variation of HTU with temperature at constant liquid flowrate and rotor speed for 30wt% solution	125
FIGURE 7.9	Variation of HTU with temperature at constant liquid flowrate and rotor speed for 55wt% solution.	125

FIGURE 7.10 Variation of HTU with temperature at constant liquid flowrate and rotor speed for 75wt% solution. 126

FIGURE 7.11 Variation of HTU with temperature at constant liquid flowrate and rotor speed for 100wt% solution 126

FIGURE 7.12 Variation of HTU with liquid flowrate at constant temperature and rotor speed for 30wt% solution. 127

FIGURE 7.13 Variation of HTU with liquid flowrate at constant temperature and rotor speed for 55wt% solution 128

FIGURE 7.14 Variation of HTU with liquid flowrate at constant temperature and rotor speed for 75wt% solution 128

FIGURE 7.15 Variation of HTU with liquid flowrate at constant temperature and rotor speed for 100wt% solution 129

FIGURE 7.16 Variation of HTU with liquid concentration at constant temperature, rotor speed, and at 40 L/min liquid flowrate 131

FIGURE 7.17 Variation of HTU with liquid concentration at constant temperature, rotor speed, and at 20 L/min. liquid flowrate 131

FIGURE 7.18 Variation of % recovery with liquid concentration at constant temperature, rotor speed, and at 40 L/min liquid flowrate. 132

FIGURE 7.19 Variation of % recovery with liquid concentration at constant temperature, rotor speed, and at 20 L/min liquid flowrate. 132

FIGURE 7.20 Comparison between current investigation and Chambers and Wall (1954) machine. 133

FIGURE 7.21 Variation of HTU with G/L on desorption of carbon dioxide from 30wt% MEA solution using air. 137

FIGURE 7.22 Effect of variation of HTU with (G/L) ratio on steam desorption of carbon dioxide from 30 wt% MEA solution @ 800 RPM. 138

FIGURE 7.23 Effect of variation of (G/L) ratio on steam desorption of carbon dioxide from 60 wt% MEA solution @ 600 and 1000 RPM. 138

Figure A-1: Viscosity.....A2

Figure A-2: Specific Heat.....A2

Figure A-3: Surface Tension.....A2

Figure A-4: Specific Gravity.....A2

Figure A-5: Refractive indices.....A3

Figure A-6: Heat of solution (25°C).....A3

Figure A-7: Volatility.....A3

Figure A-8: Heat of vaporization.....A3

Figure A-9: Boiling point composition curve for MEA.....A4

Figure A-10: Specific gravity of MEA solution.....A4

Figure A-11: Total Vapour Pressure of MEA solutions.....A4

Figure A-12: Weight Percent versus Molarity for MEA solutions.....A5

Figure B-1: Calibration chart for flowmeter (47X) at room temperature.....B1

Figure B-2: Calibration chart for flowmeter (35X) at room temperature.....B1

Figure B-3: Relationship between the air flowmeter and its gauge pressure.....B2

Figure C-1: Dimensions of RPB.....C2

Figure C-2: Expamet Configuration.....C3

Figure D-1: Sudden contraction to the liquid flow in 4-arm distributor.....D1

Figure E-1: Dimensions of the Copper Pipe.....E1

Figure G-1: The increase in CO_2 concentration in 30wt% MEA solution leads to colour change.....G3

Figure H-1: Procedure for Gas Calibration.....H1

Figure N-1: Different flow compartments in the Higee.....N1

List of Tables

Table 2.1:	Operating data for Aqueous MEA Gas Treating Plant, (Kohl and Nielsen, 1997)	10
Table 2.2:	Review of historical recommended MEA strength.	14
Table 2.3:	Absorption results using dirty MEA	31
Table 2.4:	Absorption results using new MEA	31
Table 2.5	Mass Transfer Coefficients for Gas Film Control Process	34
Table 2.6	: Mass Transfer Coefficients for Liquid Film Control Process	34
Table 2.7:	Comparison between the Higee technology and a conventional vacuum tower in water deaeration (Zhenh et al., 1997).	38
Table 5.1:	Comparison between the GCs' used by Jou et al. (1995) and the current investigation.	79
Table 5.2:	Operating conditions of GC.	82
Table 5.3:	Details of the column 1 and column 2.	82
Table 5.4:	Values of Q and m for (Atadan, 1955) equation.	86
Table 5.5:	Values of Q and m for power equation	93
Table 6.1:	Statistical summary of the loadings for the lean and the rich MEA solution for Run 6.	105
Table 6.2:	MEA peak areas calculated by the GC for Sample 1 & 2.	107
Table 6.3:	Carbon dioxide peak areas calculated by the GC for Sample 1 & 2.	107
Table 7.1:	Summary of mass transfer data for NH3-H2O and CO2-MEA-H2O systems	112
Table 7.2:	Effect of the variation of concentration and temperature on the liquid-side mass transfer resistance.	113
Table 7.3:	Reaction time x 105 (s) at different amine concentrations	117
Table 7.4:	Average enhancement factors (I) for RPB	119
Table 7.5:	High/Low enhancement factors (I) for conventional columns	119

Table 7.6:	Kinematic viscosities (centistokes) of the MEA solutions at 20° and 40°C.	124
Table A-1	The physical properties of MEA	A1
Table F-1	Experimental flooding data	F3
Table G-1	Comparison between weight technique and titration to calculate MEA strength	G2
Table J-1	(Mason And Dodge, 1936) Solubility data	J1
Table J-2	(Jou et al., 1995) Solubility data	J3
Table K-1	Experimental Solubility Data	K1
Table K-2	Linear relationships between 0.2-0.3 loading data for (Jou et al., 1995)	K2
Table L-1	Dry Runs Results	L2
Table P-1	Results of Absorption Runs for MEA Solution(100 wt%)	P1
Table P-2	Results of Absorption Runs for MEA Solution(75 wt%)	P1
Table P-3	Results of Absorption Runs for MEA Solution(55 wt%)	P2
Table P-4	Results of Absorption Runs for MEA Solution(30 wt%)	P2
Table P-5	Regeneration by Air	P3
Table P-6	Regeneration by Steam	P4

List of Photographs

Photograph 1: Doughnut shape of the packing mesh.....50
Photograph 2: Stainless steel mesh packed in the rotor.....50
Photograph 3: Position of 4-arm distributor in the "eye" of the rotor.....52
Photograph 4: A 4-arm liquid distributor.....52
Photograph 5: CO_2/Air mixture system.....53
Photograph 6: Dry steam system.....55
Photograph 7: Sampling of sweet gas.....58

CHAPTER 1

INTRODUCTION

The field of process intensification (PI) got momentum in late 1970s when ICI engineers pioneered this field. The main objective was to reduce the size of the Main Plant Items (MPI) in the bulk chemical industries in order to reduce the installation costs, by a factor of 10 or more, with the application of novel and compact technologies (Ramshaw, 1983).

Reducing the size of unit operations and/or integrating their functions can substantially save costs by reducing civil engineering and piping works. However, PI success is not only limited to its early advantage of reducing the size and weight of equipment and thus saving space, but the vision, even at that early stage, was to improve efficiency, inherent safety, as well as reducing the energy consumption and environmental impact. These advantages were accomplished due to the short residence time and low volume of multi-phase operations.

(Hendershot, 2000) supported the utilization of PI technologies in the chemical industries due to process minimization, which add inherent safety factor to the equation of plant design. The concept of PI has evolved in the last three decades, and now covers both the bulk chemicals industry and the small volume speciality chemicals production. (Green, 1998) reviewed the PI technologies currently under investigation: rotating packed beds (RPB), spinning disk reactor, compact heat exchanger, in-line mixing devices, combined chemical reactor-heat exchangers, oscillatory flow reactors, and microreactors.

Both the RPB and the spinning disk reactor technologies take advantage of centrifugal fields as stimulants for PI (Ramshaw, 1993). The wisdom of using centrifugal fields is to benefit from the fact that the dynamic behaviour of multiphase fluids is dictated by the interphase buoyancy factor $\Delta\rho g$. Therefore, increasing the centrifugal acceleration improves the slip velocity, which in turn improves the flooding characteristics and interfacial shear stress, and consequently boost mass transfer coefficient.

(Stankiewicz and Moulijn, 2000) stressed the effect of process intensification on transforming the chemical engineering field. They predicted that the intensified equipment and processing techniques would cause extinction of the traditional unit operations in the 21st Century in a similar approach to the advancement in electronics field. The vision was to apply efficient and integrated devices such as pipeline reactors or 1-2 m rotating devices as an alternative to long columns or reactors.

The industrial technology in operation throughout the world for removing acid gases involves the application of the conventional packed columns for both absorption and desorption. The main objective of this research is to develop and test a high performance mass transfer device (Higee) that is capable of absorbing and desorbing carbon dioxide using various strengths of alkanolamine solutions.

The application of Higee technology in gas sweetening field in the offshore oil industry will provide a cornerstone in plant design by critically reducing the size and weight of absorber/desorber, increasing the inherent safety of offshore sites and performing efficient mass transfer operations.

An initiative by the Norwegian government to restore CO_2 emissions in the year 2000 to the 1989 level, led to the introduction of a CO_2-tax costing oil companies a staggering US$ 355 millions in 1994. The high cost of tax forced the oil companies to seek new technologies for the reduction of greenhouse emissions (Falk-Pedersen et al., 1995). Norsk Hydro, a Norwegian energy, chemicals and metals group, declared an initiative to invest in an environmental-friendly project for the generation of electricity. Figure 1.1 shows a schematic diagram of the overall process. The feedstock to synthesis process (reformer) is natural gas (CH_4), which will produce Hydrogen as the main product and carbon dioxide as a by-product. Hydrogen will be fed to the gas and steam turbines for the production of electricity, while carbon dioxide will be injected into the Grave oil reservoir in the Norwegian continental shelf of North Sea for recovering oil. By utilizing carbon dioxide in oil recovery, a reduction of 90% emission of this greenhouse gas is attainable.

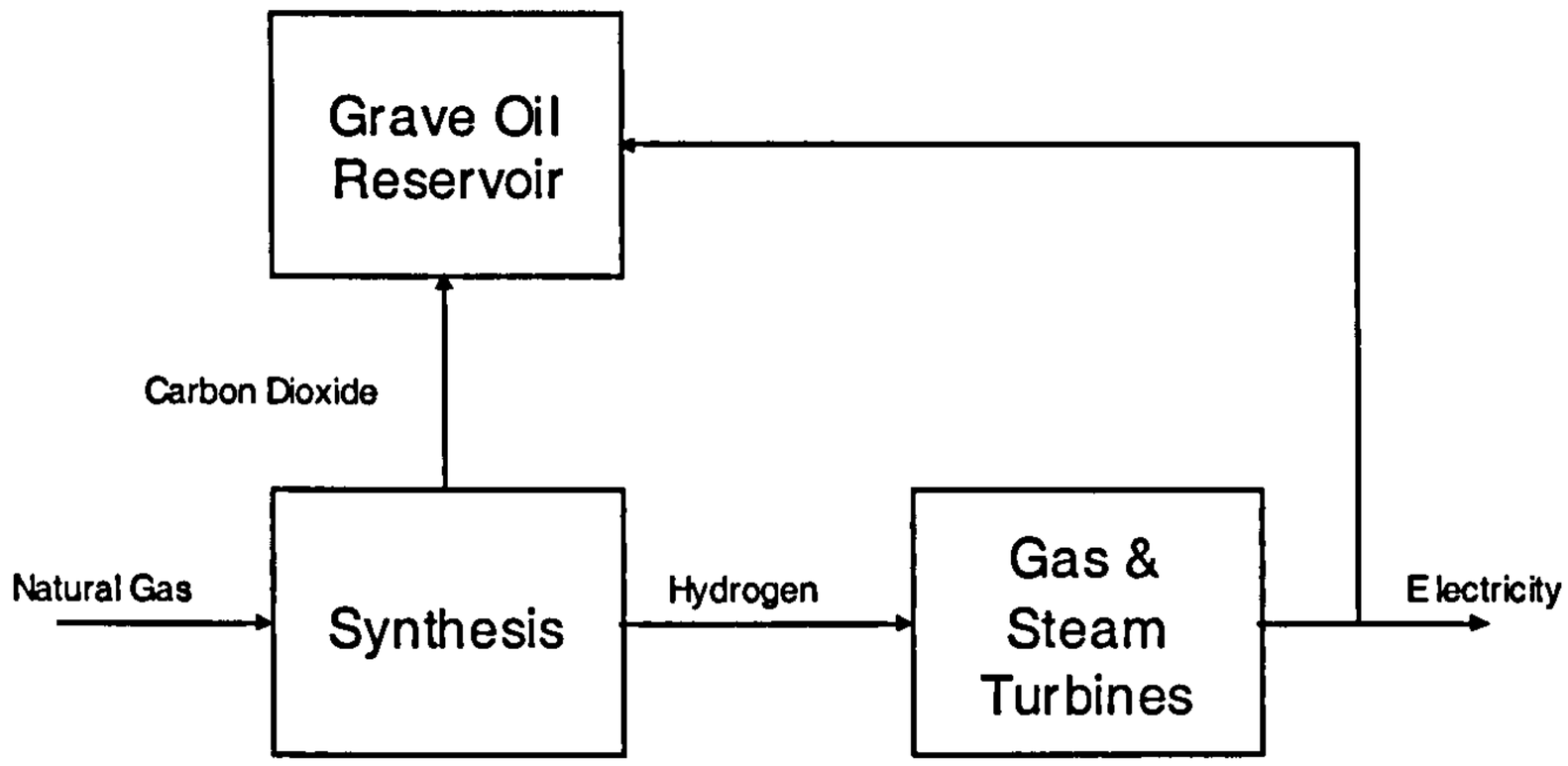

Figure 1.1: Schematic diagram of overall process for production of electricity and oil recovery.

(Green, 1999) described an overall methodology to start-up a PI industrial project as shown in Figure 1.2. The business drivers for the current research project is to utilise the concept of the compact Higee machine in offshore facilities in order to reduce CO_2-related taxes as explained earlier. The knowledge elicitation step is acknowledged in Chapter 2 with a detailed brainstorming of the concept of regenerable mass transfer, process chemistry, rate limiting step, reaction kinetics, and the rotating packed beds concept. The detailed design description of the experimental pilot plant rig is shown in Chapter 3. The flooding and solubility experiments are shown in Chapter 4. The early mass transfer studies showed that the recovery of carbon dioxide in the absorption runs were only 40% using 30wt% MEA lean solution, which was based upon the typical high-range MEA solution strength in the modern conventional absorbers. As the Higee is a radical mass transfer machine in terms of the fast residence time, the PI blockers were reviewed and it was decided to study the effect of MEA strength on mass transfer characteristics. Chapter 5 shows the absorption and desorption studies. Chapter 6 shows the conclusions and recommendations for future work. Finally, a list of appendices shows the detailed calculations, solubility data, and the gas chromatography calibrations.

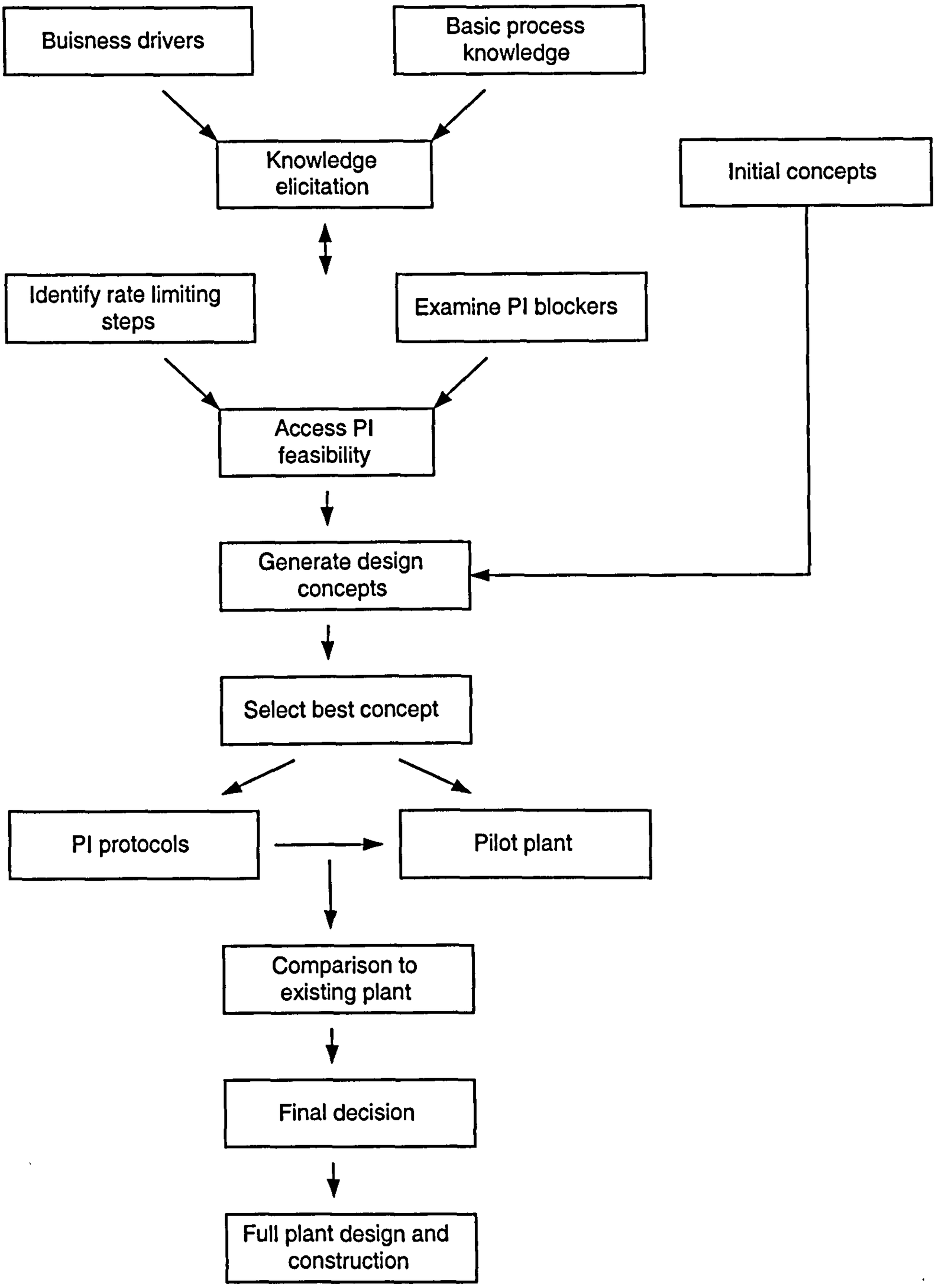

Figure 1.2: The PI methodology courtesy of (Green, 1999)

CHAPTER 2

LITERATURE REVIEW

2.1 Regenerable Mass Transfer Processes

2.1.1 Introduction

Purification of a gas stream by a liquid solvent is an important chemical engineering mass transfer operation. (Pearce, 1993) categorized acid gas removal methods into 7 groups as shown in Figure 2.1.

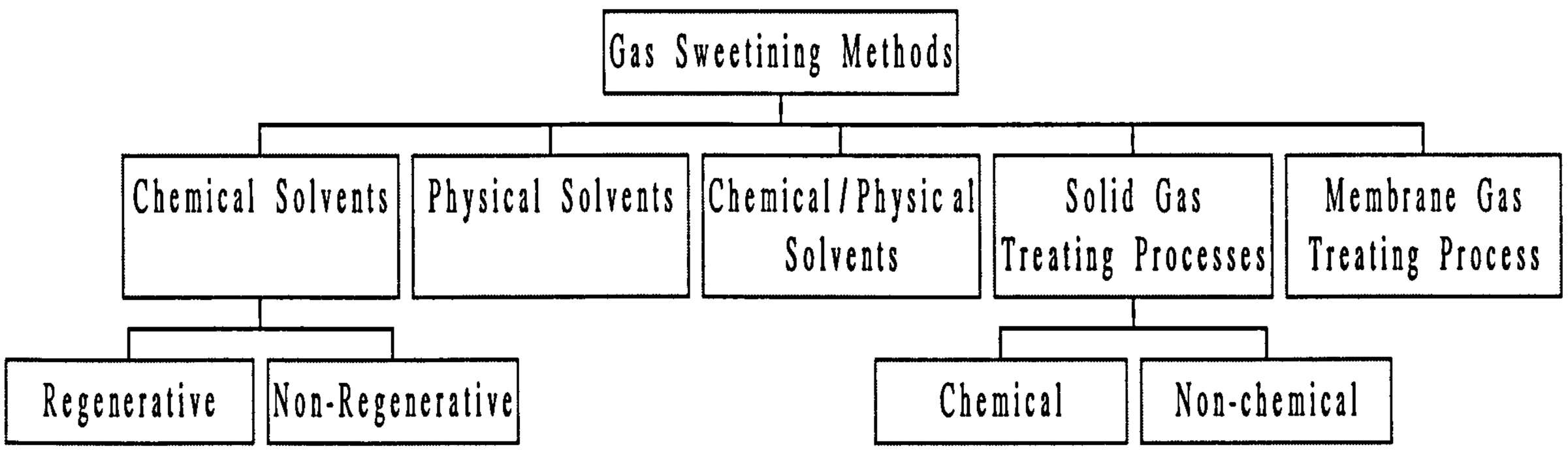

Figure 2.1: Classification of the gas sweetening methods

The liquid-vapour mass transfer operation can either be accompanied with or without chemical reaction depending on the type of the chosen solvent. The former is called chemical solvent and the latter is known as physical solvent. The criteria for choosing an appropriate solvent depend on the composition, temperature, and pressure of feed gas and the required specification on sweet gas as shown in Figure 2.2 (Tennyson and Schaaf, 1977).

From the economic point of view, chemical solvents are favourable when the partial pressure of acid gas in both the sour and sweet streams is low. Furthermore, the chemical reaction between the base liquid and the acid gas can be reversed by changing the operating condition of the process thus regenerating the chemical solvent.

The vapour-liquid equilibrium curves of the chemical solvent shows that fewer theoretical stages are required to achieve high acid gas clean-up. The shape of the equilibrium curve is due to the high ionic strength of the chemical solvents. Other advantages of chemical solvents are: higher capacity, higher degree of removal of acid gas, higher absorption mass transfer coefficient, and higher desorption mass transfer coefficient.

However, there are limitations that should be investigated, such as: cost of chemicals, high heat of absorption, corrosion, side reactions, and possible environmental concerns.

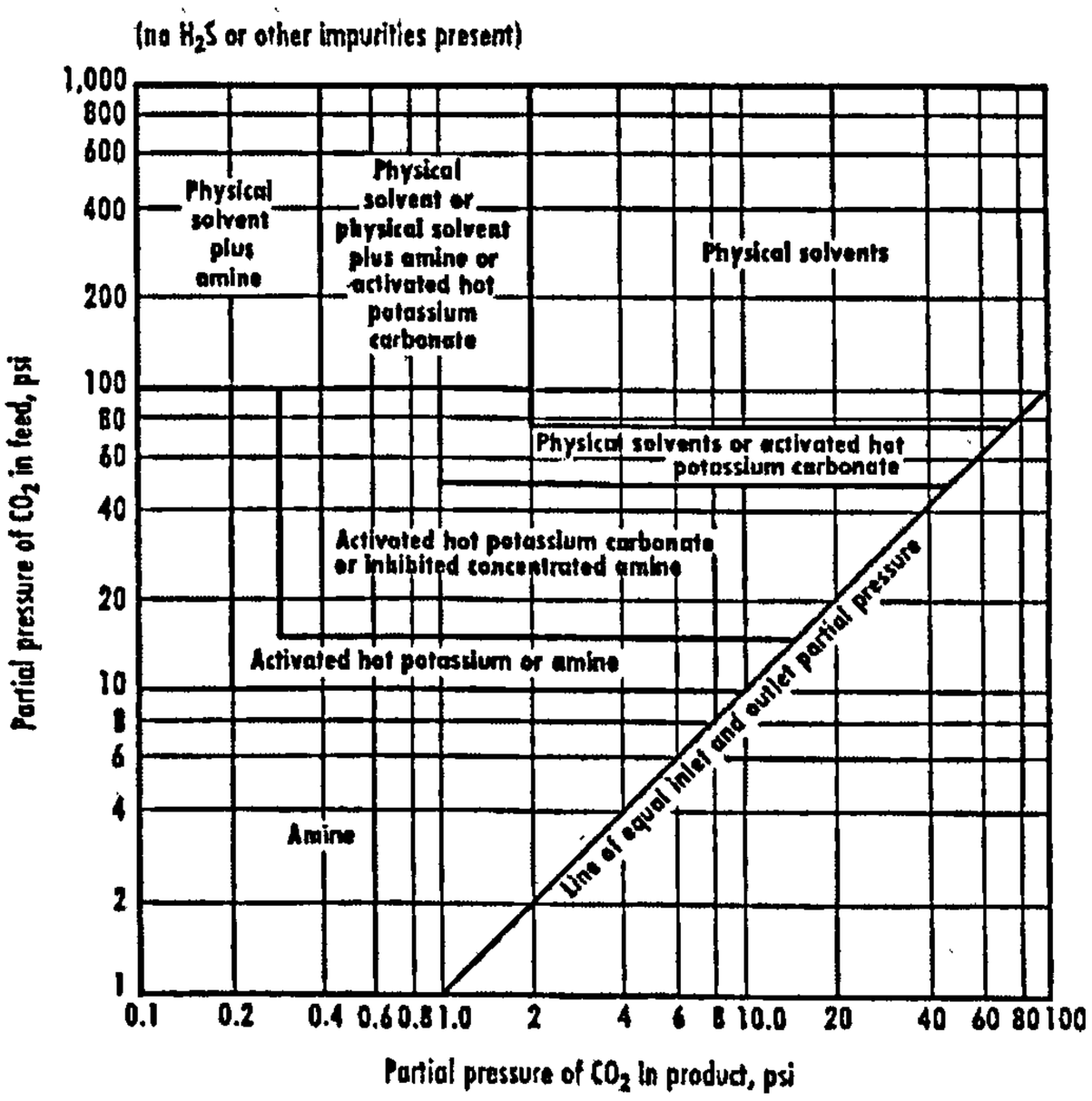

Figure 2.2: Choice of solvent in gas treating (Tennyson and Schaaf, 1977).

There are five main fields that applies gas/liquid absorption and desorption processes (Charpentier, 1982): (1) Liquid phase processes e.g. nitration, polymerisation; (2) Gas scrubbing e.g. CO_2, H_2S; (3) Pure products manufacturing e.g. H_2SO_4, HNO_3; (4) Biological processes e.g. aerobic fermentation; and (5) Multi and two phase flow e.g. oil recovery.

2.1.2 Description of the Operation of A Conventional Gas Treating Plant

Removal of the acid gases (H_2S and CO_2) or gas sweetening is an important industrial application. The removal of carbon dioxide is a common target in the manufacture of Hydrogen, ammonia, natural gas production and the recovery of CO_2 from the flue gases. The main items of a conventional gas sweetening plant are: absorber, desorber and flash drum as shown in Figure 2.3.

The lean alkanolamine solution is fed to the top of the absorber and the sour gas is fed at the bottom thus a mass transfer counter-current process takes place throughout the length of the packing. The sour components of gas stream are diffused with exothermic chemical reactions into the alkanolamine solution. The sweet gas is released at the top of absorber and a CO_2-rich alkanolamine at the bottom.

The next stage is to regenerate rich alkanolamine. The rich solution is heated up using the hot lean ethanolamine from the bottom of the desorber. It is then flashed off before being fed to the desorber in order to remove as much as possible of the flashed gases so that less steam is desirable for regeneration. The flashed liquid is then fed to the top of the desorber. The desorption takes place when the equilibrium partial pressure of carbon dioxide in the rich solution is greater than its partial pressure in the gas phase. Steam is used as a desorption medium because it provides energy to reverse the carbon dioxide and alkanolamine reaction, lowers the partial pressure of carbon dioxide in the gas phase, and provides sensible heat to raise the temperature of the rich amine to the lean amine exiting desorber.

The flashing occurs when total equilibrium vapour pressure, i.e. the sum of equilibrium partial pressure of acid gas and solvent, exceeds total pressure of the system. The kinetics of flashing is not fully understood, though, it can be considered as boiling in which nucleation governs the kinetics. A measurement system is required over the flash drum in order to define the conditions at the top of desorber. Table 2.1 shows the operating data for aqueous MEA gas treating plant.

Figure 2.4 shows the position of the operating line in the counter-current gas-liquid absorber and desorber for a chemical solvent.

2.1.3 Operating Modes

There are three modes of operation: Rich End Pinch (REP), Lean End Pinch (LEP), and Unpinched (UP). In REP and LEP the lean solvent is recycled to the top of absorber whereas for UP mode the solvent is recycled to low feed point. The packing height in REP and LEP should be large to accommodate a pinch whereas it should be small enough in UP mode to avoid existence of a pinch.

In REP a high steam rate is maintained at the bottom of desorber thus ideally a lean solvent is always fed to absorber.

2.1.4 Operating Variables

The operating variables are: (1) steam rate to desorber, (2) liquid circulation rate, (3) feed gas rate, (4) composition, and temperature, (5) pressure in the absorber and desorber, (6) composition of the lean and rich solutions and of the flashed solution, (7) composition of the gas exiting from the absorber, (8) temperatures at the lean and rich end of both absorber and desorber.

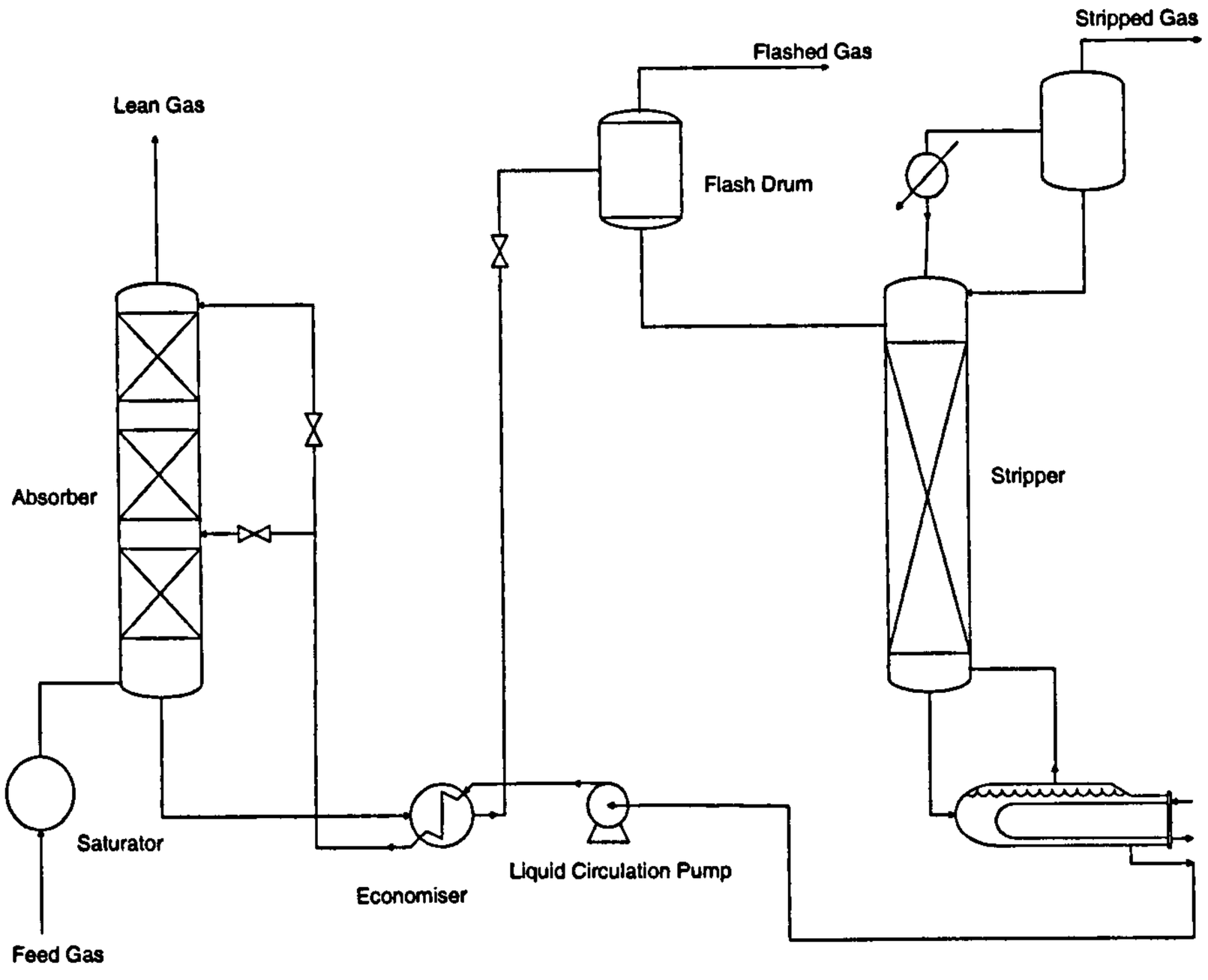

Figure 2.3: Flowsheet of a typical amine plant

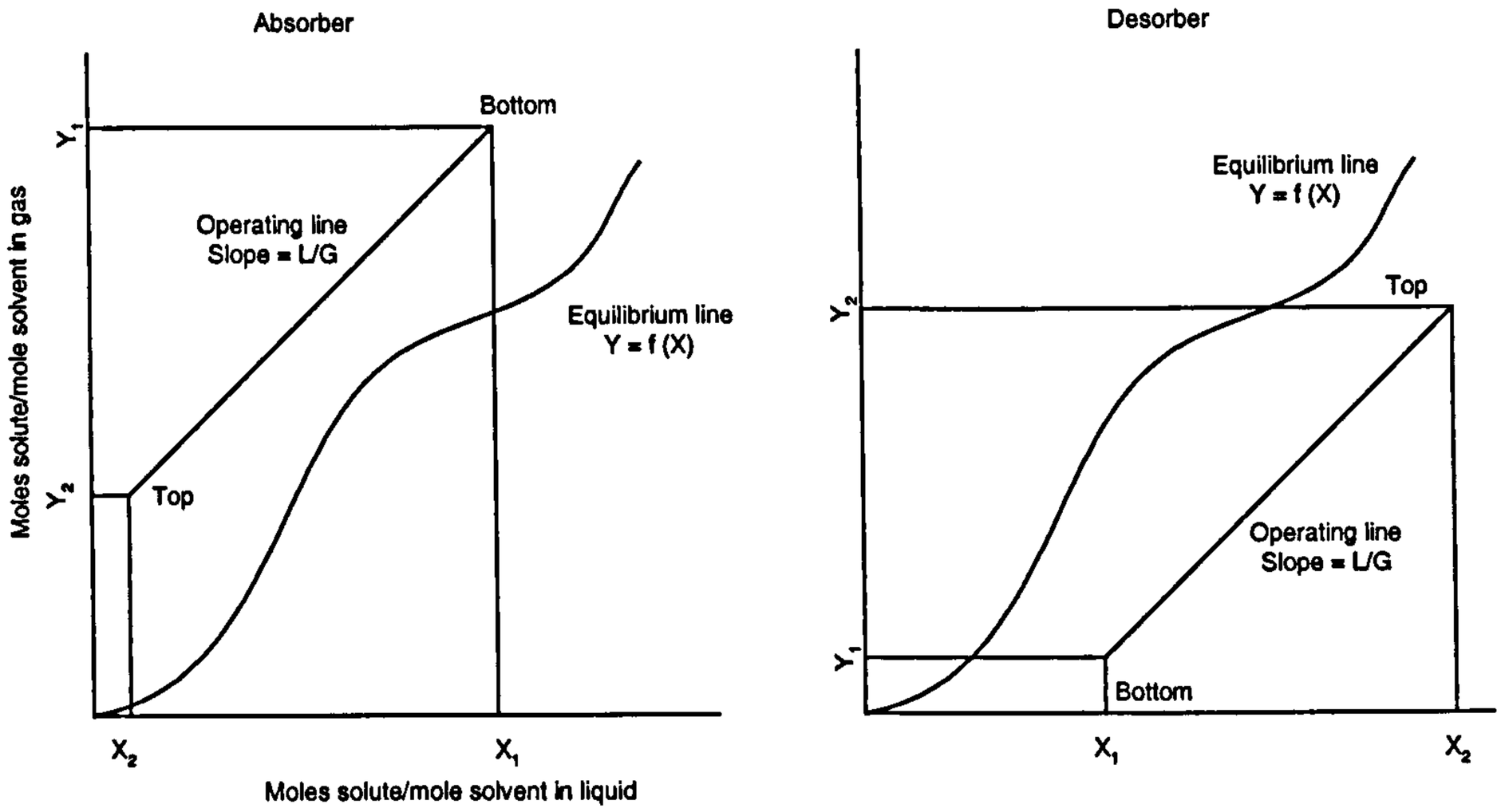

Figure 2.4: Position of the operating line in the absorber and desorber.

Table 2.1: Operating data for Aqueous MEA Gas Treating Plant, (Kohl and Nielsen, 1997)

Gas Feed rate	72 MMscfd	Solution Flow rate	2,000 gpm
%wt MEA	10-18		
Feed gas analysis		Outlet gas analysis	
CO_2, %vol	10-15	CO_2, %vol	0.1-0.3
SO_2, ppmv	10-100	SO_2, ppmv	1-5
H_2S, grains/100scf	0	H_2S, grains/100scf	0
Lean solution loading		Rich Solution Loading	
Mol CO_2/mol MEA	0.062	Mol CO_2/mol MEA	0.415
Absorber			
Number of columns	1	Diameter ID, ft	14.5
Height, ft	133	Internals	Two 23-ft beds of polypropylene saddles
Water wash	2 trays	Pressure, psig	0
Stripper			
Number of columns	1	Diameter ID, ft	12.5
Total trays	18	Wash trays	2
Pressure, psig	5-10	Bottom temperature, °C	118.3
Steam to reboiler, lb/gal of solution	1.13		

2.2 Chemistry

2.2.1 Selection of Amine

There are different types of amines applied in the industry, namely: primary (e.g. monoethanolamine - MEA), secondary (e.g. diethanolamine - DEA), ternary (e.g. triethanolamine - TEA), sterically-hindered, and mixtures of amines. The structural formulas of common amines are shown below.

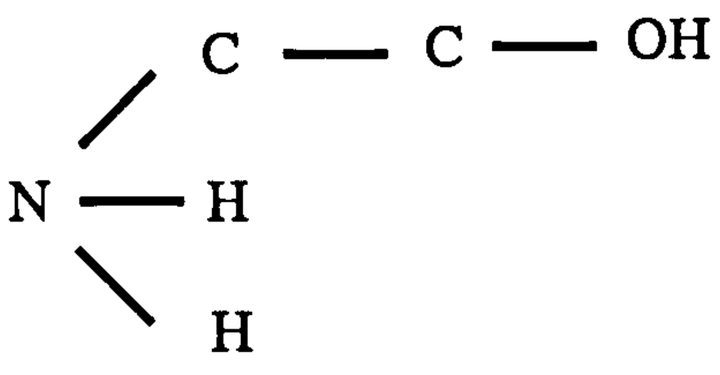

Monoethanolamine (MEA)

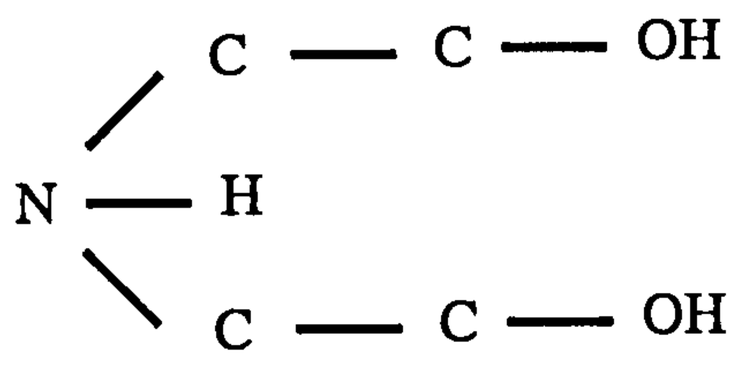

Diethanolamine (DEA)

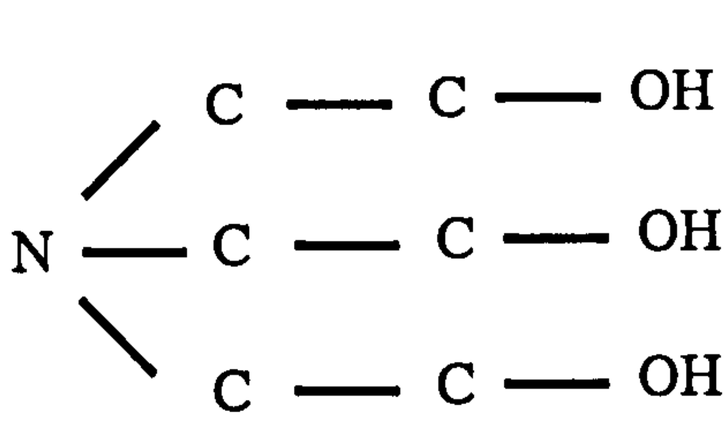

Triethanolamine (TEA)

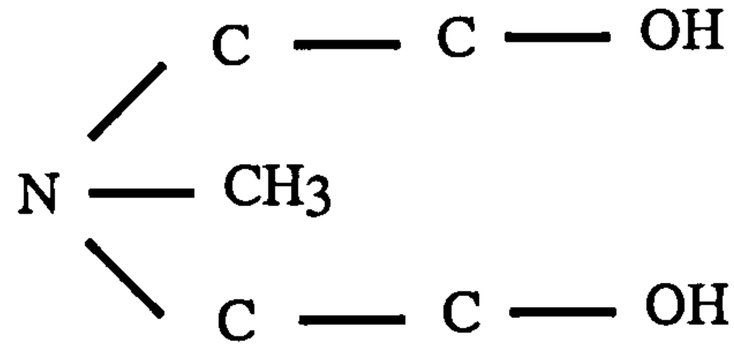

Methyldiethanolamine (MDE

Monoethanolamine (MEA) is selected as the chemical solvent throughout this research due to the availability of vast literature bank related to the laboratory scale physico-chemical data. Furthermore, MEA has a large proportion of the amine world market share (40%) as shown in Figure 2.5.

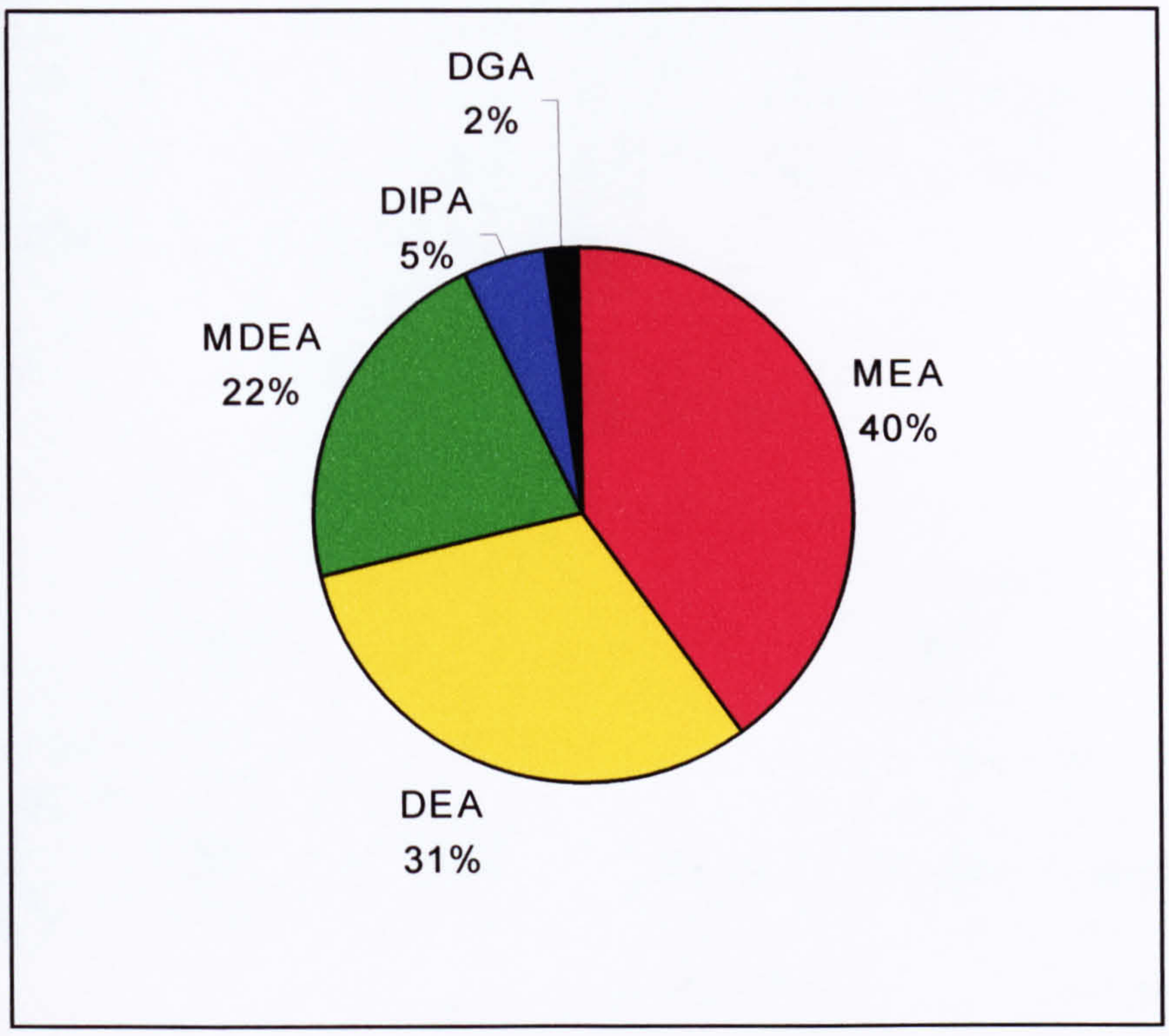

Figure 2.5: Share of MEA in amines global market (DuPart et al., 1993a)

MEA occupies a large slice of the amine market due to few factors such as: higher reaction rate, better stability, high alkalinity, cheaper, easier to reclaim, higher capacity due its lower molar mass thus minimizes the amount of solvent to be circulated, high solubility and low liquid phase mass transfer coefficient. However, its limitations are: formation of a stable carbamate, high vaporization losses due to its high vapour pressure, higher enthalpy of reaction with CO_2 (20 kcal/gmol), high corrosion rate, and formation of degradation products with oxygen.

2.2.2 Classification of Amine

Initially, Brønsted proposed a classification system for the solvents based upon three properties: dielectric constant, acidic strength, and basic strength. He came up with eight classes of solvents and denoted a plus sign to indicate predominance and a negative sign to indicate weakness or absence. Most amines were in class seven which has a positive basicity and negative dielectric constant and relative acidity.

Figure 2.6 shows the current solvent classification scheme (Popovych and Tomkins, 1981). Solvents are broadly divided into amphiprotic and aprotic. The former is capable of accepting and donating protons whereas the latter is unable to transfer

protons. The amphiprotics are further subdivided into protogenic (acidic), protophilic (basic), and neutral. Amines, which react with CO_2, are amphiprotic protophilic solvents. Water is classified as amphiprotic neutral solvent. Therefore, a mixture of water and amine exhibits basic properties.

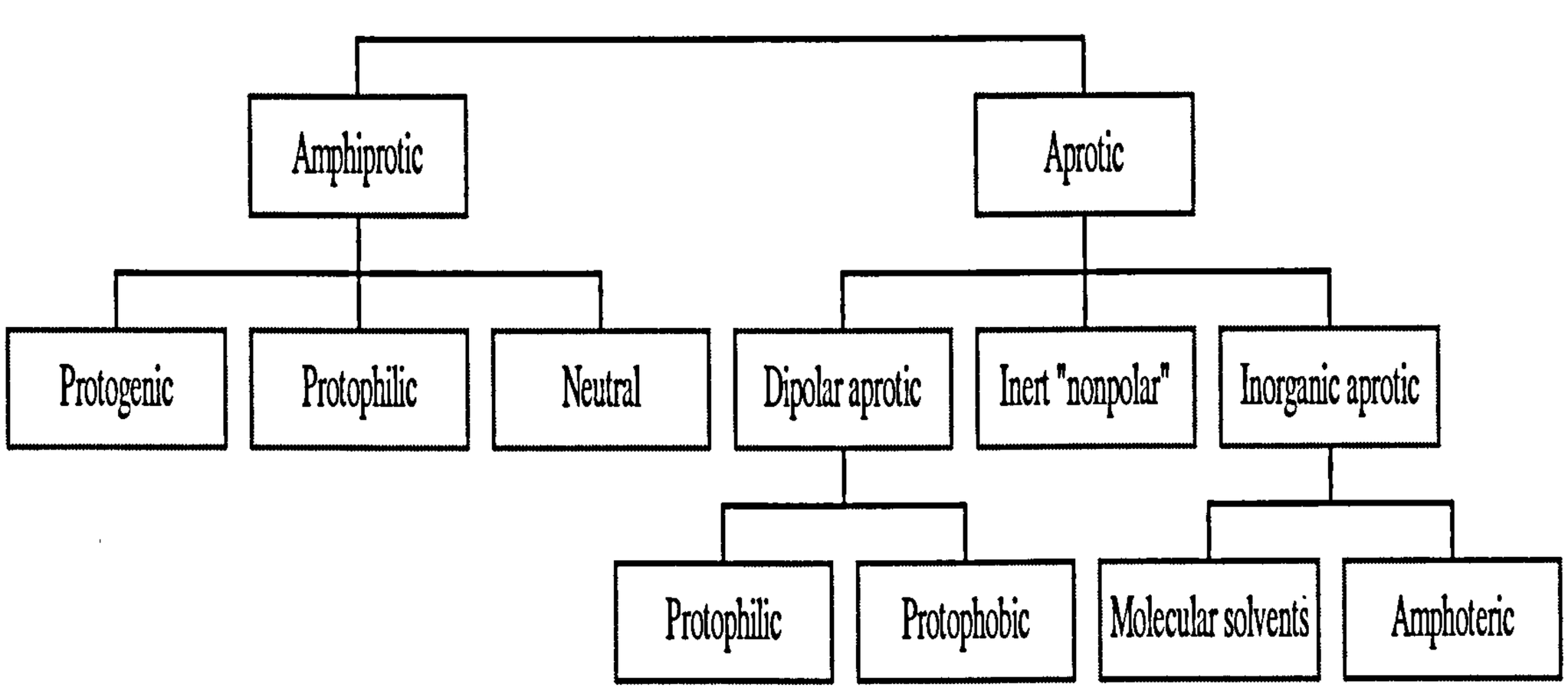

Figure 2.6: Classification of solvents

2.2.3 Amine Concentration

Choice of amine strength is not an easy decision due to the economic and technical considerations (Butwell, 1968). The economic considerations are: capital investment, utility cost, daily losses through vaporization, chemical reaction, or degradation losses. The technical considerations are: acid gas loading, degasification rates, and corrosion.

Table 2.2 reviews the recommended MEA strength in the literature. In 1960s, most of the authors recommended 15wt% MEA solution due to the lack of corrosion inhibitors and the use of carbon steel as the main material of construction. However, progress in corrosion chemistry and employment of stainless steel in sensitive parts of sweetening plant enabled the use of higher amine concentration.

Table 2.2: Review of historical recommended MEA strength.

Source	%wt. MEA	Notes
Peagan et al	15	-
(Butwell, 1968)	20	Ammonia synthesis industry: minimum difficulty in removal of CO_2 as long as rich loading is less than 0.45 mol/mol.
(Connors, 1958)	15-20	-
(DuPart et al., 1993b)	15-20	Rich loading 0.3-0.35 mol/mol
(Dingman et al., 1966)	15	Rich loading 0.35 mol/mol
(Kohl and Nielsen, 1997)	32	Add corrosion inhibitors when acid gas is only CO_2.

The drawbacks in increasing the ethanolamine concentration are: difficulty in the regeneration of strong solution, the increase of vapour pressure of carbon dioxide over the concentrated ethanolamine solution (Figure 2.8), higher heat of reaction will cause increase in the temperature thus higher vapour pressure, carbon dioxide flashing in the heat exchangers and piping prior to stripping column, high concentration of carbon dioxide in stripper, and different types of corrosion. Figure 2.7 shows that the vapour pressure of pure MEA is higher than DEA or diluted solution of MEA.

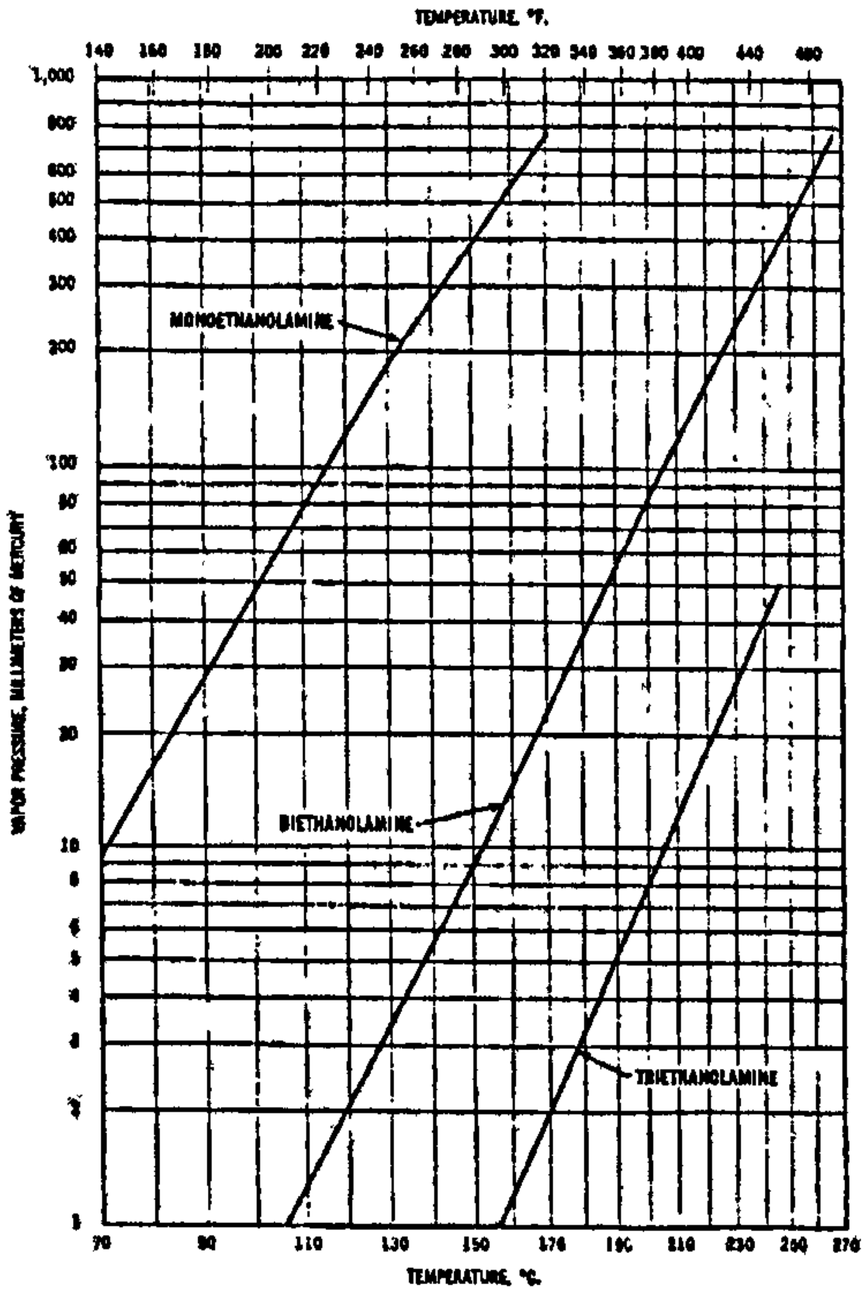

Figure 2.7: Vapour pressure of amines.

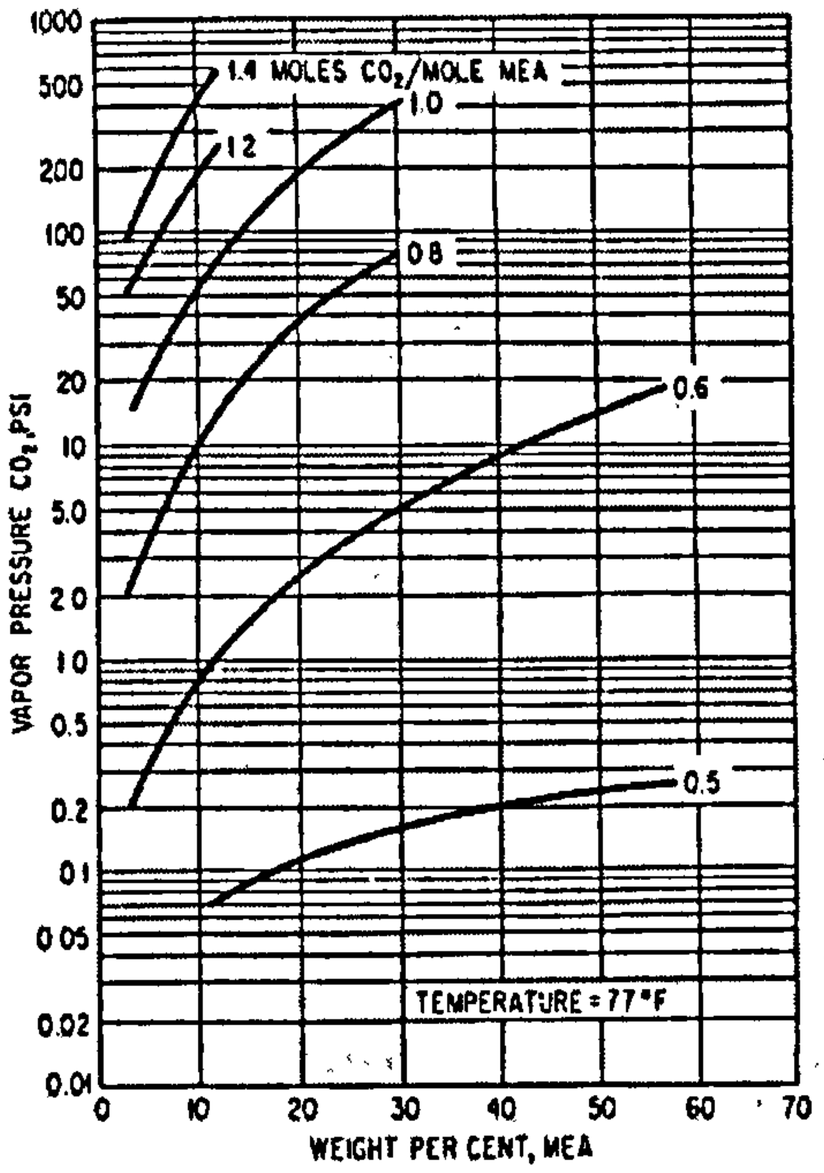

Figure 2.8: Vapour pressure of CO_2 at different MEA concentration (Kohl and Nielsen, 1997).

2.2.4 Reaction Kinetics

The reaction in the solution is between ethanolamine and acid gas (CO_2). Carbon dioxide is a Lewis acid i.e. accepts electrons. The amine has two functional groups: amine and hydroxyl. The amine provides the basicity to the chemical compound and reacts with acid gas. The hydroxyl group increases the solubility of alkanolamine in water thus reducing the vapour pressure of amines so that less is lost at the top of the absorber or stripper. Furthermore, as a consequence to the kinetics of the reaction, carbon dioxide reacts at a finite rate with amine thus the selectivity towards CO_2 can be controlled by changing the type of amine, or, in a mixed amine system, the ratio of various amines in solution.

The main reactions that occur in the solution (Kohl and Nielsen, 1997):

a) Ionization of water:

$$H_2O \longleftrightarrow H^+ + OH^- \qquad (2.1)$$

b) Hydrolysis and ionization of dissolved carbon dioxide:

$$CO_2 + H_2O \longleftrightarrow HCO_3^- + H^+ \quad (2.2)$$

c) Protonation of alkanolamine:

$$RNH_2 + H^+ \longleftrightarrow RNH_3^+ \quad (2.3)$$

Furthermore, (Astarita et al., 1983) and (Zarzycki and Chacuk, 1993) categorized main reactions according to loading level:

CARBAMATE FORMATION: It is the main reaction when loading < 0.5. The mechanism can be explained by zwitterion theorem, which determines the rate-limiting step. ($R \cong C_2H_4OH$)

$$CO_2 + 2\,RNH_2 \longleftrightarrow RNH_3^+ + RNHCOO^- \quad (2.4)$$

BICARBONATE FORMATION: It occurs at all values of loadings.

$$CO_2 + RNH_2 + H_2O \longleftrightarrow RNH_3^+ + HCO_3^- \quad (2.5)$$

$$CO_2 + H_2O \longleftrightarrow H^+ + HCO_3^- \quad (2.6)$$

$$CO_2 + OH^- \longleftrightarrow HCO_3^- \quad (2.7)$$

Direct mechanisms of bicarbonate formation are neglected due to the slow reaction rates.

CARBMATE REVERSION: It is the main reaction when the loading > 0.5.

$$CO_2 + RNHCOO^- + 2\,H_2O \longleftrightarrow RNH_2 + 2\,HCO_3^- \quad (2.8)$$

At loadings > 0.5, the reaction becomes slower thus there is a need for more residence time in the absorption apparatus.

2.2.5 The Rate Limiting Step

(Caplow, 1968) proposed a zwitterion mechanism for the bimolecular reaction of amines (not alkanolamines) with CO_2. Carbon dioxide reacts with an amine molecule to form an intermediate (a zwitterion) then this intermediate instantaneously reacts with another amine/base molecule to form a carbamate and a protonized amine/base. Thus, the forward reaction of zwitterion formation is the rate-determining step and it is first order with respect to CO_2 and RNH_2 and second order overall.

$$CO_2 + RNH_2 \underset{K_{-1}}{\overset{K_1}{\rightleftharpoons}} RNH_2^+COO^-$$

$$RNH_2^+COO^- + RNH_2 \underset{K_{-b}}{\overset{K_b}{\rightleftharpoons}} RNH_3^+ + RNHCOO^-$$

Combining Equations (2.9) and (2.10) above yields:

$$CO_2 + 2\,RNH_2 \rightleftharpoons RNH_3^+ + RNHCOO^- \qquad (2.11)$$

(Danckwerts, 1979) extended this to the absorption of CO_2 by primary, secondary and ternary alkanolamines and (Critchfield and Rochelle, 1987) introduced reversibility thus enabling to describe both mass transfer mechanisms of absorption and desorption.

(Danckwerts, 1979) derived an overall forward reaction rate equation with the assumption of quassi-steady state condition.

$$r = \frac{k_1 [CO_2][R_2NH]}{1 + \frac{k_{-1}}{\sum (k_b.[B])}} \qquad (2.12)$$

The base (B) can be any base in the solution (amine, H_2O, and OH^- species). If the second term in the denominator << 1.0 then the rate equation becomes:

$$r = k_1 [CO_2] [R_2NH] \qquad (2.13)$$

Equation 2.14 shows the zwitterion formation and Equations 2.15, 2.16 and 2.17 show three possible parallel reactions for deprotonation reactions for carbamate formation from MEA.

Zwitterion formation:

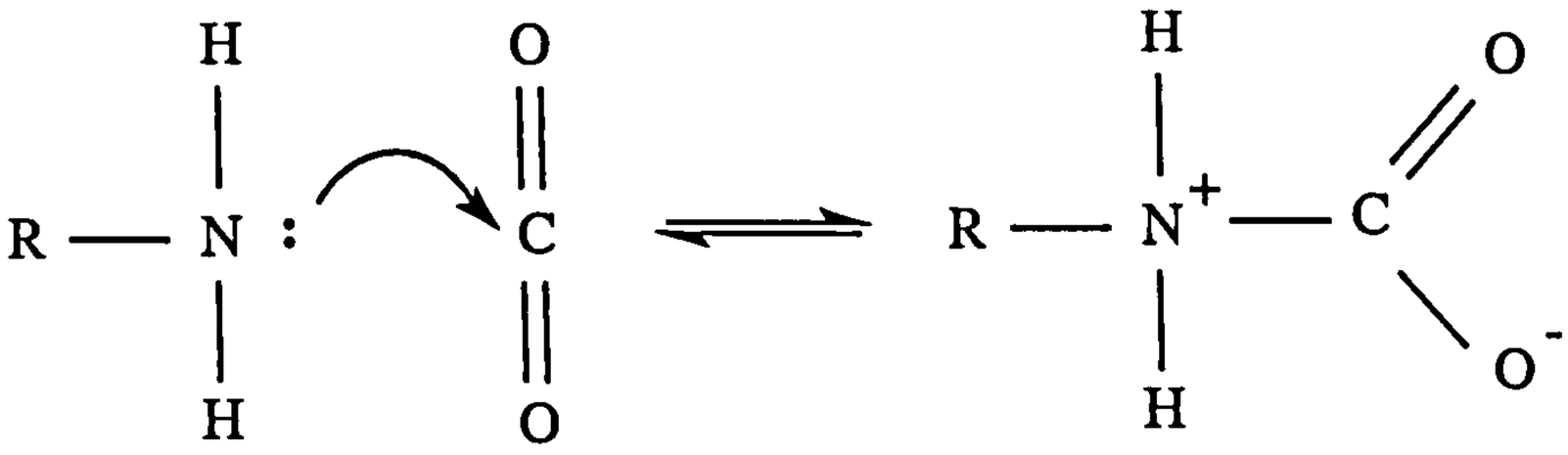

Zwitterion deprotonation (3 parallel reactions):

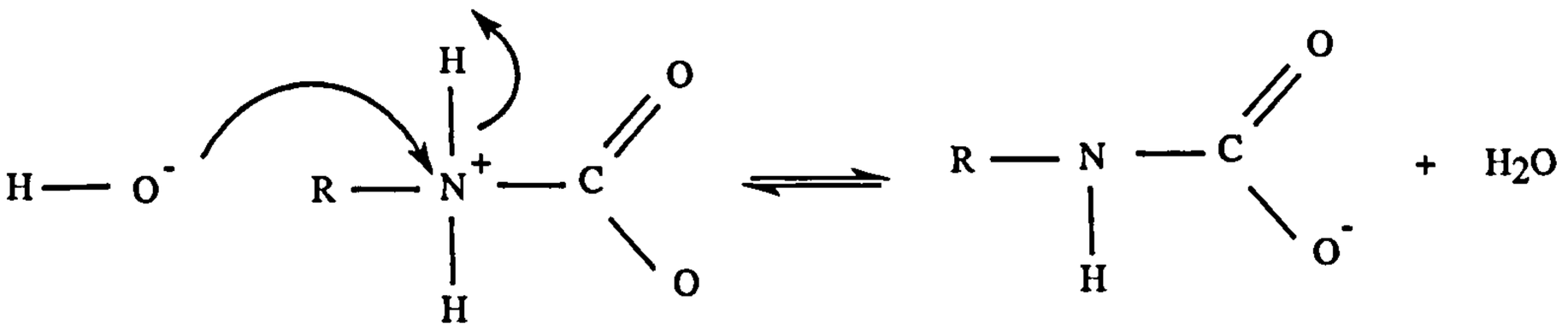

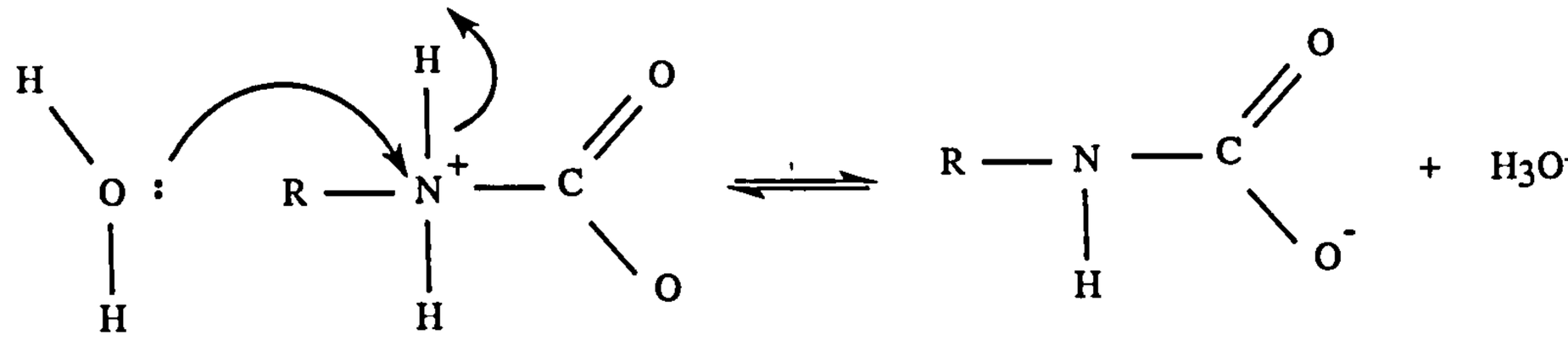

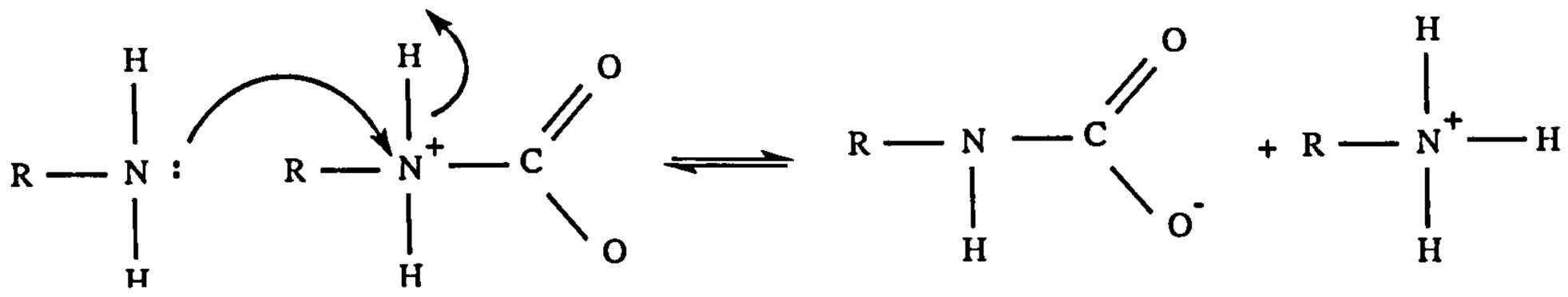

2.2.6 Kinetic Data

(Blauwhoff et al., 1984) reviewed the literature kinetic data for the amines. It was concluded that the reaction rate constant for MEA quoted by Hikita et al. (1977) fits well the kinetic data investigated by other recent sources.

The reaction between carbon dioxide and the amine is second order. Thus, the rate equation is:

$$r_{CO2} = k_2 [CO_2] [MEA]. \qquad (2.18)$$

where k_2 is the second order reaction rate constant (l/mole/s), and $[CO_2]$ and [MEA] are the concentrations of carbon dioxide and the amine respectively. In addition, k_2 value for the temperature range of 5-80°C is given by Hikita et al (1977):

$$\text{Log}_{10} k_2 = 10.99 - (2152 / T). \qquad (2.19)$$

2.2.7 Properties of Monoethanolamine (MEA)

2.2.7.1 Physical Properties

Appendix A shows the physical properties diagrams of aqueous MEA solutions: viscosity, specific heat, total vapour pressure, specific gravity, boiling point, heat of vaporization, volatility, heat of solution, refractive index, and surface tension (Atadan, 1955).

2.2.7.2 Oxidation

In the presence of free oxygen, with and without carbon dioxide, alkanolamines are degraded to form heat stable salts (Rooney et al., 1998). Oxygen reacts with alkanolamines to form heat-stable acids such as: formic acid, ammonia, substituted amide, high molecular weight polymers, glycine, glycolic acid, formic acid, acetic acid, and oxalic acid. These reactions are irreversible and produce heat-stable salts: formate, oxalate, acetate, thiocyanate, sulphate and chloride. As a result, there is a reduction in the amine available for gas removal, increase in corrosion and solution viscosity.

Thus, it is recommended that the storage tanks of ethanolamines should be blanketed with nitrogen in order to keep the air away. In case of oxygen contamination, scavengers such as sulphites and hydrazine could be injected to reduce oxygen solubility and build up of heat stable salts.

2.2.7.3 Foaming

Reduction in surface tension of amine solution by contaminants increases the foaming tendencies (Pauley, 1991). The main contaminants are oxidation and degradation products that form a thin film that is elastic and capable of encapsulating a gas bubble. The direct consequence of foam formation is the reduction in the gas treating capacity because of the reduction in the effective mass transfer area.

2.2.7.4 Diffusivity of CO_2 in Aqueous Solutions of Monoethanolamines

As mass transfer is accompanied by chemical reaction, it is impossible to obtain directly the diffusivity of CO_2 in MEA solution. However, it is possible to estimate the diffusivity of CO_2 in alkanolamines solutions using data of a non-reacting gas

such as N_2O (Versteeg and Van Swaaij, 1988). N_2O is a non-reacting gas that has similar configuration, molecular volume, and electronic structure to CO_2. The N_2O analogy was applied by (Laddha et al., 1981) to estimate the solubility of CO_2 in alkanolamine solutions. The methodology of such estimation is as follows:

Firstly, diffusivities of CO_2 and N_2O in water can be calculated:

$$D_{CO_2} = 2.35 * 10^{-6} \exp\left(\frac{-2119}{T}\right) \tag{2.20}$$

$$D_{N_2O} = 5.07 * 10^{-6} \exp\left(\frac{-2371}{T}\right) \tag{2.21}$$

Thus, the diffusivity of CO_2 and N_2O in water at 298K is $1.78*10^{-9}$ and $1.92*10^{-9}$ m^2/s respectively. Then the modified Stokes-Einstein relation can be used to calculate the diffusion coefficient of N_2O in the amine solution.

$$\left(D_{N_2O}\,\mu^{0.6}\right)_{\text{amine sol}} = \left(D_{N_2O}\,\mu^{0.6}\right)_{\text{water}} \tag{2.22}$$

The viscosities of water and 30wt% MEA at 298K are respectively $0.8937*10^{-3}$, $2.27*10^{-3}$ Pa.s. Thus, the diffusivity of N_2O in amine solution is $1.10*10^{-9}$ m^2/s. Thereafter, applying N_2O analogy to calculate the diffusivity of CO_2 in amine solution.

$$\left(\frac{D_{N_2O}}{D_{CO_2}}\right)_{\text{amine sol.}} = \left(\frac{D_{N_2O}}{D_{CO_2}}\right)_{\text{water.}} \tag{2.23}$$

Thus, the diffusivity of CO_2 in amine solution is $1.02*10^{-9}$ m^2/s.

2.3 Mass Transfer Processes

2.3.1 Physical Mass Transfer Processes

2.3.1.1 General Concepts

When liquid and gas comes into contact, mass transfer takes place between the two phases until equilibrium prevails. The laws that govern the rate of mass transfer between the two phases can only be determined by experiments.

The résistance to mass transfer between the liquid and the gas is across both sides of the interface. (Whitman, 1923) proposed splitting the driving force across the gas film and the liquid film. Therefore, the basic mass transfer equation for the transfer of component (A) across an interface for a physical solvent is:

$$N_A = k_G (P_{AG} - P_{Ai}) = k^o_L (C_{Ai} - C_{AL}) \qquad (2.24)$$

where N_A is the overall rate of mass transfer, k_G is gas film mass transfer coefficient (m/s), k^o_L is physical liquid film mass transfer coefficient (m/s), C_{Ai} is the concentration at the interface, C_{AL} is the concentration in the bulk of liquid, P_{Ai} is the partial pressure at the interface and P_{AG} is the partial pressure at the bulk of gas.

The mass transfer coefficient is linear for the physical solvents and highly non-linear for the chemical solvents. Furthermore, the fugacity is continuous across the interface.

In industry, it is more familiar the use of overall mass transfer coefficients rather than the film mass transfer coefficients. Thus, Equation (2.24) becomes:

$$N_A = K_G (P_{AG} - P_{Ae}) = K_L (C_{Ae} - C_{AL}) \qquad (2.25)$$

where P_{Ae} is the partial pressure of A in equilibrium with a solution having the composition of the main body of liquid, and C_{Ae} is the concentration of A in solution in equilibrium with the main body of gas.

The relationships between overall mass transfer coefficients and the film coefficients are:

$$\frac{1}{K_G} = \frac{1}{k_G} + \frac{H}{k^o_L} \qquad (2.26)$$

$$\frac{1}{K_L} = \frac{1}{k^{\circ}_L} + \frac{1}{H k_G} \tag{2.27}$$

Henry's Law applies when equilibrium is assumed linear in the system.

Thus, $p_i = H c_i$ (2.28)

Where H is Henry's law coefficient.

Combining Equations (2.25) and (2.28) into (2.27) yields:

$$N_A = \frac{\frac{P_A}{H} - C_{Ai}}{\frac{1}{k^{\circ}_L} + \frac{1}{H k_G}} \tag{2.29}$$

According to Equation (2.29), there are two mathematical limiting behaviours (Astarita et al., 1983):

1- Gas Phase Control:

$$\frac{k^{\circ}_L}{H k_G} \succ\succ 1 \tag{2.30}$$

Thus, $N_A = k_G (P_A - H C_{AL})$ (2.31)

Which means that the solute is very soluble (low Henry's constant value) in the liquid and therefore the resistance is mainly in the gas phase.

2- Liquid Phase Control

$$\frac{k^{\circ}_L}{H k_G} \prec\prec 1 \tag{2.32}$$

Thus, $N = k^{\circ}_L \left(\frac{P_A}{H} - C_{Ai} \right)$ (2.33)

Which implies that the resistance is mainly in the liquid i.e. the solute is less soluble in the liquid (high Henry's constant value).

In conclusion, the resistance to mass transfer in the absorption of carbon dioxide into alkanolamine solution is primarily in the gas phase because the solute is readily soluble (low Henry's constant value).

2.3.1.2 Mass Transfer Models

This section reviews briefly the theoretical models that describe the hydrodynamics of the liquid next to the gas-liquid interface. Mass transfer is a function of the fluid physical properties, concentration difference, interfacial area, and the degree of turbulence (Coulson et al., 1993). The gas absorption mass transfer mechanism can be described as follows: soluble gas diffuses to surface then dissolves in liquid and then passes into the bulk of the liquid. Different theories describe the resistance to transfer at the phase boundary and the conditions in the region of the phase boundary.

2.3.1.2.1 The Two film Theory

(Whitman, 1923) established the first theory of mass transfer between two phases. The theory indicates that mass transfer occurs between gas/liquid in a stagnant film by molecular diffusion. The total mass transfer resistance is located in the films. At the interface, a laminar layer is assumed to exist on each side of the films (Dankwerts, 1970).

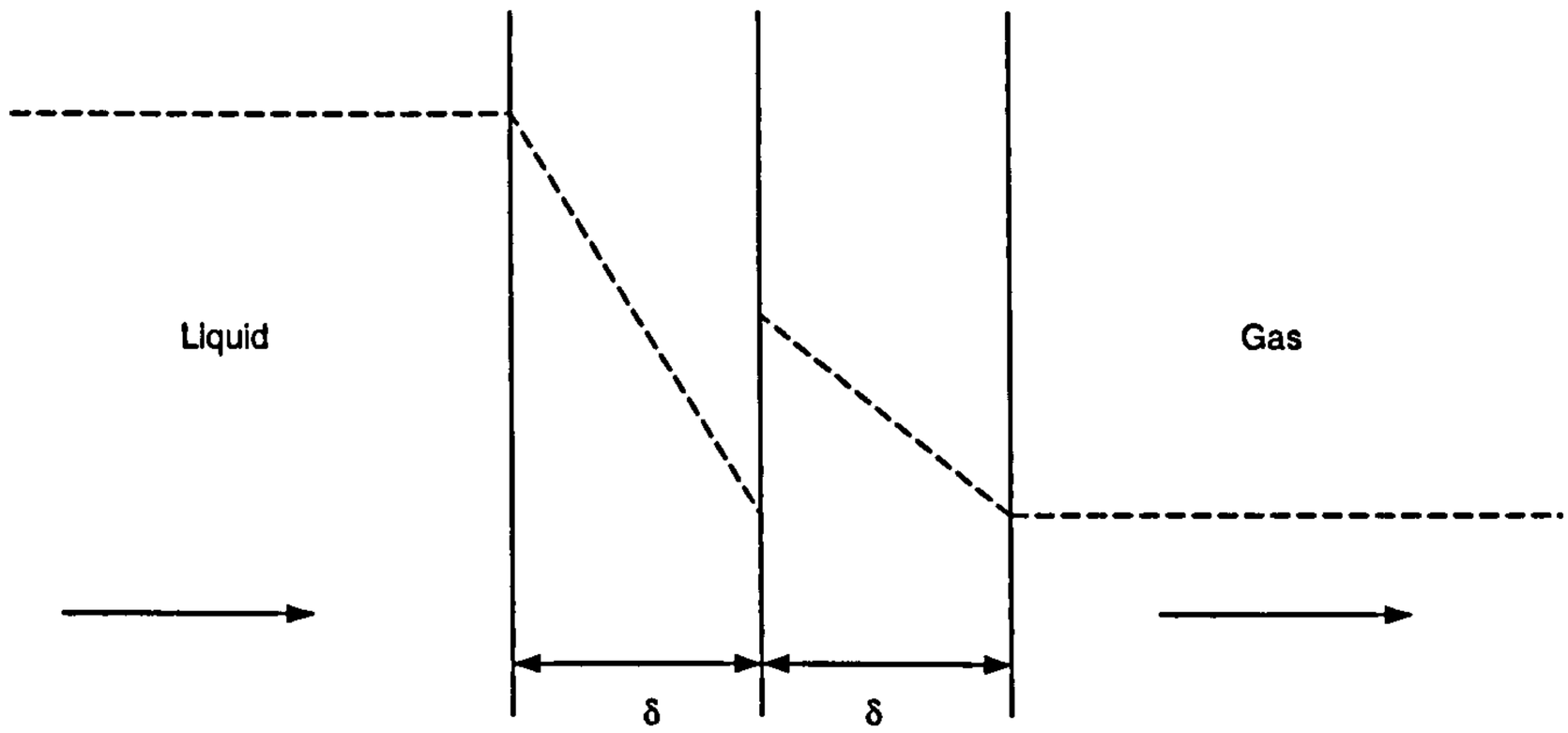

Figure 2.9: Concentration profile of physical absorption using Two-film Theory

Figure 2.9 shows both of the gas and liquid hypothetical layers on each side of the interface. The concentration gradient is linear inside each layer and the stagnant film is assumed to have a uniform thickness. Therefore, the mass transfer flux for equimolecular counter-diffusion and in the absence of a chemical reaction is:

$$N_A = D_A \frac{C_{Ae} - C_{AL}}{\delta} \tag{2.34}$$

$$\text{Thus, } K_L = \frac{D_A}{\delta} \tag{2.35}$$

2.3.1.2.2 The Penetration Theory

(Higbie, 1935) proposed a new theory for liquid-side mass transfer resistance in absorption without chemical reaction. The mass transfer was attributed to fresh material brought by eddies at interface where unsteady state transfer takes place for a fixed period at the freshly exposed surface. The mass transfer coefficient varies with the square root of diffusivity ($K_L \alpha \sqrt{D}$). The assumptions of the penetration theory as applied to packed beds are: very short exposure time, infinitely thick film, liquid flow is laminar and the liquid is completely remixed at junctions of the packing material. The only limitation of the penetration theory is the hypothesis that all mass transfer components stay on the surface/interface for the same length of time (t^*).

The average flux for instantaneous mass transfer is:

$$N = \frac{1}{t^*} \int_0^{t^*} N_{inst}(t)\, dt = 2\sqrt{\frac{D}{\pi\, t^*}} (C_i - C_L) \tag{2.36}$$

$$\text{Thus, } K_L = 2\sqrt{\frac{D}{\pi\ t^*}} \tag{2.37}$$

Where t* is the exposure time of the liquid to the gas. The driving force for the mass transfer coefficient is the difference between the interfacial concentration and the concentration in the liquid at the beginning of the short absorption period:

$$t^* = \frac{\pi\, d_p}{2\, v} \tag{2.38}$$

where d_p is the characteristic dimension (e.g. filament thickness) and v is the liquid film velocity. Equation (2.39) is based on (Nusselt, 1916) theory for fully developed laminar flow.

$$v = \left(\frac{\rho\, g\, \delta^2}{3\, \mu} \right) = \left(\frac{9\, g\, \Gamma^2}{8\, \mu\, \rho} \right)^{1/3} \tag{2.39}$$

where Γ is the liquid flowrate per unit width:

$$\Gamma = \frac{\delta^2 \, g \, \rho}{2 \, \mu} \tag{2.40}$$

Therefore, substituting Equations (2.38), (2.39), (2.40) into (2.37) yields:

$$Sh = \frac{K_L \, d_p}{D} = 0.919 \left(\frac{a_p}{a_e} \right)^{1/3} Sc^{1/2} \, Re^{1/3} \, Gr^{1/6} \tag{2.41}$$

(Davidson, 1959) developed three models based upon the Penetration Theory to predict the HTU in a packed bed for liquid phase mass transfer.

First model assumes that the bed consists of a large number of vertical and completely wetted surfaces.

$$\frac{H_L}{d_p} = 0.345 \, Sc^{1/2} \, Re_l^{2/3} \, Gr^{-1/6} \tag{2.42}$$

The second model assumes that the bed is made from a large number with randomly inclined flat surfaces of equal lengths.

$$\frac{HTU_L}{d_p} = 0.244 \, Sc^{1/2} \, Re^{2/3} \, Gr^{-1/6} \tag{2.43}$$

And the third model assumes that the bed is made from a large number of randomly inclined flat surfaces of random lengths.

$$\frac{HTU_L}{d_p} = 0.1833 \, Sc^{1/2} \, Re^{2/3} \, Gr^{-1/6} \tag{2.44}$$

2.3.1.2.3 Surface-Renewal Models

(Danckwerts, 1951) suggested that the surface of liquid has a variety of elements that exposes to the gas for different lengths of time and thus be absorbed at different rates. A distribution function f(θ) describes the distribution of surface elements. The average flux for instantaneous mass transfer is:

$$N = \int_0^\infty N_{inst}(\theta) \psi(\theta) \, d\theta = \sqrt{\frac{D_A}{\pi}} (C_{Ai} - C_{A0}) \int_0^\infty \frac{\psi(\theta)}{\sqrt{\theta}} d\theta \tag{2.45}$$

$$K_L = \sqrt{D_A \, s} \tag{2.46}$$

where "s" is the rate of surface renewal. The mass transfer rate coefficient is proportional to the square root of the diffusivity and thus similar to the penetration theory.

2.3.2 Mass Transfer Accompanied by Chemical Reaction

2.3.2.1 Introduction

A chemical solvent enhances the rate of mass transfer by chemically reacting with the solute gas. The degree of enhancement is in incorporated into the physical mass transfer equation:

$$[N_{AL}]_{chem} = [k_{AL}]_{chem} [C^*_{AL} - C_{AL}] \quad (2.47)$$

Using the two-film theory to define the mass transfer coefficient:

$$[K_{AL}]_{chem} = \frac{D_{AL}}{[\delta_L]_{chem}} \quad (2.48)$$

Equation (2.48) implies that the chemical absorption has different thickness to the physical absorption.

The ratio of physical and chemical molar fluxes is defined as the enhancement factor:

$$E = \frac{[k_{AL}]_{chem}}{[k_{AL}]_{phys}} \quad (2.49)$$

Substituting Equation (2.49) into (2.47) yields:

$$[N_{AL}]_{chem} = E\, k_{AL} [C^*_{AL} - C_{AL}] \quad (2.50)$$

where k_{AL} is the physical mass transfer coefficient.

2.3.2.2 Reasons for Higher Rate of Mass Transfer Using Chemical Solvents

Chemical reaction enhances the rate of sour gases absorption. The reason for higher absorption rates with chemical reaction can be categorized into two effects (Glasscock, 1990):

2.3.2.2.1 Equilibrium considerations

The overall gas phase mass transfer coefficient is:

$$N = \frac{P - P^*}{\frac{1}{k_g} + \frac{H}{E k_l^o}} = K_g (P - P^*) \qquad (2.51)$$

The driving force for the above equation is the difference between the partial pressures of CO_2 in the gas phase and the equilibrium partial pressure of CO_2 that corresponds to the concentration of CO_2 in the liquid phase. Chemical reactions in the liquid phase between CO_2 and basic species reduce the equilibrium partial pressure thus increasing the driving force.

2.3.2.2.2 Non-equilibrium considerations

The above overall gas phase mass transfer coefficient is similar to the equation for physical system except the existence of the enhancement factor "E". The reason that the chemical reaction enhances absorption rate is that the gas is consumed at the gas-liquid interface. The reaction causes an increase in the concentration gradient of CO_2 at the gas-liquid interface and therefore an increase in the absorption rate.

2.3.2.3 Reaction Regimes

There are three distinct reaction regimes: slow, fast and instantaneous. A dimensionless ratio Φ is a measure of relative rates of reaction and diffusion time.

$$\phi = \frac{t_D}{t_r} \qquad (2.52)$$

t_D (diffusion time) is the time available for molecular diffusion before mixing of the liquid phase makes the concentration of liquid uniform. And t_r (reaction time) is the time required by the chemical reaction to change considerably the concentration of the limiting reactant.

If $\Phi \ll 1$ then the reaction is in the slow regime and there is no rate enhancement. If $\Phi \to \infty$ then the reaction is in the instantaneous regime. An intermediate regime occurs when $\Phi \gg 1$ and called the fast regime.

(Astarita et al., 1983) quoted the reaction times for the three regimes:

Slow reaction	$t_r > 10^{-2}$ s
Fast reaction	$10^{-2} > t_r > 10^{-6}$ s

Instantaneous reaction $t_r < 10^{-6}$ s

In the case of CO_2 absorption by alkaline solutions, the magnitude of the reaction times is 10^{-5}-10^{-7} s, which implies that the reaction is in grey area between fast and instantaneous reaction.

The diffusion time, t_D, is defined as follows:

$$k_L = \sqrt{\frac{D}{t_D}} \qquad (2.53)$$

$$t_D = \frac{\delta^2}{D} \qquad (2.54)$$

where D is the diffusivity and δ is the film thickness. The range of t_D in industry is provided by (Astarita et al., 1983):

$4*10^{-3} < t_D < 4*10^{-2}$ sec

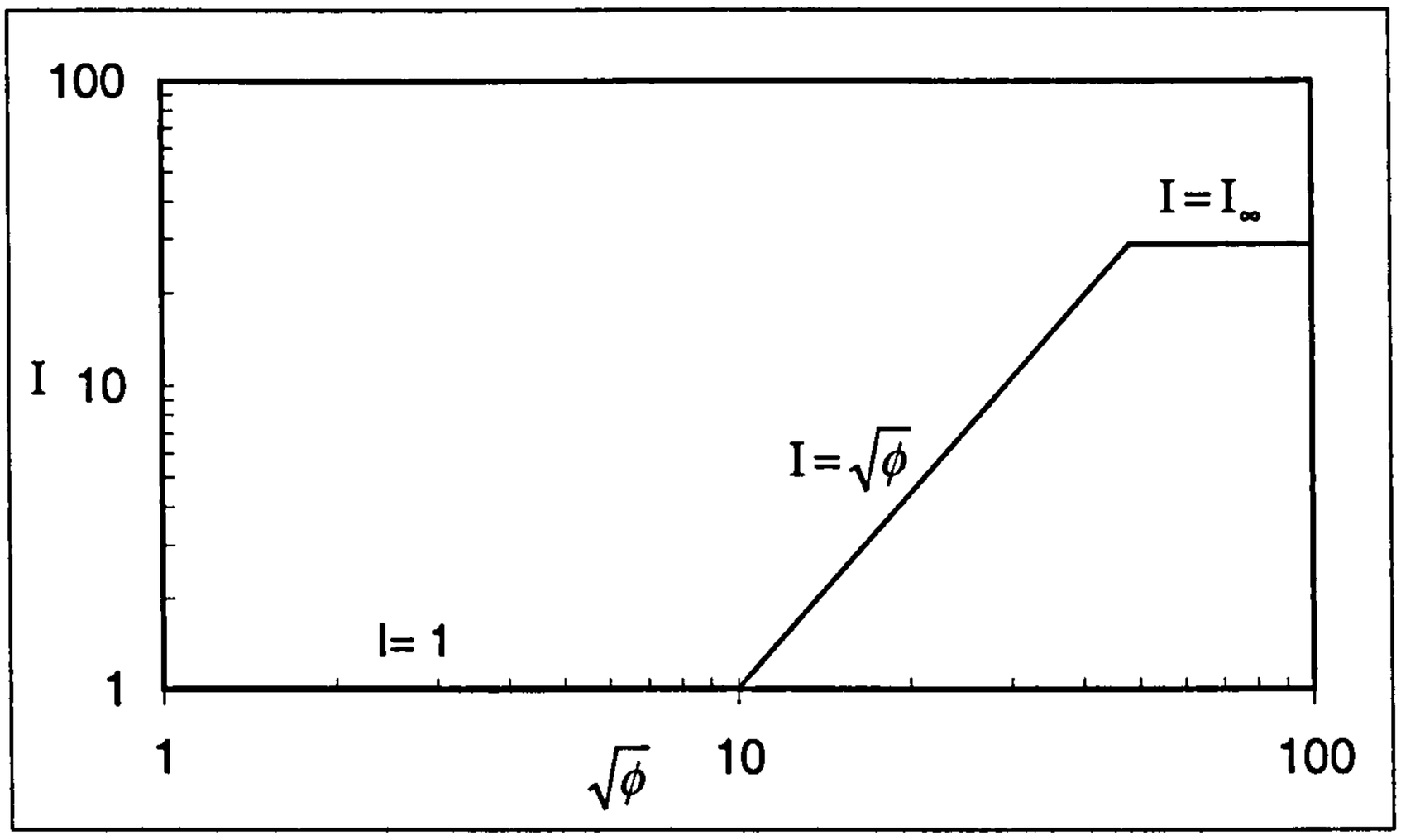

Figure 2.10: Asymptotic behaviour for I

Figure 2.10 shows the asymptotic behaviour of mass transfer accompanied by chemical reaction. The reaction between alkanolamine and carbon dioxide is very fast and as a consequence carbon dioxide is readily soluble in the alkanolamine solution.

2.4 Rotating Packed Bed (RPB)

2.4.1 Comparison Between the Classical Packed Tower and RPB

For the chemical engineer, the classical packed tower is used for different mass transfer operations such as distillation, and absorption. The tower is basically a cylindrical shell filled with different packing materials, shapes, and sizes; and positioned vertically. The gravitational acceleration is constant throughout packing and the pressure drop is due to drag forces. Liquid enters at the top of the packed column and flows downward under the influence of gravity. The gas enters at the bottom and flows upward through the packing. Thus a counter-current mass transfer takes place and the packing provides the area of contact. The efficiency of the packed tower for mass transfer depends upon the specific area of the packing and the liquid irrigation rates (Coulson et al., 1991).

On the other hand, the Higee mass transfer machine has different shape and mode of operation (Ramshaw, 1993). The Higee machine is constructed using a doughnut-shaped rotor, which is mounted on a shaft, and filled with high specific area packing. Gas phase is forced to enter from the outer periphery and flows radially inwards and passes through a rotating packed material before exiting. The liquid phase enters from the eye of the machine through a spray nozzle, which radially sprays it outwards. Therefore, a counter-current mass transfer occurs between the phases accompanied by centrifugal force. The rotational speed gives an extra degree of freedom, i.e. by selecting the specific rotational speed; both the residence time and the thickness of mass transfer film can be controlled. Furthermore, the enhanced acceleration causes higher flooding velocities and improved volumetric mass transfer coefficients. As a result, both of these features lead to a particularly compact mass transfer contactor for a given duty.

2.4.2 Background

This section details the historical development on the field of rotating packed beds:

(Chambers and Wall, 1954) designed a centrifugal absorber with 21 in. diameter and 10 in. height (Figure 2.11). The mass transfer between phases occurs in the intermesh of concentric rings and no packing was utilized. It was successfully applied in reducing the carbon dioxide concentration in the air mixture from 14% to 2% with

application of pure MEA solution. The pilot rig was made from mild steel thus the rich solution was deteriorated due to the corrosive nature of pure MEA solution. The results were not expressed in terms of gas mass transfer coefficient as the author suggested that its values could mislead the reader because Henry's Law is applicable for to short contact time.

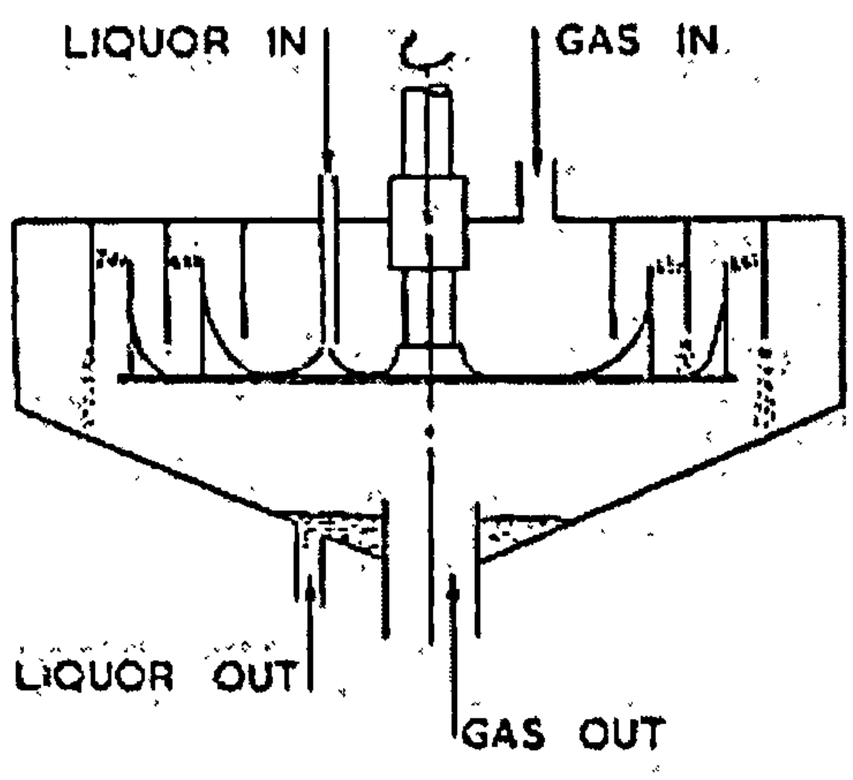

Figure 2.11: Chamber's centrifugal absorber.

Table 2.3 shows the absorption results using dirty MEA solution while Table 2.4 shows the absorption results using new MEA solution. The comparison indicated the importance of MEA solution quality which in this case was deteriorated due to metal corrosion products, oxidation products etc.

Table 2.3: Absorption results using dirty MEA.

Gas Flow (m3/hr) a	Liquid Flow (L/min) b	a / b	CO_2 in gas (%)		Absorption (kg/hr)
			In	Out	
56.63	6.44	8.79	16.3	2.3	16.01
84.95	6.44	13.19	15.8	4.5	19.82
113.27	6.44	17.58	14.3	6.6	18.37
141.58	6.44	21.98	16.3	8.7	23.22

Table 2.4: Absorption results using new MEA

Rotor speed (RPM)	Gas flow (m^3/hr)	Liquor Rate (L/min)	CO_2 in gas (%)		Absorption (kg/hr)
			In	Out	
2300	116.1	5.68	14.8	2.2	29.49
2300	209.54	5.68	14.8	4.9	43.55
2690	209.54	5.45	14.8	4.9	43.55
2690	339.80	5.68	13.6	7.2	49.45
2690	339.80	9.85	12.8	4.3	60.79
2690	396.44	11.36	14.8	5.6	78.03
2690	396.44	11.36	14.7	5.7	76.67
2690	481.39	17.05	10.2	1.3	85.29
2690	538.02	17.05	10.8	2.0	95.27
2690	566.34	17.05	12.0	2.0	114.33

(Pillo and Dahlbeck, 1960) scrubbed H_2S from coke oven gas using liquid ammonia. High efficiency was achieved by carrying out ideal counter-current washing. It was shown that the unit has lower residence time.

(Vivian et al., 1965) studied the effect of centrifugal acceleration on carbon dioxide desorption from water in a packed column mounted on a large centrifuge. The column is 6 in. ID, 1 ft high and filled with ¾ in. rasching rings. The total body force ratio of the centrifugal field to the gravity used ($r\omega^2/g$) was varied between 1-6.4. They reported that for desorption of carbon dioxide from water into air, the liquid side mass-transfer coefficient varied with centrifugal acceleration as follows:

$$K_L a \alpha \left(\frac{r\omega^2}{g}\right)^p \qquad (2.55)$$

$$0.41 \leq p \leq 0.48$$

In comparison, the correlation for mass transfer coefficient in a short wetted-wall column by Vivian and Peaceman (1956) is:

$$\frac{K_L h}{D} = 0.443 \left(\frac{4\Gamma}{\mu}\right)^{0.4} (N_{Sc})^{1/2} (gh^3\rho^2/\mu^2)^{1/6} \qquad (2.56)$$

The gravity term in the centrifuge has higher power exponent (0.41-0.48) than the gravity term in the short wetted-wall column (1/6). (Vivian et al., 1965) attributed the increase to the higher interfacial area with increasing body force due to centrifugal forces. Also, it was shown the effect of gravity upon the liquid mass transfer coefficient for different liquid flowrates.

(Podlbieiniak, 1966) invented a rotational vapour liquid contactor (deodorizer) for stripping out odour and flavour substances from triglyceride oil using steam. The machine worked well for removing low amount of impurities (0.1-0.2%) from triglyceride oil. The advantages of the machine were: short contact time between phases, reduction in oil loss due to entrainment, more efficient contact between phases and a reduction in the loss due to hydrolysis because of low residence time. Figure 2.12 shows apparatus of centrifugal contactor. The contactor is basically a cylindrical rotor mounted on a shaft. There are contacting elements in the rotor in which the gas and the liquid phases counter-currently mix. The speed of rotation is between 500-1000 RPM. The liquid phase is heated to around 450-500°F before being introduced to the machine. The vessel is kept under vacuum (1-6 mmHg) by connecting the vacuum equipment to steam outlet.

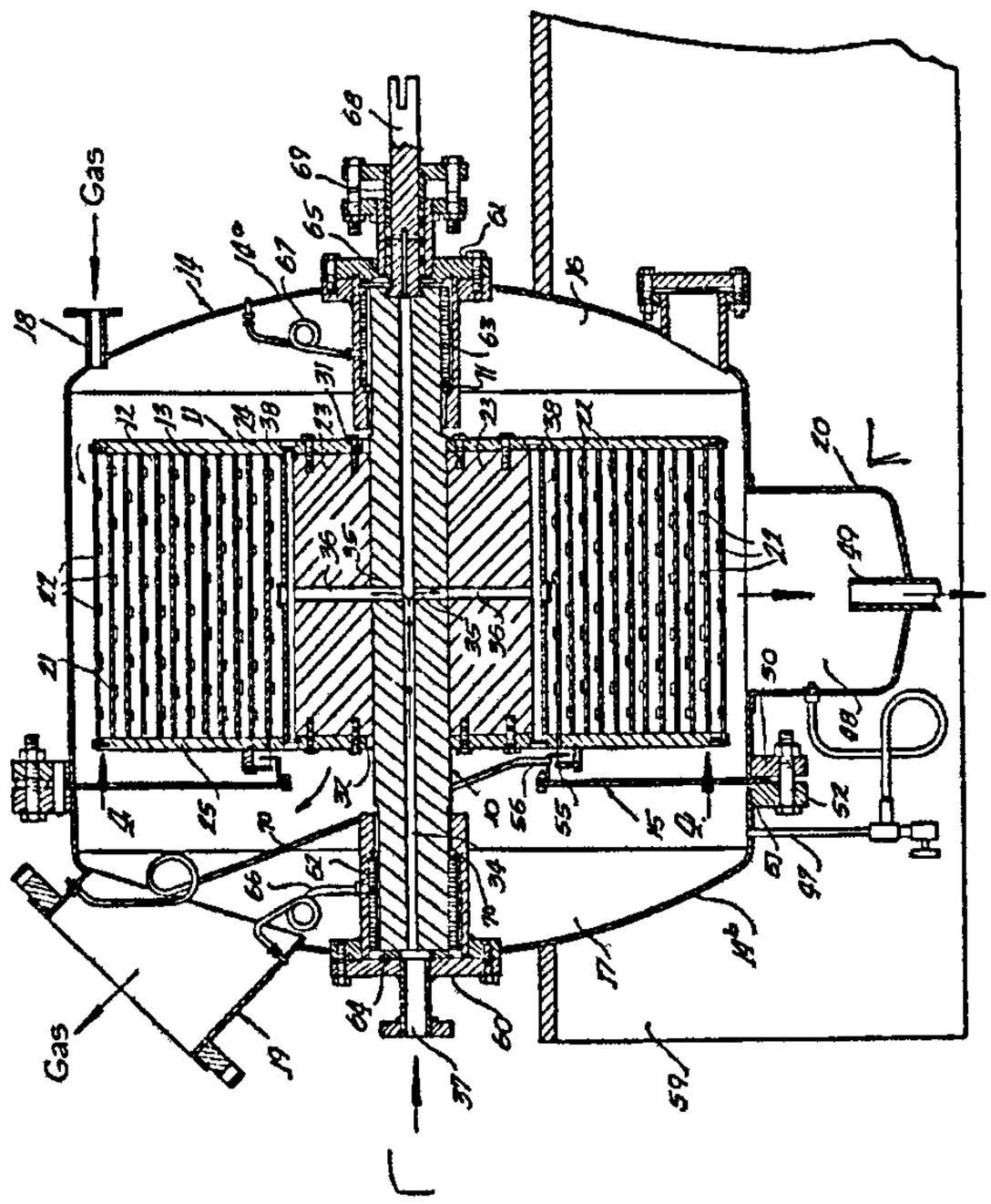

Figure 2.12: Podlbieiniak's deodrizer.

In a new milestone, in late 1970s, ICI patented the Higee concept (Mallinson and Ramshaw, 1982, Ramshaw and Mallinson, 1981). The Higee machine was constructed using a doughnut-shaped rotor, which is mounted on a shaft, and filled with high specific area packing. Liquid enters through the eye of the machine and flows outwardly throughout the packing whereas the vapour enters from the periphery of the casing and inwardly thus a counter-current mass transfer takes place. (Ramshaw and Mallinson, 1981) showed that both the gas and the liquid film controlled mass transfer coefficients for water-oxygen system and ethanol-methanol system respectively, increase substantially in comparison to a stationary column as shown in Table 2.5 and Table 2.6.

Table 2.5: Mass Transfer Coefficients for Gas Film Control Process

Permeable Element	Rotation Speed (RPM)	Mean Acceleration (m/s^2)	$K_G * 10^8$ (m/s)	$\frac{K_G a}{(K_G a)_{grav}}$
Glass Beads	1000	760	3.94	4
	1750	2354	4.83	5
Stainless Steel Gauze	1000	760	10.8	8
	1750	2354	12.69	9

Table 2.6: Mass Transfer Coefficients for Liquid Film Control Process

Permeable Element	Water Flow rate * 10^5 m^3/s	Rotational Speed (RPM)	Mean Acceleration (m/s^2)	$K_L * 10^5$ m/s	$\frac{K_L a}{(K_L a)_{grav}}$
1 mm Glass Beadsd	3	1250	1197	21.2	37
	3	1500	1727	24.9	42
	5	1500	1727	20.3	41
	5	1750	2354	21.7	44
Copper Gauze	4	1500	1727	19.4	27
	4	1750	2354	20.6	28
	6	1500	1727	26.7	29
	6	1750	2354	31.5	34

The mean acceleration, a_m, was defined by:

$$a_m = \left(2\pi \frac{N}{60}\right)^2 \left(\frac{r_o + r_i}{2}\right)^{1/2} \tag{2.57}$$

where N is the rotation speed per minute (RPM), r_o and r_i are the outer and inner radii of the packed bed respectively.

(Tung and Mah, 1985) showed that the penetration theory was capable of describing the liquid mass transfer behaviour in the Higee machines. It was found that the mass transfer coefficient predicted by the penetration theorem was as accurate as the experimental data. The following set of equations was developed to calculate the mass transfer coefficient based upon the following assumptions: complete mixing of liquid at the junctions of packing materials, falling film and negligible shear.

$$K_L = \sqrt{\frac{4D}{\pi t}} \tag{2.58}$$

$$t = \frac{\pi d_p}{2v} \tag{2.59}$$

$$v = \left(\frac{\rho g \delta^2}{3\mu}\right) = \left(\frac{9 g \Gamma^2}{8 \mu \rho}\right)^{1/3} \tag{2.60}$$

$$\Gamma = \frac{\delta^2 g \rho}{2\mu} \tag{2.61}$$

$$Sh = \frac{K_L d_p}{D} = 0.919\left(\frac{a_p}{a_e}\right)^{1/3} Sc^{1/2} Re^{2/3} Gr^{-1/6} \tag{2.62}$$

(Bucklin et al., 1988) investigated the application of Higee in H_2S removal with MDEA. The loading of acid gas was unexpectedly high. There was 25% error in accuracy of analysis due to use of dry chemical analysis and that influenced the calculations of mass balances. Also, higher circulation of amine and increase in thickness of packing was not possible due to flooding of rotor.

(Keyvani and Gardner, 1989) investigated the operating characteristics of RPB and published a model for the pressure drop characteristics of RPB, residence time distribution, and power required by RPB using air-CO_2-H_2O system. It was shown that contrary to conventional columns, the pressure drop for dry and wet beds at constant liquid and gas flowrates was $\Delta P \alpha \omega^2$. The packing in use was aluminium foam metal with a 92% porosity and has a specific surface area of 600-300 m^2/m^3.

The speed of the rotor was 500-2000 rpm (60-1000g). Average HTU achieved was 1.4-4.0 cm.

(Al-Shaban et al., 1992) showed using hydrodynamics studies on a large centrifugal water deoxygenator (1 m diameter) the existence of a non-uniformity bubble distribution throughout the radial length of the rotor. It was shown that the potential savings on the offshore installations besides reduction in space and weight.

(Singh et al., 1992) stripped efficiently VOCs from ground water using centrifugal liquid contactor (Figure 2.13). Their flooding curve underestimated the classical Sherwood flooding correlation curve. The mass transfer data was presented using the area of transfer unit (ATU) as shown in Equation 2.63 and 2.64. Equation 2.65 correlates geometry of gas-liquid contactor and mass transfer:

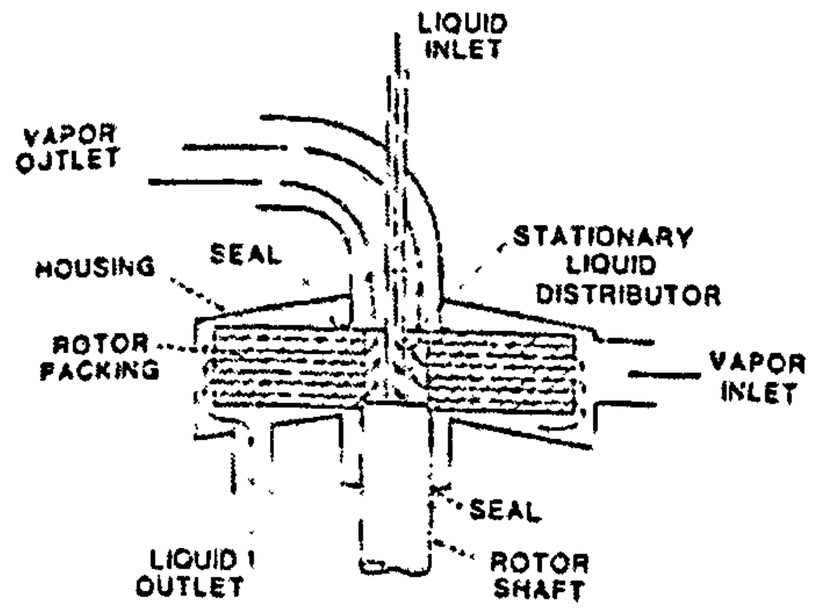

Figure 2.13: Singh's stripper

$$ATU=\left(\frac{34000}{a_t^{\,2}}\right)\left(\frac{L'}{\mu_L a_t}\right)^{0.6}\left(\frac{\rho_L^{\,2} g}{\mu_L^{\,2} a_t^{\,3}}\right)^{-0.15} \tag{2.63}$$

$$ATU=\frac{Q}{l\,K_L a} \tag{2.64}$$

$$ATU\frac{\ln\left[\left[\frac{X_1-Y_2/H}{X_2-Y_2/H}\right]\left(1-1/S\right)+\left(1/S\right)\right]}{\left(1-1/S\right)}=\pi\left(r_o^{\,2}-r_i^{\,2}\right) \tag{2.65}$$

(Liu et al., 1996) investigated the pressure drop dependency on the flowrates of the liquid and gas besides the influence of rotor speed. The gas film mass transfer coefficient for stripping ethanol solution using air was influenced by gas and liquid flowrates as well as by the rotor speed. They developed a correlation that predicts the overall gas-film mass transfer coefficient for RPB and his experimental data were within ± 30% of the calculated values.

$$\frac{K_G\, a\, RT}{D_G\, a_t^{\,2}} = 3.111*10^{-3} Re_{Ga}^{\,1.163} Re_{La}^{\,0.631} Gr_G^{\,0.25} \qquad (2.66)$$

The design equation for gas mass transfer is:

$$\frac{G_m}{z\, K_G\, a\, p_t} \frac{\ln\left[(1-S)\dfrac{Y_1 - H_c X_2}{Y_2 - H_c X_2} + S\right]}{\left(1 - 1/S\right)} \pi\left(r_2^{\,2} - r_1^{\,2}\right) \qquad (2.67)$$

$$\text{Where } ATU_G = \frac{G_m}{z\, K_G\, a\, p_t} \qquad (2.68)$$

(Kelleher and Fair, 1996) studied the distillation of cyclohexane/n-heptane in a Higee contactor. The mass transfer efficiency, pressure drop, and hydraulic capacity were modelled and investigated. The design of RPB was based upon ATU concept because Higee is in a polar coordinate system. Equation (2.69) shows the design equation:

$$\pi\,(r_o^{\,2} - r_i^{\,2}) = (ATU)\,(NTU) \qquad (2.69)$$

where the ATU term was defined as follows:

$$ATU_L = \frac{L}{\rho_L\, h\, K_L\, a_e} \qquad (2.70)$$

$$ATU_G = \frac{L}{\rho_G\, h\, K_G\, a_e} \qquad (2.71)$$

(Burns and Ramshaw, 1996) showed by a visual study that the type of liquid flow in RPB is determined by centrifugal acceleration. The maximum speed of the rotor was 1620 RPM, and with a declon packing which has a porosity of 0.95 and a surface area of 1500 m^2/m^3. At low rotational speeds (300-600 RPM) the liquid travelled in rivulets then changed to droplet flow at higher rotational speed (600-800 RPM). The rivulet flow lead to the highest maldistribution of the liquid and the gas within the packing; while the droplet flow increased the wetting of the packed bed.

(Zhenh et al., 1997) applied the Higee technology for water deaeration. Two Higee machines were manufactured in order to reduce the oxygen content of water from 6-14 ppm to less than 50 ppb using natural gas as the stripping medium. Table 2.7 compares the Higee technology with the conventional vacuum tower. It is apparent

that the weight, height, and the quality of mass transfer operation favour the new technology especially in offshore operations.

Table 2.7: Comparison between the Higee technology and a conventional vacuum tower in water deaeration (Zhenh et al., 1997).

	Vacuum Tower	Higee Technology
Number of units	1	2
Capacity (T/d)	10,000	2 x 6,000
Platform Area (m^2)	30	2 x 10
Height (m)	14	3
Weight (T)	60 (dry) 130 (operation) 180 (full of water)	2 x 10 2 x 10.5 2 x 11
Residual O_2 in water (ppm)	1 (Summer) 2-3 (Winter)	< 0.05 < 0.05
Power (kW)	155	2 * 160

(Waldie and Harris, 1998) investigated the performance of the high intensity contactor in stripping dissolved aromatics from water. The machine was not mechanically rotating (like Higee); instead the centrifugal force was generated by injecting the liquid phase tangentially into a permeable tube through which the gas flows counter-currently. It was found that the volumetric mass transfer coefficient, K_{La}, was hundreds times more and has lower H_{OL} in comparison to the conventional packed column.

$$\text{Number of transfer units, } N_{OL} = \frac{\log\left[\frac{x_2}{x_1}\left(1-\frac{1}{S}\right)+\frac{1}{S}\right]}{1-\frac{1}{S}} \qquad (2.72)$$

Where the stripping factor is, $S = \frac{HG_m}{PL_m}$ (2.73)

(Trent et al., 1999) developed a commercial RPB as a reactive stripper for the production of HOCl. The unit had a product yield greater than 90%. The overall gas-side mass transfer coefficient was 40-60 s^{-1}.

(Sanilya et al., 2001) investigated the gas the phase mass transfer operation using a centrifugal contactor with wire-gauze packing (porosity 0.91 and specific surface area 2196 m^2/m^3). The gas phase mass transfer coefficient in the RPB was lower than its value in the packed column due to maldistribution of the liquid. Figure 2.14 shows their experimental unit. Equation 2.74 determines the average volumetric mass transfer coefficient:

$$k_g a_e = \frac{Q_g}{\pi a} \frac{\ln\left(c_c / c_o\right)}{\left(r_o^2 - r_i^2\right)} \quad (2.74)$$

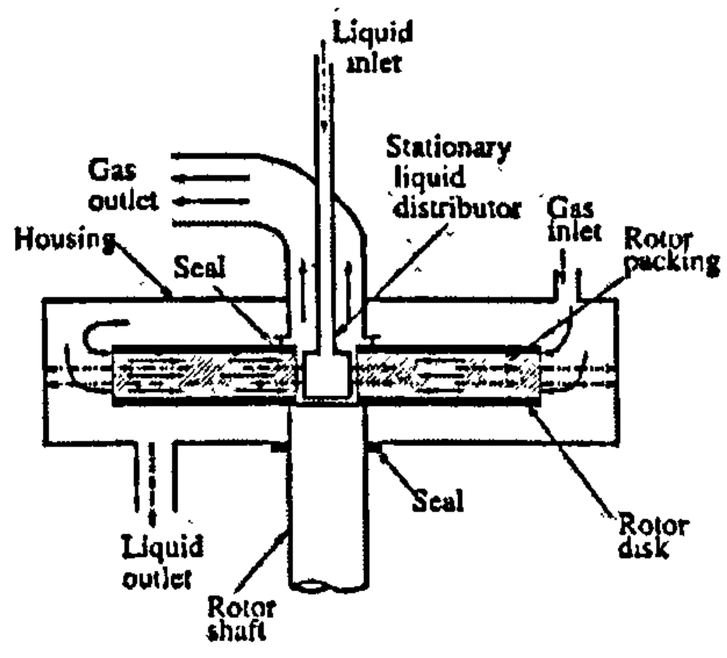

Figure 2.14: Sanilya's centrifugal contactor.

2.4.3 Packed Bed Design

2.4.3.1 Mass Transfer Equations in RPB

Figure 2.15 shows a schematic diagram of the RPB. The solute mass balance on a differential volume on the gas is presented in Equation (2.75):

$$\{\text{Solute accumulation}\} = \{\text{Solute flow in minus out}\} - \{\text{Solute lost by absorption}\}$$

There is no solute accumulation, thus:

$$\{\text{Solute flow in minus out}\} = \{\text{Solute lost by absorption}\} \quad (2.76)$$

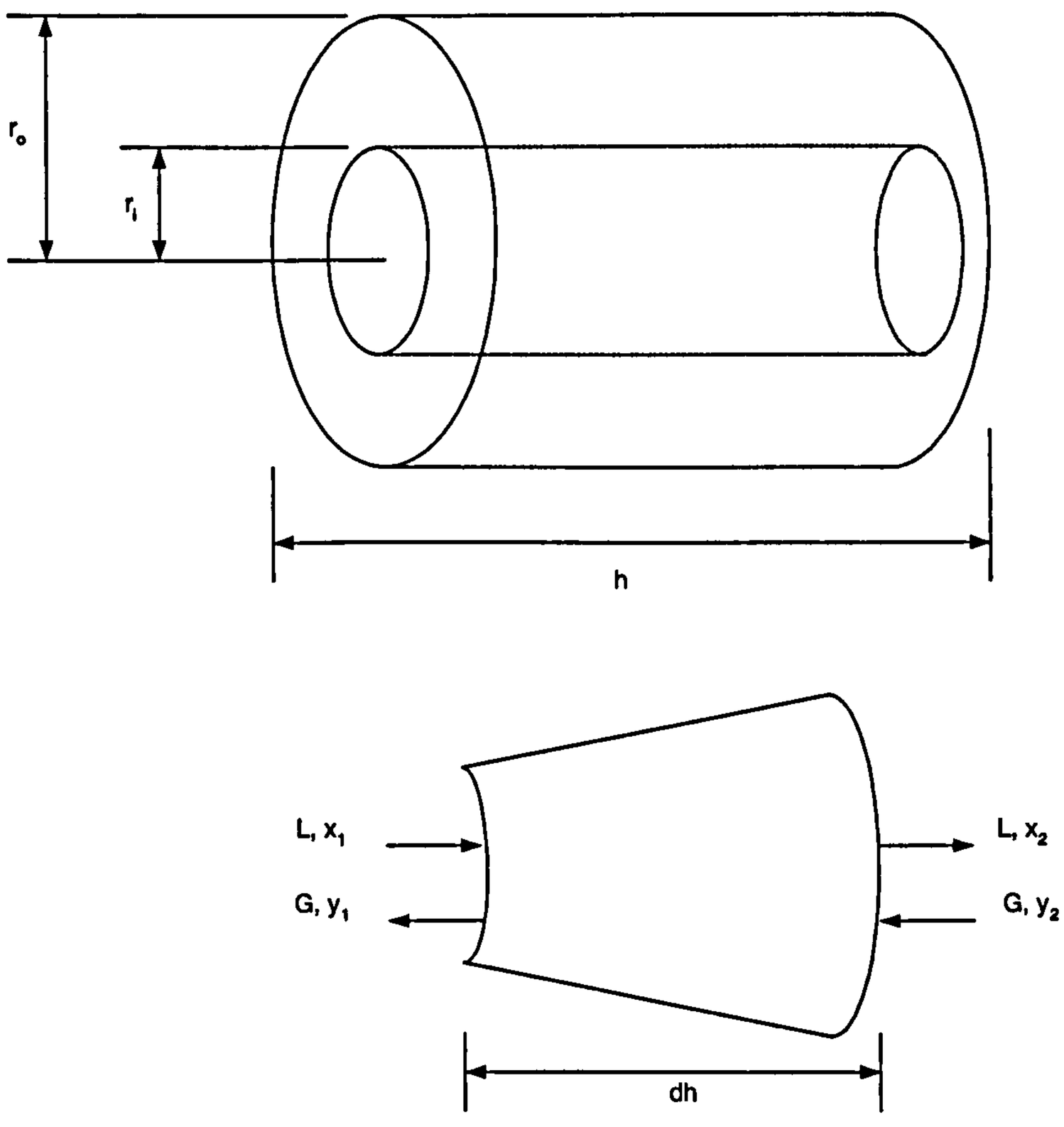

Figure 2.15: A section of counter-current mass transfer in RPB

The cross section area of RPB is:

$$S = 2\pi (r_o - r_i) = 2\pi\, dr \quad (2.77)$$

Thus, the differential volume is,

$$dV = 2\pi\, r\, h\, dr \quad (2.78)$$

The amount of carbon dioxide in the air/CO_2 mixture passes the differential volume of RPB is G moles/area^2.hr and therefore the rate of mass transfer of gas to the liquid is:

$$d(Q_G y) = K_G a (y - y^*) dV \qquad (2.79)$$

where a is the interfacial area per unit volume of packing section and dV is the differential volume of packing. Integrating the above equation and rearranging for the volume of bed:

$$V = \frac{Q_G}{K_G\, a} \int_{y_1}^{y_2} \frac{dy}{y - y^*} \qquad (2.80)$$

It can be expressed in terms of the height of the bed as follows:

$$H = \frac{Q_G}{A\, K_G\, a} \int_{y_1}^{y_2} \frac{dy}{y - y^*} \qquad (2.81)$$

Or in a more familiar way:

$$H = \frac{G}{\rho\, K_G\, a} \int_{y_1}^{y_2} \frac{dy}{y - y^*} \qquad (2.82)$$

Where A is the cross sectional area. The integral part is known as the Number of Transfer Units (NTU) and the terms (Q_G/A K_G a) or (G / ρ K_G a) represents the Height of a Transfer Unit (HTU).

The total height of a packed bed can be found from the following equation:

$$H = HTU * NTU \qquad (2.83)$$

The packed height is substituted with the radial depth (R_o-R_i). Therefore, the number of transfer units can be expressed as follows:

$$NTU = \frac{R_o - R_i}{HTU} \qquad (2.84)$$

where R_o and R_i are the outside and the inside radii of the bed.

CHAPTER 3

EXPERIMENTAL FACILITY

3.1 Objective of the Experiments

The objective of this chapter is to provide a detailed description of the design of the experimental facility. It is used to gather both flooding and gas-liquid mass transfer data for carbon dioxide/ethanolamine solution system. Flooding behaviour of ethanolamine solution is determined visually. There are two different mass transfer modes of operation for this prototype: absorption of carbon dioxide from air/CO_2 mixture by different concentrations (30, 50, 80, 100 wt%) of ethanolamine solution; and desorption of carbon dioxide from ethanolamine solution by steam or air.

The following sections describe rig flowsheet, mechanical details of the RPB, Air/CO_2 system, steam delivery system, and outlines the sampling procedures for both gaseous and liquid streams.

3.2 Flowsheet of the Rig

Figure 3.1 shows the flowsheet of the experimental facility. Ethanolamine solution is stored under a nitrogen blanket in the polypropylene feed tank (420 L). The feed tank is usually 60-70% full and it is equipped with a level indicator. A three-way valve configuration allows the feedstock to be routed into three directions. Firstly, route **A** allows the feedstock to be continuously recycled back to the feed tank in order to have a homogenous solution batch or it could be applied to route the product batch back to the feed tank after finishing an experimental run. Secondly, path **B** allows the homogeneous feedstock to be routed to a closed circuit heating system in order to raise its temperature. Finally, path **C** allows the prepared ethanolamine solution to be pumped to the Higee rig. There are two polypropylene diaphragm valves (George Fischer, Type 315) prior to flowmeters (35 SX, and 65P) to control manually the amount of irrigation rate to the Higee rig. The calibration charts of both the flowmeters are shown in Appendix B. The flameproof magnetic drive centrifugal pump (Totton Pumps Limited) has a flowrate of 380 L/min, 23 m head, and it is made from PVDF. All the pipelines are made from polypropylene except two stainless steel

pipelines extended from the Higee rig to the product tank in order to tolerate hot and corrosive ethanolamine solution during the desorption runs. The Higee rig is inside a flameproof enclosure, which is equipped with a ventilation system.

The gas phase could either be CO_2/air mixture or steam depending on the mode of the operation. The liquid product is routed to product tank via two stainless steel (42 mm OD) pipes. Stainless steel is used because during the stripping operation the temperature can exceed 100°C. The product gas is ventilated to the atmosphere via an exhaust fan.

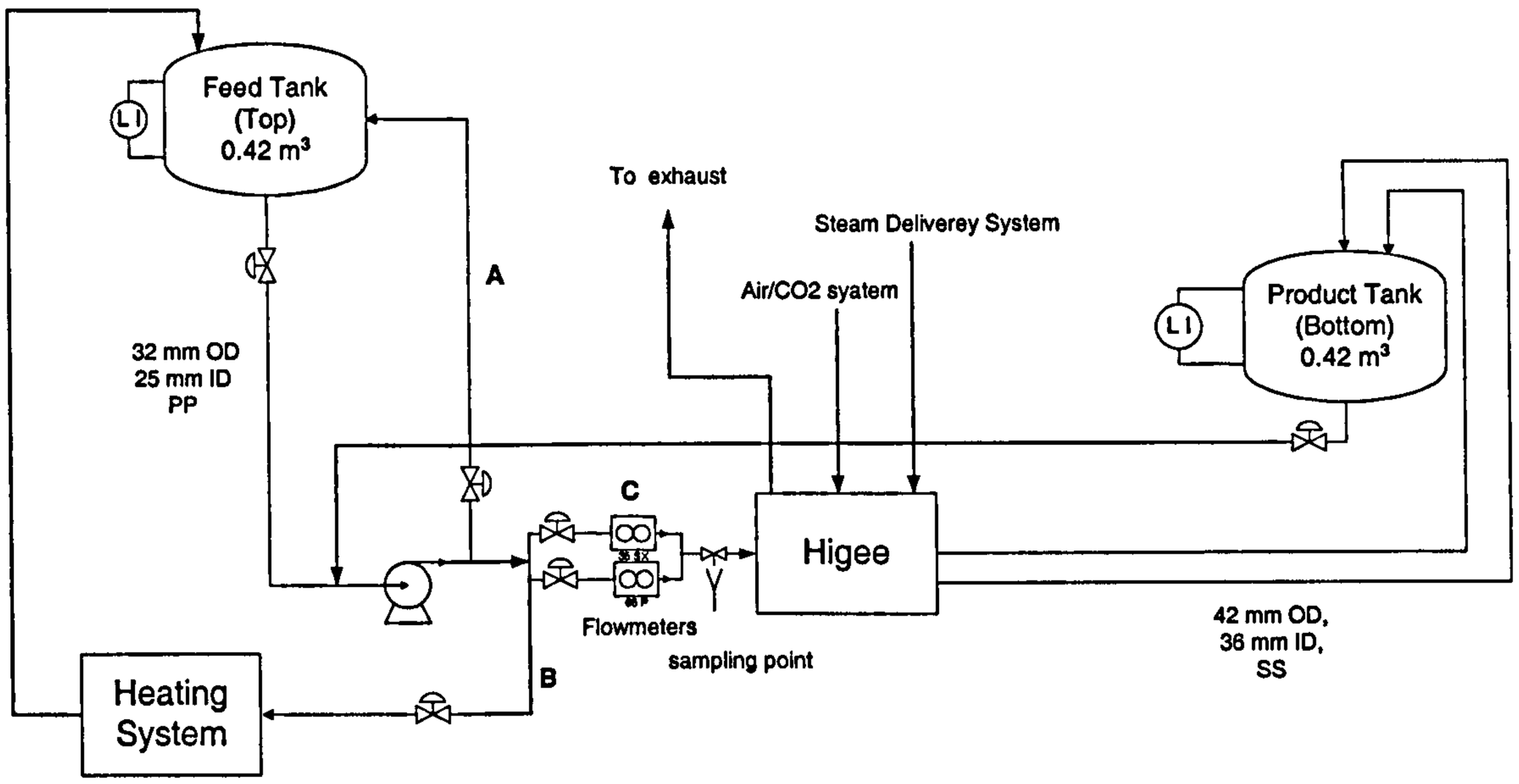

Figure 3.1: Flowsheet of experimental facility

3.3 Material of Construction

Due to the corrosive nature of loaded ethanolamine solution, it was decided to use only stainless steel and polypropylene as the material of construction for the rig. The rotor is entirely made from stainless steel whereas the piping and the storage tanks are made from polypropylene. In addition, the liquid sample tubing is made from stainless steel to avoid contamination of the ethanolamine sample.

There are many sources in the literature that highlights the importance of the material of construction selection for amine application. (Hawkes and Mago, 1971) indicated that the ethanolamine solution is not corrosive to steel but becomes corrosive when loaded with acidic gas.

(Wong et al., 1985) highlighted factors that contributes to the corrosiveness of ethanolamine solution such as: type of amine, amine concentration, acid gas loading, elevated temperature, acid gas flashing from solution, solution degradation products, and heat-stable salts. However, the two most important factors are: amine concentration and acid gas loading.

(Dingman et al., 1966) recommended alternative ways to minimize the corrosion in MEA units. They recommended MEA solution strength of 15wt% as a design basis because of its lower corrosion rate and greater processing flexibility. The maximum total recommended acid gas loading for rich MEA solution is 0.35 mol CO_2/mol MEA as shown in Figure 3.3 and the maximum lean loading is 0.1-0.15. Furthermore, it was recommended to apply less stripper pressure in order to minimize the temperature of regeneration that could degrade the solution as shown in Figure 3.2.

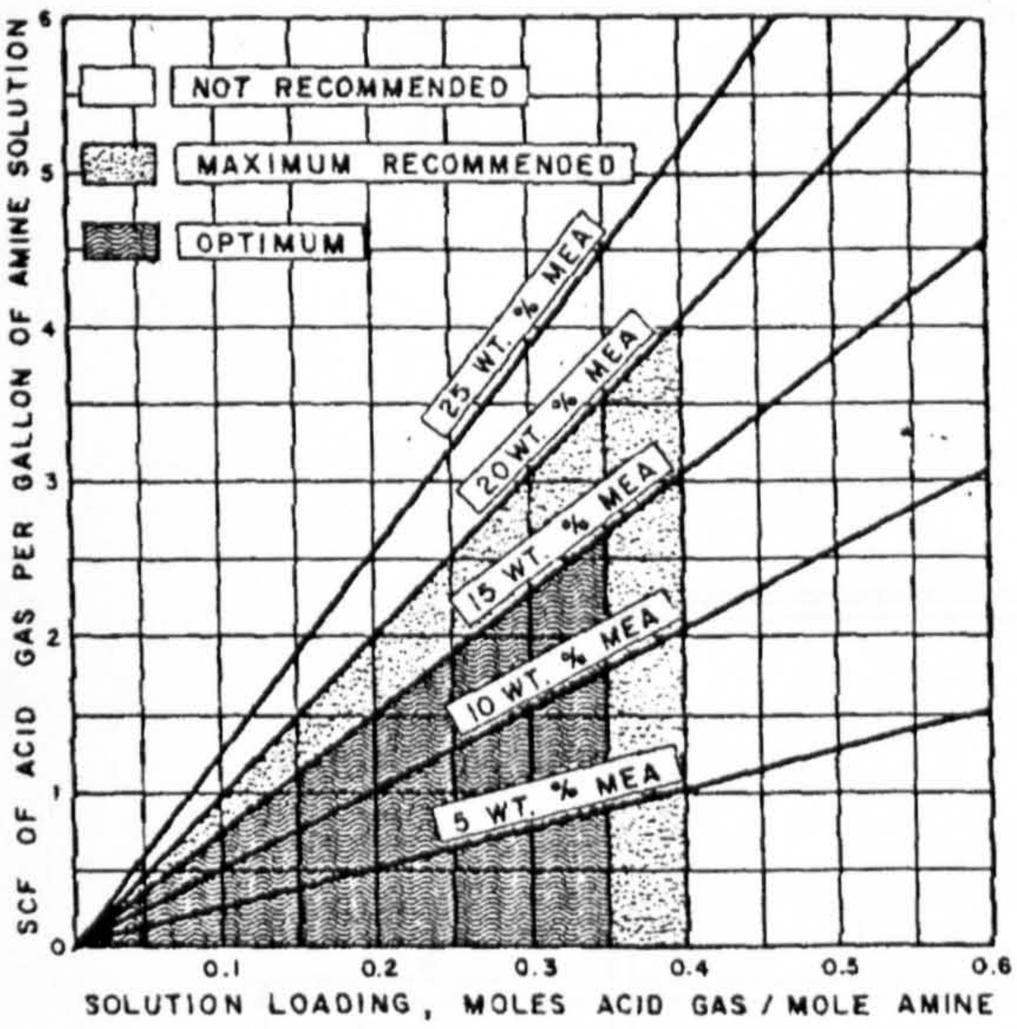

Figure 3.3: Optimum and recommended amine strength.

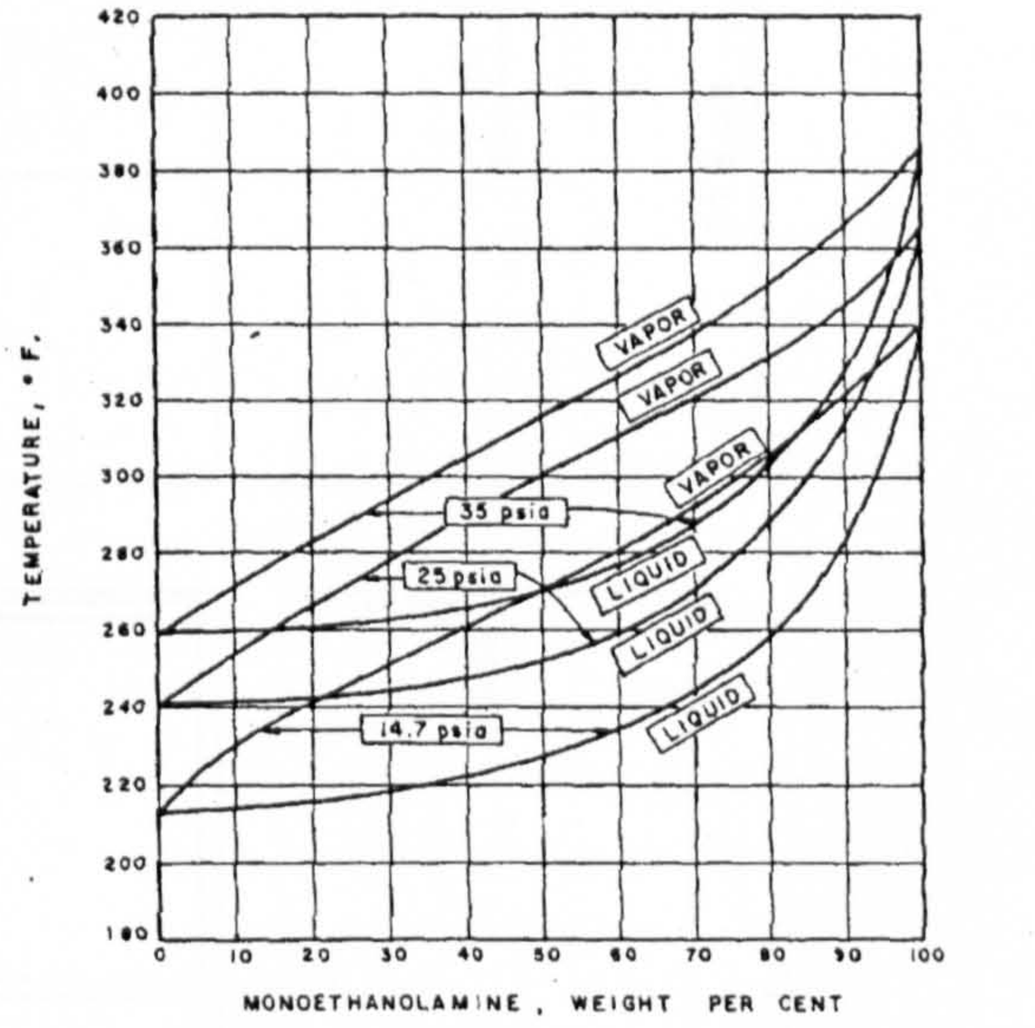

Figure 3.2: Phase equilibrium data for MEA solutions.

(DuPart et al., 1993b) advised the use of stainless steel rather than carbon steel because the corrosion rate for stainless steel is <0.1 mm. per year whereas it is 103.0 mm. for carbon steel when experiments were conducted to absorb carbon dioxide using 20wt% MEA solution at 115°C. Furthermore, it was pointed out that the potential of acid gas flashing is higher for stronger amine concentrations because they can not achieve high mol/mol equilibrium rich loadings as the lower strength amines.

3.4 Rig Support Frame

Figure 3.4 shows the mechanical details of the Higee support frame. The frame was sufficiently rigid to withstand any out of balance forces during rotor operation for upto speed of 1000 RPM. The upper part holds a RPB, a buffer tank and a motor. The lower part is kept for holding the inlet gas-sampling vessel. The structure is made from mild steel and it is painted in order to avoid corrosion in the case of ethanolamine spillage. In addition, the height of structure allows the RPB to be visually inspected during the flooding operation.

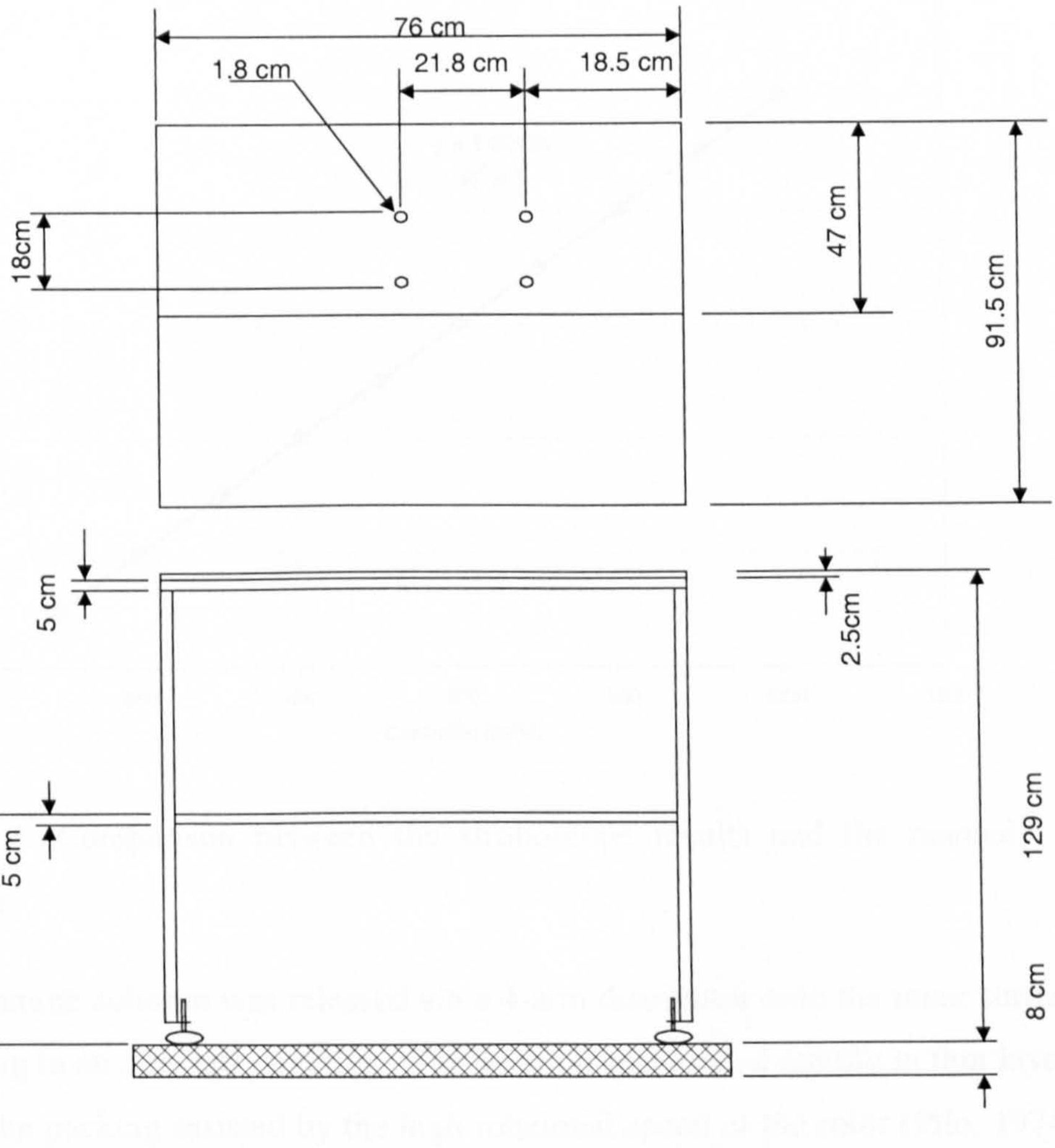

Figure 3.4: The Rig Support Frame

3.5 Rotor

Figure 3.6 shows the cross sectional view of the rotor. A belt connects the stainless steel horizontal shaft to a motor.

The speed of the rotor is varied with a manual controller. A stroboscope was used to calibrate the rotational speed of the bed. The instrument emits flashes on the rotating bed and hence determines the exact number of flashes per minute. Figure 3.5 shows that the stroboscope results were in good agreement with the manual controller.

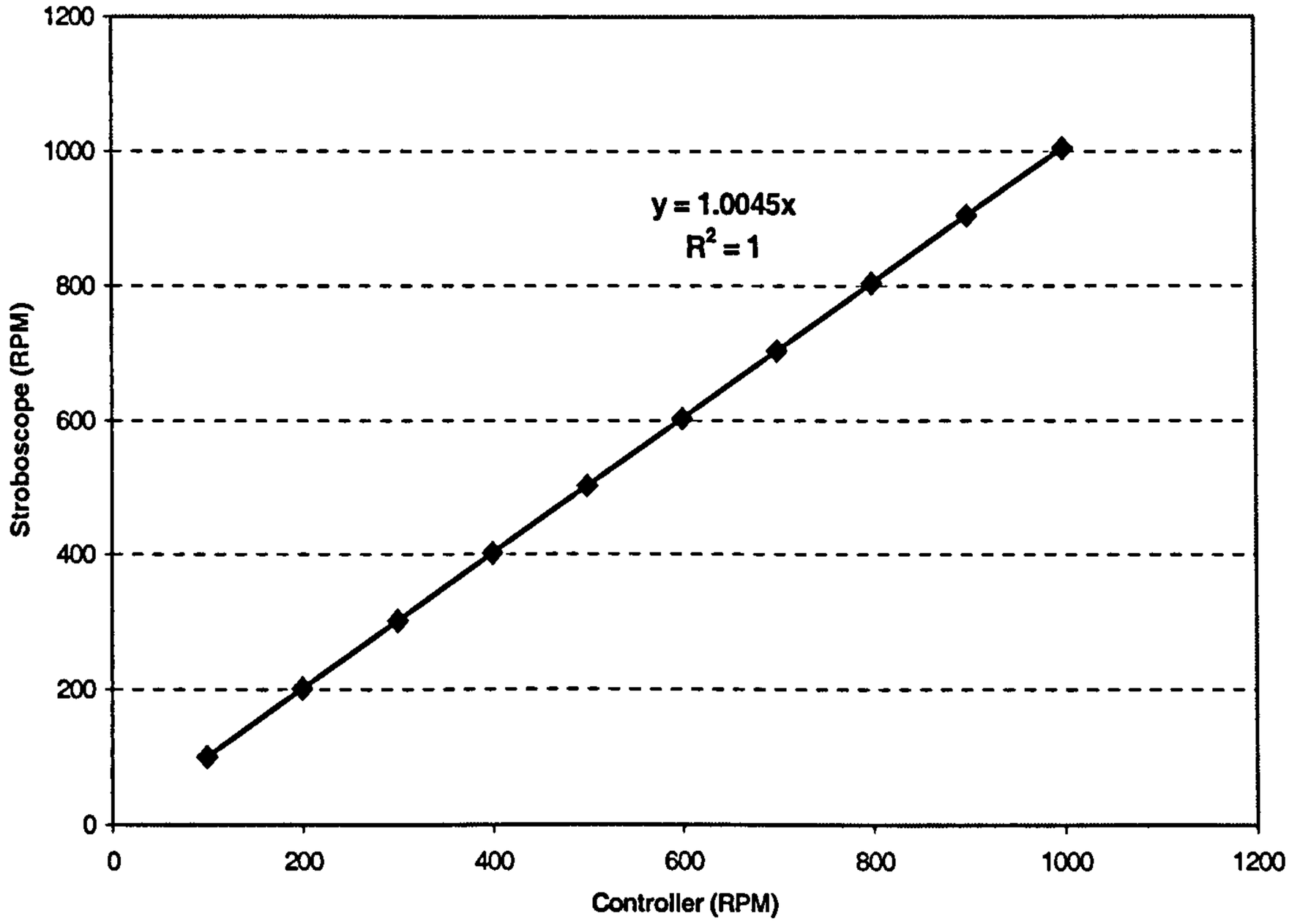

Figure 3.5: Comparison between the stroboscope results and the manual controller.

The ethanolamine solution was released via a 4-arm distributor onto the inner surface of the packing in an outward direction. The solution accelerated rapidly in thin layers throughout the packing assisted by the high rotational speed of the rotor (Pilo, 1974). The formation of thin layers enhanced mass transfer due to large surface to volume ratio. According to visual analysis carried out in this department by (Burns and Ramshaw, 1996), the rotational speed of rotor was the main influence on the type of flow in a RPB. The experimental runs were conducted at 600-1000 RPM rotor speed, which implies that the type of the flow in the RPB was droplet flow and hence less maldistribution of the liquid in the RPB and thus better mass transfer operation.

The carbon dioxide/air mixture entered via a rotary union (Deublin, part number 450-191-029) positioned at the end of the horizontal shaft and then passes into the gas plenum chamber before entering 72 holes drilled in the stainless steel disc located on the outer side of packed bed. It then flows inwardly within the packing in a counter-current direction to the flow of the ethanolamine solution. The flow of carbon dioxide/air mixture was turbulent prior to reaching the Higee rig in order to ensure better mixing between the gas and the liquid inside the packed bed.

In the desorption runs, all the components of the absorption experiments remained the same with the exception of the rotary union (Deublin, part number: 525-086-026) which must be replaced in order to safely handle the saturated steam.

Details of the rotor are shown in Figure 3.7. The packed bed was sandwiched between the stainless steel disc and the perspex disc. The dimensions of the packed bed are 398 mm OD, 156 mm ID, and an axial depth of 52 mm. The packing material occupies 25 mm of the axial thickness and a 27 mm polypropylene disc spacer occupies the remaining depth. The purpose of reducing the size of the packed bed axial thickness was to increase the flooding velocity of the RPB. Furthermore, it allowed better wetting of the packing by the ethanolamine solution.

Figure 3.8 shows the details of the stainless steel disc. The diameter of disc is 454 mm and there are 72 holes drilled on the circumference in order to allow feed gas to enter from gas plenum. The overall gas flow area passed into the packing is $3.619*10^{-2}$ m^2. On the other hand, the dimensions of the perspex disc are 454 mm OD and 130 mm ID. There are 8 equi-spaced cut-outs of 3mm deep in the perspex disc to allow liquid an exit path. In addition, the perspex was used as a transparent front cover in order to aid the visual observation of the packed bed during operation. Also, the rotor was completely sealed in order that the ethanolamine solution does not come into contact with the outside atmosphere and thus be subjected to degradation. A splash-guard encloses the rotor with its chimney leading to an exhaust fan.

The peripheral liquid lute seal has two functions. Firstly, it allows the ethanolamine solution to discharge from the RPB into the buffer tank. Secondly, it forces the sour gas towards the 'eye' of the RPB. Directing the path of the sour gas towards the 'eye' of the rotor is a simple engineering mechanism, which depends upon the difference in the liquid levels as shown in the magnification of liquid seal in Figure 3.6. The

stainless steel lip allows build up of liquid head, which is higher than the inside head thus forcing the sour gas towards the 'eye' of the rotor.

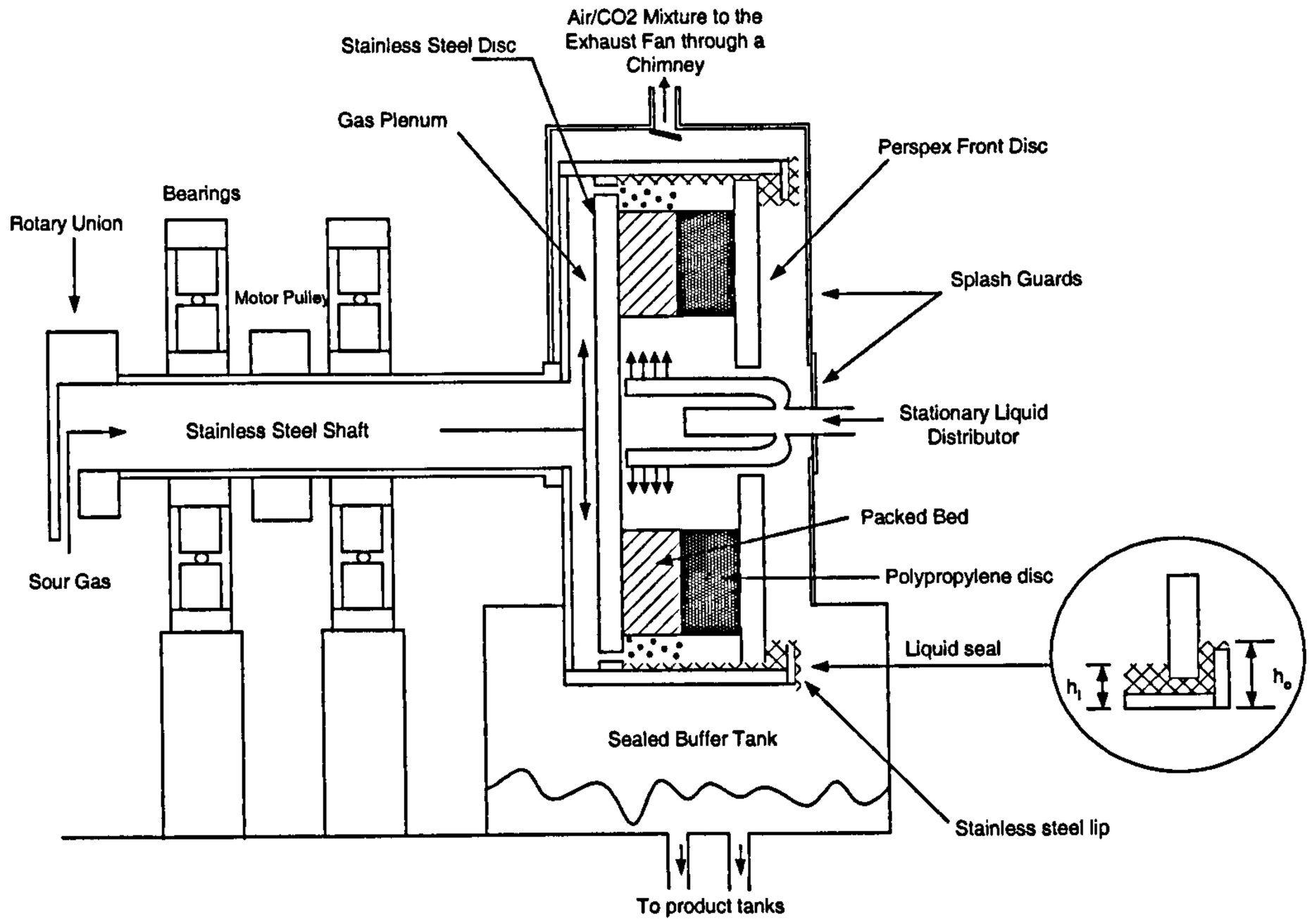

Figure 3.6: Cross sectional view of the Higee rig

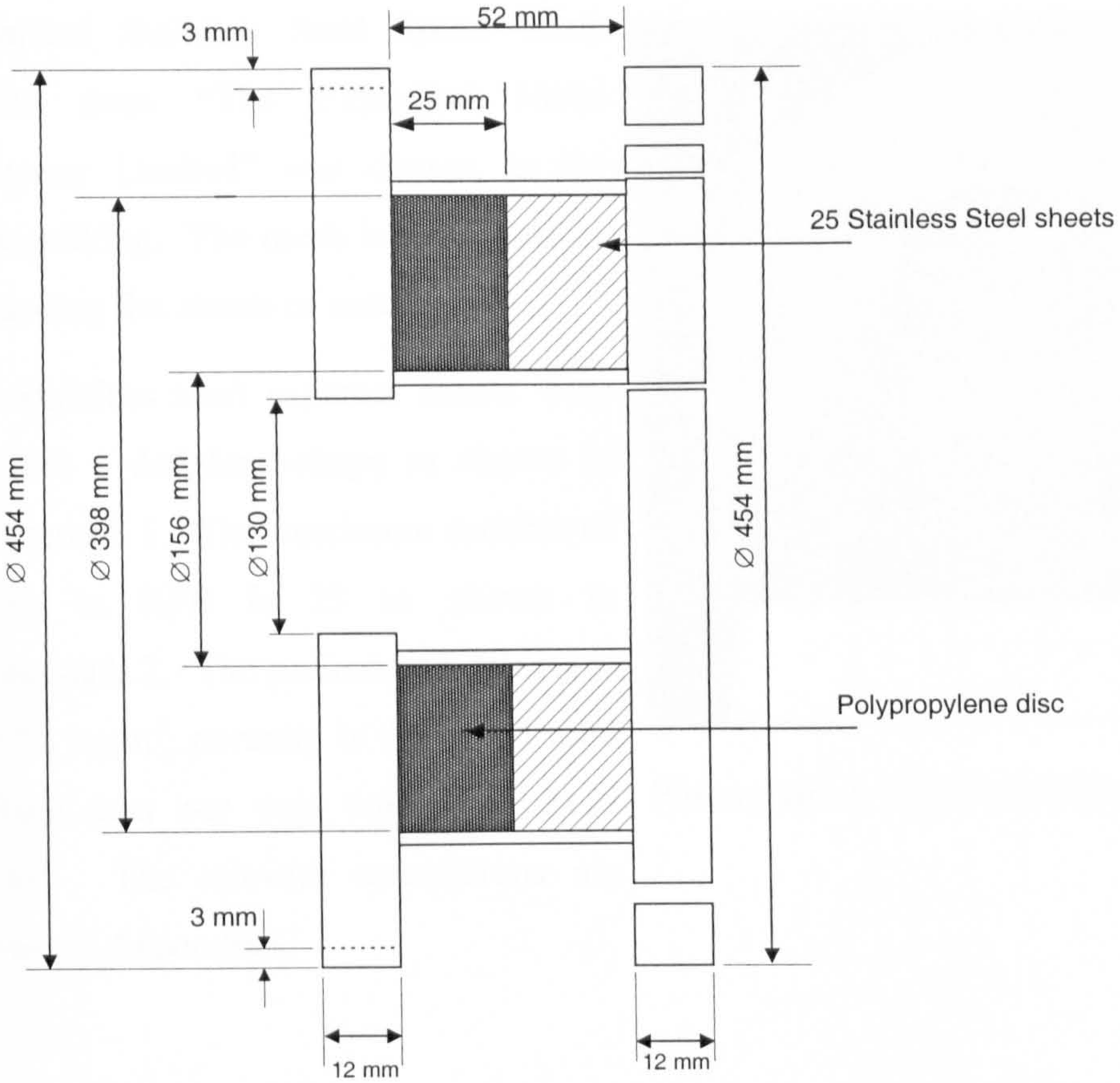

Figure 3.7: Cross sectional view of the rotor

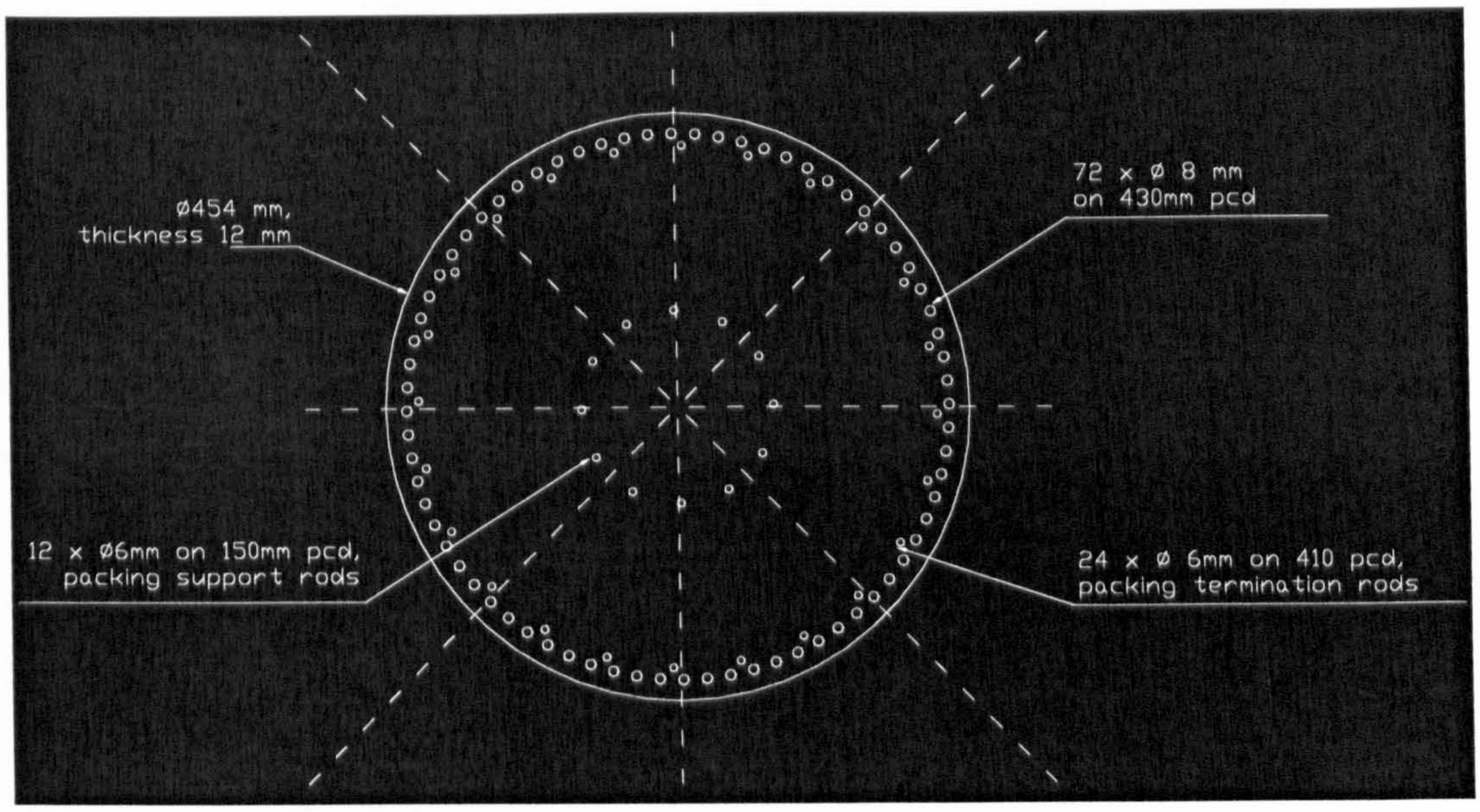

Figure 3.8: Details of the stainless steel disc

3.6 Packing

Expanded Stainless Steel Small Mesh (707S) from "The Expanded Metal Company Limited" was chosen as the rotor packing. The mesh is fabricated by expanding flat sheets of metal.

The stainless steel expamet sheets were cut into a doughnut-shape as shown in Photograph 1. The maximum number of sheets in RPB is 25 as shown in Photograph 2. The packed bed density is 1877.8 kg/m^3, porosity is 0.76, and total surface area per unit volume is 2132 m^2/m^3. The relevant calculations are shown in Appendix C

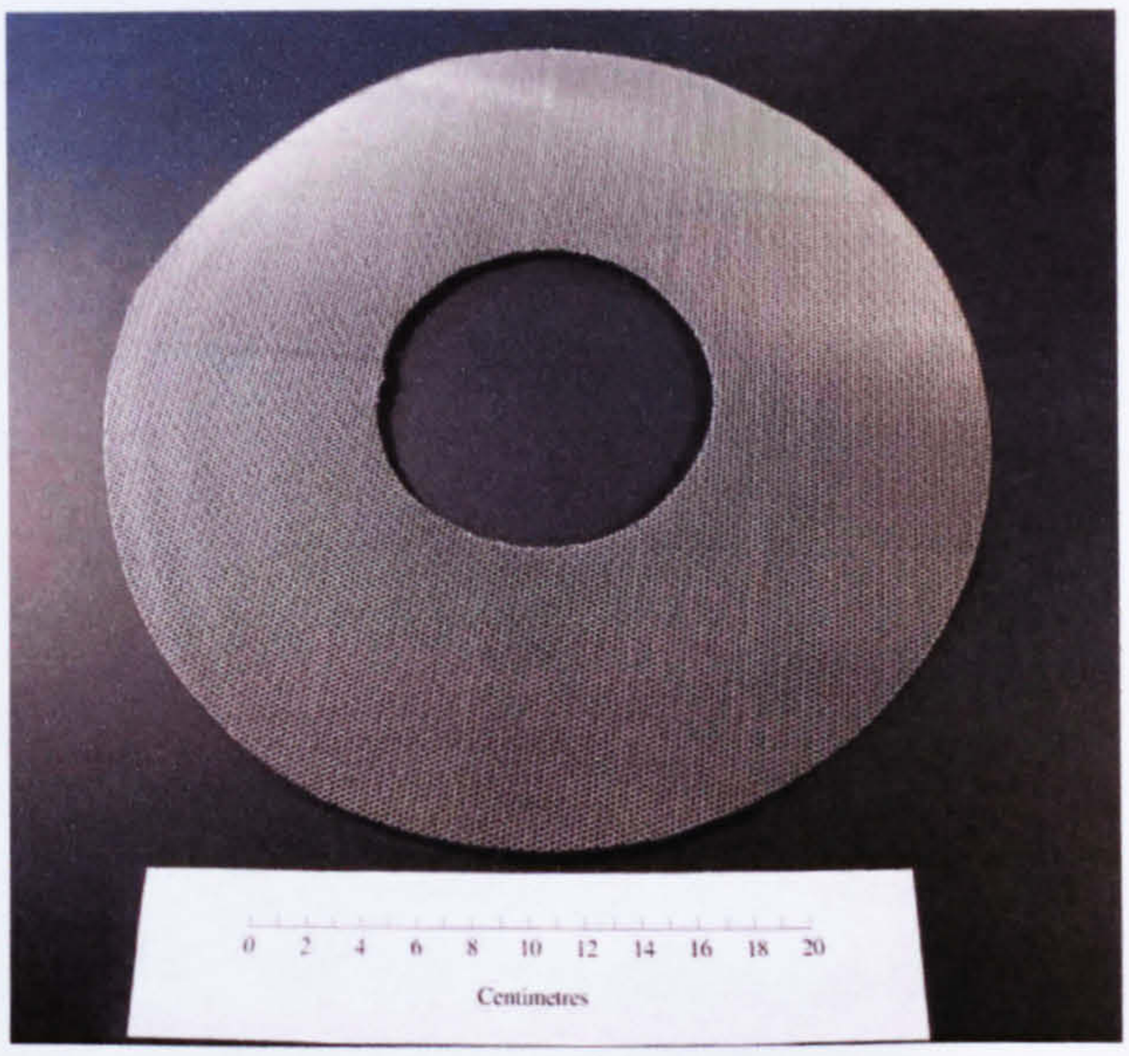

Photograph 1: Doughnut shape of the packing mesh

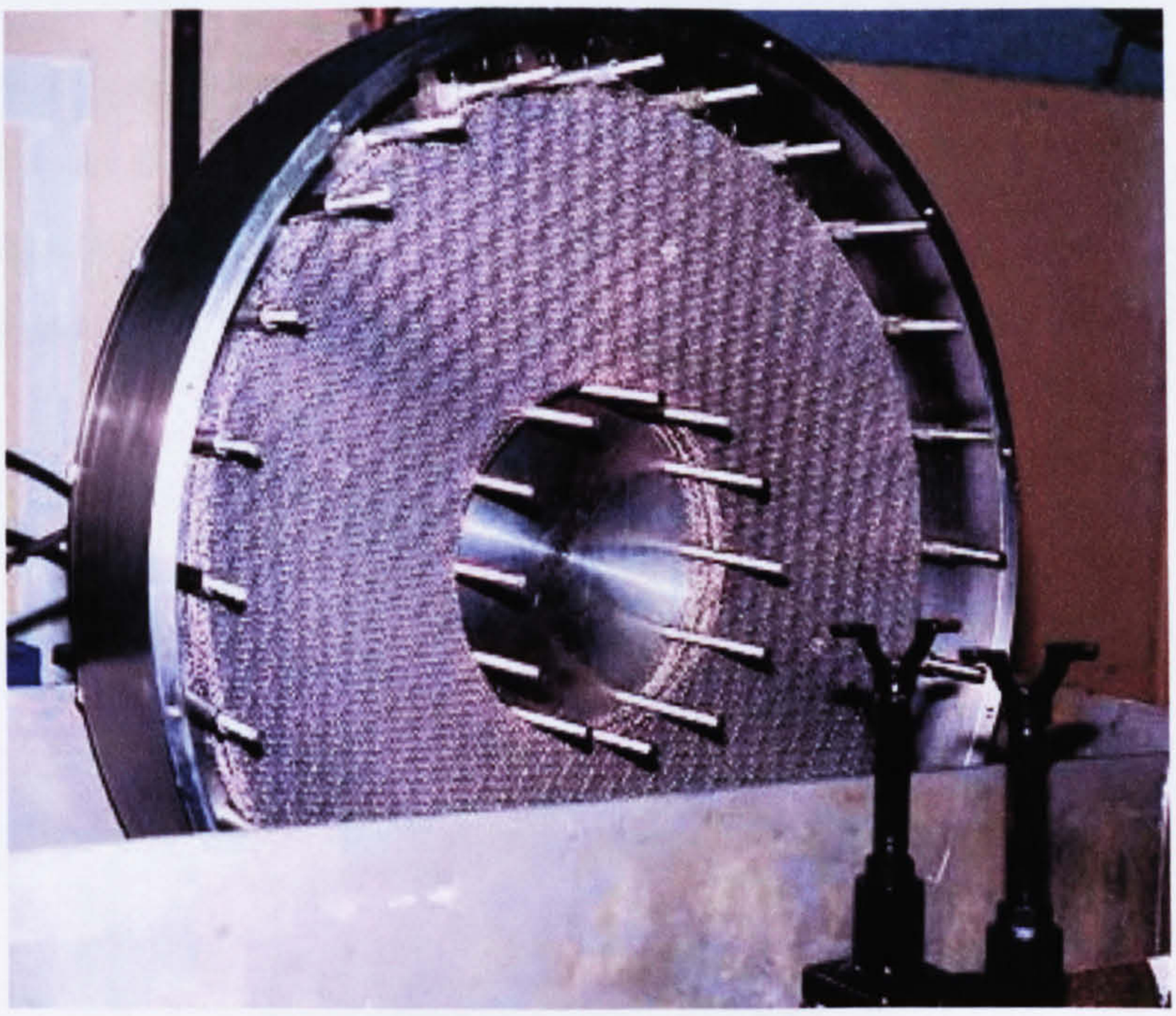

Photograph 2: Stainless steel mesh packed in the rotor

3.7 Liquid Distribution to the RPB

Ethanolamine solution irrigates the RPB using a stationary stainless steel 4-arm distributor as shown in Figure 3.9. There are 8 holes drilled in each arm, each of 2 mm diameter parallel to the radial direction with 45° spacing. The pressure drop across the distributor is 68.24 kPa based upon an ethanolamine solution flowrate of 50 L/min and taking into account *vena contracta* of flow (Appendix D). Photograph 3 shows the position of the distributor in the eye of the RPB and Photograph 4 shows the details of the distributor.

In the absence of the 4-arm liquid distributor, free vortices are created inside the 'eye' of the rotor and cause the formation of a low-pressure region and hence alter the composition of any representative sweet gas sample. The presence of the 4-arm liquid distributor is to substantially reduce any effect of such vortices. In addition, the rotation of the packed bed causes the formation of forced vortices inside the 'eye' of the rotor but in a similar fashion the 4-arm distributor reduces any such effects. The shape of the 4-arm liquid distributor is engineered in order to break off both the free and the forced vortices and hence reduces substantially any effects of windage in the liquid distribution area.

The distributor irrigates the packed bed in a more uniform way with the application of 32 holes, which jets liquid in a short trajectory. Furthermore, experiments proved that the 4-arm distributor achieved lower HTU values compared to a single pipe distributor (Hassan-beck, 1997).

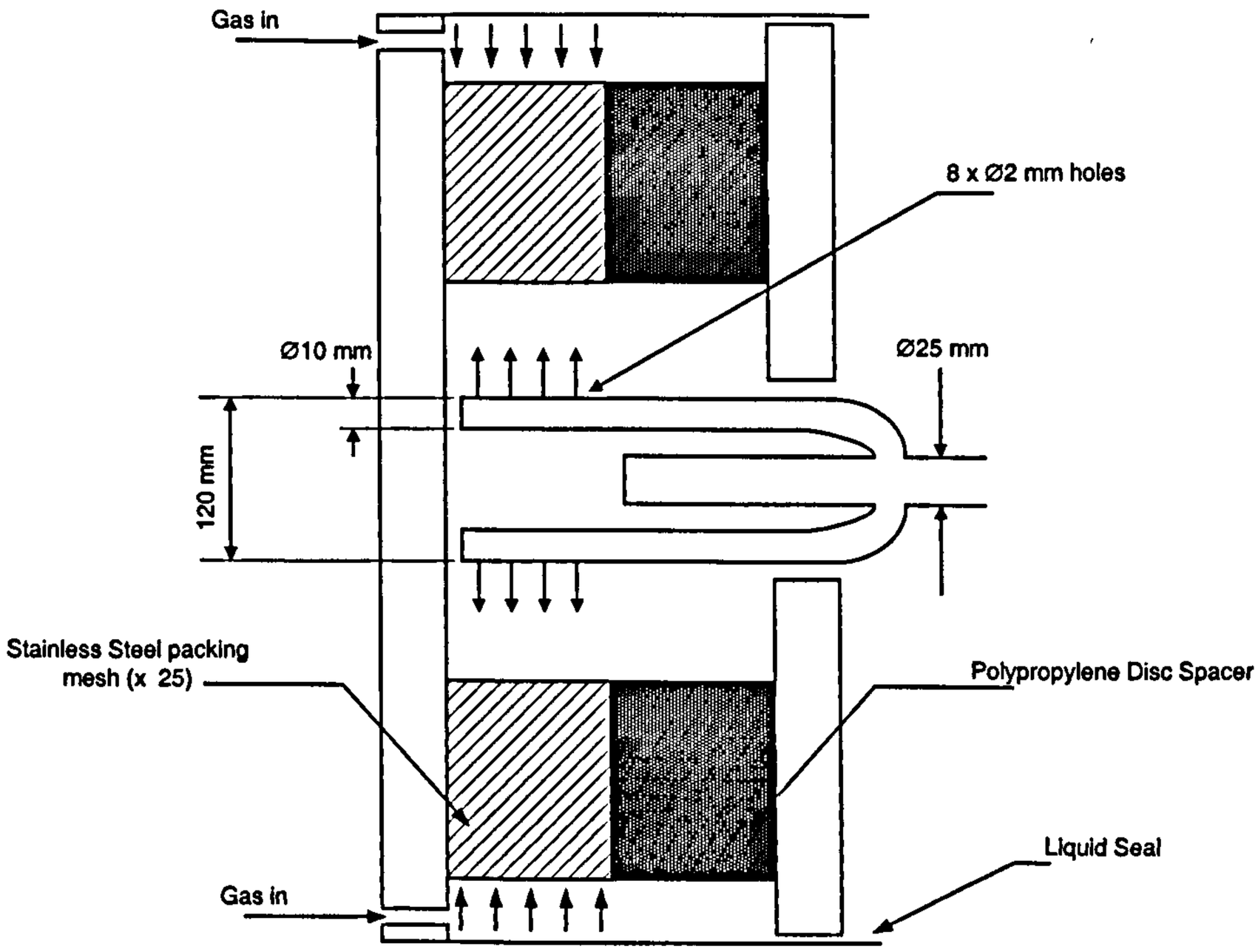

Figure 3.9: Irrigation of RPB with 4-arm distributor.

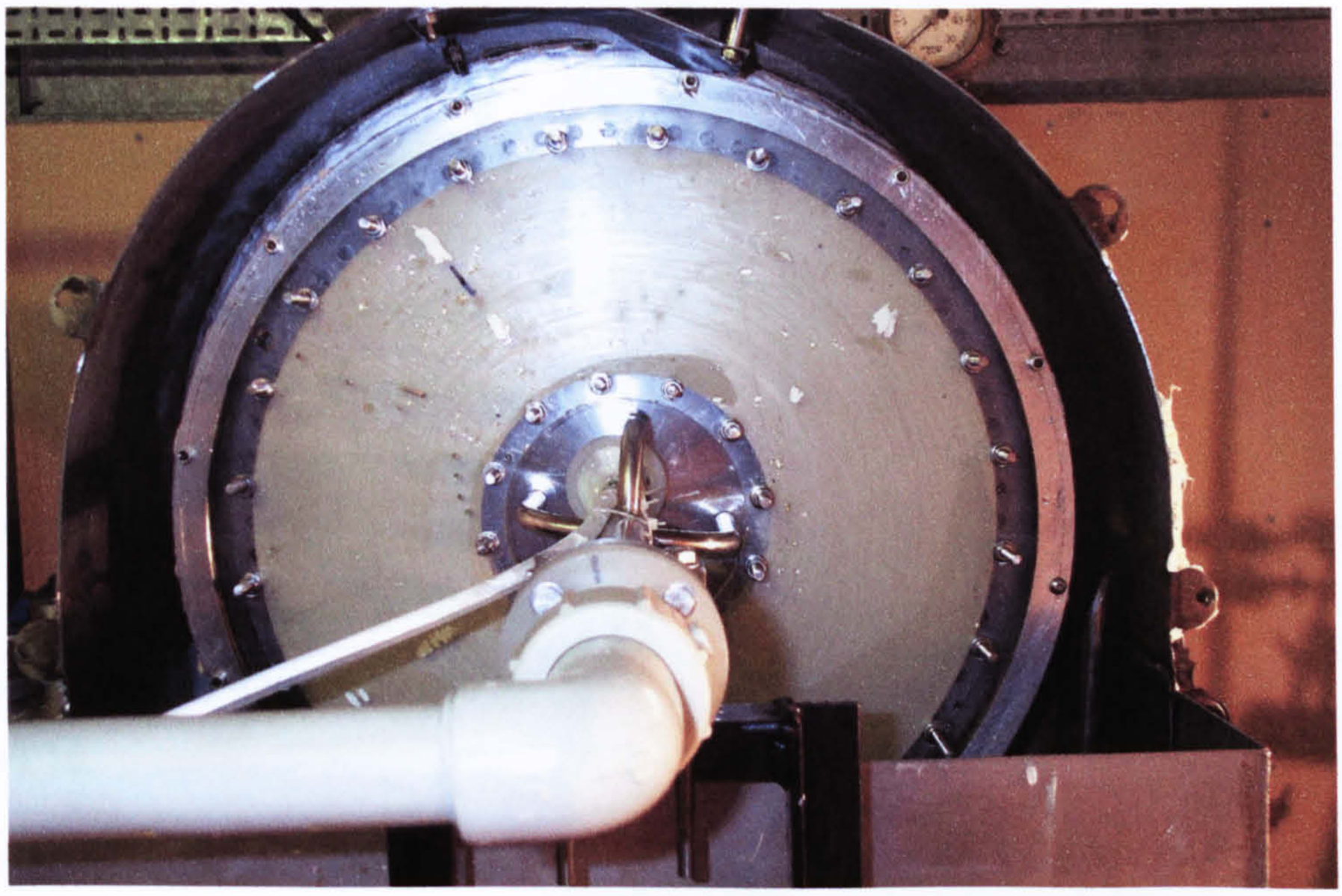

Photograph 3: Position of 4-arm distributor in the "eye" of the rotor.

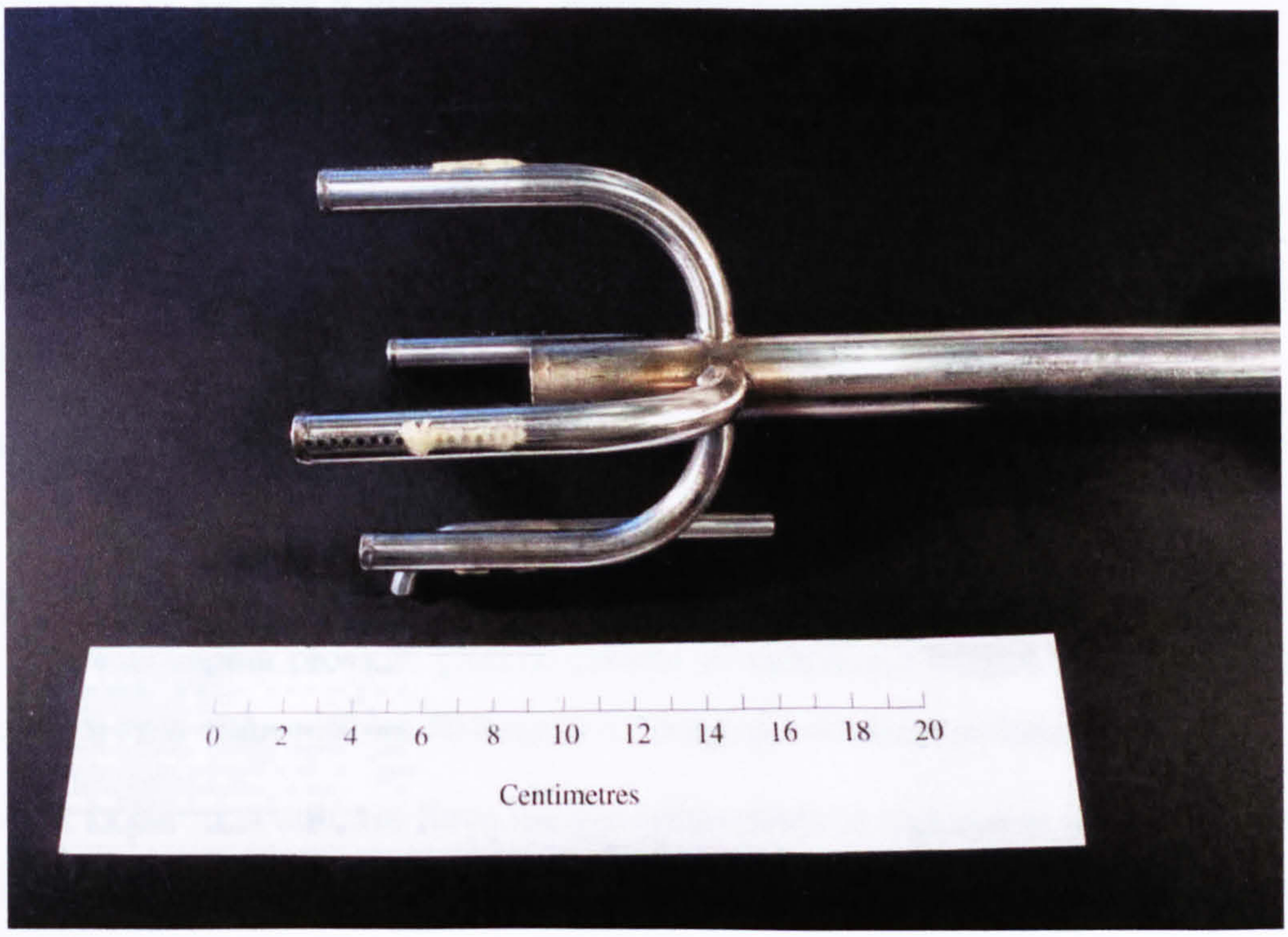

Photograph 4: A 4-arm liquid distributor

3.8 Carbon dioxide / Air Mixture

The purpose of the system is to deliver a steady, turbulent and homogeneous flow of carbon dioxide and air mixture (sour gas) to the Higee rig for the duration of experiment, which is approximately 15 minutes. The air-CO_2 system is shown in the Photograph 5 and a flowsheet of the system is shown in Figure 3.10.

Photograph 5: CO_2/Air mixture system

Air is supplied from the department's main compressor (Belleiss Morcom) with a maximum pressure of 55 psi and a maximum delivery of 203 m^3/min.

A non-return valve is installed in the air pipeline in order to prevent carbon dioxide backflow and thus eliminating any contamination to the departmental air. A flowmeter, a thermocouple and a pressure gauge measure the macroscopic properties of air.

The carbon dioxide source was a single BOC cylinder with a capacity of 34 kg (@ 50 bar, 15°C). The flow of carbon dioxide from the cylinder is a steady state, steady-flow throttling process across a restriction. Carbon dioxide is stored in liquid form but due to its vapour pressure gaseous carbon dioxide is discharged from the cylinder. The pressure is reduced from 50 barg to 4.5 barg at a constant enthalpy.

In order to ensure a uniform flow, the gas temperature is restored to its ambient value by passing it through a copper coil immersed in a water tank. The 10 m copper coil with 4.50 mm inside diameter provides 0.87 kW heat to the cold carbon dioxide as shown in Appendix E. Figure 3.11 shows the temperature of carbon dioxide after the heat exchanger and the departmental air stream. It shows that the temperature profile of both of the gaseous streams becomes stable after 10 minutes of operation. It clearly shows that the temperature decreases with time because the carbon dioxide

bottle becomes colder. Therefore, the pressure and the temperature of the stream are measured in order to make the necessary corrections in the mass balance calculations. Finally, both the air and the carbon dioxide streams are combined and allowed to have a sufficient length of distance to mix in order to ensure homogeneity before being fed to the Higee rig.

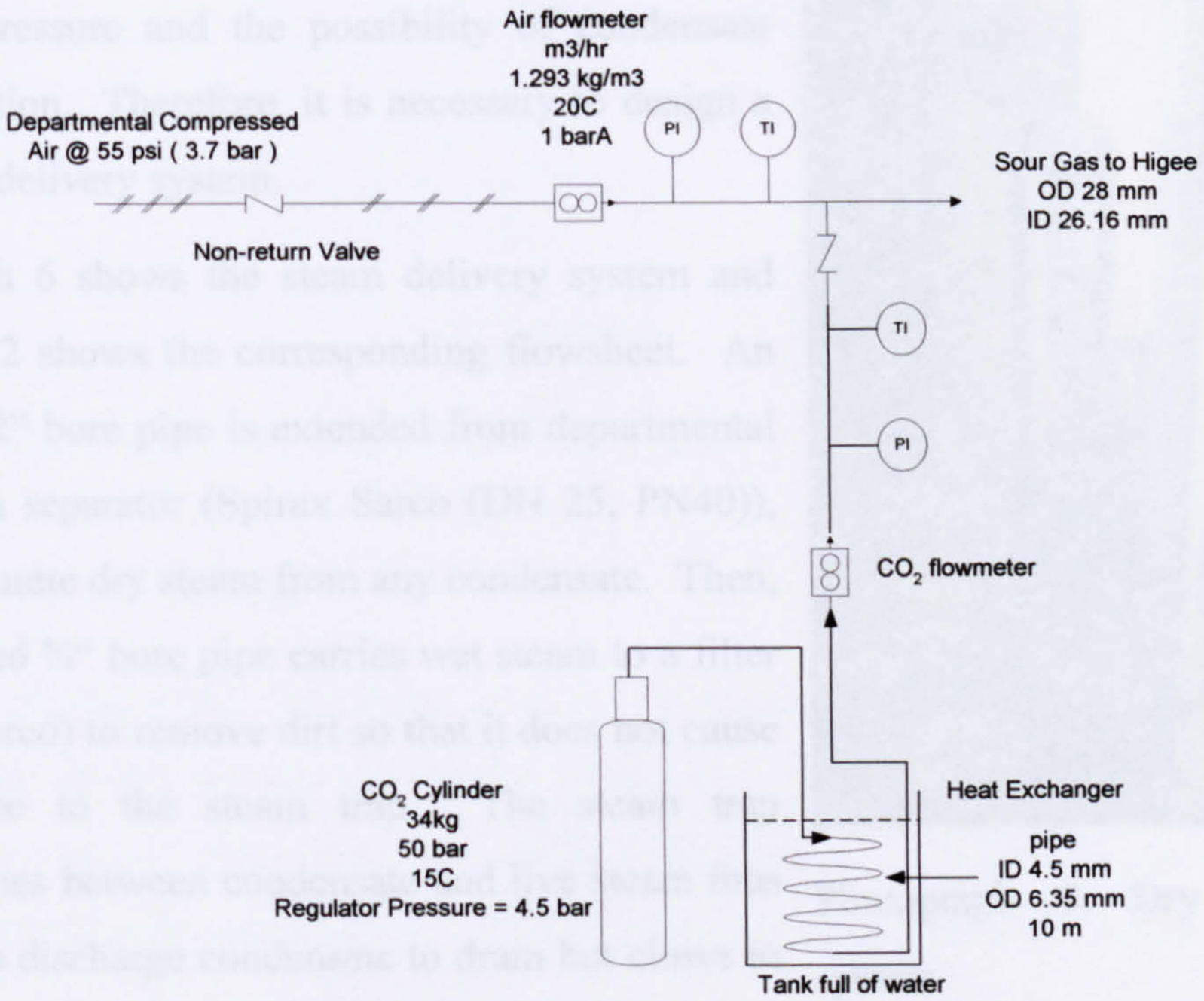

Figure 3.10: Flowsheet of CO_2/Air system

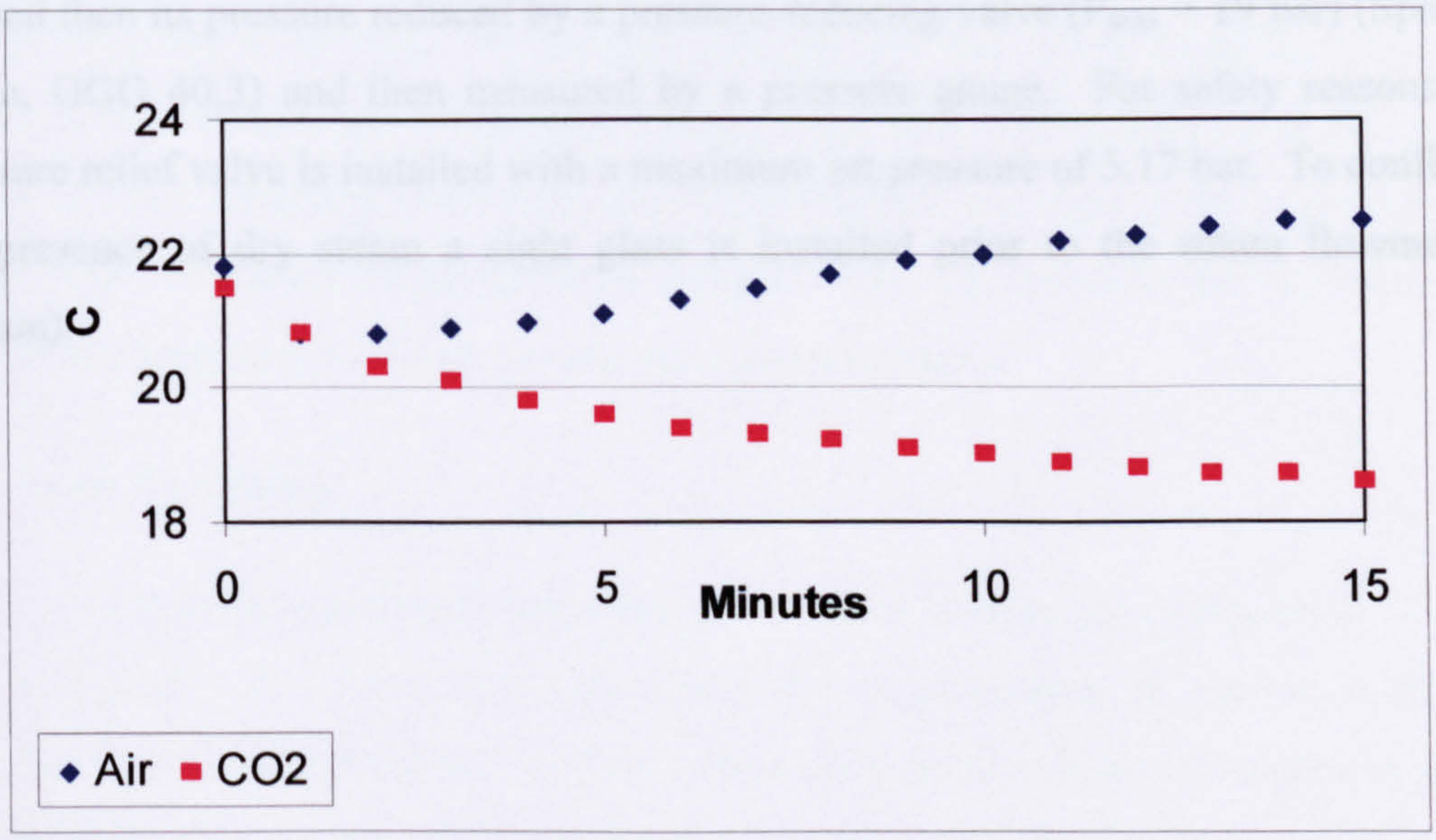

Figure 3.11: Effect of time on the temperature of CO_2/Air Stream

3.9 Dry Steam System

The purpose of the steam system is to deliver a maximum flowrate of 300 kg dry and saturated steam per hour to the Higee rig. However, departmental steam can not be routed directly to the pilot rig due to its high pressure and the possibility of condensate contamination. Therefore, it is necessary to design a dry steam delivery system.

Photograph 6: Dry steam system

Photograph 6 shows the steam delivery system and Figure 3.12 shows the corresponding flowsheet. An insulated 2" bore pipe is extended from departmental steam to a separator (Spirax Sarco (DN 25, PN40)), which separate dry steam from any condensate. Then, an insulated ¾" bore pipe carries wet steam to a filter (Spirax Sarco) to remove dirt so that it does not cause any failure to the steam trap. The steam trap distinguishes between condensate and live steam thus it opens to discharge condensate to drain but closes to trap the steam.

On the other hand, an insulated 1" bore pipe carries dry steam, which is initially filtered then its pressure reduced by a pressure-reducing valve (P_{max} = 19 bar) (Spirax Sarco, GGG 40.3) and then measured by a pressure gauge. For safety reasons, a pressure relief valve is installed with a maximum set pressure of 5.17 bar. To confirm the presence of dry steam a sight glass is installed prior to the steam flowmeter (Nixon).

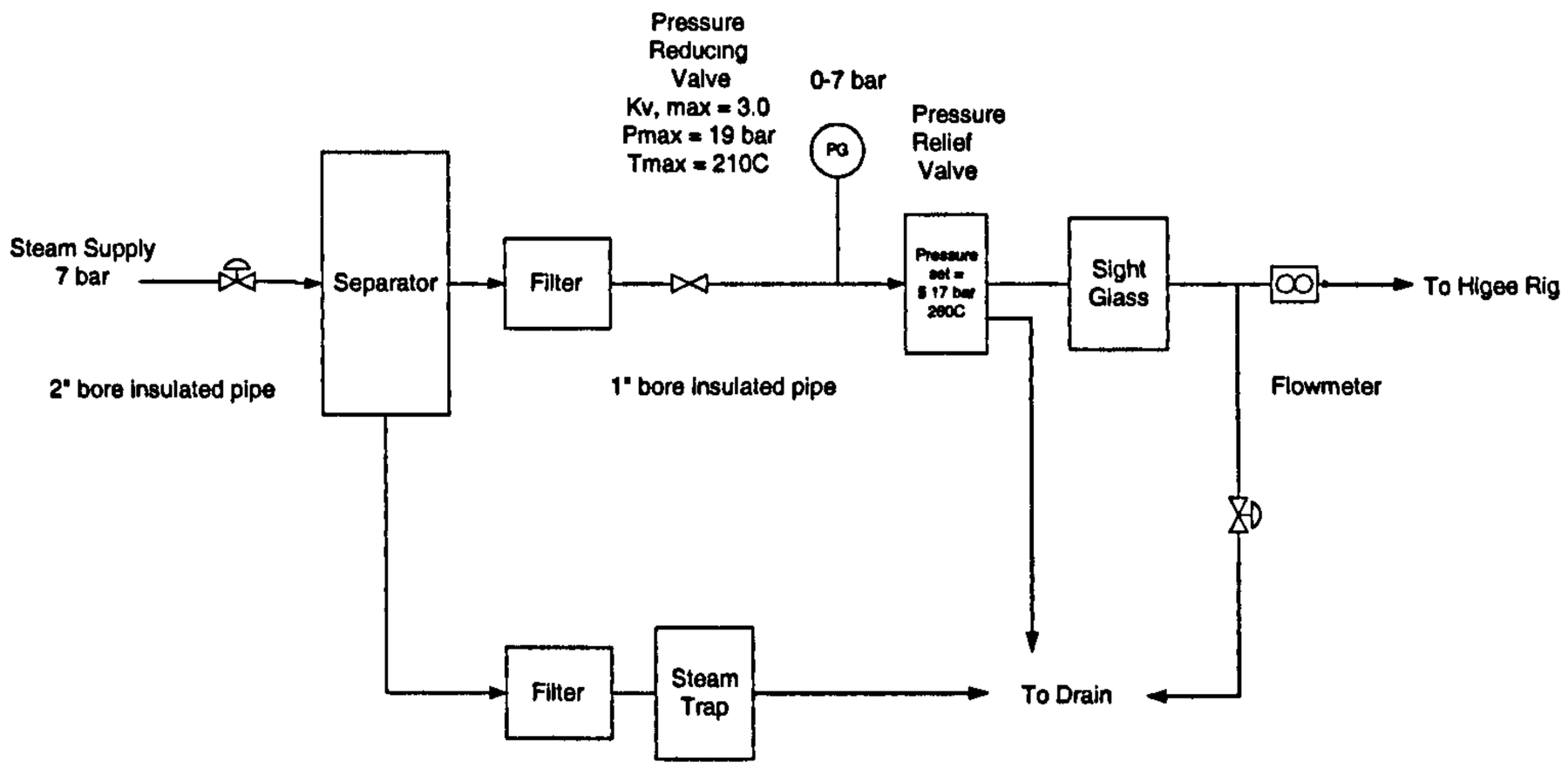

Figure 3.12: Flowsheet of steam delivery system

3.10 Liquid Sampling

For each experimental run, three samples of ethanolamine solution were taken. Figure 3.13 shows the liquid sampling positions. A lean ethanolamine solution sample is taken prior to the liquid distributor. After counter-current absorption/desorption operation in the Higee, two rich ethanolamine solution samples are taken. The rationale of taking two rich ethanolamine solution samples is to investigate the end effects. A stainless steel sample line (**A**) is extended to a position as close as to the periphery of the RPB in order to collect liquid droplets as they emerge from the liquid seal. A stainless steel sample line (**B**) is extended from the bottom of the buffer tank. The liquid samples are collected in sealed 250 mL glass flasks. All the sampling point lines are flashed before and during the experimental run in order to collect a representative sample. The rich ethanolamine samples are usually analysed within 24 hours using gas chromatography.

3.11 Gas Sampling

For each absorption/desorption run, there is a need to analyse the composition of the inlet and outlet gas phase and specifically the concentration of carbon dioxide. Section 3.8 shows the preparation of the carbon dioxide/air mixture. Samples of sour gas are taken prior the gas mixture is fed to the Higee using four 10 mL syringes.

Sweet gas samples were taken from the 'eye' of rotor as shown in Figure 3.14. The sweet gas is passed from the 'eye' of RPB to a gas sample vessel via 8mm teflon piping. The sweet gas is then discharged via a rotary vacuum pump (Speedivac, model ES35) to the atmosphere. Four 10 mL syringes were used to collect samples from the gas-sampling vessel as shown in Photograph 7. It was decided to take four samples per experiment for each gas sampling point in order to ensure that correct and representative data was recorded. It is important to ensure that no liquid is vacuumed into the lines so that only dry samples were collected. The tips of the syringes were covered in order to avoid air leakage. The sour and sweet gas samples were immediately analysed using gas chromatography and they were not kept overnight to avoid contamination. Section 5.2 shows the dry run experiments that were carried out to ensure that representative sweet gas samples were withdrawn from the 'eye' of the rotor.

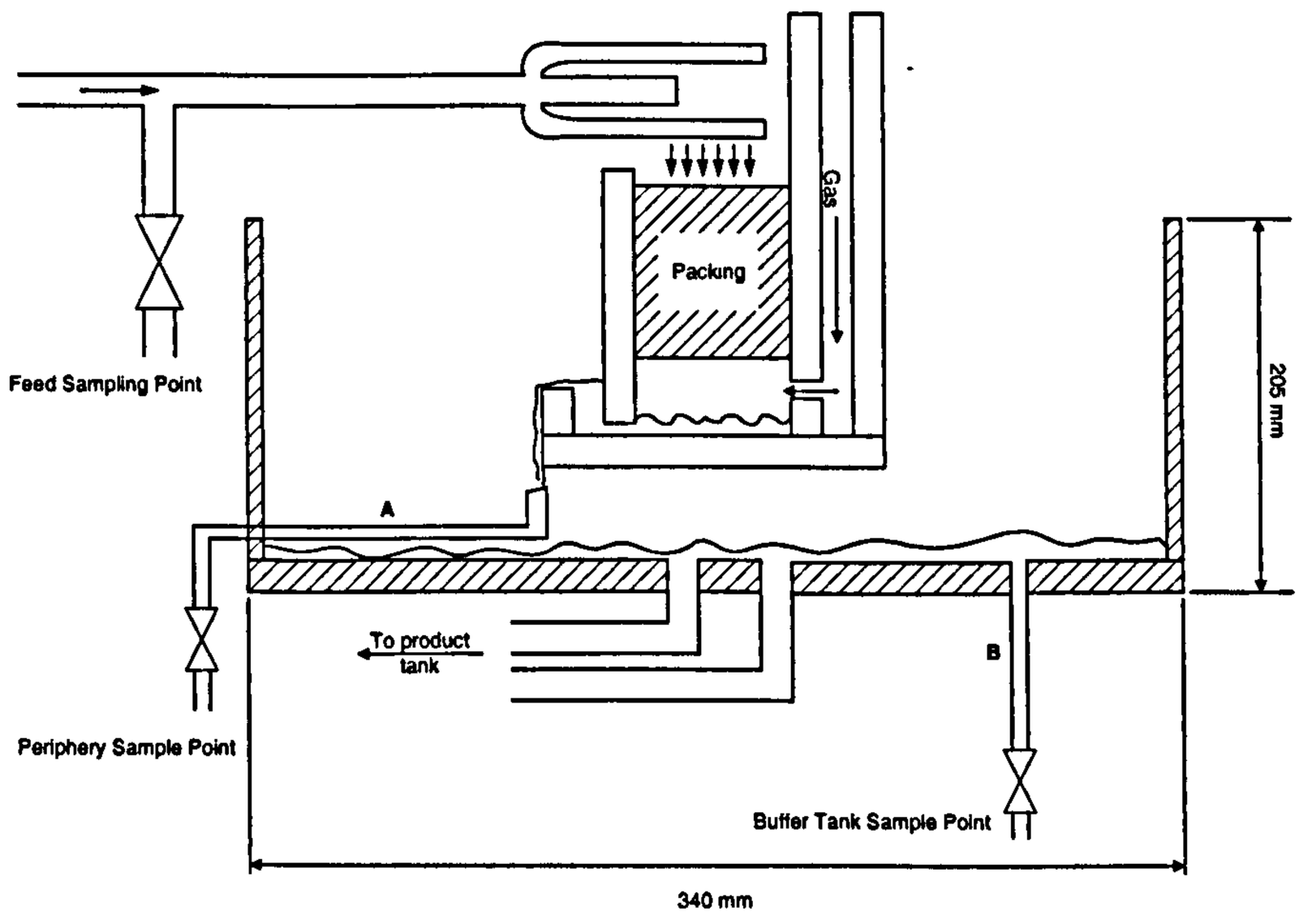

Figure 3.13: Positions of liquid sampling

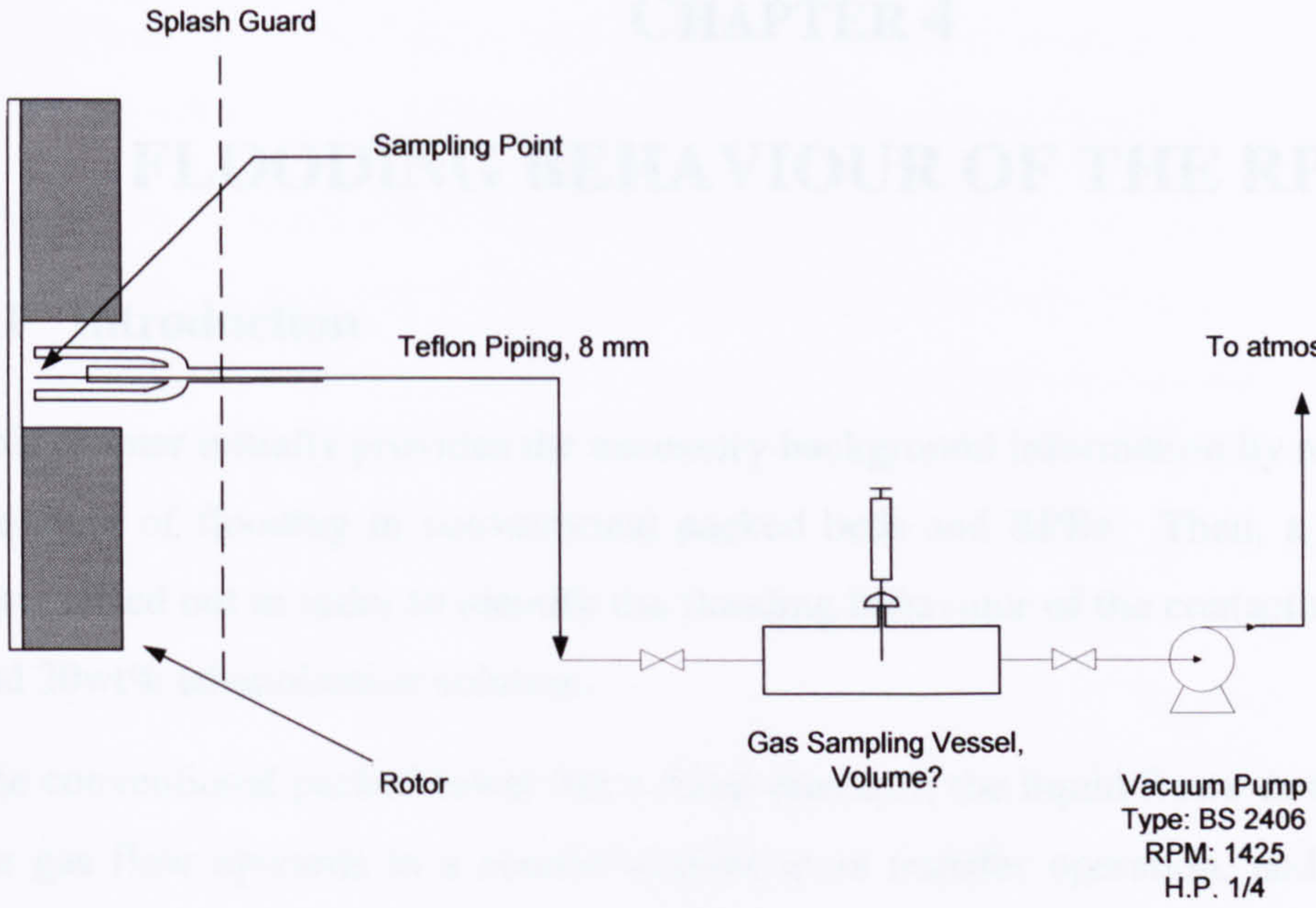

Figure 3.14: Positions of gas sampling

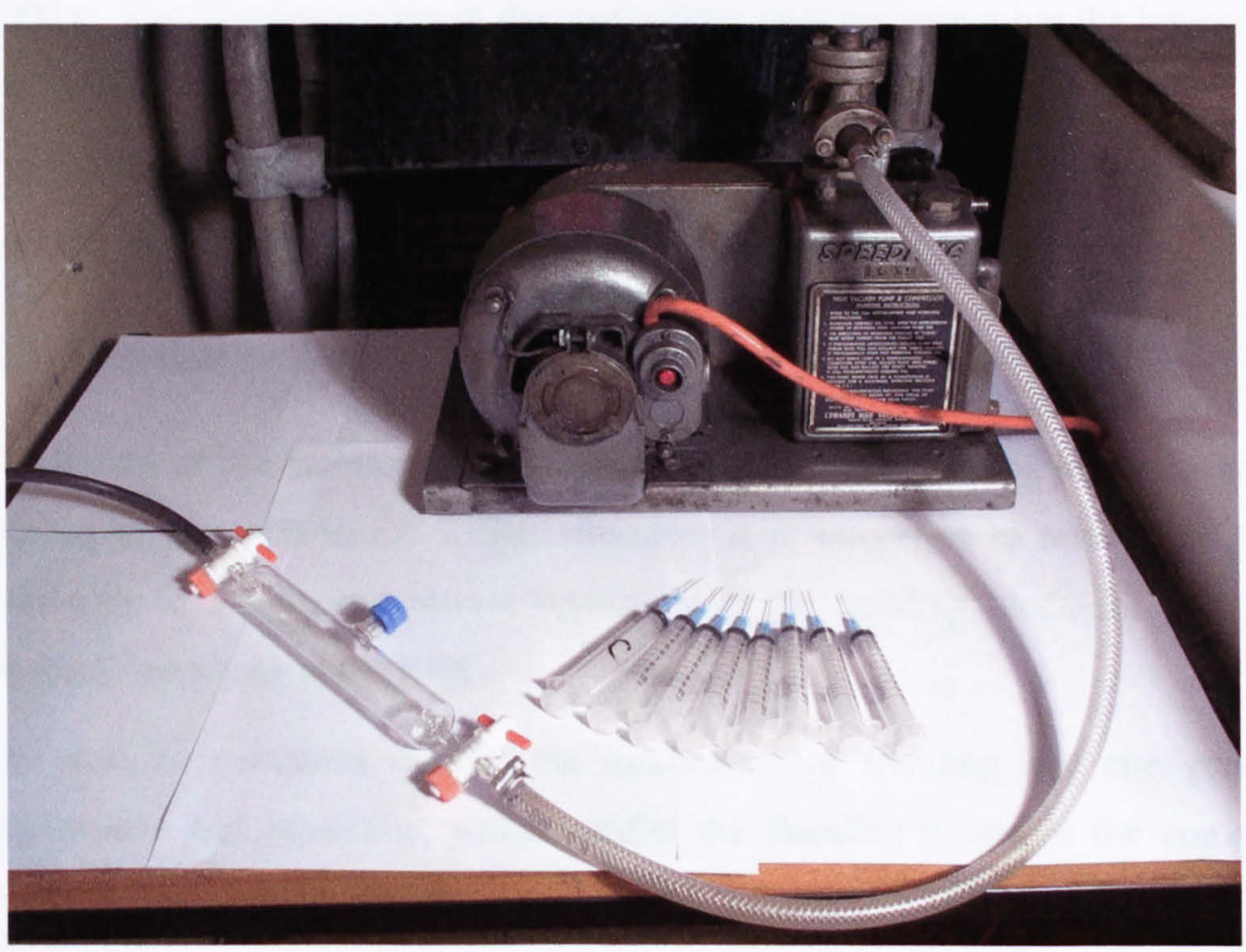

Photograph 7: Sampling of sweet gas

CHAPTER 4

FLOODING BEHAVIOUR OF THE RPB

4.1 Introduction

This chapter initially provides the necessary background information by reviewing the literature of flooding in conventional packed beds and RPBs. Then, a visual study was carried out in order to identify the flooding behaviour of the contacting fluids: air and 30wt% ethanolamine solution.

The conventional packed tower has a fixed diameter, the liquid flows downwards and the gas flow upwards in a counter-current mass transfer operation, and the column operates at 1 g. As a consequence, the flooding occurs throughout the column.

In contrast, the RPB has a variable area of contact due to the doughnut-shape of the rotor, the liquid flows outwardly and the gas flows inwardly, and it operates at 100-1000 g. The flooding occurs in the 'eye' of the rotor because it has the lowest 'g' and the highest mass fluxes.

The measurement of pressure drop across the RPB was not carried out as this subject was already investigated and modelled by other authors.

4.2 Literature Review

The review of the literature is divided into two sections: flooding in the conventional packed towers, and in the RPBs. Initially, it is important to review the flooding behaviour in the packed towers because it is the building block for studying the flooding behaviour in the RPB.

The next two sections discuss the mechanism of flooding and cite generalized expressions and equations, which predict the flooding points in the conventional packed towers and the RPBs.

4.2.1 Flooding in Packed Towers

It is important that the packed tower should not reach the flooding conditions during operation. Therefore, it is necessary to predict the maximum flux-rate of the liquid

and the gas; as well as the liquid flux-rate that should provide sufficient wetting to the packed bed. The actual liquid and the gas flux-rates are determined by a combination of the knowledge of the limiting capacity and an economic feasibility studies.

(White, 1935) carried out experiments on air/water system in order to visualize the flooding mechanism in a packed bed. The air flowrate was gradually increased over the packing at a constant flow of water. It was observed that there is a gradual increase in the amount of liquid held-up in the packing as well as the formation of gas bubbles. As a consequence, the liquid hold-up caused the reduction of the channel area available for the gas flow. Three flow regimes were defined as shown in Figure 4.1: (1) the pressure drop increases with the second power of the gas velocity at low gas flowrate; (2) the pressure drop increases more rapidly with the second power of the gas velocity at higher gas flowrate; (3) a great increase in the pressure drop with a slight increase in the gas velocity. The transition from the first to the second flow regimes was defined as the loading point and the transition from the second to the third flow regimes was defined as the flooding point.

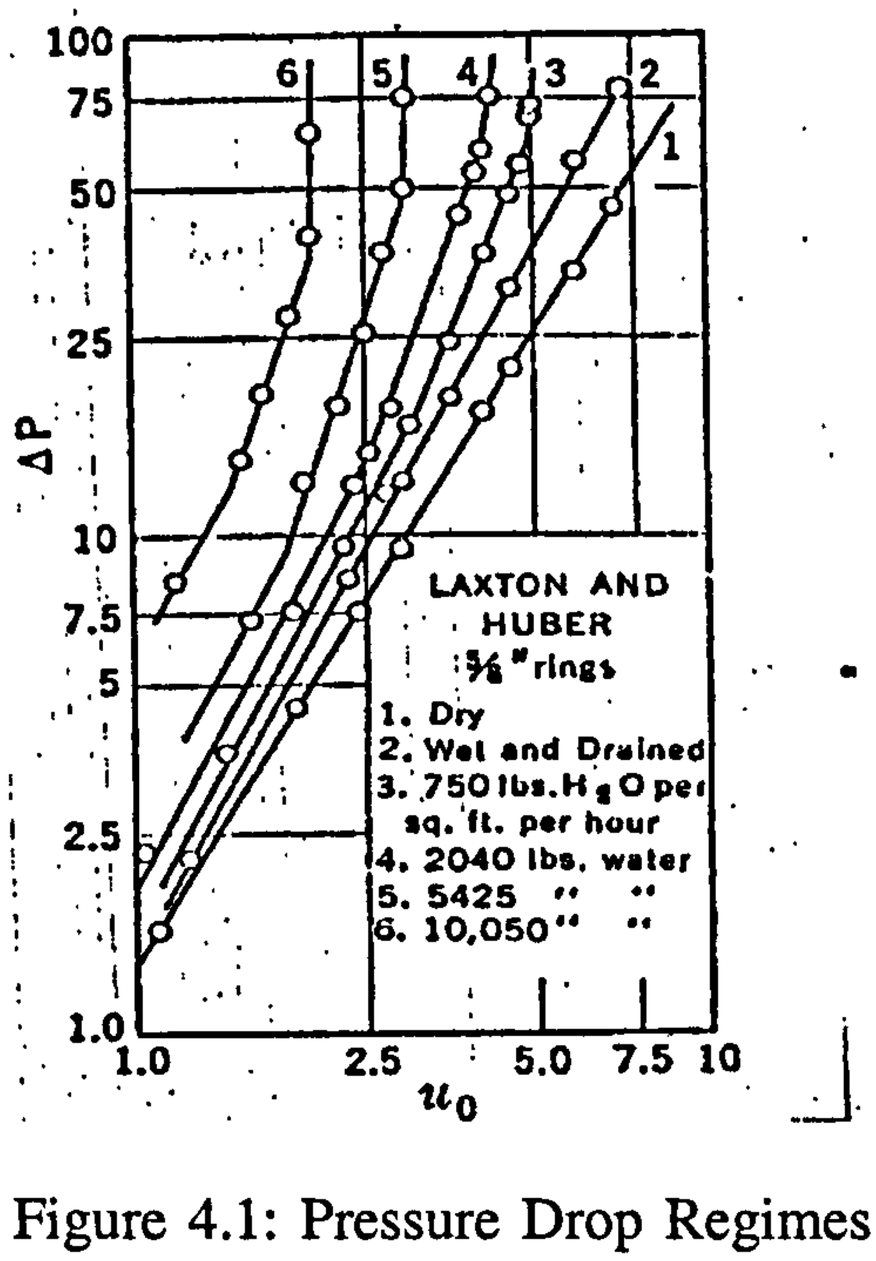

Figure 4.1: Pressure Drop Regimes in a Packed Column.

Prior to (Sherwood et al., 1938), most of the experimental flooding velocities were conducted on air/water system. (Sherwood et al., 1938) investigated the effect of the

physical properties of gas and liquid on the flooding velocities. A widely-used generalized correlation was developed and presented in a log-log diagram (Figure 4.2):

$$\left(\frac{u_o{}^2 S}{g\,F^3}\right)\left(\frac{\rho_g}{\rho_L}\right)\mu^{0.2} \text{ vs.} \left(\frac{\mathrm{L}}{\mathrm{G}}\right)\left(\frac{\rho_g}{\rho_L}\right)^{0.5} \tag{4.1}$$

where u_0 is the superficial gas velocity, S is the surface area of packing, g is the acceleration of gravity, F is the fraction of free volume in packing, L is the superficial mass velocity of liquid, G is the superficial mass velocity of gas, ρ_G and ρ_L are the density of gas and liquid respectively. There are two distinct lines: dumped Raschig rings and stacked rings. The flooding velocities for stacked rings are higher than the Raschig rings. The gravity term (g) is included in the ordinate term in order to have a dimensionless ratio:

$$\frac{(\text{gas velocity based on free area})^2}{\text{hydraulic mean radius}} = \frac{\left(u_0/F\right)^2}{F/S} = \frac{u_o{}^2 S}{F^3} \tag{4.2}$$

(Piche et al., 2001) expressed the ordinate for (Sherwood et al., 1938) figure as a mathematical function of the abscissa for dumped rings.

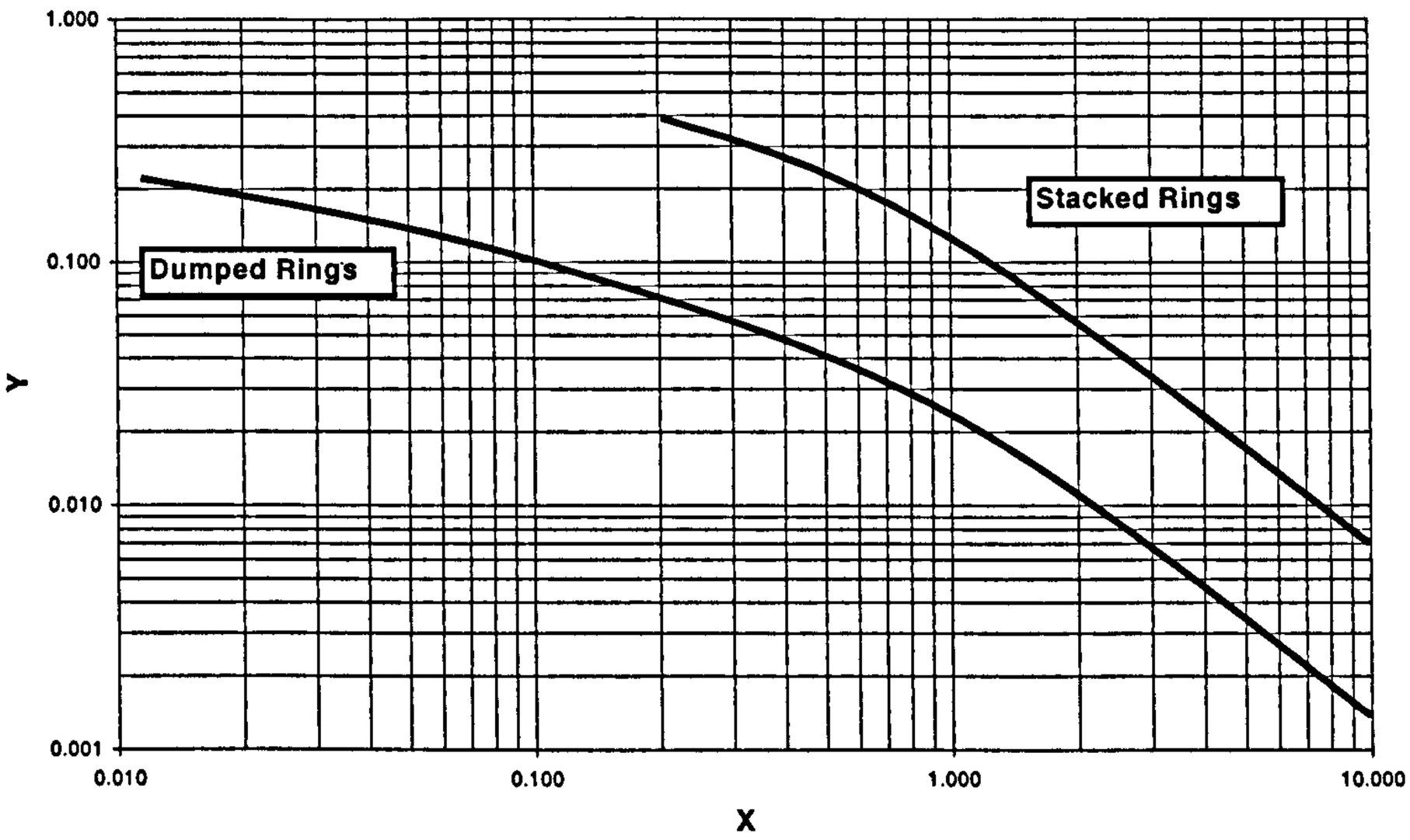

Figure 4.2: Flooding Diagram by Sherwood

$$\log(Y) = -0.2866\log^2(X) - 1.0997\log(X) - 1.6784 \qquad (4.3)$$

(Szekely and Mendrykowski, 1972) showed that the Sherwood plot described well the flooding behaviour of high-density liquid (up to 13.6 g/cm3) and high interfacial tension liquid (up to 500 dynes/cm).

(Silvey and Keller, 1966) argued that there is not a consistent definition of flooding point. In fact, around 10 definitions of the flooding point were cited and they were not considered meaningfully equivalent. However, they did not propose a new approach for correlating packed tower capacity but only highlighted the need for a new one. Figure 4.3 shows the discrepancies of the flooding data around the (Lobo et al., 1945) correlation on a linear scale.

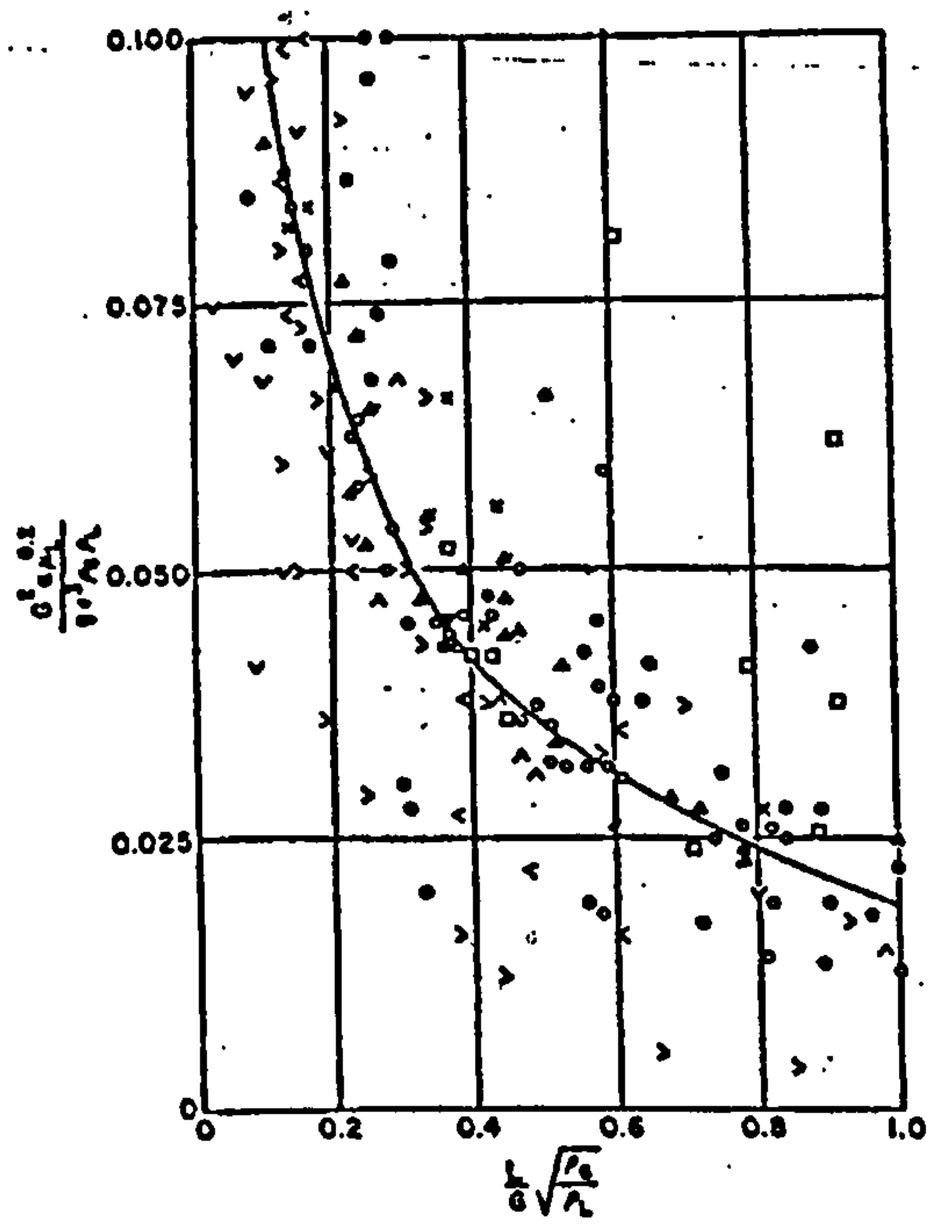

Figure 4.3: Discrepancies on (Lobo et al., 1945) Correlation

(Sarchet, 1942) compared the value of the visual flooding velocity with the corresponding graphical flooding velocity. It was shown that the visual flooding data for different type of packing materials were 15-20% below the graphical flooding points. The visual study showed that at low gas velocities the gas was the continuous phase and when flooding was approached the gas became the discontinuous phase.

(Hutton et al., 1974) proposed a mechanism for flooding in packed columns. The analysis showed that flooding is initiated by (1) instability due to the interaction between the pressure gradient and liquid hold-up at a constant gas and liquid flowrates; and (2) wave type instability. In comparison, flooding is initiated only by wave type instability in wetted-wall columns (Cetinbudaklar and Jameson, 1969).

(Piche et al., 2001) applied artificial neural network computing and dimensional analysis to generate a flooding capacity correlation of randomly dumped packed beds for a wide range of data in absorption and distillation. The correlation absolute average relative error was 16.1% and a standard deviation of 20.4%. The study identified the physical properties that influence the flooding capacity in a packed bed, namely: liquid superficial velocity, liquid viscosity, gas density, bed porosity, packing surface area, and column diameter. Their investigation highlighted the limitations of earlier flooding correlations in terms of accuracy and the generalization. In addition, a better method of statistical analysis was applied to improve the prediction of the flooding.

4.2.2 Flooding in Rotating Packed Bed

Flooding occurs in the 'eye' of the RPB because it has the lowest centrifugal acceleration and the mass fluxes are highest. Understanding the dynamics of flooding could explain the higher hydraulic capacity and the enhancement to the mass transfer of the Higee.

The Sherwood correlation (Figure 4.2) can be modified in order to accommodate the high speed of the RPB. The physical properties (density) and the superficial mass flowrates of the liquid and the gas fix the value of abscissa, $X = \frac{L}{G}\sqrt{\frac{\rho_G}{\rho_L}}$. Therefore, the ordinate value, $Y = \frac{U_g^{\,2}.a_p}{g.\varepsilon^3}\left(\frac{\rho_G}{\rho_L}\right)$, is fixed.

The value of the gravitational acceleration (g) in the ordinate has to be replaced with $(r_i\omega^2)$ where ω is the rotational speed and r_i is the inside radius.

It is expected that higher values of the gas velocity and/or the specific surface of packed bed are achieved by accelerating the rotational speed of the packed bed

because the ratio of the gas and the liquid densities as well as the voidage remains constant in the ordinate formula.

As a consequence, the increase in gas velocity leads to higher throughput and thus higher hydraulic capacity of the Higee. In addition, the higher packing density material (a_p) may be expected to lead to better contact and mixing of the liquid/vapour phases, better mass transfer operation, and thus achieving lower HTU values.

(Kelleher and Fair, 1996) flooding data deviated only within 10% of the values predicted by (Sherwood et al., 1938). The flooding point was identified by a sudden increase in the pressure drop when it was plotted against the rotational speed.

(Lockett, 1995) showed that Wallis model could be used as a better alternative for predicting the flooding behaviour in structured packing than the widely used Sherwood Plot. The flooding experiments were conducted on air/water system and the packed bed was a corrugated aluminium foil with specific surface area of 1770 m^2/m^3. The pressure drop of 500 Pa/100 rpm was the criterion used to identify the flooding point.

(Keyvani and Gardner, 1989) performed pressure drop experiments at constant liquid rates and variable RPM and gas flowrates. It was concluded that the pressure drop is proportional to RPM and gas flowrates. However, the flooding point was not clearly defined by an abrupt and sudden change in the pressure drop as the classical case in the conventional packed beds. This behaviour could be due to the fact that only the total pressure drop was measured; which was a combination of the pressure drop across the rotor, and the pressure drop between the housing and the spinning rotor.

(Singh et al., 1992) defined flooding in terms of a critical operating speed in which the pressure drop increase by ≥500 Pa/100 rpm.

(Hassan-beck, 1997) carried out both visual and pressure drop flooding experiments on a RPB using water and air. Figure 4.4 shows his visual flooding data results. The pressure drop results at the flooding point showed that there is no sudden hike.

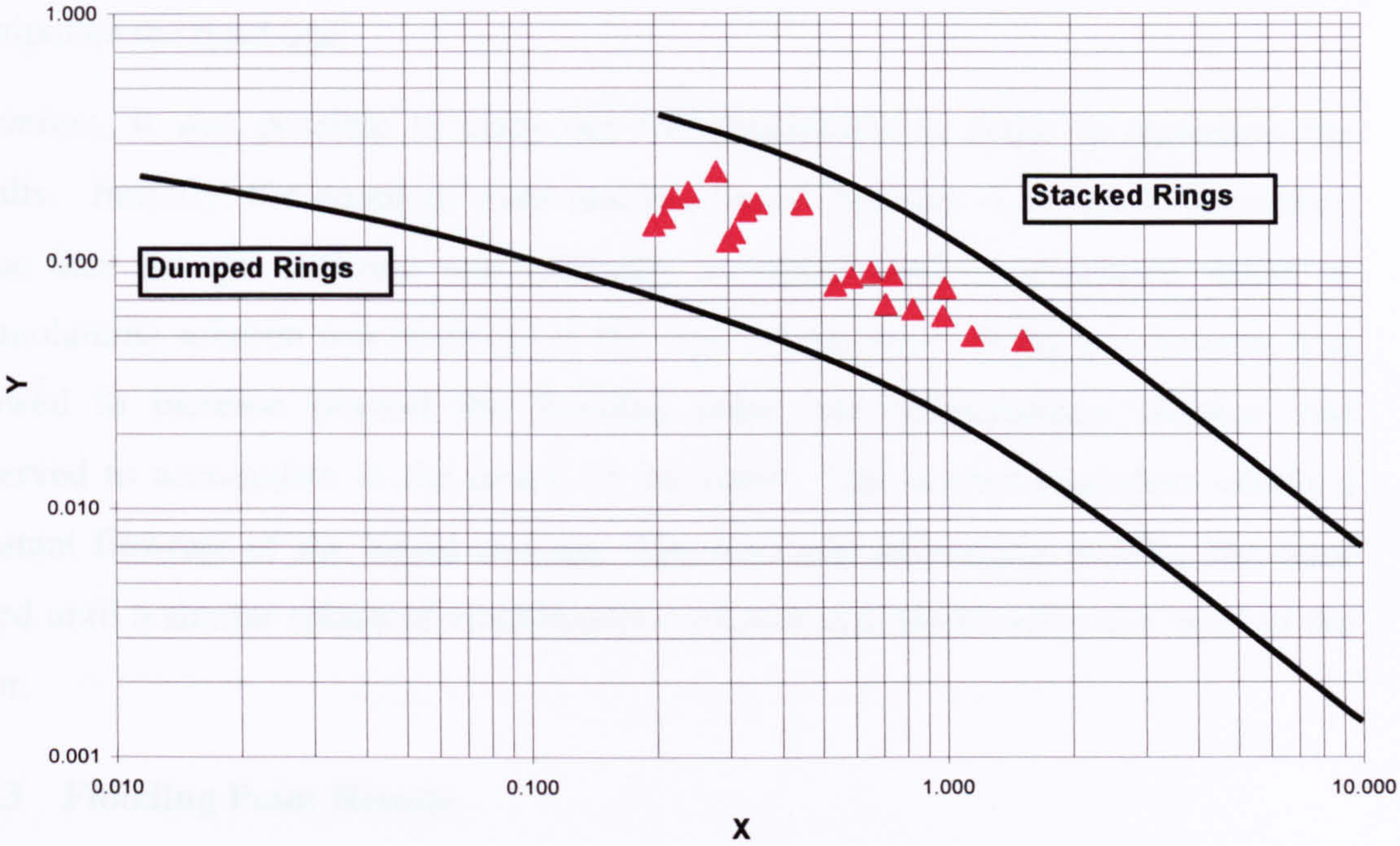

Figure 4.4: (Hassan-beck, 1997) visual flooding data on Sherwood plot.

The identification of flooding point in the Higee machine by a substantial increase in the pressure drop was observed by (Kelleher and Fair, 1996) and (Singh et al., 1992). These flooding points did not deviate significantly from those predicted by Sherwood correlation. However, (Keyvani and Gardner, 1989) and (Hassan-beck, 1997) did not observe similar increase in pressure drop.

4.3 Visual Study of the Flooding Behaviour in RPBs

4.3.1 Flooding Experimental Facility

The flooding experiments were conducted on the experimental facility that was fully described in Chapter 2. The liquid phase is 30wt% ethanolamine solution and the gaseous phase is air supplied from the department's compressor.

4.3.2 The Procedure for the Determination of the Flooding Point

The three operating variables that influenced the flooding point are: speed of rotor (RPM), liquid flowrate (L), and gas flowrate (G). The procedure for visual

determination of the flooding point is to neutralize two of the operating variable and manipulate the third one.

Therefore, it was possible to carry out two procedures in order to reconfirm the results. Initially, the speed of rotor and the liquid flowrate were set to a constant value then the gas flowrate was gradually increased until an excessive splash of ethanolamine solution was observed in the 'eye' of the rotor. If the gas flowrate was allowed to increase beyond the flooding point, the ethanolamine solution was observed to accumulate in the centre of the rotor. The second procedure entails a constant flowrate of the liquid and gas then similarly decreasing steadily the rotor speed until a similar splash of ethanolamine solution was observed in the 'eye' of the rotor.

4.3.3 Flooding Point Results

4.3.3.1 Sherwood Correlation

The specific combinations of gas flowrate, liquid flowrate and rotor speed for each flooding point enables the calculation of the abscissa and the ordinate in the Sherwood Plot. A detailed illustrative example of such calculation is shown in Appendix F.

The flooding point data are tabulated in Appendix F and presented on Sherwood Plot in Figure 4.5. It is shown that the flooding velocities in the Higee are higher than those for dumped rings. In fact, the flooding points data are closer to the stacked rings profile. In comparison, (Singh et al., 1992) found that Sherwood correlation for dumped rings underestimates the rotational speed limit for Sumitomo packing but it was in good agreement with wire gauze packing. In addition, a second-order polynomial curve fit was proposed for the experimental data (Equation 4.4); and Figure 4.5 compares their curve with Sherwood correlations for dumped and stacked rings and the current investigation data.

$$\log y = -2.27 - 1.14 \log(x) - 0.17 [\log (x)]^2 \qquad (4.4)$$

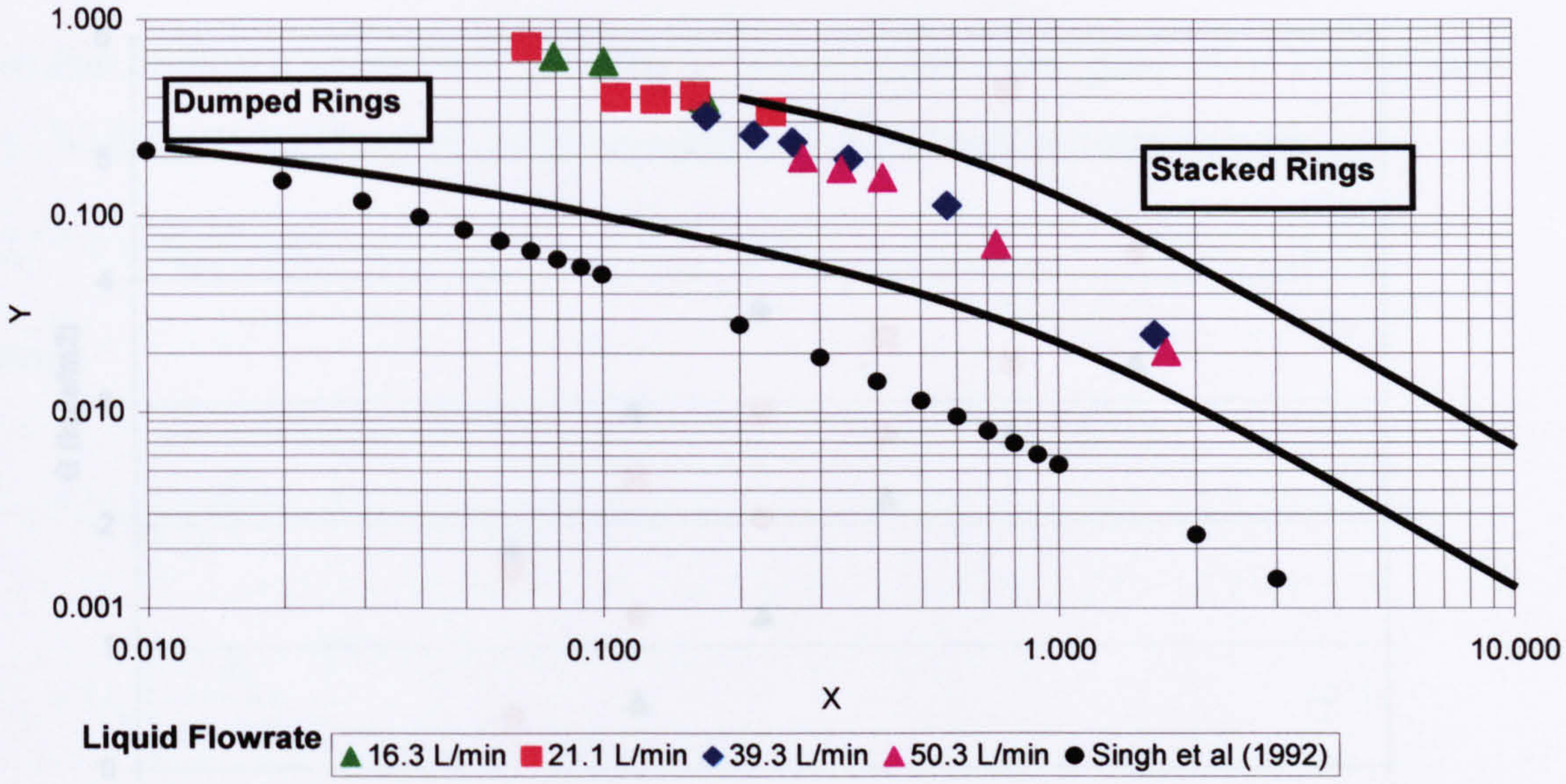

Figure 4.5: Flooding behaviour at different liquid flowrates.

The relationships between the three operating variables are illustrated in Figure 4.6 and Figure 4.7. It is evident from Figure 4.6 that increasing the RPM, at a constant liquid flowrate, allows a higher gas flowrate and thus corresponds to a higher flooding velocity. This implies that increasing the rotational speed of the bed increases the capacity of the Higee. In addition, Figure 4.6 shows that the gas flowrate increases as the liquid flowrate decreases at a constant RPM.

Another representation of the data is shown in Figure 4.7. It shows that increasing the RPM leads to a reduction in the L/G ratio at a constant liquid flowrate. This implies an increase in the gas flowrate and hence leads to a higher capacity for the Higee.

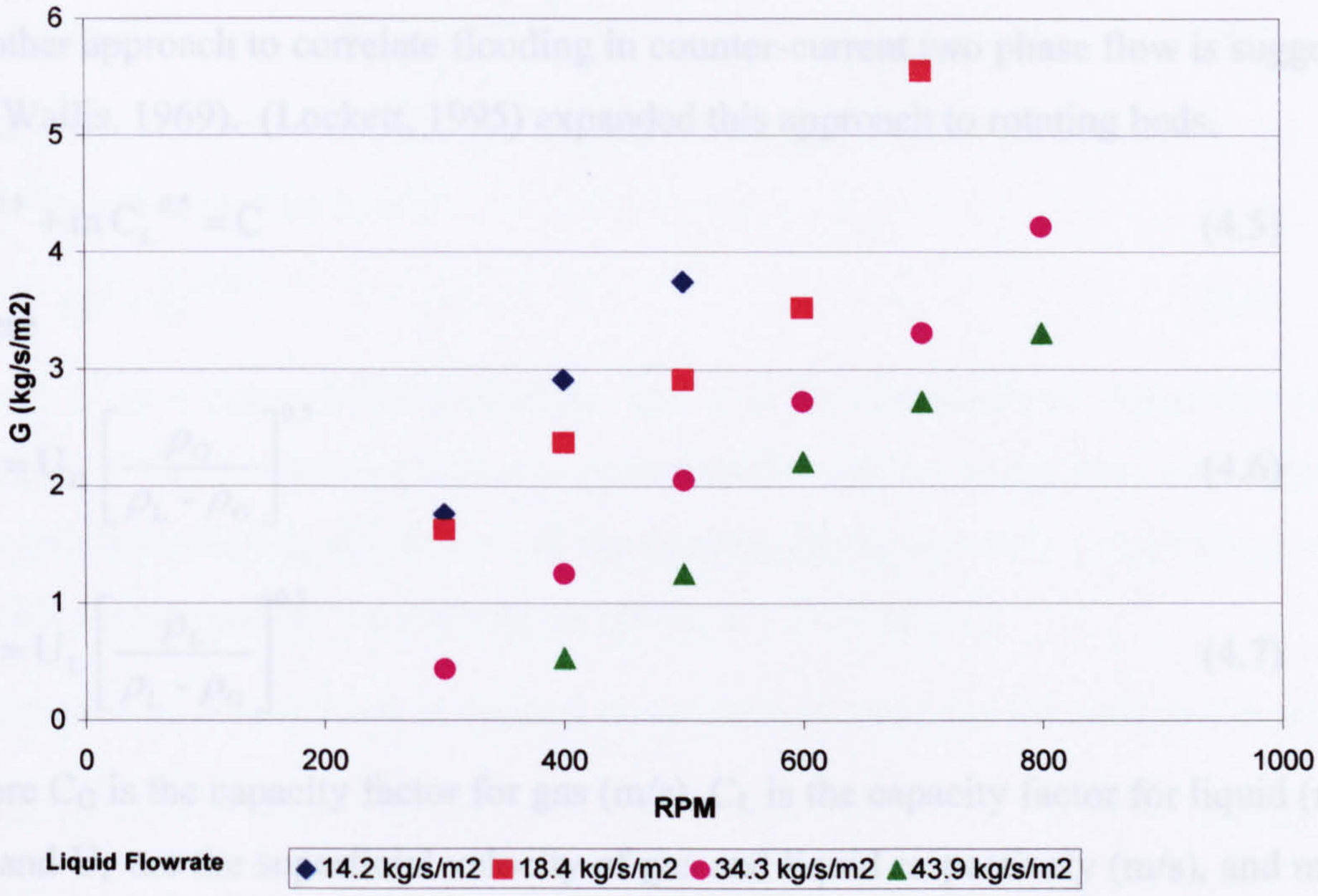

Figure 4.6: Flooding gas flowrate vs. RPM at varying liquid flowrate.

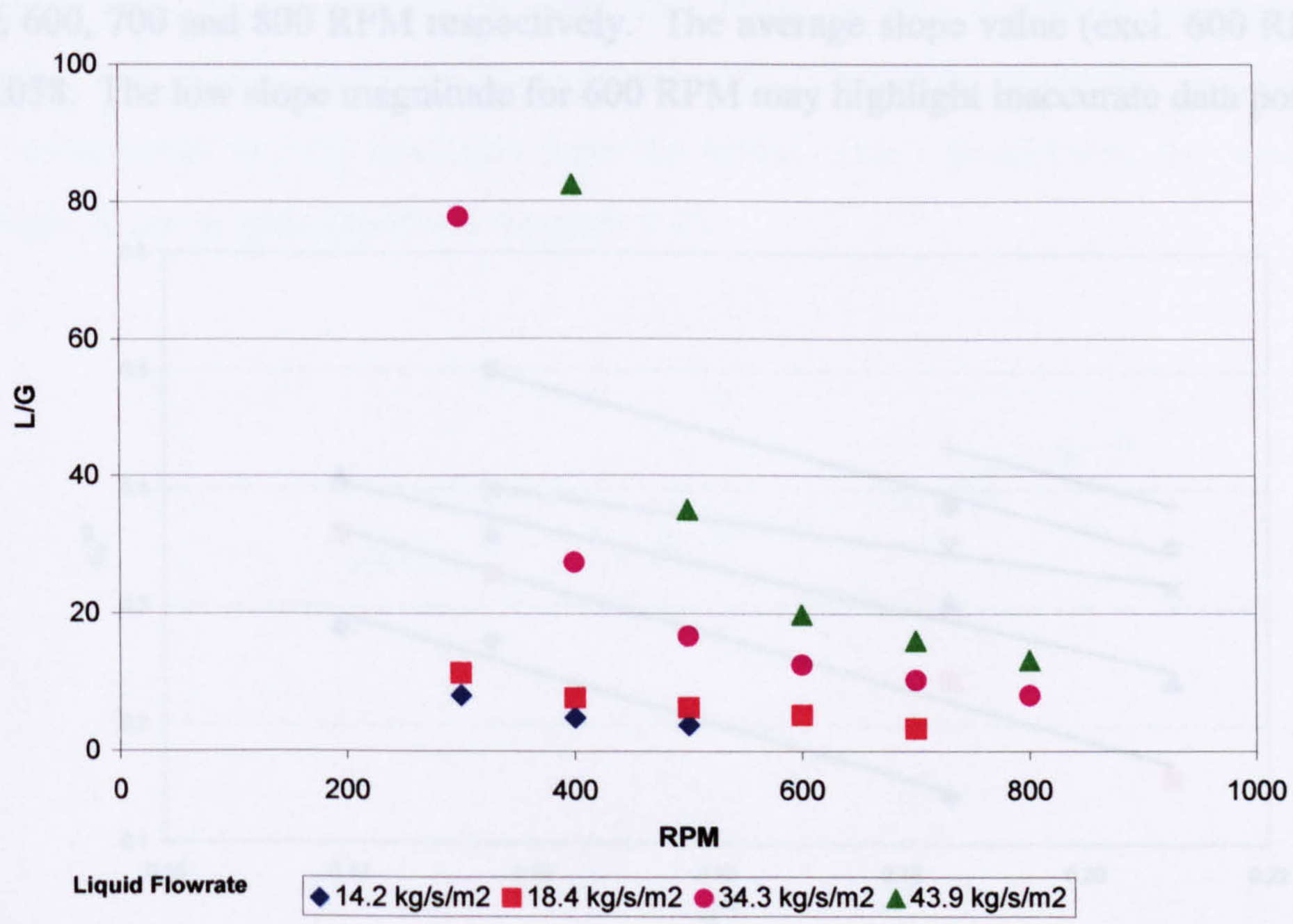

Figure 4.7: L/G vs. RPM at varying liquid flowrate

4.3.3.2 Wallis Correlation

Another approach to correlate flooding in counter-current two phase flow is suggested by (Wallis, 1969). (Lockett, 1995) expanded this approach to rotating beds.

$$C_G^{0.5} + m\,C_L^{0.5} = C \tag{4.5}$$

where

$$C_G = U_G \left[\frac{\rho_G}{\rho_L - \rho_G}\right]^{0.5} \tag{4.6}$$

$$C_L = U_L \left[\frac{\rho_L}{\rho_L - \rho_G}\right]^{0.5} \tag{4.7}$$

where C_G is the capacity factor for gas (m/s), C_L is the capacity factor for liquid (m/s), U_G and U_L are the superficial velocity of gas and liquid respectively (m/s), and m and C are constants.

Figure 4.8 shows the flooding diagram using Wallis method. The slopes of straight lines were 2.245, 2.195, 1.745, 1.100, 2.067, and 2.036 for speed rotor of 300, 400, 500, 600, 700 and 800 RPM respectively. The average slope value (excl. 600 RPM) is 2.058. The low slope magnitude for 600 RPM may highlight inaccurate data points.

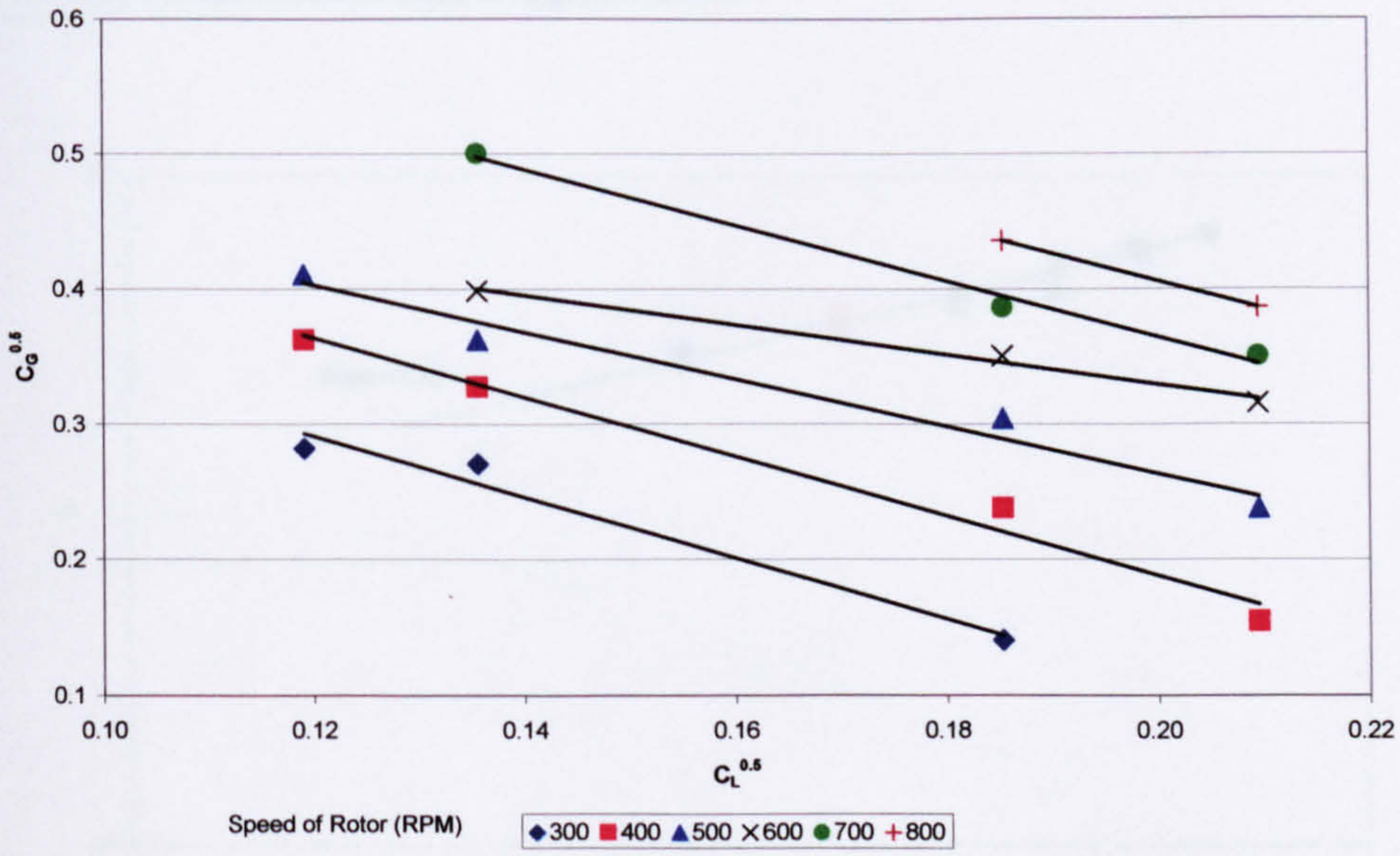

Figure 4.8: Flooding data using Wallis Plot

The constant (C) in Equation (4.5) is defined as follows:

$$C = C' (g.d)^{0.25} \quad (4.8)$$

Thus, it is possible to include the rotation of the packed bed as the gravity (g) term could be substituted by $(r.\omega^2)$.

$$C = C' (\omega^2 r\, d)^{0.25} \quad (4.9)$$

Where C' is a dimensionless constant, and d is the characteristic dimension of the packing. If the structured packing is geometrically similar, as the case with expamet, then the characteristic dimension of the packing (d) is inversely proportional to the specific surface area of the packing (a) (Note: $a = 2132\ m^2/m^3$).

A dimensional acceleration is defined as the ratio of rotor acceleration to the gravity.

$$N_g = \frac{r\,\omega^2}{g} \quad (4.10)$$

Substituting Equation (4.10) into (4.11) yields:

$$C = A\, a^{-0.25}\, N_g^{\ 0.25} \quad (4.11)$$

Equation (4.5) can be used to calculate C. Then, varying C with N_g as shown in Figure 4.9 in order to calculate the exponent of N_g. The slope of the line is 0.22 and that corresponds to 13% deviation from the initial value. In addition, the value of constant A can be calculated and it equals 2.29.

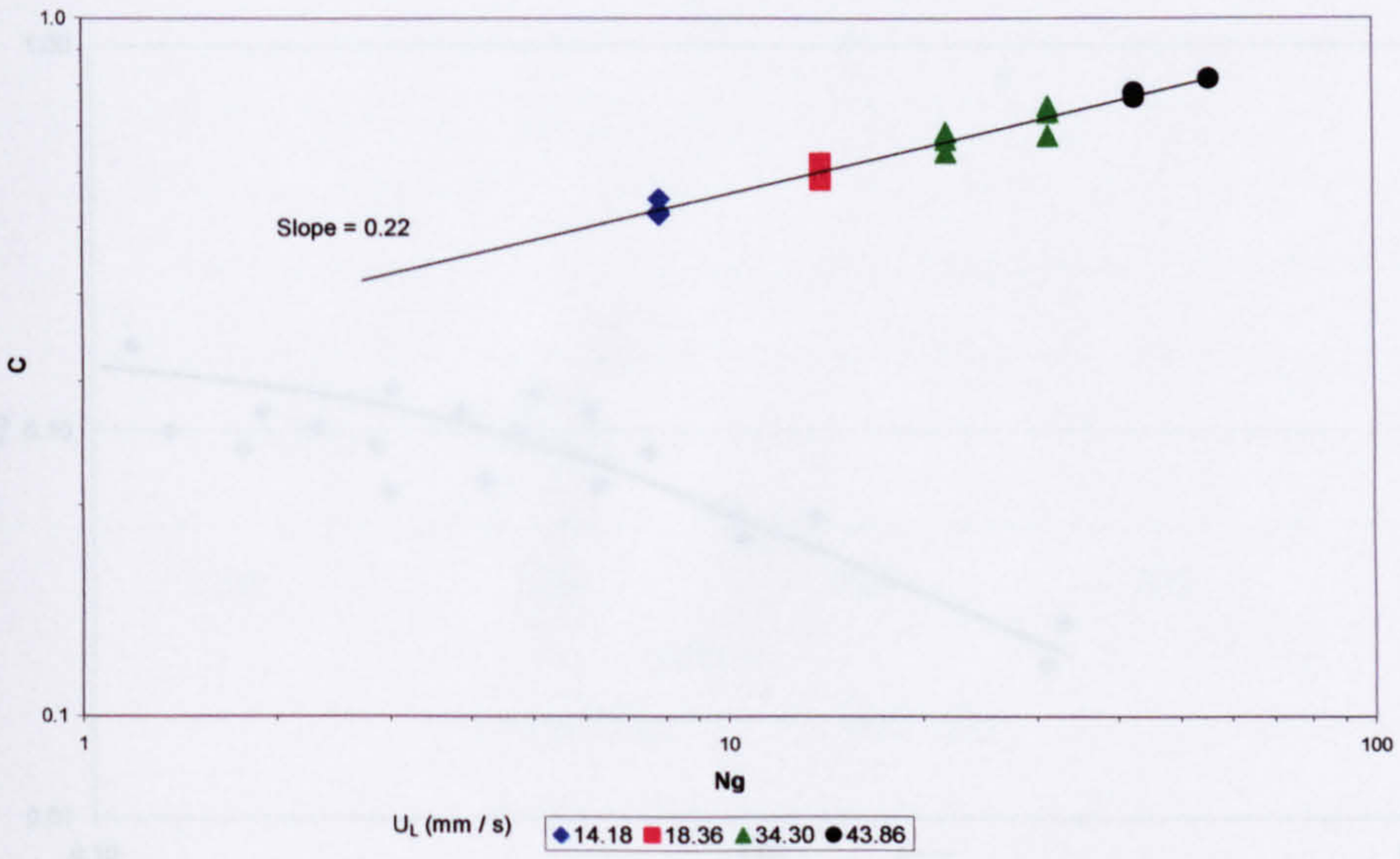

Figure 4.9: Variation of C with N_g

The value of the exponent on (a) is assumed to be –0.25 as there is no available data to investigate the variation of C with (a).

Therefore, the Wallis equation that could be used to predict the flooding behaviour in the expamet packing in the rotating beds is:

$$C_G^{0.5} + 2.058\, C_L^{0.5} = 2.29\ a^{-0.25}\ N_g^{0.22}\ \mu^{-0.03} \qquad (4.12)$$

The viscosity term is added as a minor correction and it is the ratio of the liquid viscosity to that of water at 70°F. The viscosity of water is 10 cP and the viscosity of 30 wt% MEA solution is 2.8 cP and hence the correction factor is 1.04.

(Lockett, 1995) correlated a relationship between Sherwood and Wallis flooding representations. Equation (4.13) shows such relationship, which varies C_G with $\frac{L}{V}\sqrt{\frac{\rho_G}{\rho_L}}$ and the flooding data are plotted in Figure 4.10.

$$C_G = \left[\frac{2.29\ a^{-0.25}\ N_g^{0.22}\ \mu^{-0.03}}{1+2.058\left(\frac{L}{V}\left(\frac{\rho_G}{\rho_L}\right)^{0.5}\right)^{0.5}}\right]^2 \qquad (4.13)$$

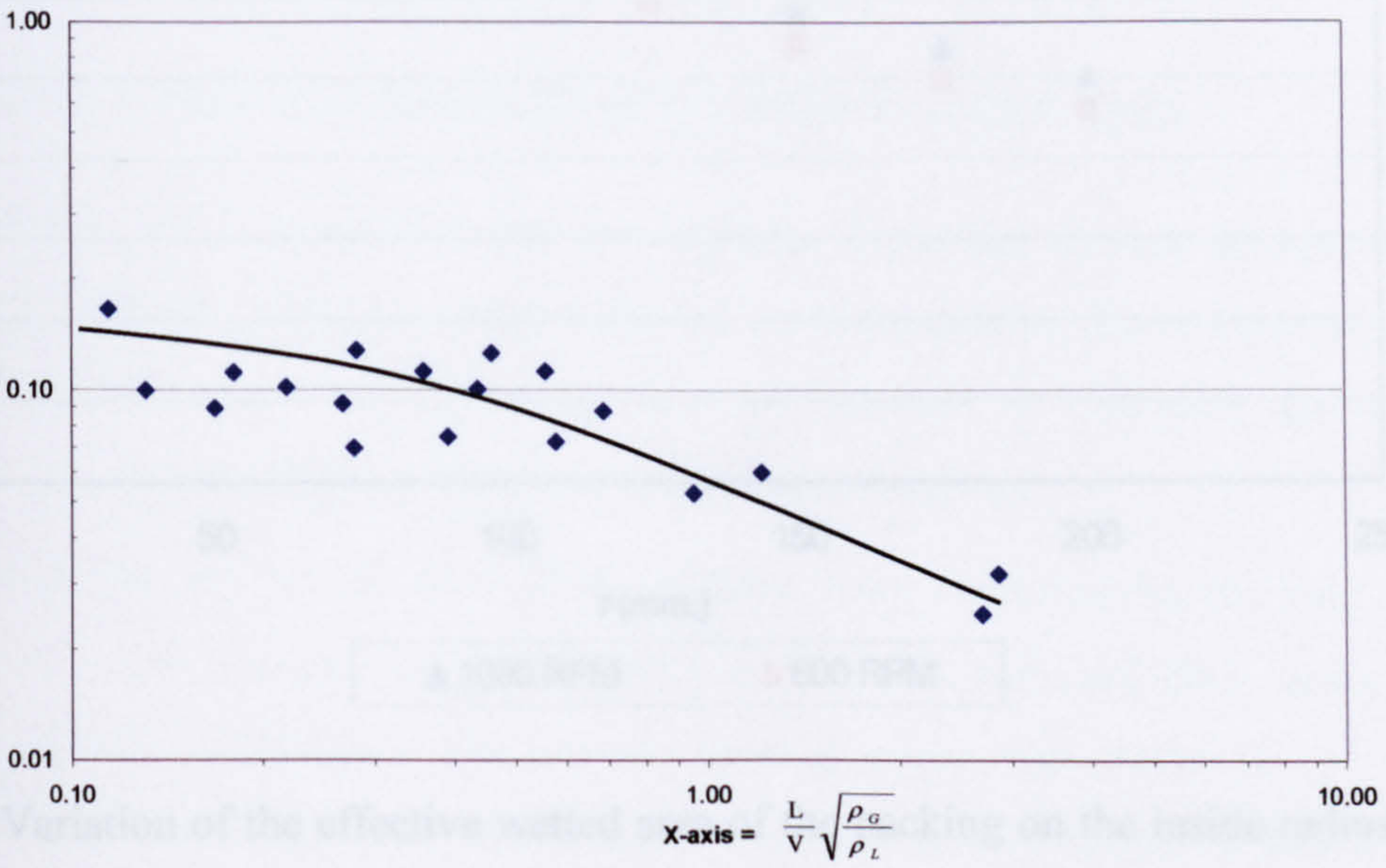

Figure 4.10: Sherwood-Wallis flooding plot.

Equation (4.13) shows that Sherwood and Wallis correlations are closely related. However, it is thought that Wallis method is a better way of representing flooding data because the data are organized in straight lines, which makes it easier to remove outliers.

4.3.4 The Effective Wetted Area of the RPB.

The purpose of this section is to illustrate theoretically the profile of the effective wetted area (a_w) with the divergence of the ethanolamine solution through the cross section of the packed bed. (Onda et al., 1968) correlation is utilized to predict the effective wetted area of the conventional packed bed. Appendix F shows the necessary modifications to Onda's correlation in order to be applied for the RPBs. The wetted area is assumed to be similar to the effective interfacial area in the Higee due to its small packing sizes (Kelleher and Fair, 1996).

Figure 4.11 shows that the effective wetted area of the RPB decreases with the increase in the radius of the RPB. The outer radius of the packed bed is approximately 17% less wet than the inside radius. Furthermore, the correlation shows that the RPB is wetter at higher rotor speeds. However, (Munjal et al., 1989) explained the reasons for the Onda's correlation for gravity flow to under-predict the effective gas-liquid interfacial area for rotating beds.

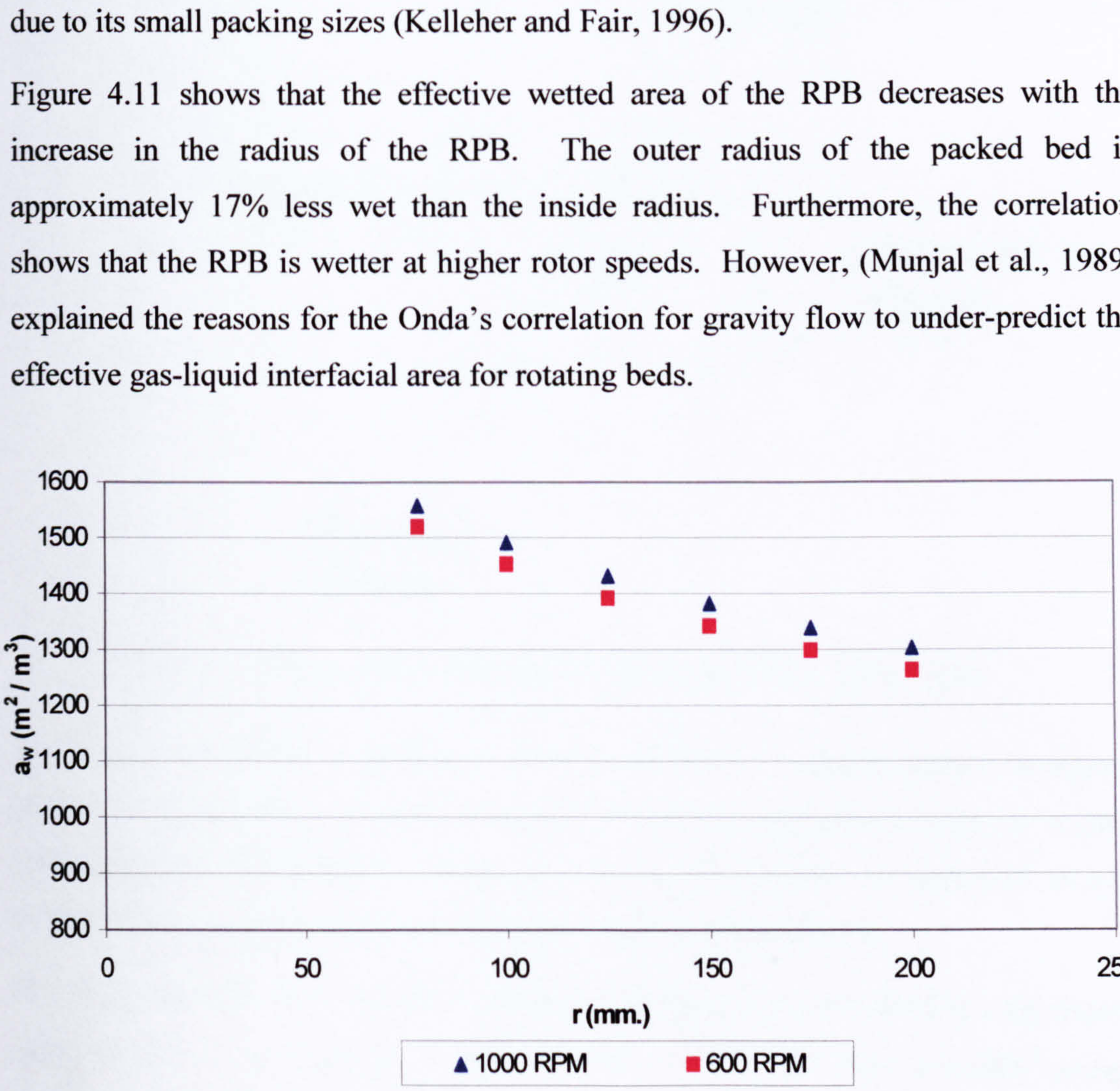

Figure 4.11: Variation of the effective wetted area of the packing on the inside radius and the RPM.

CHAPTER 5

Method of Analysis and Solubility Experiments

5.1 Introduction

Figure 5.1 shows the components of the mass balance that should be analysed accurately. Therefore, it is vital to measure the concentration of carbon dioxide in the sour/sweet gas samples and the concentration of carbon dioxide in the ethanolamine solution.

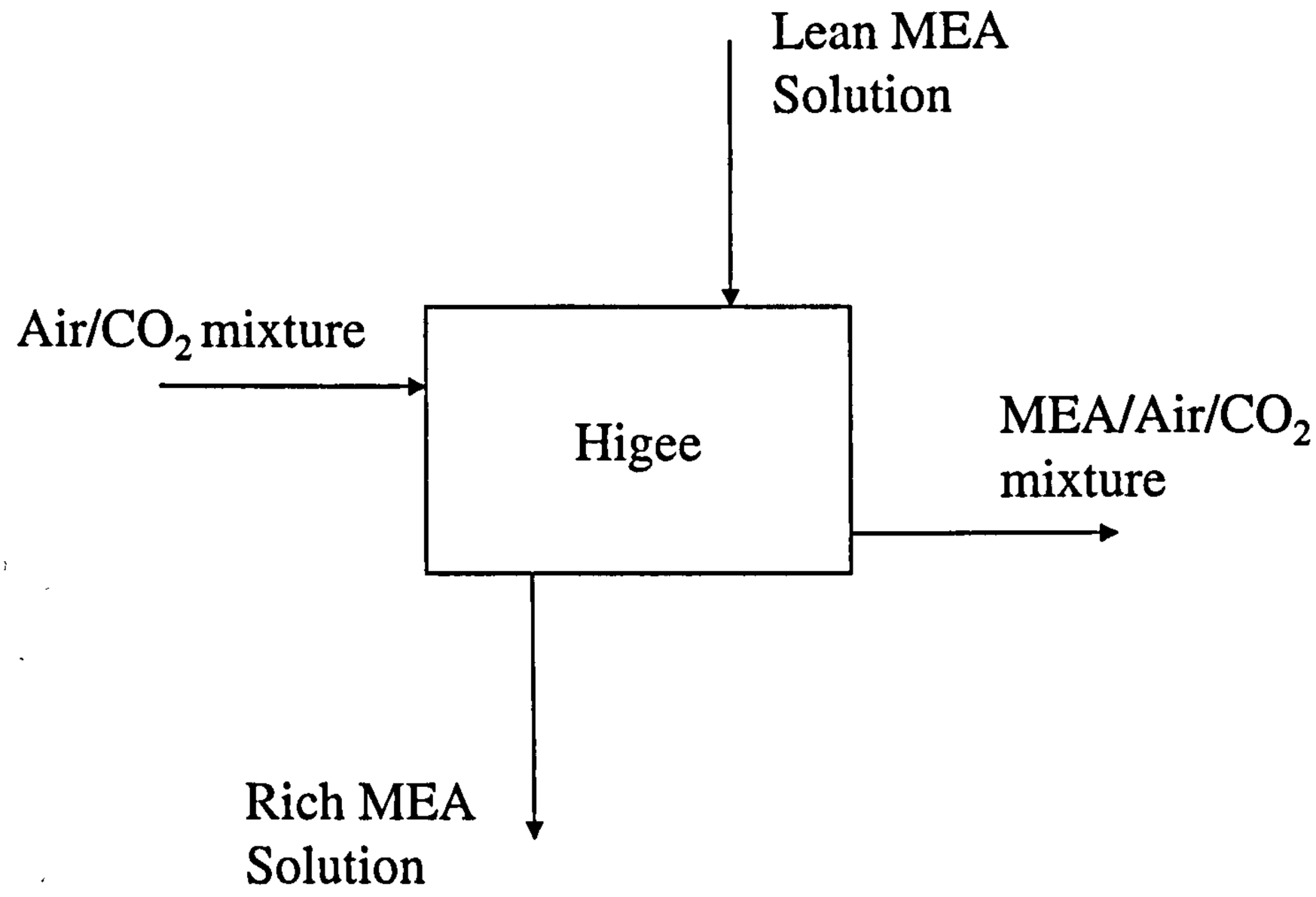

Figure 5.1: Mass balance across the Higee rig for absorption cycle.

There are three ways to determine the concentration of carbon dioxide in aqueous ethanolamine solutions: physical, indirect and gas chromatography. Early co-workers used chemical and indirect methods but with the advance in chemical analysis technologies gas chromatography became another popular option.

The CO_2 solubility data for 30 wt.% MEA solution were measured for the loading range of 0.2-0.3 mol carbon dioxide/mol MEA at 25°, 40°, 60°, and 80°C using a simple equilibrium technique. The chosen loading range was based upon the industrial interest. In addition, the results of the experiments were modelled and then

compared against (Jou et al., 1995) solubility data as most of the solubility data for other investigators were at higher loading ranges.

5.2 Determination of the carbon dioxide concentration in an aqueous ethanolamine solution

5.2.1 Chemical Methods

This section reviews the titration and analytical methods applied to determine the concentration of carbon dioxide in ethanolamine solution.

(Mason and Dodge, 1936) tried unsuccessfully to apply titration methods to determine the amount of carbon dioxide in the ethanolamine solution. Therefore, another analytical technique was considered. It was based upon acidifying the heated solution, then absorbing the evolved carbon dioxide by ascarite[1].

Figure 5.2 shows the Modified Knorr's method to determine the amount of carbon dioxide in carbonates. The carbon dioxide is evolved from the carbonates by an acid then absorbed by caustic and weighed (Furman, 1962).

(Jones et al., 1959) determined the concentration of carbon dioxide in aqueous monoethanolamine by two methods: precipitation as carbonate with barium chloride or modified Knorr procedure. The latter method involves the acidification of the sample with sulphuric acid then the solution was heated in order to evolve carbon dioxide. After that, carbon dioxide was swept from the reaction vessel with nitrogen and then passed over a tube containing a CO_2 absorbent. The results obtained using the modified Knorr method were preferred because the precipitation method gave lower amounts of carbon dioxide at higher gas loadings due to the formation of carbamates.

(Jeffery and Kipping, 1962) developed a gas-chromatographic method for determining the concentration of carbon dioxide in rocks and minerals; and its results were in good agreement with those obtained by the traditional methods. It was then further developed in order to determine the concentration of carbon dioxide in

---

[1] Ascarite: Sodium hydroxide-asbestos preparations, used as absorbent for carbon dioxide (Bennett, 1986).

ethanolamine solutions. The CO_2-MEA mixture was boiled with a diluted orthophosphoric acid and the reaction liberates carbon dioxide. The gas was then passed to a gas chromatograph in order to detect its concentration with a thermal conductivity cell. However, it was necessary to calibrate the instrument with each new batch of samples because of continuous deterioration to the chromatographic column.

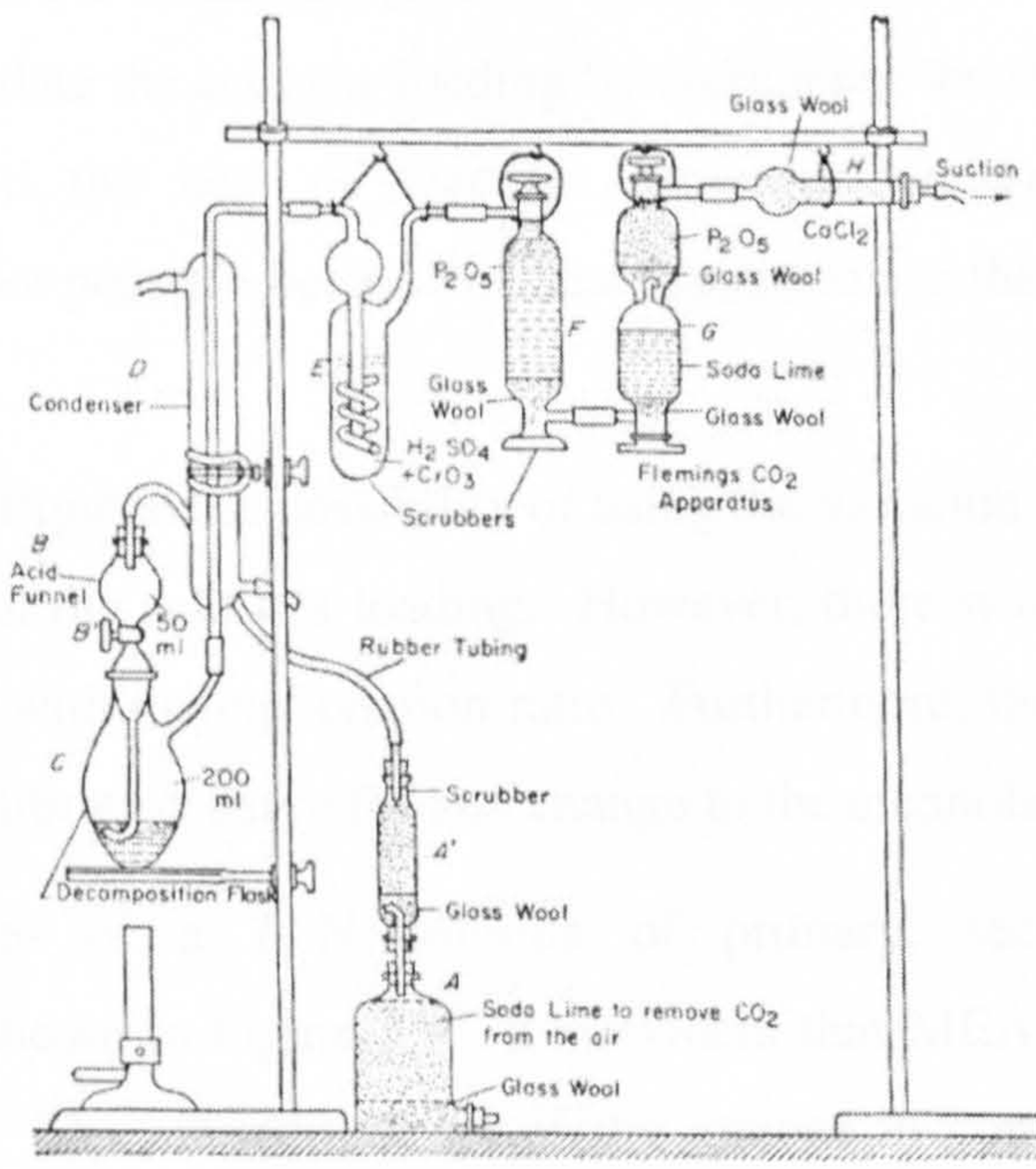

Figure 5.2: Modified Knorr Method

(Jou et al., 1995) used a precipitation-titration method to analyse the liquid sample. The aliquot was added to 0.1 mol/dm^3 $BaCl_2$ in order to precipitate the carbonate as $BaCO_3$. After two days of aging in order to allow $BaCO_3$ particles to agglomerate, the mixture was filtered and then washed with distilled water until the pH of the filtrate was 5.0-5.6. Then, the distilled water was added to the precipitate and it was titrated against 0.1 mol/dm^3 HCl.

The limitations of the above methods are: the analysis time is long and could take in excess of two days, the potential need for a large liquid sample, and the need to be careful with small details as a slight error in the experimental procedure could produce a larger error in the results.

5.2.2 Indirect Methods

The direct methods depend on finding a physical property of the ethanolamine solution that could vary in a sensible way during carbonation. The potential properties were: viscosity, refractive index, surface tension, specific gravity, pH, and electrical conductivity. (Atadan, 1955) concluded that the deviation for most of these properties was small with the increase of carbonation.

The reaction between the ethanolamine and carbon dioxide is exothermic. Therefore, it is possible to calculate the acid gas loading by correlating the rise in the temperature of the solution and the heat of reaction. However, accurate measurement of temperature rise is not possible because of heat dissipation to the gas phase and to the equipment.

(Moore, 1986) investigated the possibility of using the variation of refractive index as a tool for finding out the acid gas loading. However, there was a small variation of the refractive index with the carbonation ratio. Furthermore, there was the necessity to produce a new calibration curve for any change to the ethanolamine solution.

The titration curves of a 2 N solution of primary, secondary and tertiary ethanolamines are shown in Figure 5.3. It is evident that MEA has higher alkalinity than other amines. The smooth curves of the amines in comparison to the KOH solution were due to the presence of non-ionized species (Kohl and Nielsen, 1997). Furthermore, the pH was reduced from 12.8 to 9.1 when the loading was increased from 0 to 0.5 mol CO_2/mol MEA. In addition, Figure 5.4 shows that the pH decreases as the temperature rises. The pH was reduced from 12.5 to 11.9 when the temperature increased from 70°F to 130°F. Similarly, the disadvantage is the need to calibrate for each different ethanolamine solution composition.

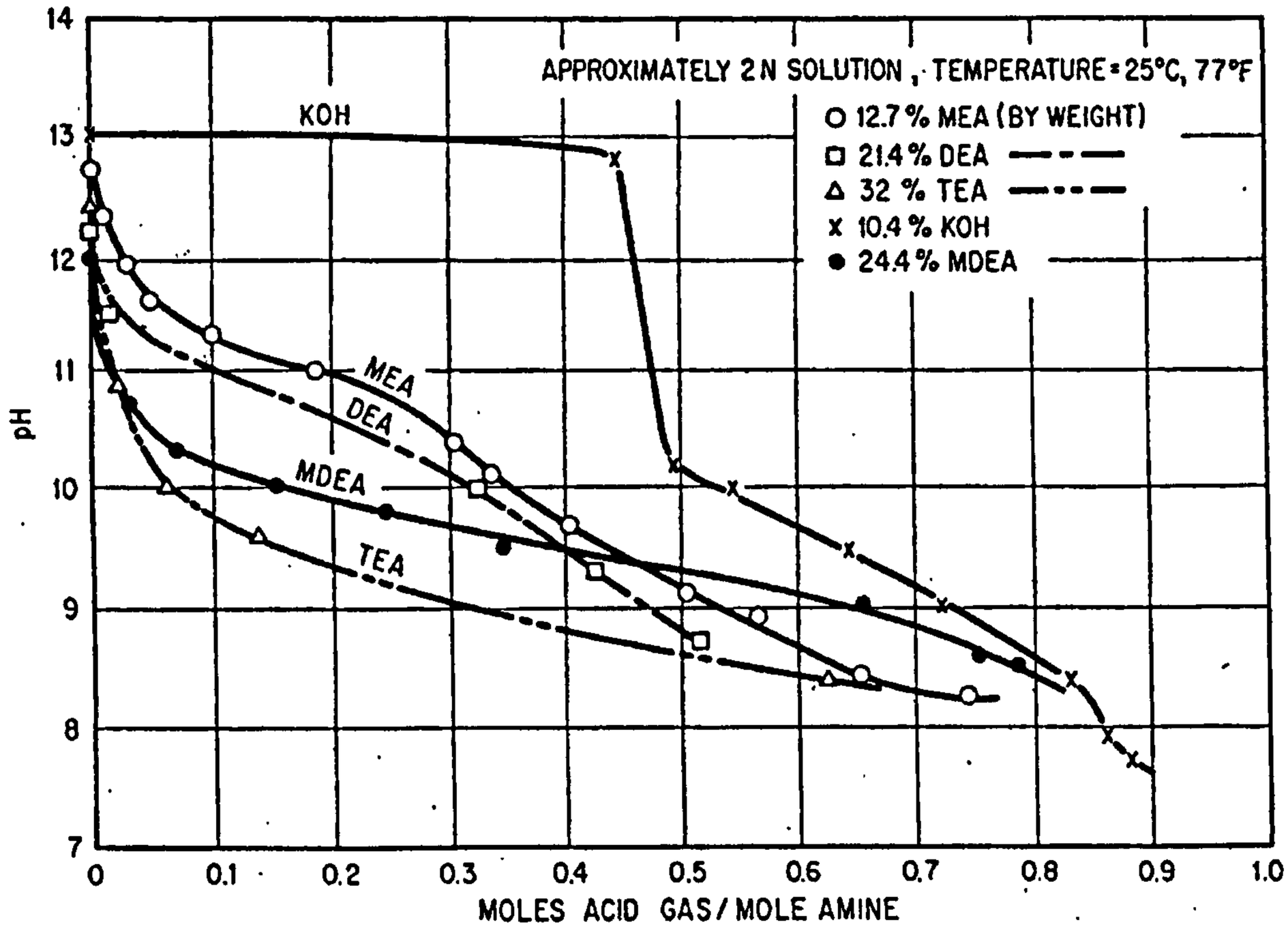

Figure 5.3: Variation of pH with acid loading for different amines and KOH.

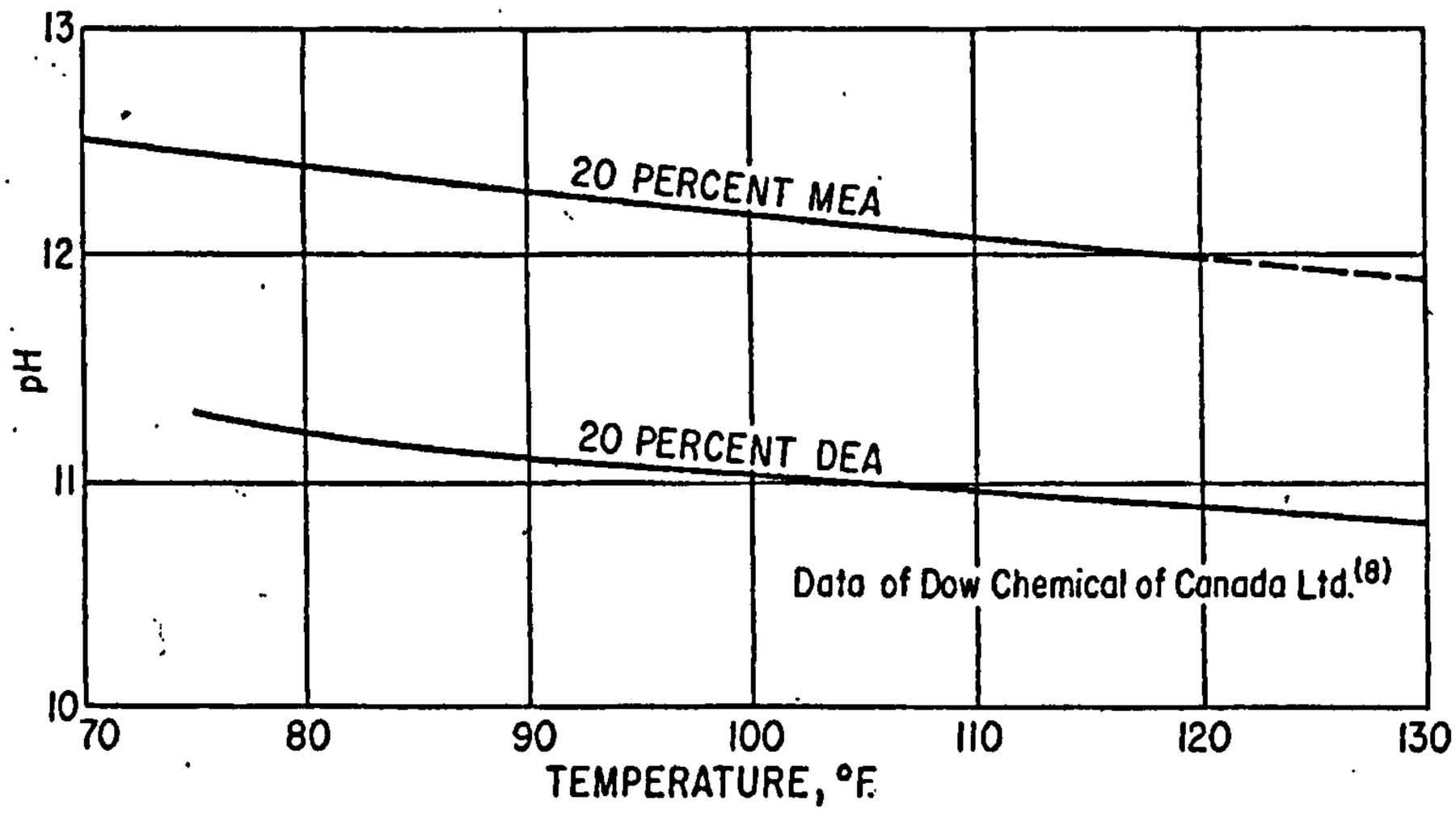

Figure 5.4: Variation of pH with temperature for 20wt% MEA and DEA.

5.2.3 Gas Chromatography

This method was introduced in 1950s and since then it has became a popular technique for the analysis of liquid and gas samples because it provides on-line detection of the eluted species, high resolution; and produces fast, repeatable and reliable results.

(Pearce et al., 1993) described the operating conditions of a Hewlett-Packard Model 5880 chromatograph used by The Dow Gas Conditioning Laboratory. A 1 μL liquid solution was injected into the sample port. The carrier gas was helium and two different columns were used to detect alkanolamine and carbon dioxide by a thermal conductivity detector. However, hydrochloric acid was injected every fourth sample in order to pretreat the carbon dioxide column and another pre-treatment method was used for the alkanolamine column in order to obtain repeatable results. (Moore, 1986) applied similar operating conditions for his PhD work on carbon dioxide absorption by diethanolamine solution.

(Jou et al., 1982, Jou et al., 1993, Jou et al., 1995) had performed solubility experiments in alkanolamine solutions at different temperatures, pressures, and concentrations. The equipment and procedures for their experiments changed over the years. As shown in Table 5.1, a comparison is made between the current investigation gas chromatograph and (Jou et al., 1995).

Table 5.1: Comparison between the GCs' used by Jou *et al.* (1995) and the current investigation.

	Jou *et al.* (1995)	Current Investigation
Column	1.63 m * 3.175 mm Stainless steel packed column of chromosorb 104	Refer to Table 5.3.
Detector	TCD	FID
Oven temperatures Injection port Column Detector	 300°C 250°C 200°C	 375°C 100-150°C 250°C
Carrier gas, flowrate	He, 22 cm^3/min.	He, 10.8 cm^3/min.
Injection volume	5 µL	0.2 µL
Retention time CO_2 H_2O MEA	 0.44 min 1.04 min 8.20 min	 4.28 min. - 7.02 min

5.3 Analysis Method: Gas Chromatography

Figure 5.5 shows a schematic diagram of the gas chromatography developed by Unicam Chromatography (UK) to detect the concentration of carbon dioxide in the gaseous phase and the concentration of carbon dioxide and ethanolamine in the aqueous solution.

The retention time of the liquid and gas samples were 10 minutes and the results were accurate and repeatable. In addition, only 0.2 μL of liquid sample and 10mL gaseous sample were required.

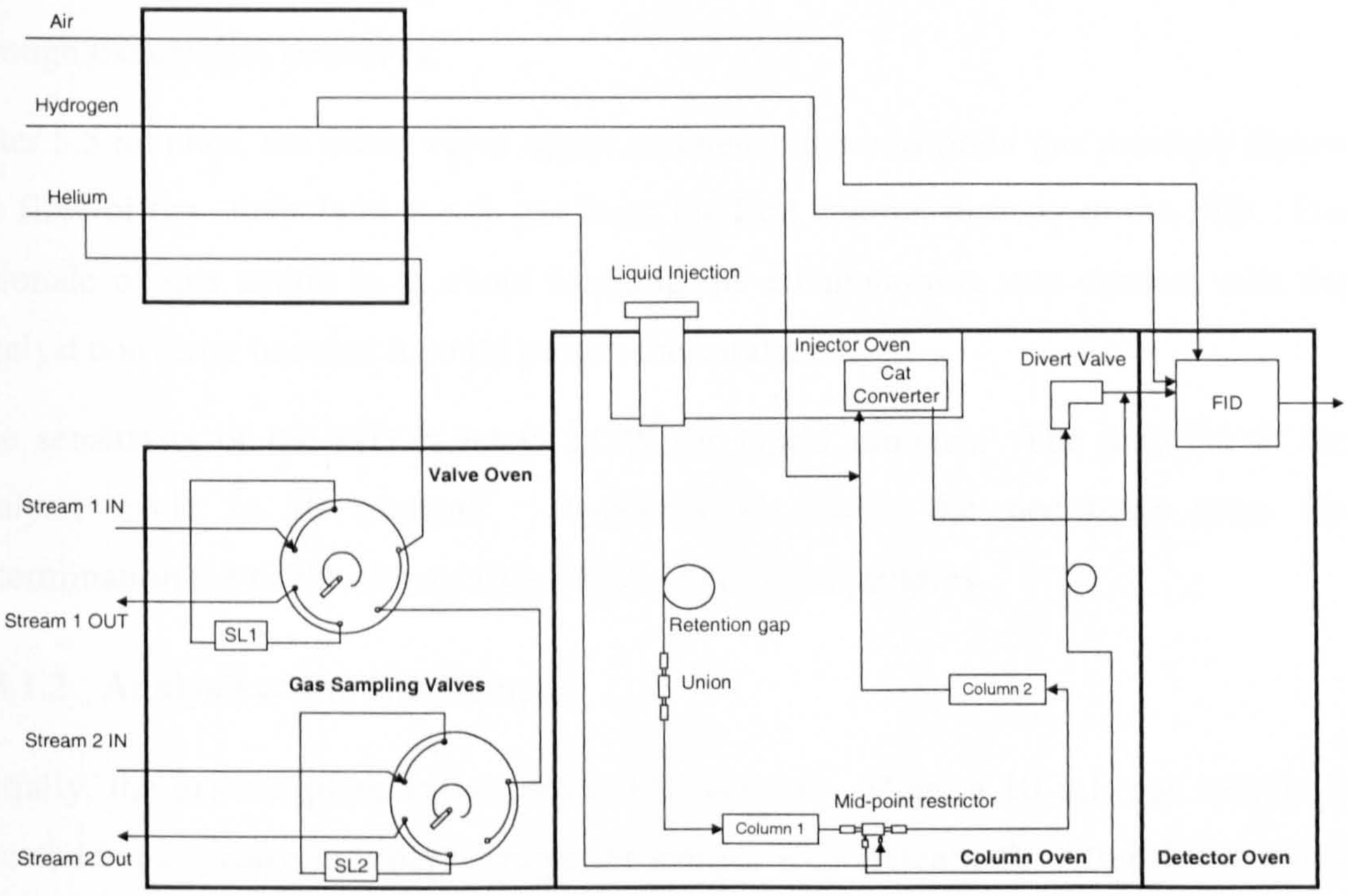

Figure 5.5: Schematic diagram of the gas chromatography

5.3.1 Description of the Process

5.3.1.1 Analysis of the Liquid Sample.

A total volume of 0.2 μL liquid sample is injected manually through a rubber septum into the sample injector port with the aid of a 1 μL Hamilton syringe. The barrel of the syringe is made from glass and the needle is stainless steel. The entire sample is contained in the needle (Harris, 1991). The liquid sample is vaporized in the injector

port as the temperature of the injector oven reaches 375°C. The operating conditions of the process are shown in Table 5.2.

The gaseous sample is then mobilized through the first column by helium. Both carbon dioxide and air (O_2, N_2) will diffuse through the first column much faster than the ethanolamine. The second column separates carbon dioxide from air. Both columns operate at 100°C and their details are shown in Table 5.3.

Carbon dioxide is then catalytically converted to methane using hydrogen. A Flame Ionization Detector (FID) detects the organic gas (methane). The divert valve is closed during this stage thus forcing the flow of carbon dioxide towards the FID through the catalyst converter.

After 5.5 minutes, the divert valve opens and hence the mid-point gas pressure directs the flow of the ethanolamine-rich gas from the first column directly to the FID. The rationale of this action is to avoid bringing the ethanolamine into contact with the catalyst converter because it could poison the catalyst.

The sensitivity of the FID is set to LOW for liquid samples. The duration of the analysis cycle is 10 minutes. Appendix G shows the necessary steps for determination the calibration of CO_2-MEA-H_2O liquid samples.

5.3.1.2 Analysis of the Gas Sample.

Initially, the gas sampling valves are in fill position. Then, a 10 mL gas sample is injected via a syringe in order to purge the sample loop (stream 2). After that, another 10 mL gas sample fills the sample loop, which is then brought inline with the carrier stream.

The combined gaseous mixture is then flushed onto column 1 while the divert valve is closed. The carbon dioxide elutes from column 1 through column 2 to the catalytic converter where it is converted to methane and detected by the FID. Finally, the ethanolamine (if present) reaches the end of column 1 then the divert valve opens and ethanolamine elutes via the valve to the detector.

The sensitivity of the FID is set to MEDIUM and the duration of analysis cycle is 10 minutes. Appendix H shows the calibration steps for CO_2-air sample.

Table 5.2: Operating conditions of GC.

Detector Oven Temperature	250°C	Polarity	REAR
Injector Oven Temperature	375°C	Backing Off	+
Auxiliary (Valve) Oven Temperature	150°C	Output	1 Volt.
Column Oven Temperature	100°C	Ramp 1	25°C/min
Initial Time	1 min.	Upper Time	8 min.
Upper Temperature	150°C		
FID Amplifier Settings - Methods 1 and 3 - Method 2	 LOW MED		

Table 5.3: Details of the column 1 and column 2.

	Column 1	Column 2
Tubing Material	Fused Silica	Silcosteel
Length	25 m	1 m
Diameter	0.53 mm (ID)	1/8" O.D.
Stationary Phase	CP Wax for Amines	Carbosieve S-II 80-100 mesh
Film Thickness	2.0 μm	
Activate/Preheat	200°C	225°C
Preheat time	2hrs	16hrs

5.3.2 FID (Flame Ionization Detector)

Figure 5.6 shows a schematic diagram of a typical FID. The effluents from column 1 and 2 are mixed with hydrogen and air before being burned in the FID. The carbon atoms of organic materials (methane and MEA) produce CH radicals that are ionized in a hydrogen-oxygen flame.

$$CH + O \rightarrow CHO^{+} + e^{-}$$

The Hydrogen flame contains a significant amount of free electrons due to the ionization and the flow of electrons causes hydrogen flame to have an electrical conductivity. The electrical conductivity of a hydrogen flame is small but with the introduction of organic vapours it increases and can be recorded (Littlewood, 1970).

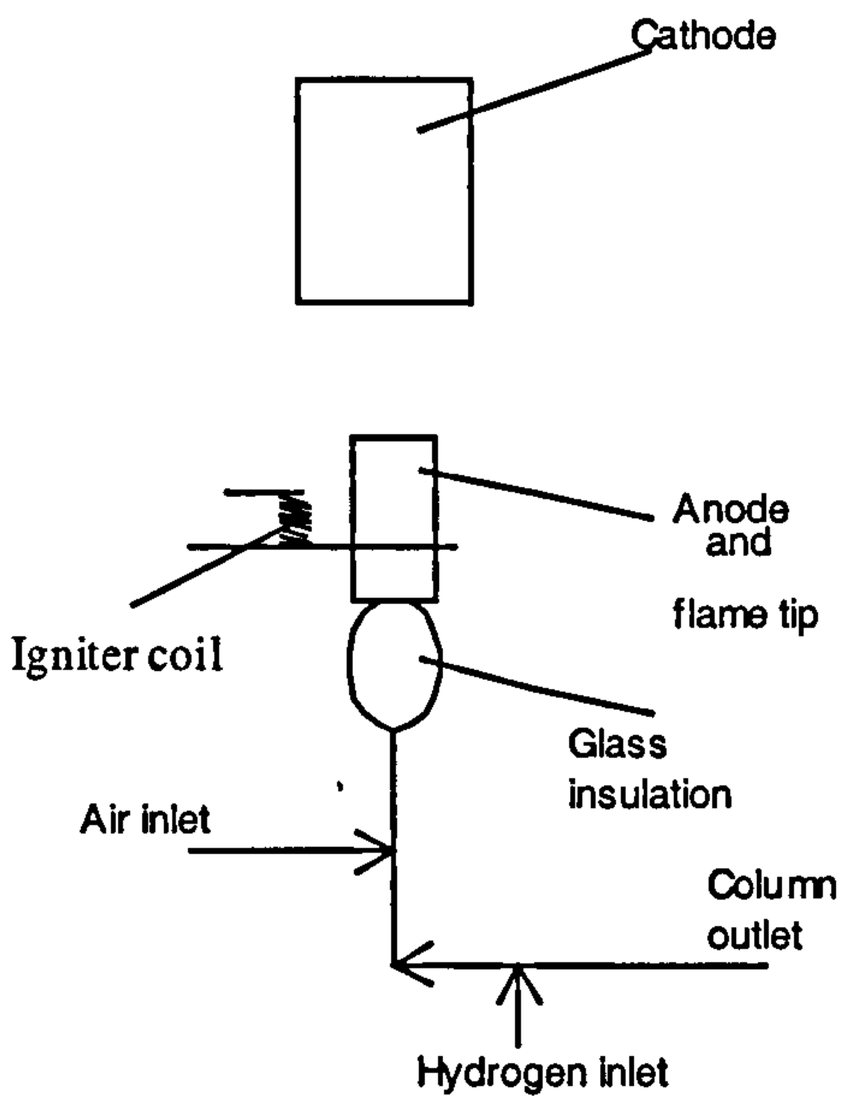

Figure 5.6: Main components of the FID

A FID is insensitive to inorganic compounds such as: H_2O, CO_2, and O_2. In addition, the sensitivity of the FID is two orders of magnitude more than the Thermal Conductivity Detector (TCD).

5.3.3 The Carrier Gas

The mobile phase chosen for the process is helium. It provides good resolution at high flowrates (10.8 ml/min) due to rapid diffusion of the solutes through it. In addition, helium enhances rapid equilibrium between the mobile and the stationary phases in the columns and hence achieves a smaller H.E.T.P. (Harris, 1991).

5.3.4 GC output

Figure 5.7 shows a typical output signal from the FID detector to the liquid solute concentration. The chromatogram shows two components: the small peak on the left represents carbon dioxide and it has a 4 minutes retention time. The second peak represents monoethanolamine and it has a retention time of 6.5 minutes.

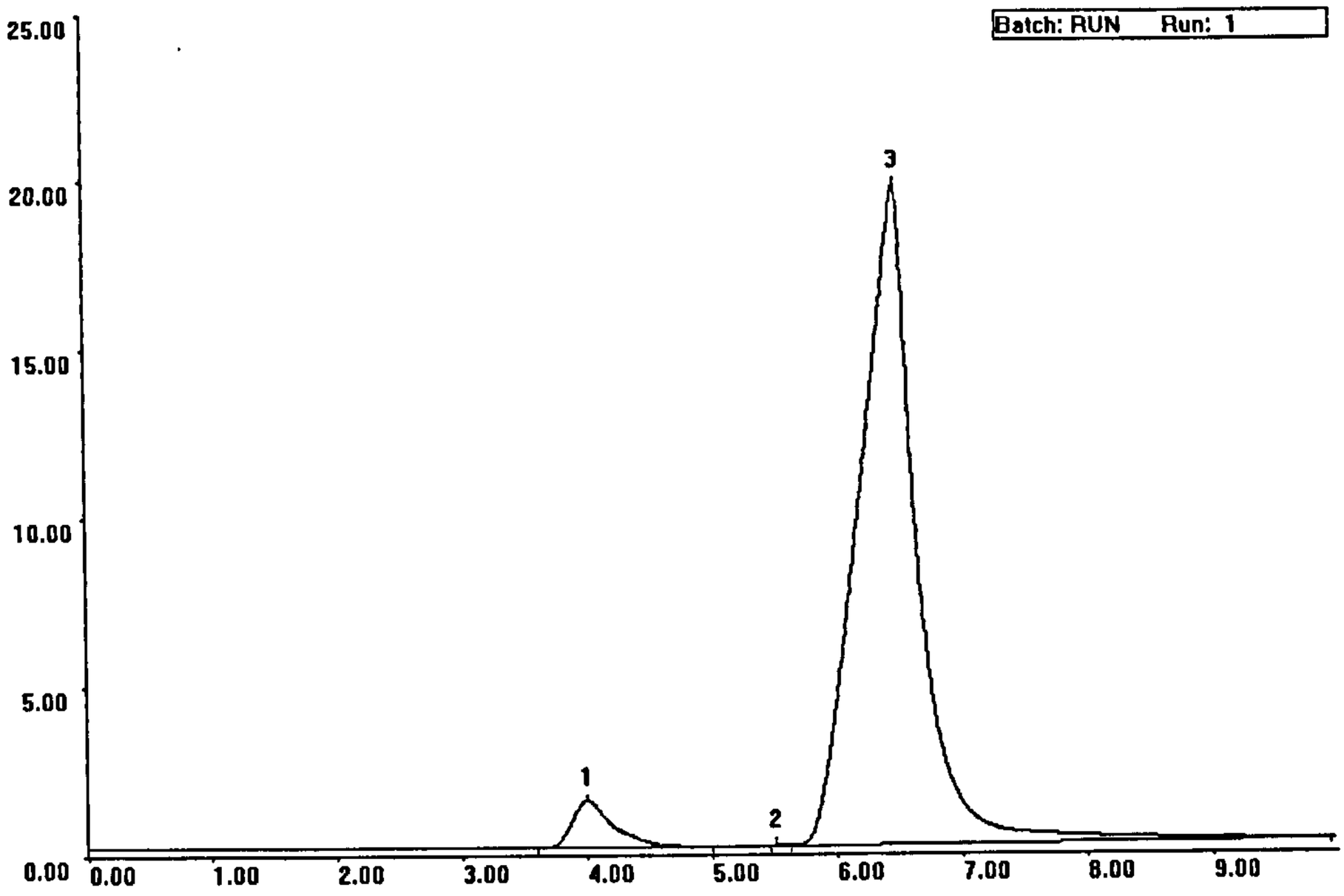

Figure 5.7: A typical chromatogram for CO_2 and MEA peaks in liquid sample.

5.4 Solubility Experiments

5.4.1 Introduction

The solubility data determine the maximum amount of the gas species that the reactive liquid can absorb under specific conditions of temperature, pressure, and concentration. In addition, it estimates the driving force when calculating the rate of absorption.

The equilibrium solubility data of CO_2 in ethanolamine solutions are mostly for low amine strength (<30wt%) due to the use of low amine concentrations in the industrial applications in order to avoid corrosion problems in mild steel equipment. However, higher concentrations are possible nowadays due to the use of stainless steel and corrosion inhibitors.

5.4.2 Literature Review

(Mason and Dodge, 1936) presented carbon dioxide equilibrium data in MEA solutions (3, 12, 30, 56, and 74 wt%) at temperatures of 0°, 25°, 50°, and 75°C and at partial pressures of carbon dioxide ranging from 1.38-99.85 kPa. A curve fitting method was used to correlate the data. The equilibrium data relevant to this research are shown in Appendix J.

(Atadan, 1955) extended the earlier solubility data to a wider range of operating conditions: 0-600 psia, 0-75°C, and 0.5-12.5N MEA. In addition, he proposed a solubility equation:

$$s = Q P^m \qquad (4.1)$$

where s is the solubility (mol CO_2/mol MEA), P is the partial pressure of carbon dioxide (psia), Q and m are parameters that depend upon the temperature and the strength of MEA(Table 5.4).

Table 5.4: Values of Q and m for (Atadan, 1955) equation.

Normality	Temperature °C	Q	m	Normality	Temperature °C	Q	m
2.5	30	0.525	0.137	7.5	30	0.457	0.106
	50	0.469	0.132		50	0.430	0.089
	70	0.371	0.140		70	0.405	0.069
5.0	30	0.387	0.154	10	30	0.566	0.031
	50	0.418	0.122		50	0.469	0.058
	70	0.375	0.125		70	0.421	0.058

(Jones et al., 1959) carried out solubility experiments for acid gases in MEA solution (15.3 wt%). In short, a 500 in^3 stainless steel equilibrium vessel containing 2 L of 15.3 wt.% MEA solution was held in a thermostatic oil bath and rocked for 2 hours in order to establish equilibrium. The solubility data were in good agreement with those obtained by (Mason and Dodge, 1936).

(Deshmukh and Mather, 1981) developed a thermodynamic model for the solubility of CO_2/H_2S in alkanolamine solutions for a wide range of temperatures, partial pressures and concentrations. The model incorporates both the dissociation of electrolytes in the aqueous solution and the vapour-liquid equilibrium of acid gas species (i.e. fugacities and activity coefficients). The model was in a good agreement with the experimental data of CO_2/MEA system at all temperatures and normalities.

As part of their solubility experiments, (Lee et al., 1974) studied the solubility of CO_2 in 30wt% MEA solution at 40° and 100°C. The partial pressure of CO_2 was ranging from 0.167 – 959.6 psia. Similarly, (Shen and Li, 1992) studied the solubility of CO_2 in 30wt.% MEA solution at temperatures of 40°, 60°, 80°, and 100°C; and at partial pressure of carbon dioxide ranging from 1.1 – 1975 kPa. The concentration of carbon dioxide was determined by titration and the gas chromatography technique was used to analyse the vapour samples. In addition, (Nasir and Mather, 1977) studied the solubility of CO_2 in 30wt% MEA solution at 100°C; and the partial pressure of carbon dioxide was ranging from 0.00214-2.96 kPa. The precipitation and titration method was used to analyse the liquid samples and gas chromatography was used to analyse

the gas samples. Furthermore, (Murrieta-Guevara et al., 1993) studied the solubility of CO_2 in 30wt.% MEA solution at 30°, 50° and 100°C and the partial pressure of carbon dioxide ranging from 1.5-2120.3 kPa.

(Jou et al., 1995) published a wide range of experimental solubility data of CO_2 in 30wt.% MEA solution at a temperature range of 0°, 25°, 40°, 60°, 80°, 100°, 120° and 150°C and the partial pressure of CO_2 ranging from 0.001-20,000 kPa (Jou et al., 1995). The liquid samples were analysed by both the precipitation-titration method and a chromatographic technique; and the gas sample were analysed by a gas chromatograph. Figure 5.8 shows the solubility of CO_2 in a 30wt.% MEA solution. Their experimental data was in good agreement with the model developed by (Deshmukh and Mather, 1981).

Figures 5.9, 5.10, 5.11 and 5.12 compare their results with the work of other researchers. Generally, it is evident from the Figures that their data are lower than the other solubility results. The deviation in Figure 5.11 was attributed to the method of analysis of the liquid sample by (Lee et al., 1974); and the noticeable deviation behaviour of the trend in Figure 5.9 was attributed to the use of unsuitable apparatus by (Nasir and Mather, 1977).

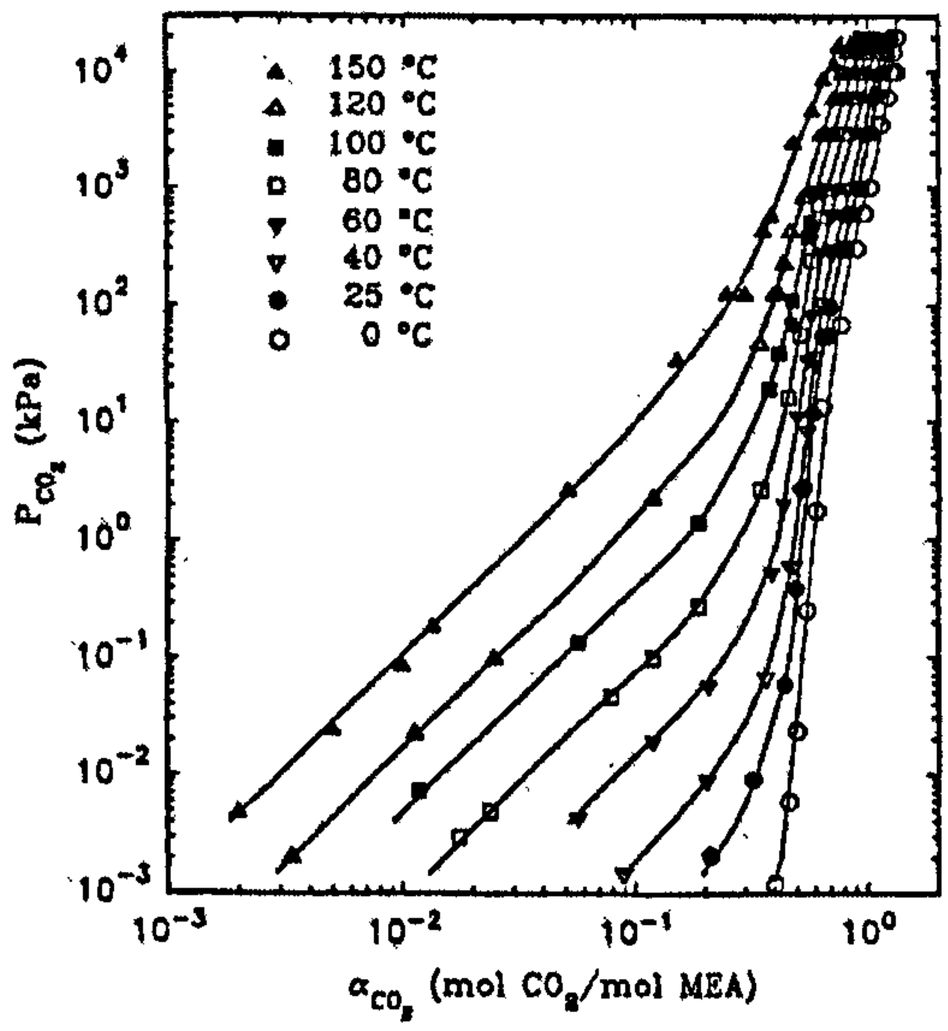

Figure 5.8: Solubility data for 30wt% MEA solution (Jou et al., 1995).

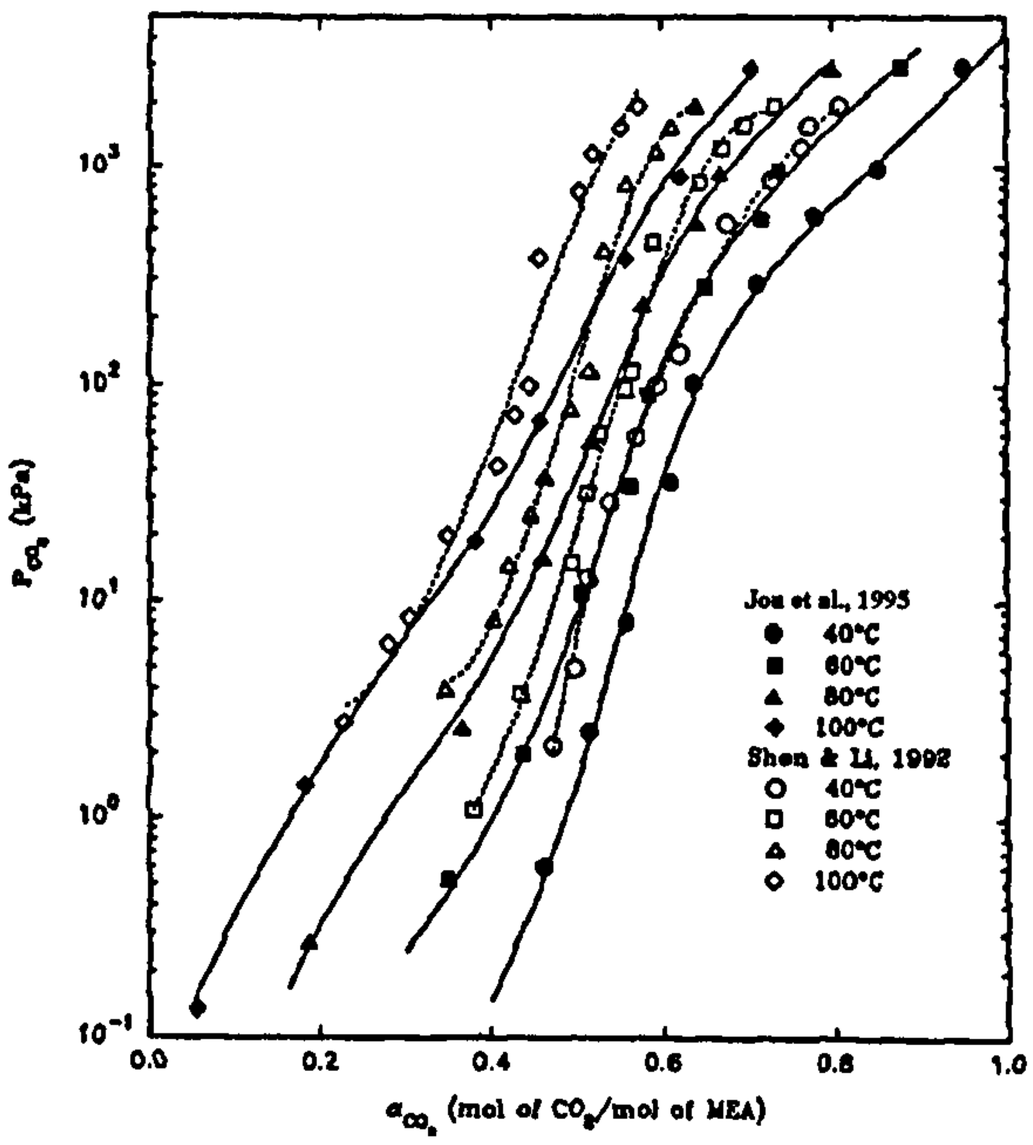

Figure 5.9: Comparison of solubility data of (Jou et al., 1995) against (Shen and Li, 1992).

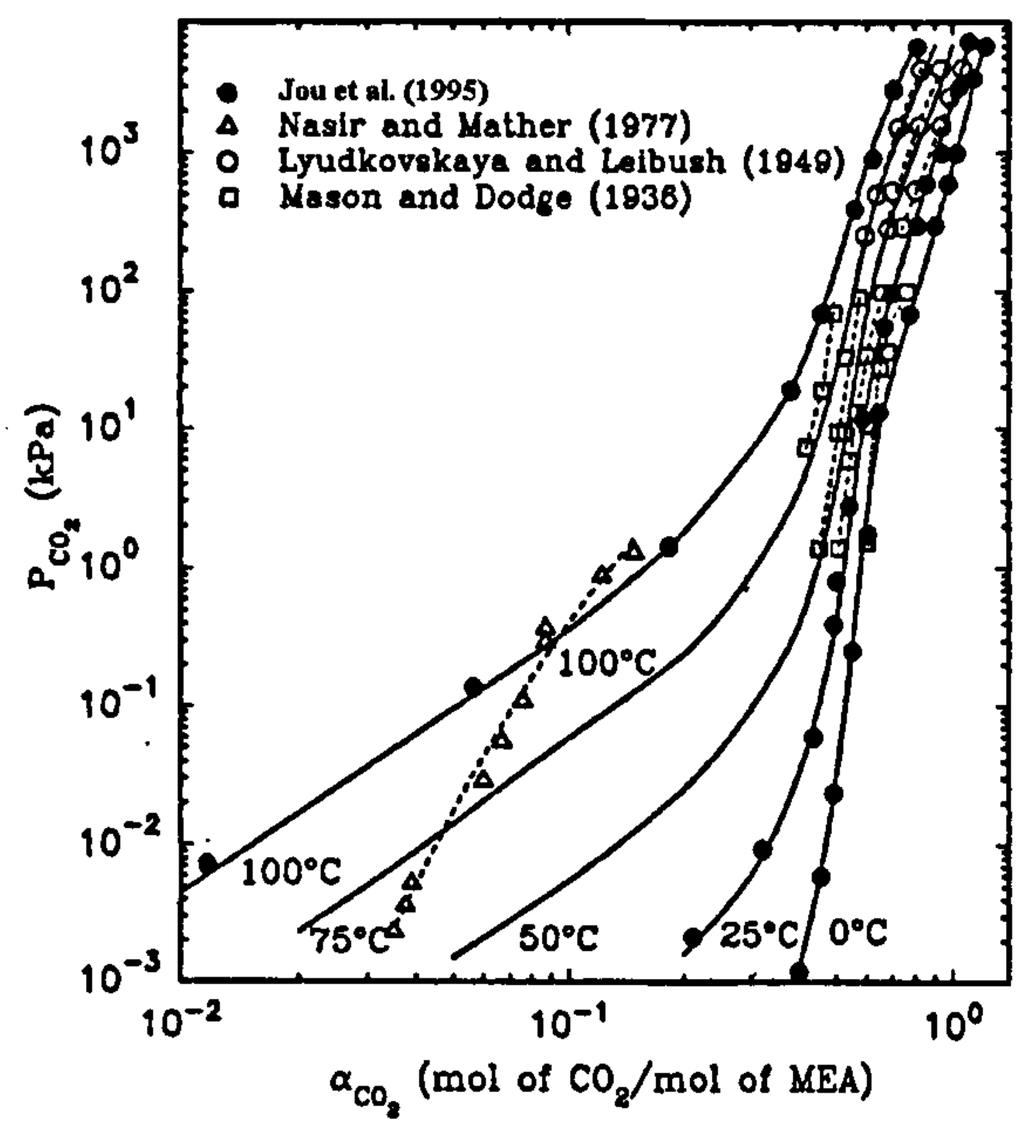

Figure 5.10: Comparison of solubility data of (Jou et al., 1995) against (Mason and Dodge, 1936) and (Nasir and Mather, 1977).

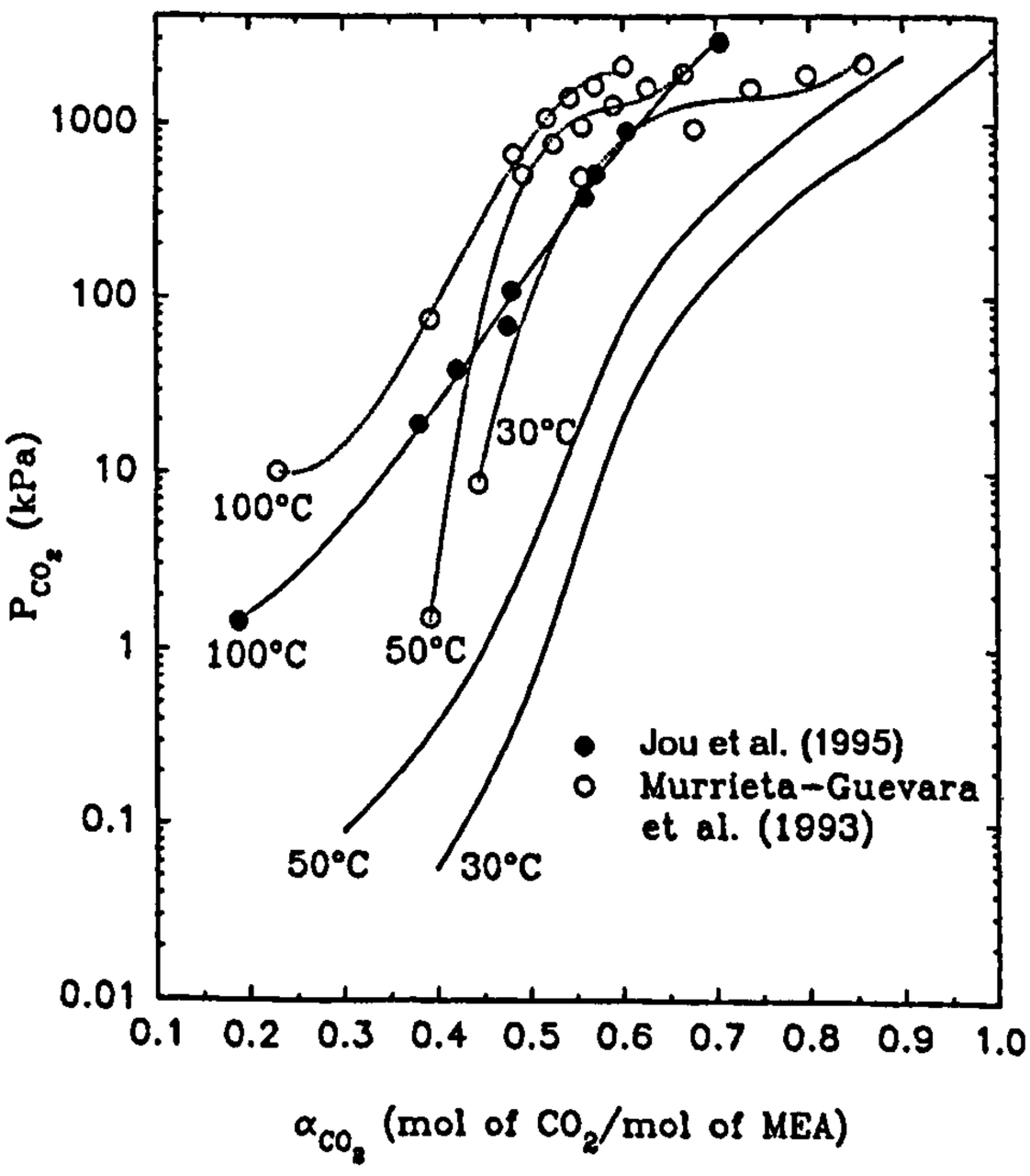

Figure 5.11: Comparison of solubility data of (Jou et al., 1995) against (Murrieta-Guevara et al., 1993)

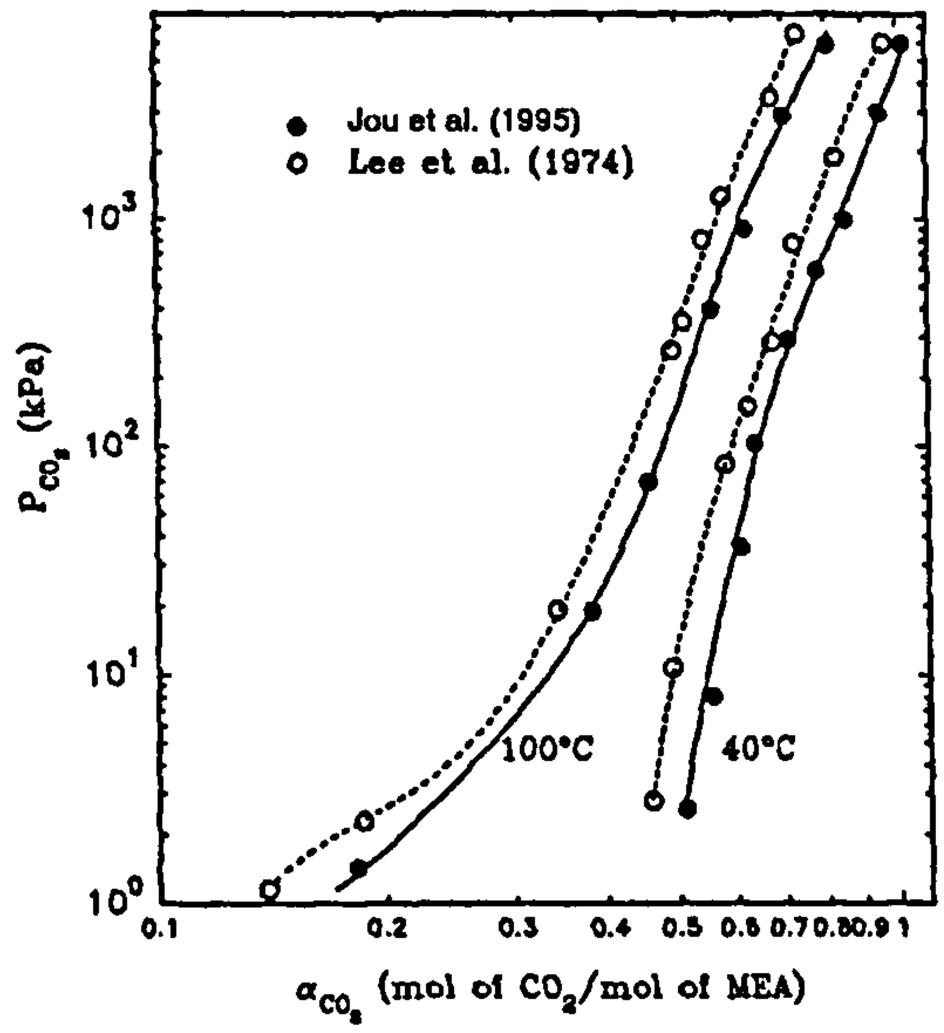

Figure 5.12: Comparison of solubility data of (Jou et al., 1995) against (Lee et al., 1974).

5.4.3 Solubility Experiments

5.4.3.1 Materials and Equipment

The amine solutions were prepared from distilled water and 99+ % strength analytical ethanolamine (Sigma). The MEA solution was made to the desired strength. Table G1 in Appendix G shows a comparison between the determination of amine strength by weight against titration with bromophenol blue indicator. The difference between the two methods was a mere 0.5%. Oxygen-free nitrogen (@ 175 bar, 15 °C) and a carbon dioxide cylinder with a capacity of 34 kg (@50 bar, 15°C) were supplied from BOC. The carbon dioxide is stored in liquid form; but due to its vapour pressure gaseous carbon dioxide is discharged from the cylinder.

The pre-saturator is a 250 mL glass flask, which is approximately half filled with distilled water. A glass leg was immersed inside the water and bubbles a uniform flow of CO_2/N_2 mixture. The flow of the gas mixture was controlled by two needle valves. The saturated gaseous mixture was then directed to the equilibrium vessel.

The 1 L glass equilibrium vessel is shown in Figure 5.13. There are 3 openings to the vessel. The gas mixture was allowed to enter the vessel through V1. The prepared MEA solution was injected into the vessel through V3 via a syringe. In addition, V2 was kept open during the loading of carbon dioxide into the ethanolamine in order not to pressurize the glass vessel.

The equilibrium vessel was rocked at a rate of 100 rpm for 24 hours in a shaker platform using Sanyo Orbital Incubator (Model IOX400.XX2.C). The equilibrium vessel was kept inside the incubator at a specific temperature environment. The maximum allowed temperature was 60°C.

For solubility experiments at 80°C, the equilibrium vessel was immersed in a water bath. Plastic balls were put afloat on the surface of the water in order to reduce its vaporization rate. The temperature in both the incubator and the water bath was controlled to ± 0.1°C.

5.4.3.2 Experimental Procedure

The calibrations procedures and charts for determining the concentration of carbon dioxide and ethanolamine in the liquid and gas samples are shown in Appendices G, H and I.

Figure 5.13 shows a schematic diagram for the preparation of the equilibrium vessel. Initially, the 1 L flask was purged with a saturated N_2/CO_2 mixture. The flowrate of N_2/CO_2 mixture was controlled by two needle valves. A gaseous sample was analysed in order to check that a moderate initial carbon dioxide concentration was achieved in order to accelerate the loading of carbon dioxide into the ethanolamine solution. Then, 5 mL of the prepared 30wt% ethanolamine solution was injected into the flask through V3. The solution was continuously bubbled with the CO_2/N_2 mixture and the liquid samples were constantly analysed in order to check the loading. The target loading range is 0.2-0.3 mol CO_2/mol MEA. Figure 5.14 shows the increase in carbon dioxide peak with time.

After achieving the required loading, both V1 and V2 were closed. After that, the sealed flask was either taken to the incubator if the solubility temperature is 60°C or below; or taken to the water bath for 80°C solubility experiment. After 24 hours, both the liquid and gas samples were analysed. The liquid sample was taken carefully and slowly by a 1 μL Hamilton syringe in order to avoid both the degassing of carbon dioxide and/or the creation of air bubbles in the needle of the syringe. In addition, the body of the needle was cleaned with a tissue prior of being injected into the sample port.

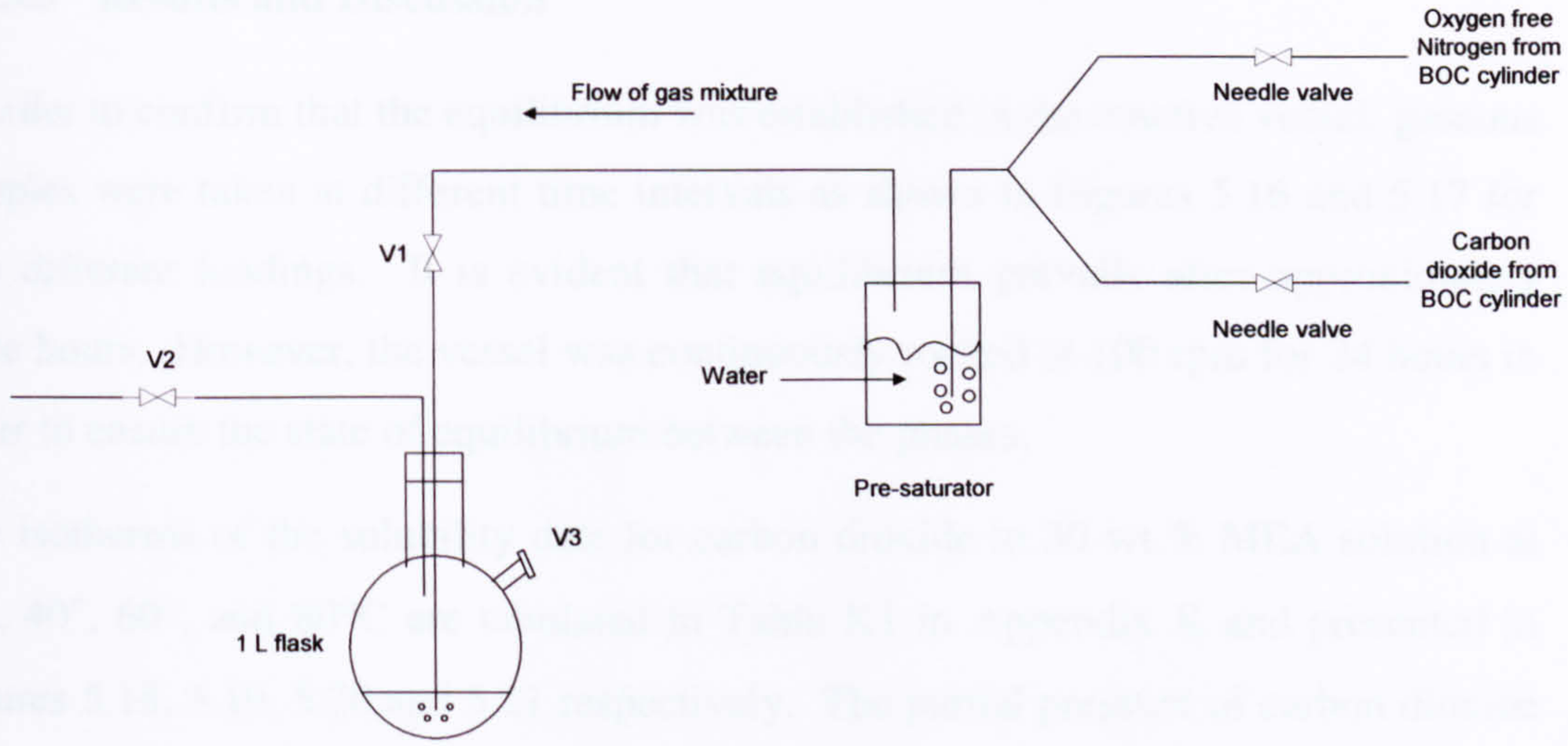

Figure 5.13: Loading of Carbon Dioxide into the Ethanolamine Solution in the Equilibrium Vessel

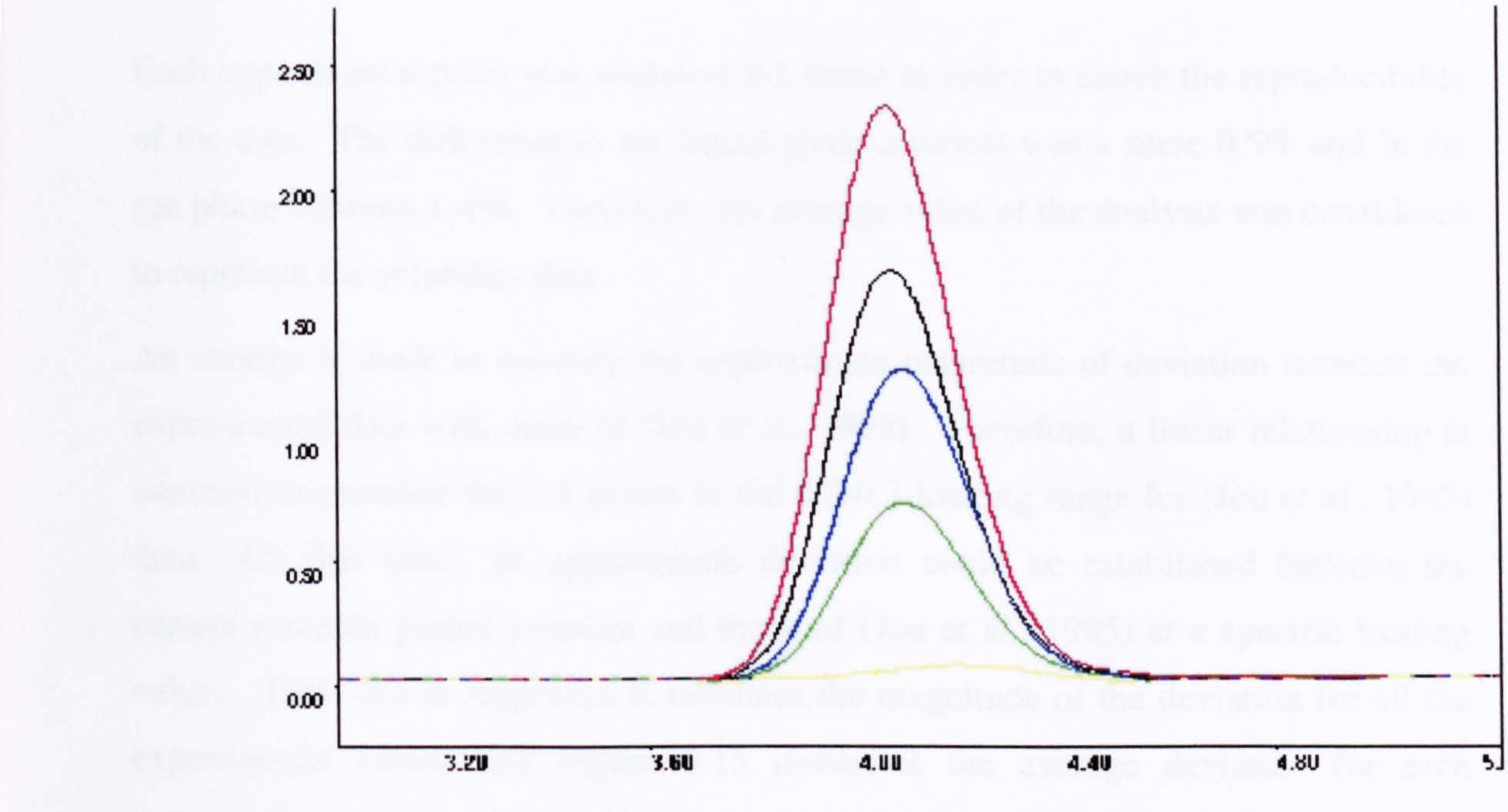

Figure 5.14: The increase of the carbon dioxide peak in the solution with time.

5.4.3.3 Results and Discussion

In order to confirm that the equilibrium was established in the reactive vessel, gaseous samples were taken at different time intervals as shown in Figures 5.16 and 5.17 for two different loadings. It is evident that equilibrium prevails after approximately three hours. However, the vessel was continuously rocked at 100 rpm for 24 hours in order to ensure the state of equilibrium between the phases.

The isotherms of the solubility data for carbon dioxide in 30 wt.% MEA solution at 25°, 40°, 60°, and 80°C are tabulated in Table K1 in Appendix K and presented in Figures 5.18, 5.19, 5.20,and 5.21 respectively. The partial pressure of carbon dioxide was ranging from 0.006442 – 2.39 kPa. Those figures show that the solubility data are higher than those of (Jou et al., 1995). The higher deviation behaviour is similar to the results of other researchers in the solubility field.

The solubility data at different temperatures were presented on linear graphs rather than the usual log-log graphs because the loading range was 0.2-0.3 and it was easier to show the deviation between the current data and those obtained by (Jou et al., 1995).

Each experimental point was analysed 2-3 times in order to check the reproducibility of the data. The difference in the liquid phase analysis was a mere 0.5% and in the gas phase between 1-4%. Therefore, the average value of the analysis was considered to represent the solubility data.

An attempt is made to quantify the approximate magnitude of deviation between the experimental data with those of (Jou et al., 1995). Therefore, a linear relationship is assumed to correlate the 2-3 points in the 0.2-0.3 loading range for (Jou et al., 1995) data. On that basis, an approximate deviation could be established between the current research partial pressure and those of (Jou et al., 1995) at a specific loading value. Table K2 in Appendix K tabulates the magnitude of the deviation for all the experimental values and Figure 5.15 illustrates the average deviation for each temperature group. Figure 5.15 shows that the error decreases with the rise in temperature, which could be attributed to the possibility of less accuracy at low CO_2 partial pressures.

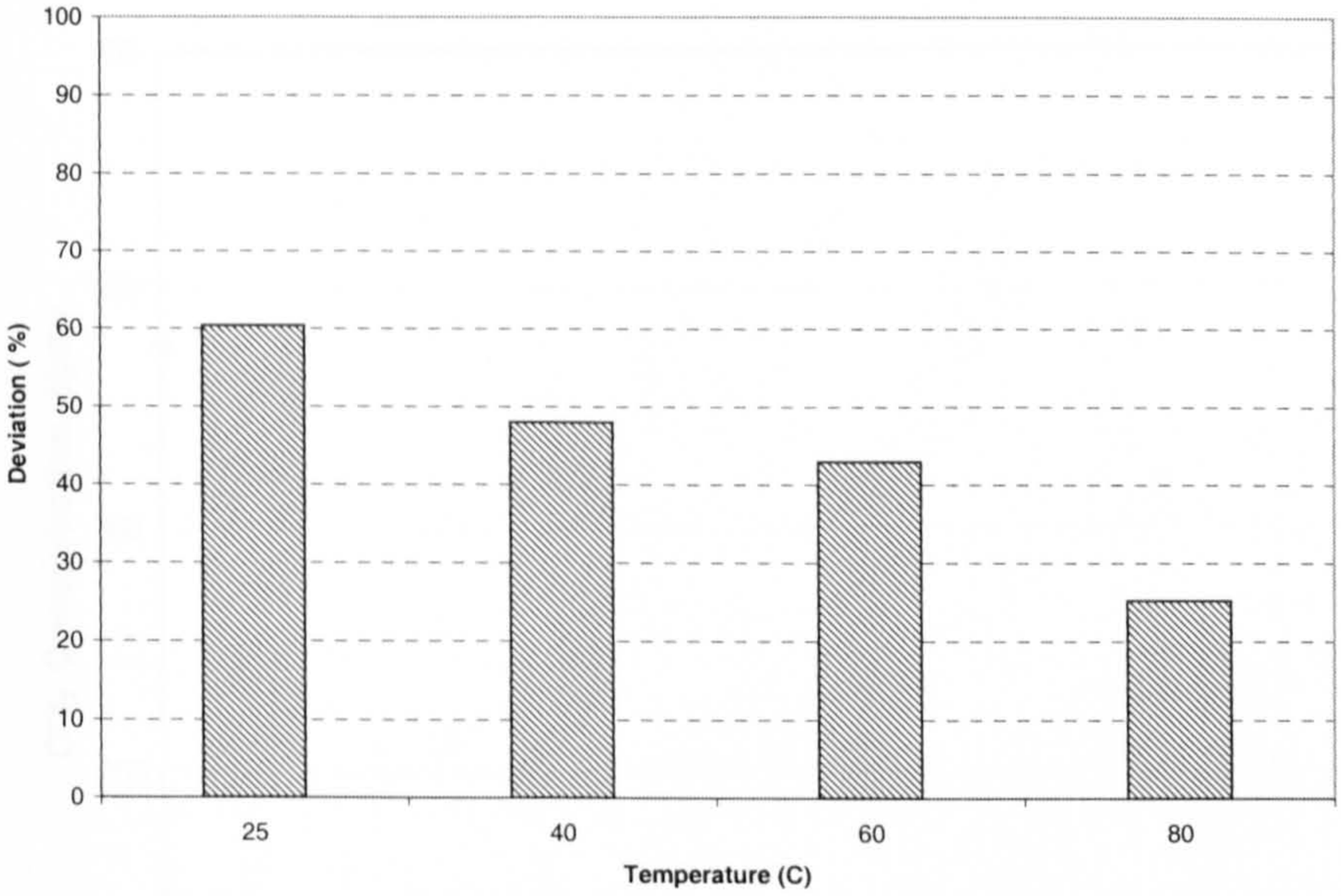

Figure 5.15: Percentage deviation between the solubility data and (Jou et al., 1995).

5.4.3.4 Correlation of Data

The solubility data for 30 wt% MEA solution at 25°, 40°, 60°, and 80°C between 0.2-0.3 loading were modelled in a similar fashion to the method used by (Atadan, 1955). The model is based upon the power equation and the values of Q and m are presented in Table 5.5:

$$s = Q\,P^{m} \qquad (4.1)$$

where s is the solubility (mol CO_2/mol MEA), P is the partial pressure of carbon dioxide (kPa), Q and m are parameters that depend upon the temperature.

Table 5.5: Values of Q and m for power equation.

Temperature (°C)	Q	m	Coefficient of determination (r^2)
25	6.2539	4.5447	0.98759
40	51.6652	5.1455	0.99350
60	370.3773	5.1964	0.99971
80	839.2923	4.5108	0.99924

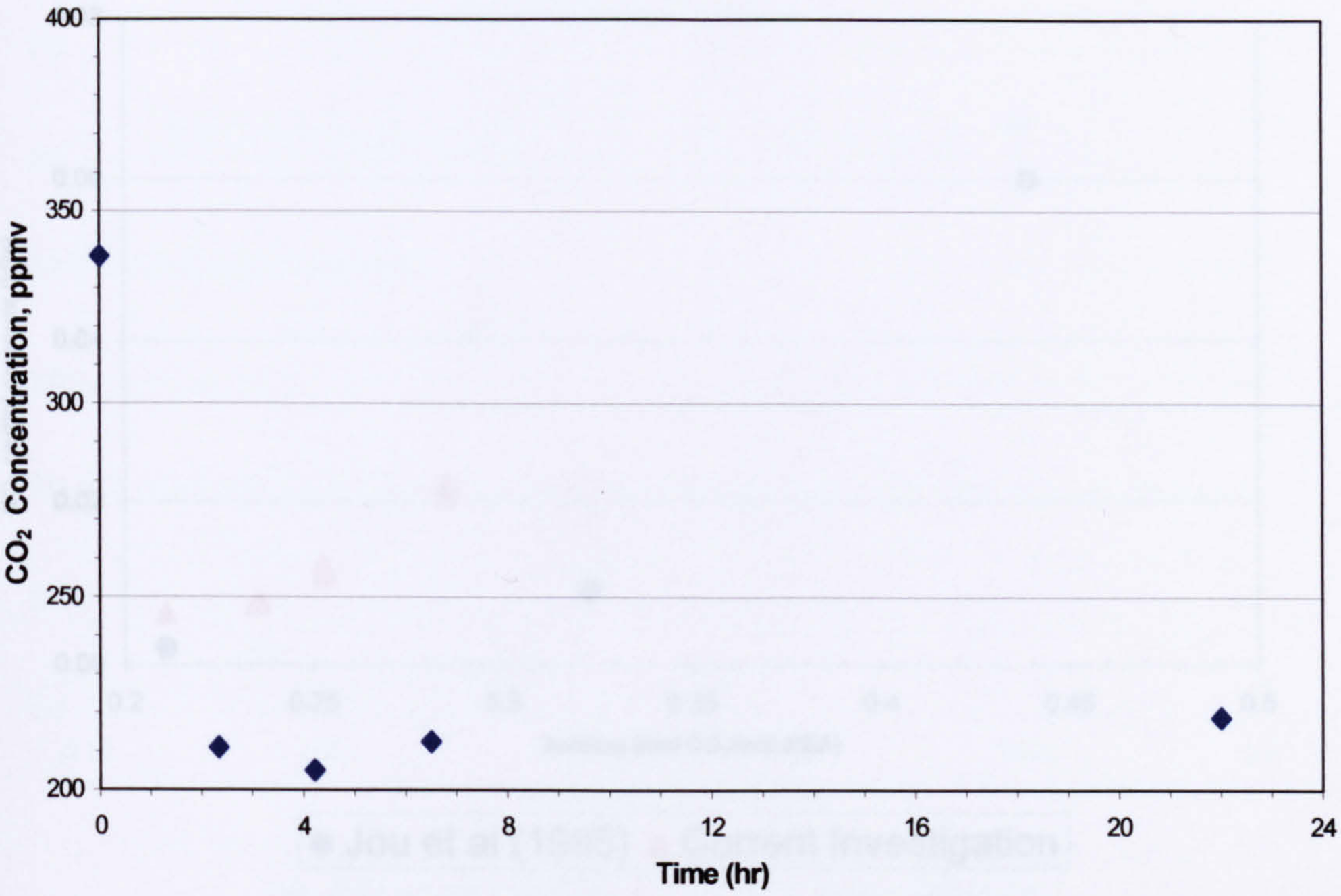

Figure 5.16: Carbon dioxide concentration vs. Time at 0.285 loading and @ 25°C.

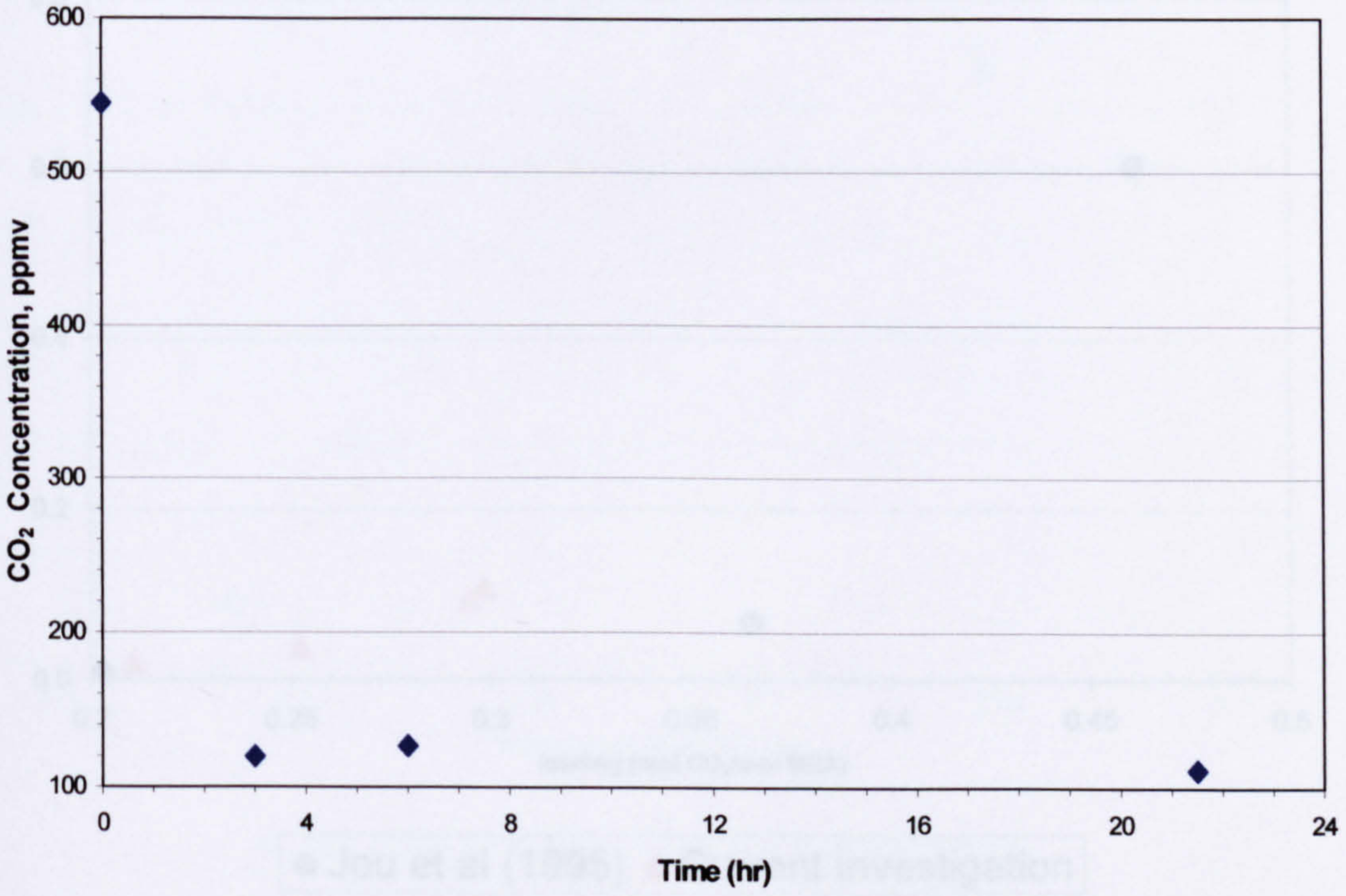

Figure 5.17: Carbon dioxide concentration vs. Time at 0.248 loading and @ 25°C.

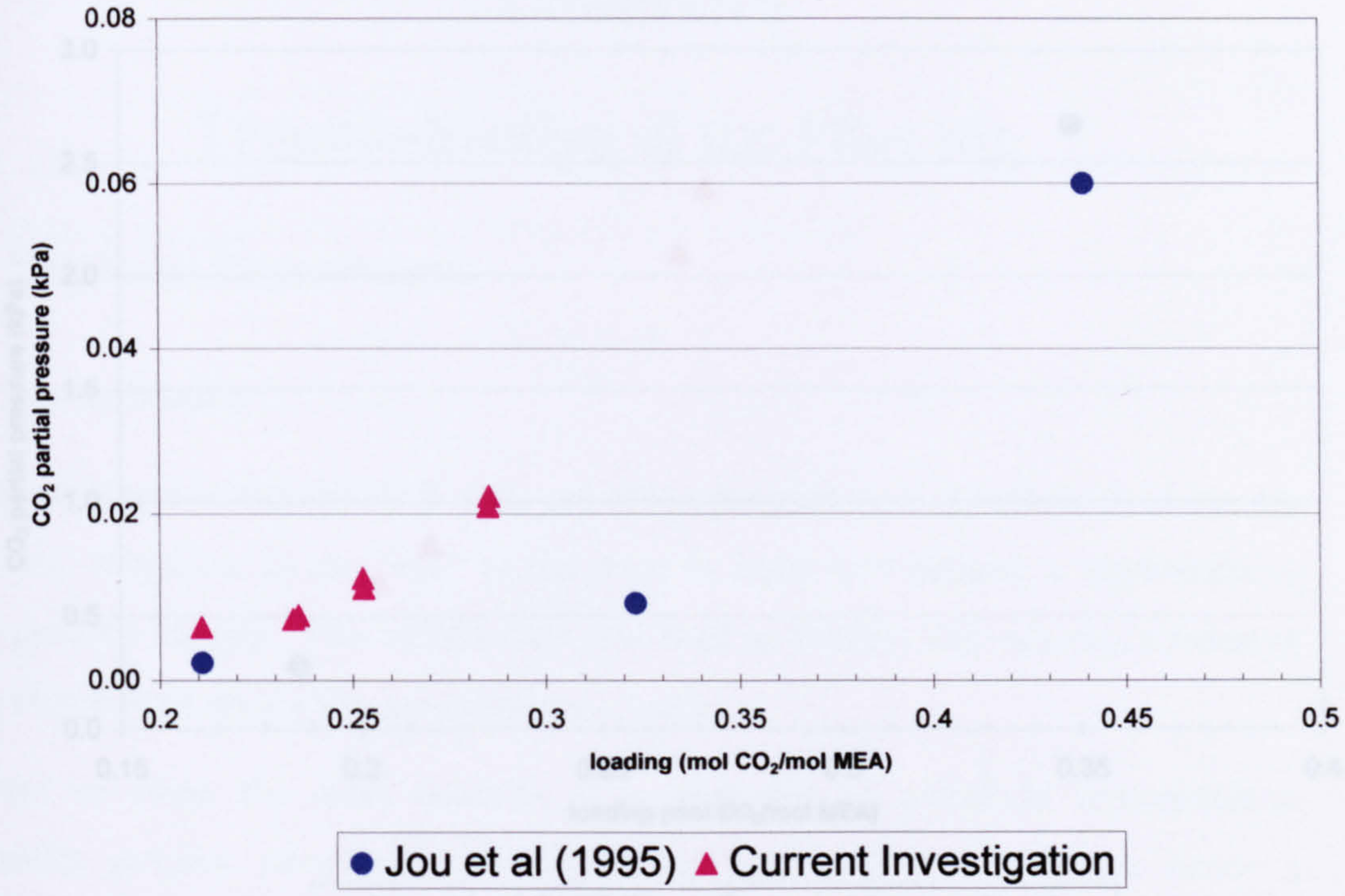

Figure 5.18: Comparison of solubility data with those of Jou et al (1995) @ 25°C.

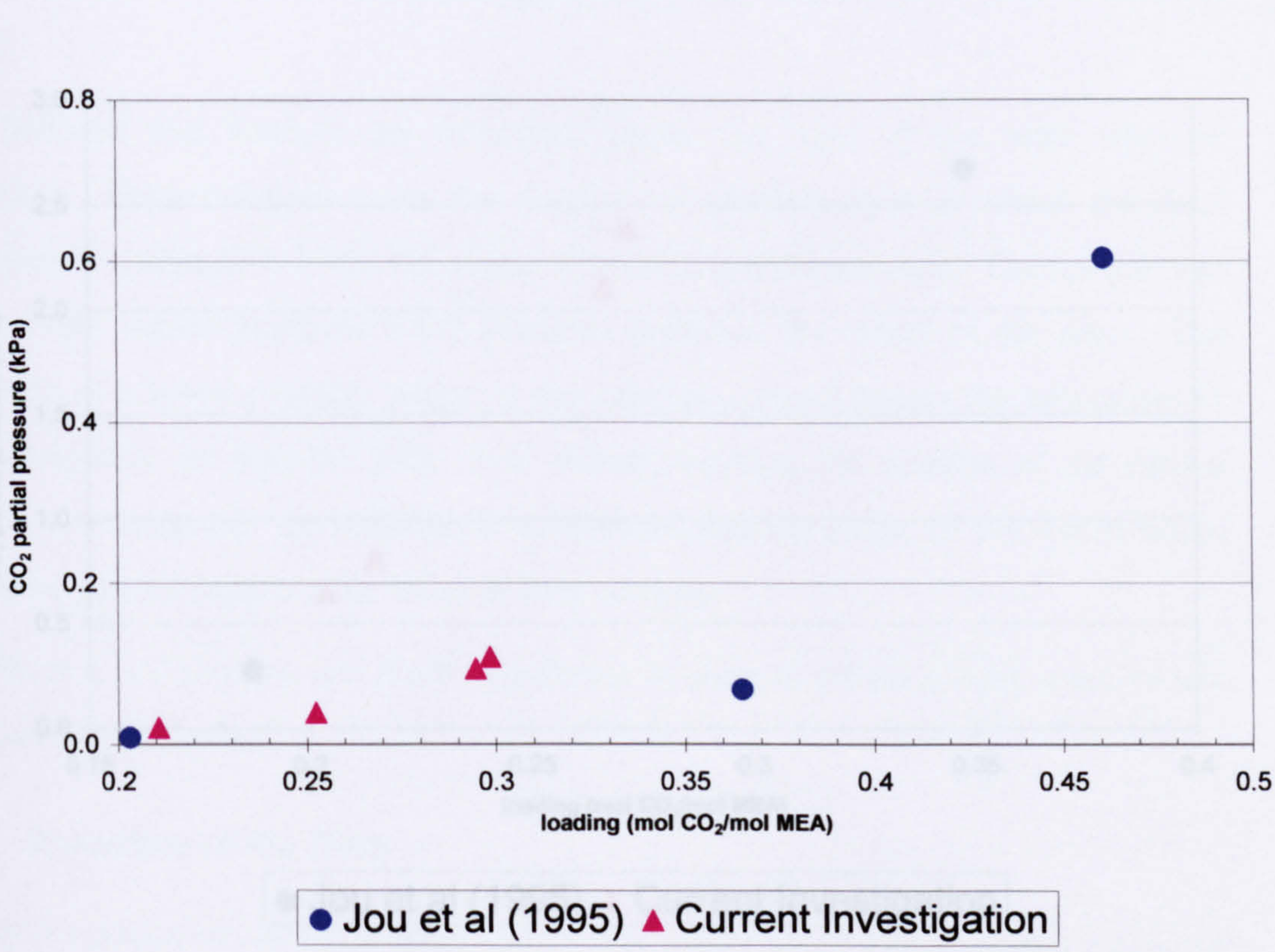

Figure 5.19: Comparison of solubility data with those of Jou et al (1995) @ 40°C.

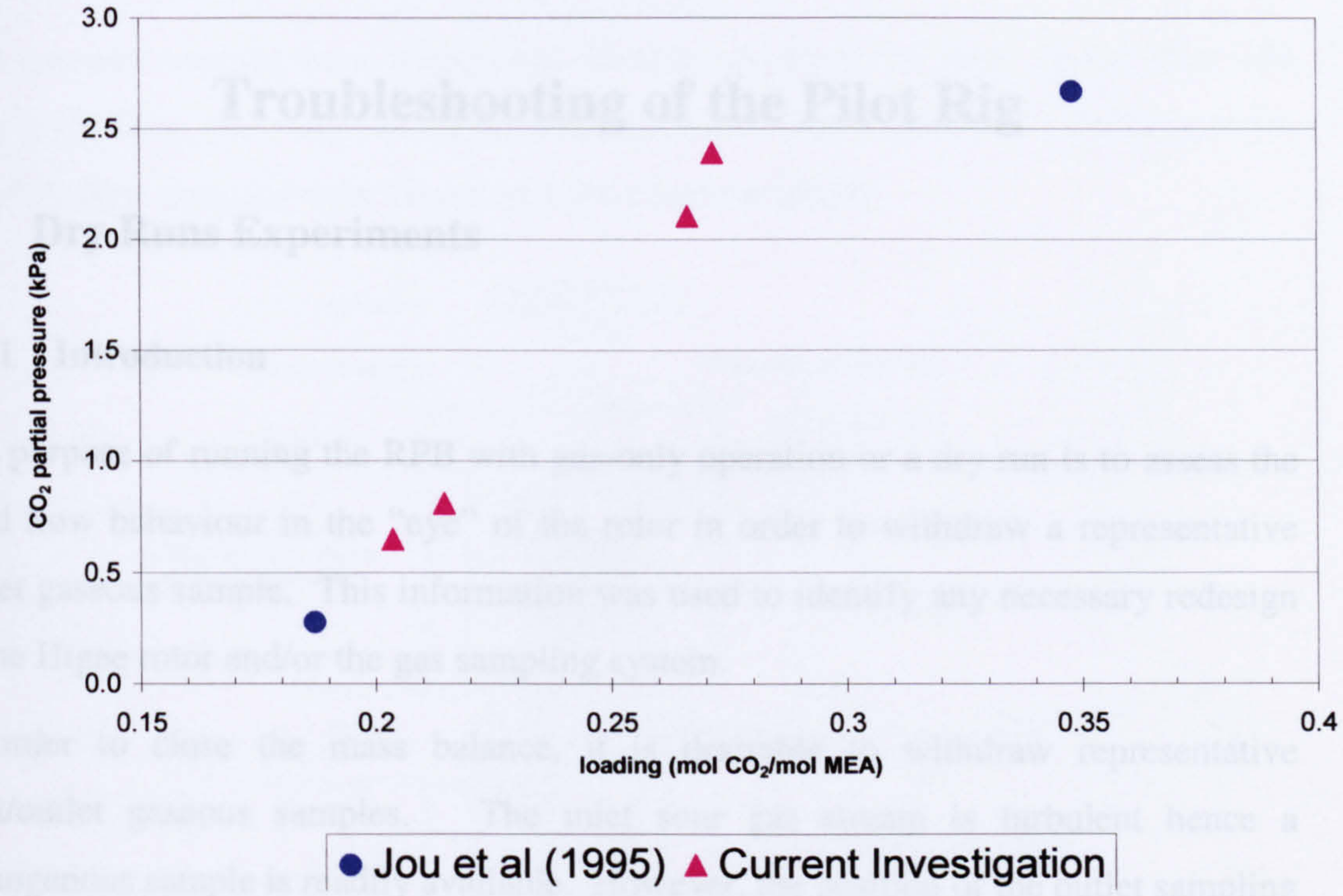

Figure 5.20: Comparison of solubility data with those of Jou et al (1995) @ 60°C.

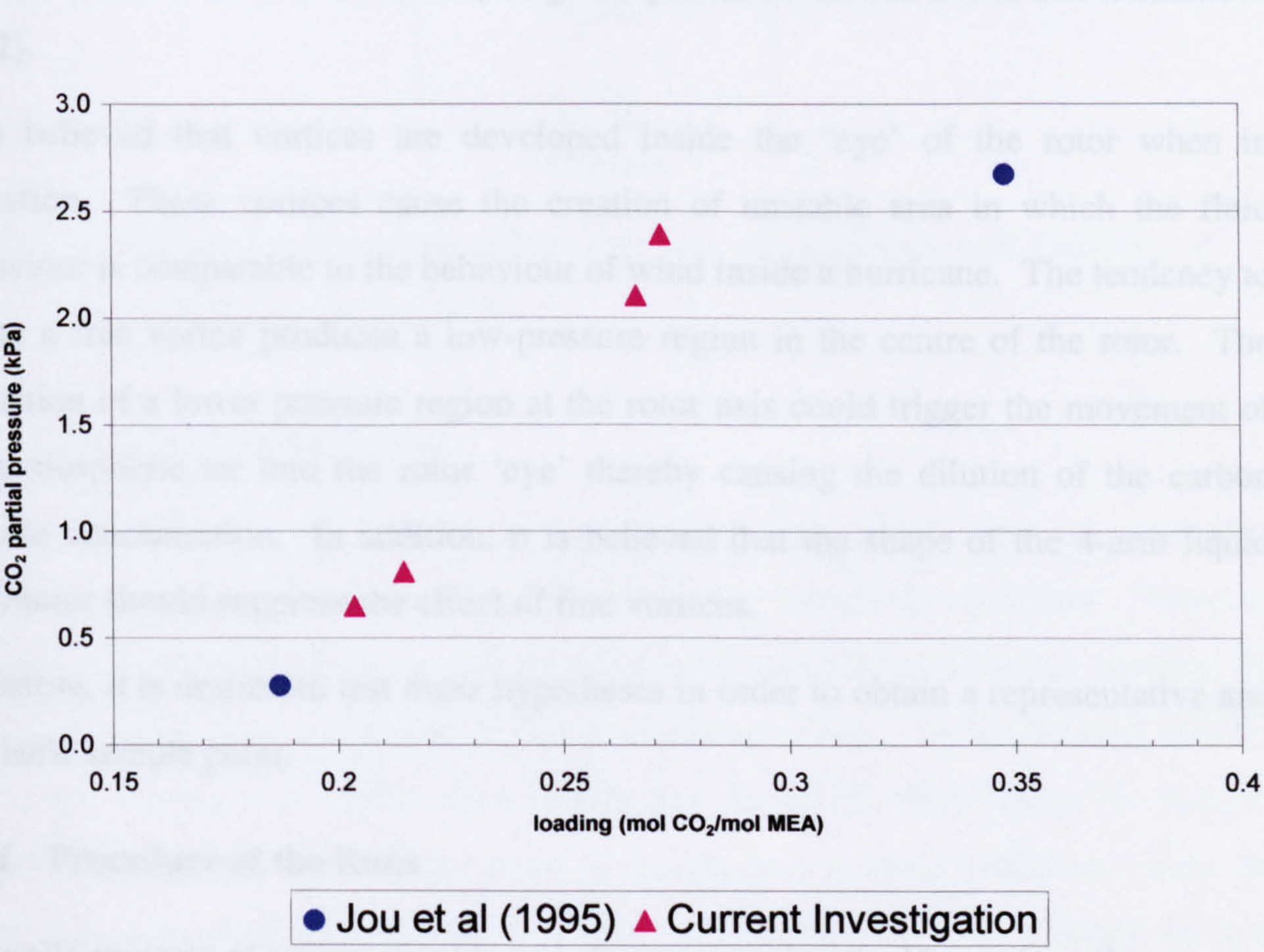

Figure 5.21: Comparison of solubility data with those of Jou et al (1995) @ 80°C.

CHAPTER 6

Troubleshooting of the Pilot Rig

6.1 Dry Runs Experiments

6.1.1 Introduction

The purpose of running the RPB with gas-only operation or a dry run is to assess the fluid flow behaviour in the "eye" of the rotor in order to withdraw a representative outlet gaseous sample. This information was used to identify any necessary redesign of the Higee rotor and/or the gas sampling system.

In order to close the mass balance, it is desirable to withdraw representative inlet/outlet gaseous samples. The inlet sour gas stream is turbulent hence a homogenous sample is readily available. However, the position of the outlet sampling point and its corresponding composition provide some uncertainties as similar problems were encountered in early Higee experiments carried out in ICI (Ramshaw, 2001).

It is believed that vortices are developed inside the 'eye' of the rotor when in operation. These vortices cause the creation of unstable area in which the fluid behaviour is comparable to the behaviour of wind inside a hurricane. The tendency to create a free vortex produces a low-pressure region in the centre of the rotor. The formation of a lower pressure region at the rotor axis could trigger the movement of the atmospheric air into the rotor 'eye' thereby causing the dilution of the carbon dioxide concentration. In addition, it is believed that the shape of the 4-arm liquid distributor should suppress the effect of free vortices.

Therefore, it is desired to test these hypotheses in order to obtain a representative and a reliable sample point.

6.1.2 Procedure of the Runs

A 2-vol% mixture of carbon dioxide and air was routed to the Higee rig and a gaseous sample was withdrawn on entry. The mixture was allowed to pass through the packed bed in the absence of the aqueous ethanolamine solution. The RPB was run at

different speeds 0, 500, 800, and 1000 RPM in order to assess the effect of the rotor speed on the composition of the sour gas mixture.

Two gaseous samples were withdrawn: Sample (A) from the 'eye' of the rotor and sample (B) from inner edge of the packed bed as shown in Figure 6.1. All the gaseous samples were analysed with the aid of a gas chromatograph.

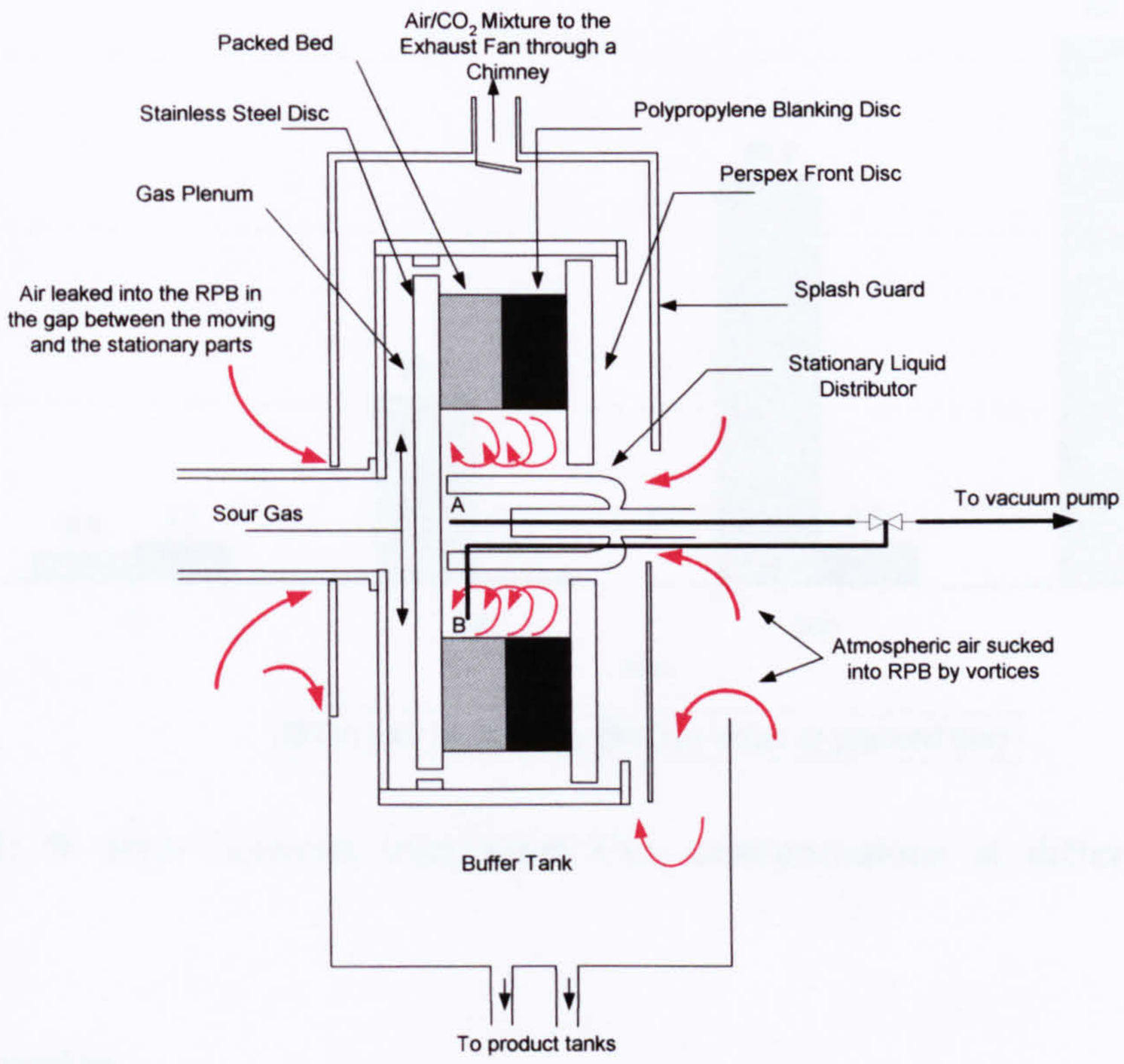

Figure 6.1: Sampling points: (A) eye; (B) periphery and positions of air leakage into the RPB

6.1.3 Results of the Dry Runs

As noted above, all the inlet/outlet gaseous samples should have an equivalent composition because there is no liquid/vapour mass transfer in operation. However, Figure 6.2 and Table L1 shows that there is a high percentage difference between the inlet and outlet gas composition in the preliminary trials. It is observed that the difference increases at higher rotor speeds and the errors were higher for samples withdrawn from the 'eye' of the rotor in comparison to those withdrawn from the inner edge of packed bed. A typical example to calculate the error between the inlet and the outlet gas composition is shown in Appendix L.

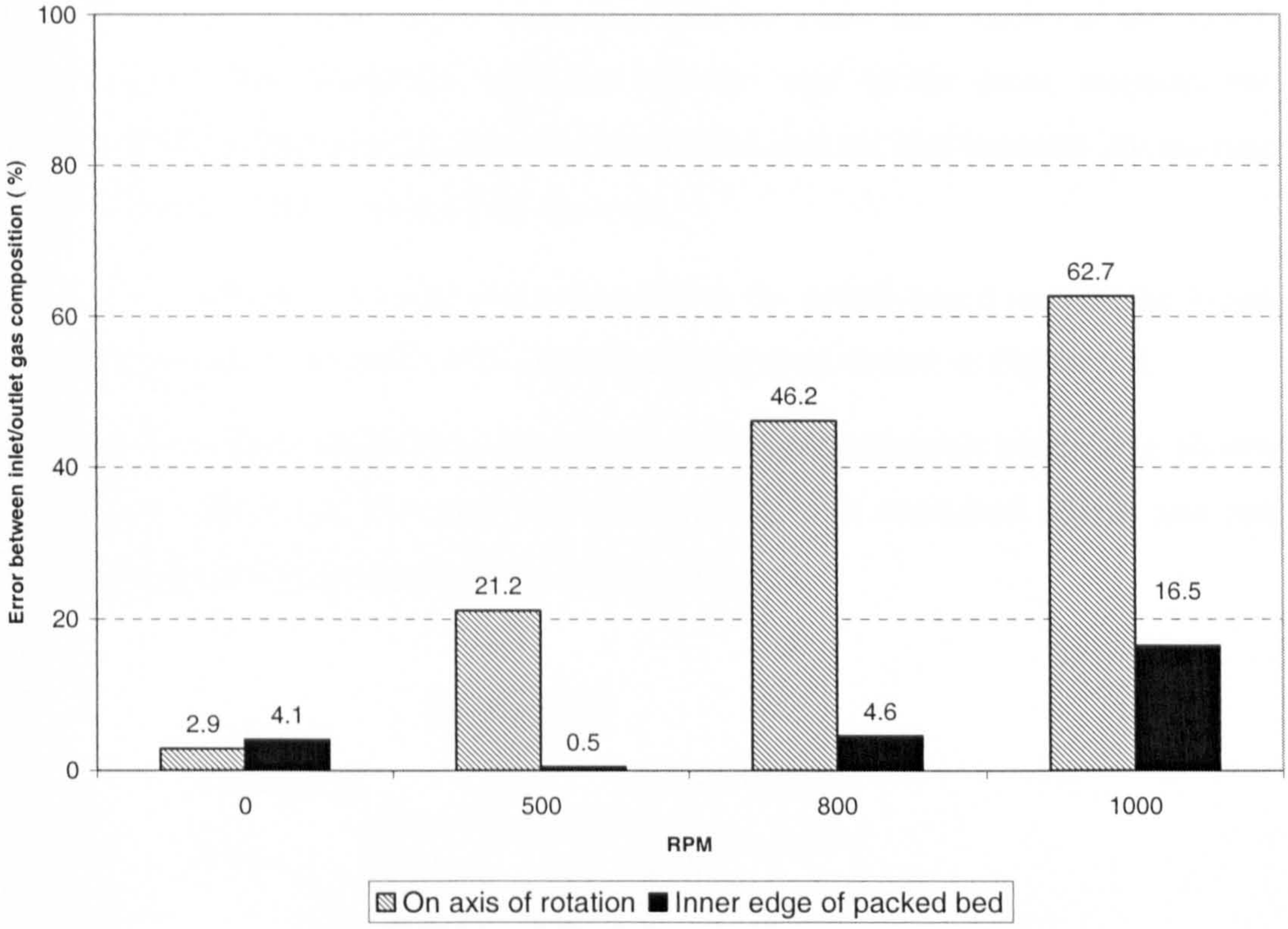

Figure 6.2: % error between inlet/outlet CO_2 concentrations at different sampling locations.

6.1.4 Discussion

The increase in the magnitude of the error between the inlet and the outlet composition was due to the dilution of carbon dioxide concentration by the atmospheric air. The air is leaked into the system due to the formation of a low-pressure regime inside the rotor envelope. Free vortices inside the 'eye' of the rotor creates a low-pressure regime coupled with high angular velocity of the gas.

There are two types of vortices developed inside the rotor: free and forced. The forced vortices are developed because the angular velocity of the inflowing gas is virtually the same of the rotating packed bed by virtue of the gas-rotor frictional interaction.

The 4-arms of the liquid distributor should minimize the effects of free vortex by suppressing its movement. In addition, identifying the positions of air leakage could minimize the effect of the free vortex.

6.1.5 Troubleshooting of the Rig

The possible locations that air can be leaked into the rotor: the vicinity of the splash guard that the 4-arm distributor is placed into the 'eye' of the rotor; secondly the upper part of the buffer tank as shown in Figure 6.1, and the gap between the moving and the stationary parts at the back of the rotor.

Initially, a transparent extension was connected to the splash guard next to the 4-arm distributor and hence the front cover was totally sealed as shown in Figure 6.3.

Another set of experiments showed that the error was significantly reduced as shown in Figure 6.4. However, the error was still great at high rotational speeds and can cause discrepancies in the calculations of mass balance.

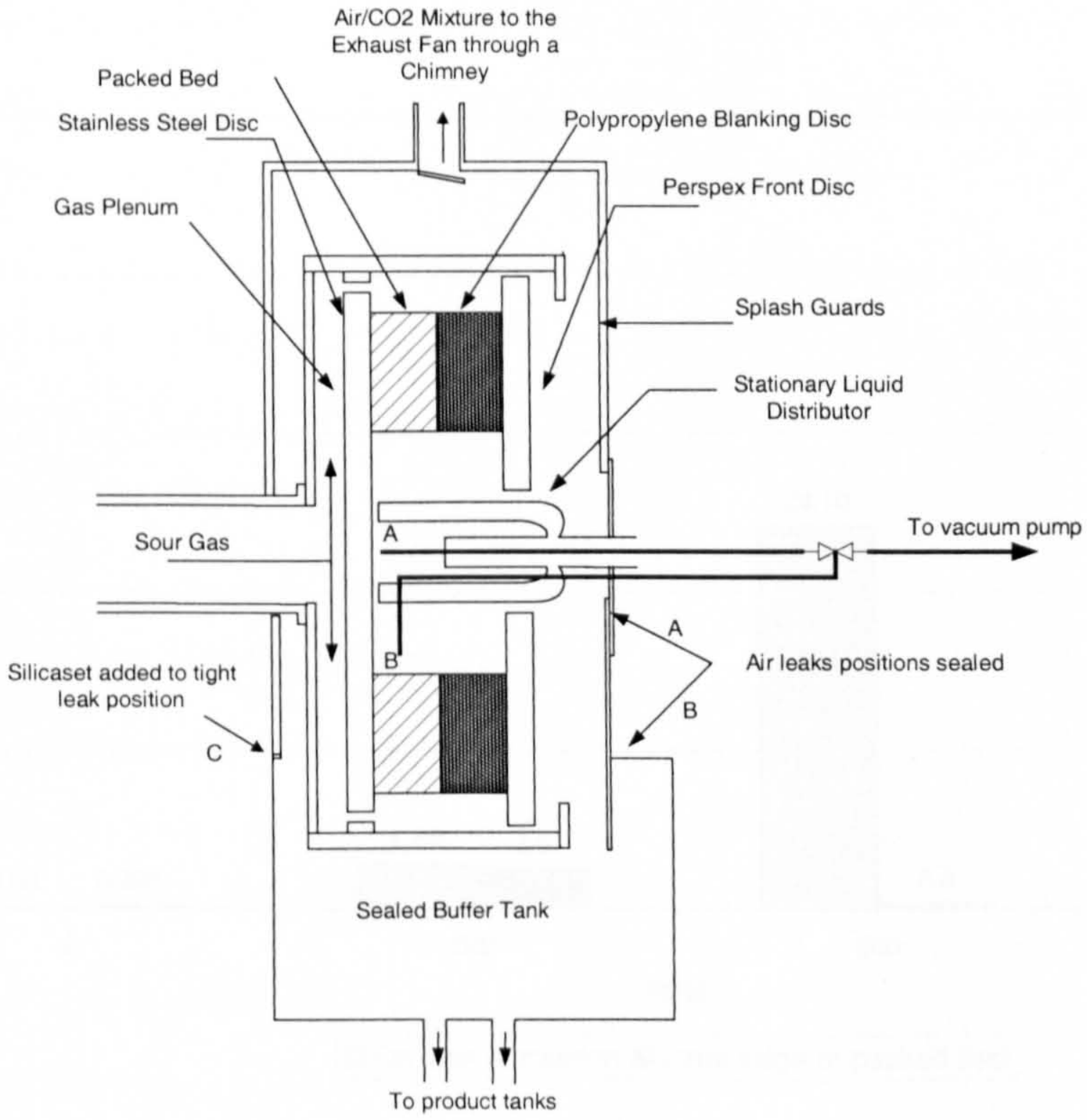

Figure 6.3: Air leakages blocked

Therefore, it was decided to seal any discontinuity between the splash guard and the buffer tank as shown in Figure 6.3 at points A, B, and C. In addition, the gap between the moving shaft and the stationary splash guard at the back of the rotor is kept to a minimum. Furthermore, silicone adhesive was applied in all the contacting surfaces

between the splash guard and the buffer tank in order to completely seal the system from the outside medium.

The last two experimental runs in Table L1 shows that the error was reduced substantially for eye measurements to a mere 0.9% at low sour gas flowrate (110 m^3/hr) and 0.7% at high gas flowrate (155 m^3/hr) when the rotor is operated at maximum speed (1000 RPM).

It was decided to collect a gaseous sample from the 'eye' of the rotor in preference to the inner edge sampling point. The latter was discarded because it was very close to the inside surface of the RPB and hence the ethanolamine solution was vacuumed into the teflon piping causing contamination to the gaseous sample.

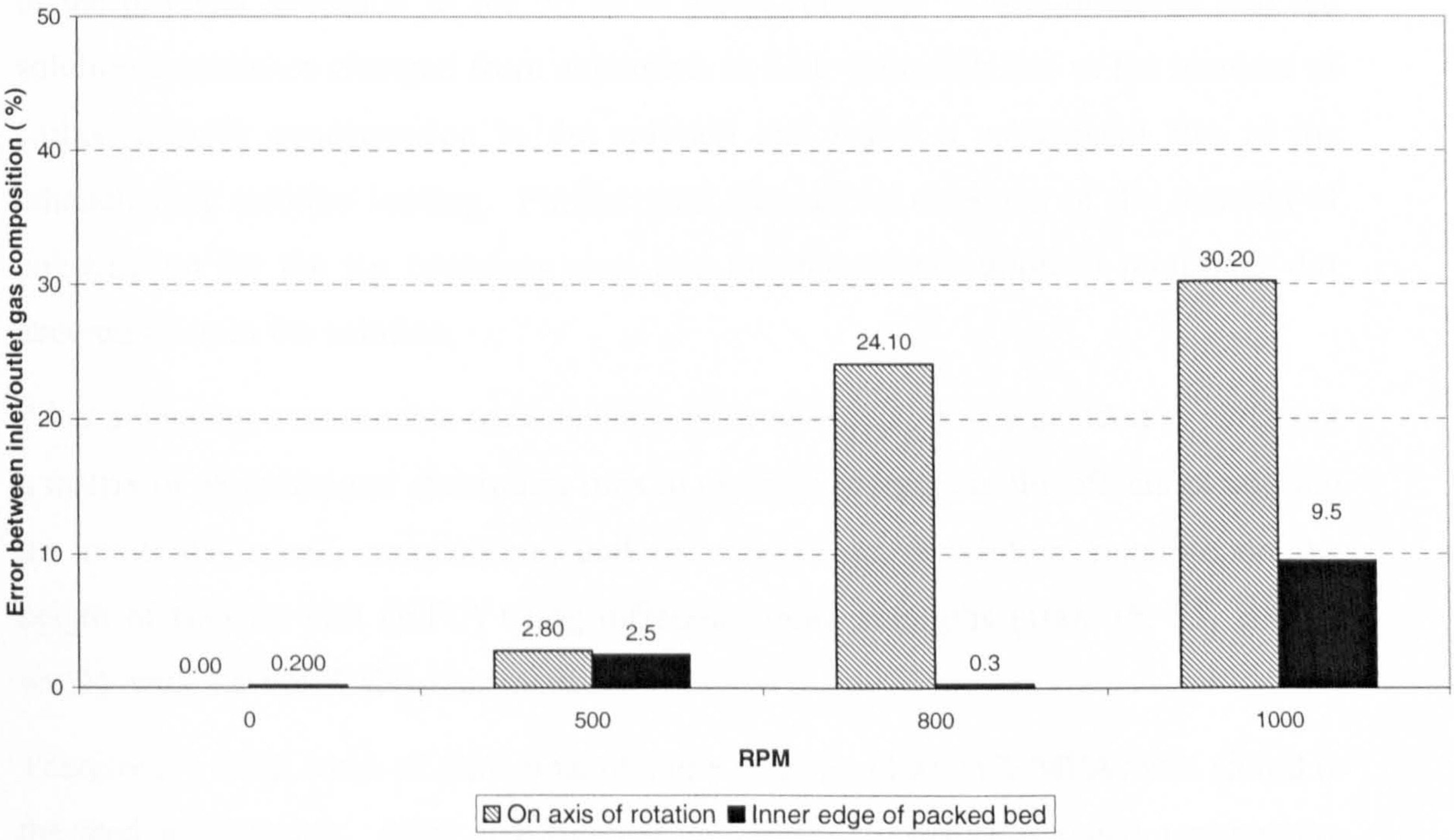

Figure 6.4: % error between inlet/outlet CO_2 concentrations after initial modifications to the Higee rig.

6.2 Absorption Runs

6.2.1 Introduction

The initial absorption runs were used as an exercise to close the mass balance across the rig and to obtain preliminary mass transfer results. The concentration of MEA solution was downgraded from 85wt% to 30wt% by blending with distilled water. The operational difficulties encountered with the mass balance were clarified and statistically analysed.

The preliminary mass transfer results indicated that the overall gas phase Height of Transfer Unit (HTU_{OG}) was approximately 20 cm at ethanolamine solution flowrate of 20 L/min and at a room temperature of 20°C.

However, the extensive absorption runs over a six-month period caused deterioration of the physical condition of the 30 wt.% MEA solution. It was observed that the solution appearance changed from colourless to dark yellowish due to the increase of carbon dioxide concentration in the solution and hence a subsequent rise in the ethanolamine solution loading. Furthermore, the careful selection of the material of construction for the rig (stainless steel and polypropylene) allowed minimum dirt accumulation in the solution.

After achieving a reasonable mass balance error accuracy, it was decided to carry out a matrix of experimental absorption runs in order to investigate the effects of varying the rotational speed, temperature, and the ethanolamine solution flowrate on the height of transfer unit (HTU) using different amine strengths (100, 75, 55, and 30 wt.%) with 4.0 vol.% CO_2/Air mixture.

Therefore, a fresh batch of pure ethanolamine solution (100 wt% MEA) was stored in the feed storage tank. After investigating the effects of rotational speed, temperature and the liquid flowrate at constant ethanolamine concentration, the solution was diluted with distilled water in order to downgrade the amine strength to the next level.

6.2.2 Mass Balance Across the Higee Rig

6.2.2.1 Operational Procedure

The flowsheet of the process is available in Section 2.2 and the descriptive explanations of the experimental components were previously stated in Chapter 2.

The following procedure was carried out for each mass transfer experimental run: The ventilation exhaust was switched ON in order to safeguard the working environment around the Higee rig as it reduces the build up of carbon dioxide concentration in the pilot plant enclosure. Then, any previous accumulated solution was drained from the liquid sampling points.

In order to ensure uniform feed composition, the aqueous MEA solution was circulated between the feed and the product reservoirs for approximately 15 minutes. Then, the circulation pump was switched off and most of the MEA solution was kept in the feed reservoir. After that, the Higee rotor was accelerated to approximately half of the intended experimental run speed and then the feed valve was opened gradually to the desired flowrate. The rotor speed was then gradually increased to the desired RPM.

A turbulent and uniform CO_2/air mixture (sour gas) was delivered to the Higee rig as described in Section 2.8. The temperature and the pressure of each gaseous component were measured in order to make the necessary corrections in the mass balance calculations. Appendix B shows the calibration charts for the aqueous ethanolamine amine solution flowmeters and the relationship between the air flowrate and its gauge pressure.

The Higee rotor was run for approximately 5-10 minutes before representative gas/liquid samples were withdrawn as described in Section 2.10 and 2.11.

After the experimental run was completed (approximately 15 minutes), the ethanolamine solution pump was switched off and both the air and the carbon dioxide valves were closed. Then, the speed of the rotor was gradually reduced to a standstill. Finally, the ventilation exhaust was allowed to operate for a further 15 minutes in order to secure the pilot plant enclosure.

6.2.2.2 Results and Discussions

Twelve absorption experimental runs were carried out using 30wt% MEA solution batch. The purpose of the exercise was to close the mass balance across the Higee; and to ascertain the behaviour and the effectiveness of the mass transfer operation. The solution strength (30 wt.%) was selected based upon the advice of the industrial sponsor (Eimer, 1999), which reflected the typical higher-range MEA solution concentration applied in the gas sweetening plants.

The results of the experimental runs for the analysis of sour gas stream, sweet gas stream, lean MEA solution, rich MEA solution (periphery), and rich MEA solution (tank) are presented in Table O-1 in Appendix O.

The concentration of carbon dioxide in the sour gas stream was initially 2 vol.% for the first 10 experimental runs then it was doubled to 4 vol.% for the last 2 runs. The speed of the rotor was set at 1000 RPM for most of the runs in order to attain the highest possible absorption efficiency (Note: the maximum feasible rotor speed was 1000 RPM due to safety and mechanical limitations as disclosed in Section 2.4). The flowrate of the lean MEA solution was progressively increased from 12 L/min (2x runs) to 20 L/min (5x runs) and finally to 50 L/min (5x runs). The rationale of increasing the lean MEA solution flowrate was to investigate the effect of increasing the L/G ratio.

The high Re number ($5*10^4$-$1.3*10^5$) of the combined air/CO_2 stream in the feed indicates that the flow of the sour gas mixture is turbulent and hence a well mixed gaseous stream is delivered to the Higee rig.

A typical calculation of mass balance across the Higee rig is shown in Appendix M. It was evident that the magnitude of the error was higher using 2 vol.% CO_2 sour gas stream (Run 1-10) in comparison to 4 vol.% (Run 11 & 12).

Figure 6.5 and Table 6.1 illustrate the dilemma of the mass balance deviation. For example, an increase by +0.0045 in the average loading of the rich MEA solution sample for Run #6 could substantially reduce the mass balance error from 60% to 6.5%. Similar behaviour was verified in other runs.

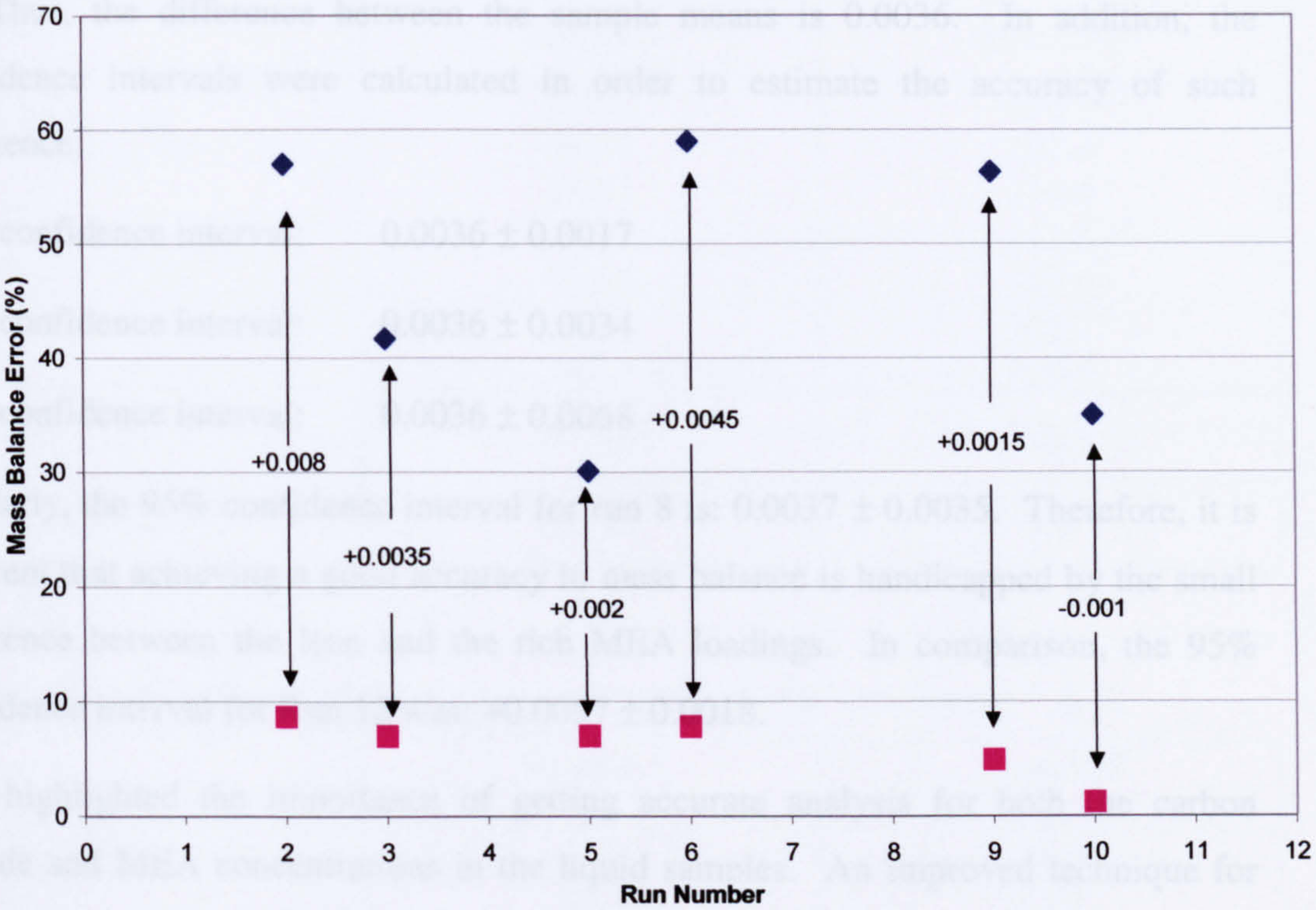

Figure 6.5: The effect of a slight change of the loading on mass balance (Periphery Samples).

Table 6.1 shows a statistical summary of the replicate loading results for the lean and the rich (periphery) MEA solution. The coefficient of variation for the lean and the rich solution are 0.27% and 0.61% respectively. Thus, it is clear that a good agreement is achieved between the replicate loading measurements.

	Lean Solution	Rich Solution (Periphery)
Number of samples	2	2
Mean	0.1106	0.1142
Median	0.1106	0.1142
Standard deviation	0.0003	0.0007

Table 6.1: Statistical summary of the loadings for the lean and the rich MEA solution for Run 6.

However, the mass balance calculations depend on the magnitude of the difference between the average lean and the rich MEA solution loadings. Assuming that the two

solutions are independent random samples with means of 0.1106 and 0.1142 for Run 6. Thus, the difference between the sample means is 0.0036. In addition, the confidence intervals were calculated in order to estimate the accuracy of such difference:

80% confidence interval: 0.0036 ± 0.0017

90% confidence interval: 0.0036 ± 0.0034

95% confidence interval: 0.0036 ± 0.0068

Similarly, the 95% confidence interval for run 8 is: 0.0037 ± 0.0035. Therefore, it is apparent that achieving a good accuracy in mass balance is handicapped by the small difference between the lean and the rich MEA loadings. In comparison, the 95% confidence interval for Run 12 was: $+0.0057 \pm 0.0018$.

This highlighted the importance of getting accurate analysis for both the carbon dioxide and MEA concentrations in the liquid samples. An improved technique for the delivery of the 0.2 μL liquid sample into the gas chromatograph port by the Hamilton syringe was identified: (1) the sample was purged x10 times into the syringe, (2) a 1 μL sample was initially withdrawn from the sample flask then the excess volume was purged out, (3) the long stainless steel syringe's needle was cleaned with a tissue, (4) the syringe was inserted inside the gas chromatograph sample port for approximate duration of 3 seconds, (5) the sample was then injected and after that the syringe was removed and finally the gas chromatograph RUN button was pressed.

Tables 6.2 and 6.3 show that the technique was successful in reducing the distribution range of the peak area for both MEA and CO_2 (Note: there are two different samples thus higher peak areas for the second sample).

The standard deviation of the MEA peak was improved from 6.2% to 1.3% and similarly the standard deviation of the CO_2 peak was improved from 6.4% to 1.5%.

Table 6.2: MEA peak areas calculated by the GC for Sample 1 & 2.

	Sample 1	Sample 2
MEA Peak Area	179.2 181.1 182.1 196.3 173.9 167.3 162.1	208.1 207.4 214.6 211.5 207.6 208.7 206.4
Average	177.4	209.2
Standard deviation	11.1	2.8

Table 6.3: Carbon dioxide peak areas calculated by the GC for Sample 1 & 2.

	Sample 1	Sample 2
CO_2 Peak Area	21.6 23.7 23.7 23.5 26.1 22.7 21.6	26.9 27.0 27.9 27.3 26.5 27.0 26.7
Average	23.3	27.0
Standard deviation	1.5	0.4

The American Society for Testing Materials (ASTM) T_n test was carried out to identify any carbon dioxide concentration outliers in the gas phase data but it was shown that all the data were not significantly deviated from the average and hence no measurements were discarded (Skoog et al., 1992). However, very few data were discarded in results of the absorption runs in the next section.

It was evident that the use of higher carbon dioxide concentration would increase the accuracy of the mass balance. Therefore, the concentration of carbon dioxide in the sour stream was increased to 4 vol.% for Run #11 and #12. As a consequence, the mass balance error was reduced to a maximum of 12.8%. Any further improvement to the magnitude of the error was restricted by the low value of the loading increase. For example, the loadings for run #11 and #12 were increased from 0.1294 and 0.1343 to 0.1348 and 0.1400 respectively. Thus, the difference between the lean and

the rich aqueous MEA solution loadings were 0.0054 and 0.0052. In addition, the repeatability of the liquid sample analysis proved that the deviation in the third and fourth decimal point was unavoidable and hence even taking the average value of the loading had its limitations.

As a consequence, it is clear from the mass balance calculations that the difference in the loadings in the liquid phase is small in relation to their absolute value and the expectation of 10% mass balance closure was unrealistic. Hence, it was decided to base all the mass transfer performance calculations on the gas phase carbon dioxide concentrations that could be measured most accurately. The accuracy of gas phase measurements was in the range of 1-10%. In addition, the purpose of the absorption process is to lower the sour carbon dioxide concentration thus it is more convenient to employ overall gas phase mass transfer parameters.

CHAPTER 7

Mass Transfer Studies

7.1 Introduction

This chapter describes the mass transfer experiments carried out to determine the efficiency of the Higee in the absorption and the desorption of carbon dioxide from different alkanolamine solutions strengths.

Section 7.2 describes briefly the chemical absorption using two-film theor. Section 7.3 theoretically determines residence time, reaction time, and diffusion time. Section 7.4 investigates the effects of rotational speed, temperature, and alkanolamine flowrate at different amine strengths (100, 75, 55, and 30 wt%) in the absorption runs. Section 7.5 compares Higee mass transfer machine with conventional column. Section 7.6 shows the results of the desorption experiments using either air or steam as the regenerative medium. Finally, Section 7.7 shows the significance of the end effect in the mass transfer machine.

7.2 Application of Two-Film Theory in Absorption with Chemical Reaction

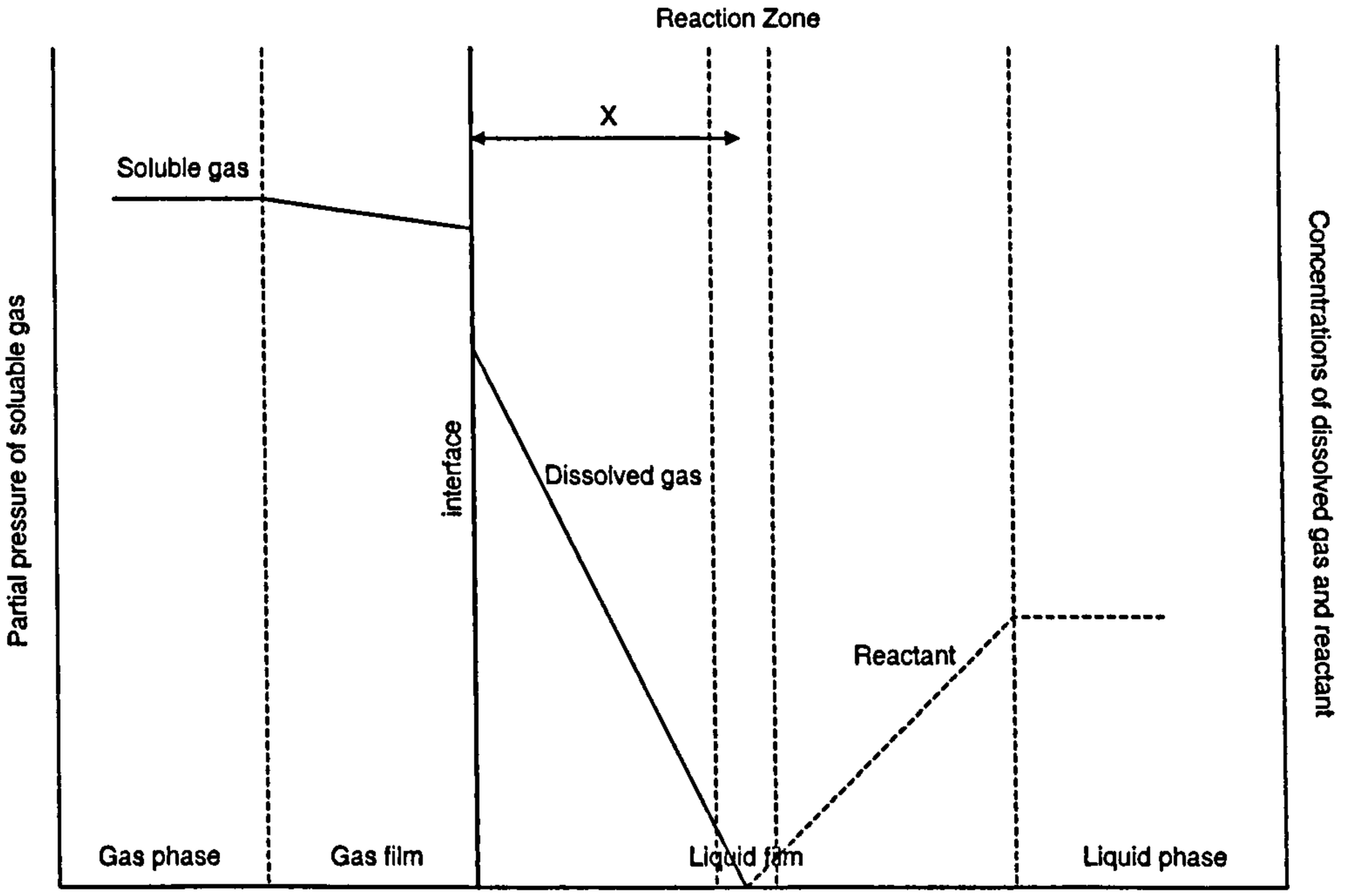

Figure 7.1: Concentration gradients of mass transfer accompanied by a chemical reaction.

(Sherwood and Pigford, 1952) described the profiles of the reactants and the products of a rapid second order irreversible chemical reaction in the liquid phase (Figure 7.1) using steady state two-film theory.

The absorption process proceeds as follows: the solute gas (A) diffuses through the gas film then dissolve and reacts with the absorbent (B) in a reaction zone in the liquid film. As a consequence of the chemical reaction, the amount of (B) will reduce in the liquid film and hence fresh quantities will diffuse from the liquid bulk to the interface. In fact, the diffusion of (B) from the liquid bulk to the reaction zone forces the diffusion of (A) in the liquid film thus the reaction zone is a small distance away from the gas/liquid interface.

The concentration of the dissolved gas and the absorbent are assumed to be negligible in the reaction zone. The thickness of the reaction zone is assumed to be small compared to the liquid film thickness. The reaction zone is assumed to be at a distance X from the gas/liquid interface. The magnitude of the distance X is a function of the diffusivities of the solute gas (A) and the absorbent (B) as well as the concentration of (B) in the liquid solution (Morris and Jackson, 1953).

If the soluble gas reacts at the surface of the liquid then the gas film controls the rate of the absorption. If the reaction occurs in a narrow zone within the liquid film then the rate of absorption is controlled by the rate of diffusion in the liquid as the rate of reaction is much higher then the rate of diffusion.

7.2.1 Mass Transfer Control

7.2.1.1 Fundamental Equations

The followings show mathematically that the absorption of carbon dioxide by MEA solution is controlled by the liquid phase using the two-film model (Eimer, 2000).

The basic mass transfer equation for the transfer of component (A) across an interface for a physical solvent is:

$$N_A = k_G (P_{AG} - P_{Ai}) = k^o_L (C_{Ai} - C_{AL}). \quad (7.1)$$

Where k_G and k_L are gas-film transfer coefficient and liquid-film transfer coefficient respectively. If the solution is in equilibrium and obeys Henry's Law then it is possible to combine both resistances:

$$\frac{1}{K_G} = \frac{1}{k_G} + \frac{H}{k^o{}_L} \text{ ; and } \frac{1}{K_L} = \frac{1}{k^o{}_L} + \frac{1}{Hk_G} \qquad (7.2)$$

where K_G and K_L are the overall gas-phase transfer coefficient and liquid phase transfer coefficient respectively.

For mass transfer accompanied by a chemical reaction, the enhancement factor should be introduced into the above equation in order to incorporate the acceleration to mass transfer in the liquid film by the chemical reaction.

$$\frac{1}{K_G} = \frac{1}{k_G} + \frac{H}{k^o{}_L E} \text{ ; and } \frac{1}{K_L} = \frac{1}{k^o{}_L E} + \frac{1}{Hk_G} \qquad (7.3)$$

It is possible to calculate the enhancement factor (E) using:

$$E = \sqrt{M} \qquad (7.4)$$

where M is defined by (Dankwerts, 1970).

$$M = \frac{D_{CO_2} k_1}{\left(k^o{}_L\right)^2} \qquad (7.5)$$

where k_1 is the rate coefficient for the pseudo first order reaction.

$$k_1 = k_2 [MEA] \qquad (7.6)$$

where k_2 is the kinetic rate constant and it is given by (Hikita et al, 1977) for the temperature range of 5-80°C:

$$\text{Log}_{10}\, k_2 = 10.99 - (2152 / T). \text{ (l/mole/s)}. \qquad (7.7)$$

Table 7.1 compares liquid film controlled system (absorption of carbon dioxide by MEA) and gas film controlled system (absorption of ammonia by water).

The calculations show that the resistance to mass transfer for the absorption of carbon dioxide by 30 wt.% MEA solution is in the liquid film. Furthermore, a spreadsheet was developed to verify the effect of the variation of temperature and MEA concentration on the liquid side resistance to mass transfer. Table 7.2 shows that the liquid side resistance decreases with higher temperatures and concentrations.

Table 7.1: Summary of mass transfer data for NH_3-H_2O and CO_2-MEA-H_2O systems

	NH_3-H_2O	CO_2-MEA-H_2O	Reference
MEA Concentration, mol/m^3	-	4919	
Diffusion Coefficient, m^2/s	$1.64*10^{-9}$	$1.02*10^{-9}$	(Cussler, 1997) for NH_3-H_2O, Section 2.2.7.4 for amine system.
Henry's Coefficient, $bar.m^3/mol$	0.0000165	0.02977	(Perry and Green, 1984), (Eimer, 1994)
Diffusion Time (t_d), sec. Low value High value	 0.004 0.04	 0.004 0.04	(Astarita et al., 1983)
$k_L^o = (D/t_d)^{1/2}$, m/s			
Low value	0.000640	0.000505	
High value	0.000202	0.000160	
Average	0.000421	0.000333	
k_G, $mol/(m^2.bar.s)$	4	4	(Cussler, 1997)
Danckwerts' M	-	200.7	(Dankwerts, 1970)
Enhancement Factor, E	1	14.2	
$1/k_G$, $m^2.bar.s/mol$	0.25	0.25	
H/k_L^o, $m^2.bar.s/mol$	0.043	6.3	
% liquid resistance	15	96	

Table 7.2: Effect of the variation of concentration and temperature on the liquid-side mass transfer resistance.

	MEA Solution Concentration (wt.%)			
Temperature (°C)	**30**	**55**	**75**	**100**
20	96	95	94	93
40	94	92	90	89

7.2.1.2 Mathematical Limiting Behaviour

Furthermore, a mathematical limiting behaviour was devised by (Astarita et al., 1983) to determine the position of the resistance to mass transfer:

A- Gas Phase Control:

$$\frac{k_L}{H\,k_G} \succ\succ 1$$

Which means that the solute is very soluble (low Henry's constant value) in the liquid and therefore the resistance is mainly in the gas film.

B- Liquid Phase Control

$$\frac{k_L}{H\,k_G} \prec\prec 1$$

Using the data available in Table 7.1, the value of $(k_L/H.k_G)$ is 5.81 for NH_3-H_2O system, indicating gas phase control. For the CO_2-MEA-H_2O system $(k_L/H.k_G)$ is 0.039 indicating liquid phase control.

7.2.1.3 Plate Efficiency

In addition, (Kohl, 1956) observed that the chemical absorption of carbon dioxide by alkanolamines gave 8-25% plate efficiency. In comparison, the gas film controlling processes (such as the absorption of ammonia) gave >80% plate efficiency. Therefore, it was concluded that the absorption of carbon dioxide is a liquid film controlling process.

7.3 Time Parameters in the Higee

7.3.1 Residence Time

The purpose of this section is to theoretically calculate the residence time of the liquid in the rotor. (Munjal et al., 1989) proposed an approximate analytical expression that predicts the thickness of asymptotic liquid film in the RPBs. The assumptions of the model were reviewed by (Basic and Dudukovic, 1995). It was assumed that the packing surface was completely wetted (i.e. $a_p = a_w$), and the liquid flows through the RPB in the forms of films. In addition, the coriolis and gravitational forces were considered negligible.

$$h = \left(\frac{3\nu\Gamma}{g} \right)^{1/3} \tag{7.8}$$

where h is the film thickness (m), ν is the kinematic viscosity of the liquid (m^2/s), Γ is the liquid flowrate per unit width (m), and g is the gravitational acceleration (m/s^2).

In a RPB, the above parameters can be defined as:

$$g = r\,w^2 \tag{7.9}$$

$$\Gamma = \frac{Q_L}{x} \tag{7.10}$$

$$x = 2\pi\, r\, Z\, a_w \tag{7.11}$$

where x is the unit width (m), a_w is the wetted area per unit volume (m^2/m^3), r is the radial position (m), and Z is the axial depth of the packing material (m). Combining Equation (7.9), (7.10) and (7.11) into (7.8) yields:

$$h = \left(\frac{3\nu Q_L}{(2\pi\, r\, Z\, a_w)(r\,\omega^2)} \right)^{1/3} \tag{7.12}$$

The volume of the liquid films in the packed bed could be calculated by using:

$$V = \int_{r_1}^{r_2} h_{RPB}\, a_w\, 2\pi\, r\, Z\, dr \tag{7.13}$$

The result of the integration yields:

$$V = \left(\frac{3\nu\, Q_L}{2\pi Z a_w \omega^2} \right)^{1/3} (a_w\, 2\pi Z)\left[r_2^{4/3} - r_1^{4/3} \right] \qquad (7.14)$$

Hence, the residence time is the ratio of the volume and the liquid volumetric flowrate:

$$t_{res} = \frac{V}{Q_L} \qquad (7.15)$$

If we consider an example: (30wt% MEA solution at 40°C)

$r_2 = 0.199$ m, $r_1 = 0.078$ m, $Z = 0.025$ m, $\omega = 105$ rad/s (1000 RPM).

$\rho = 1005$ kg/m^3 $\nu = 1.5*10^{-6}$ m^2/s $a_w = 2132$ m^2/m^3,

$Q_L = 0.66$ kg/s $= 0.66*10^{-3}$ m^3/s

Thus, $V = 2.6*10^{-4}$ m^3.

Hence the residence time $t_{res} = 0.39$ s.

Similarly, the residence time for the experimental runs was calculated at different amine strengths, liquid flowrates, and rotor speeds.

Figure 7.2 shows the residence time for different amine concentrations at a liquid flowrate of 40 L/min and at 40°C. It shows that the more concentrated amine solution has higher residence time due to its higher kinematic viscosity or shear stress. Furthermore, the increase of the rotor speed leads to shorter residence time due to the acceleration of the liquid by the centrifugal forces.

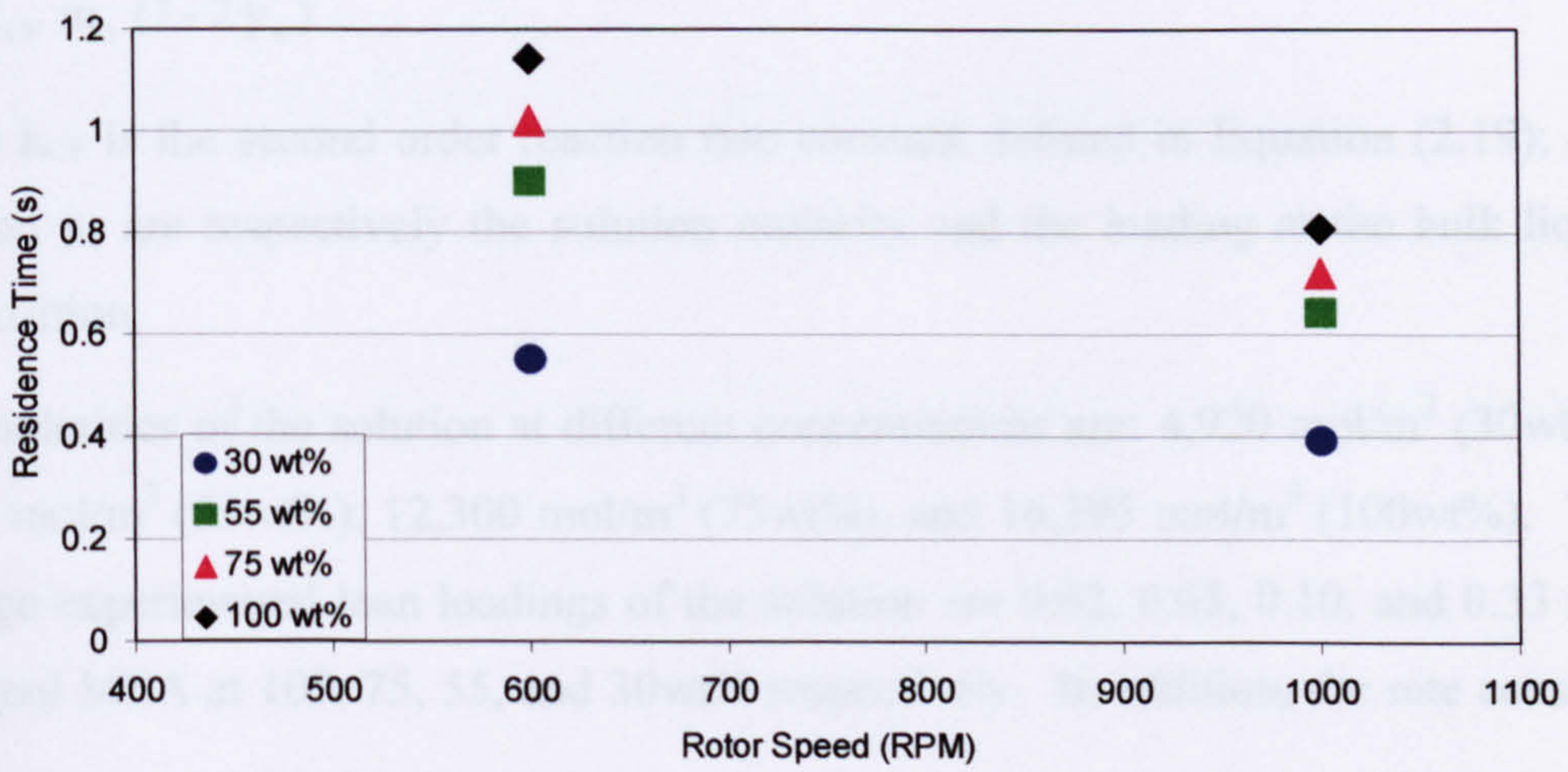

Figure 7.2: Residence time for different amine strengths at 40°C and 40 L/min.

Figure 7.3 shows the effect of liquid flowrate and temperature at constant MEA strength (30 wt%) on the residence time. The irrigation of the RPB with higher liquid flowrates leads to shorter residence time due to higher liquid superficial velocities. Furthermore, the temperature rise of the ethanolamine solution causes the reduction of the viscous forces and consequently leads to shorter residence time.

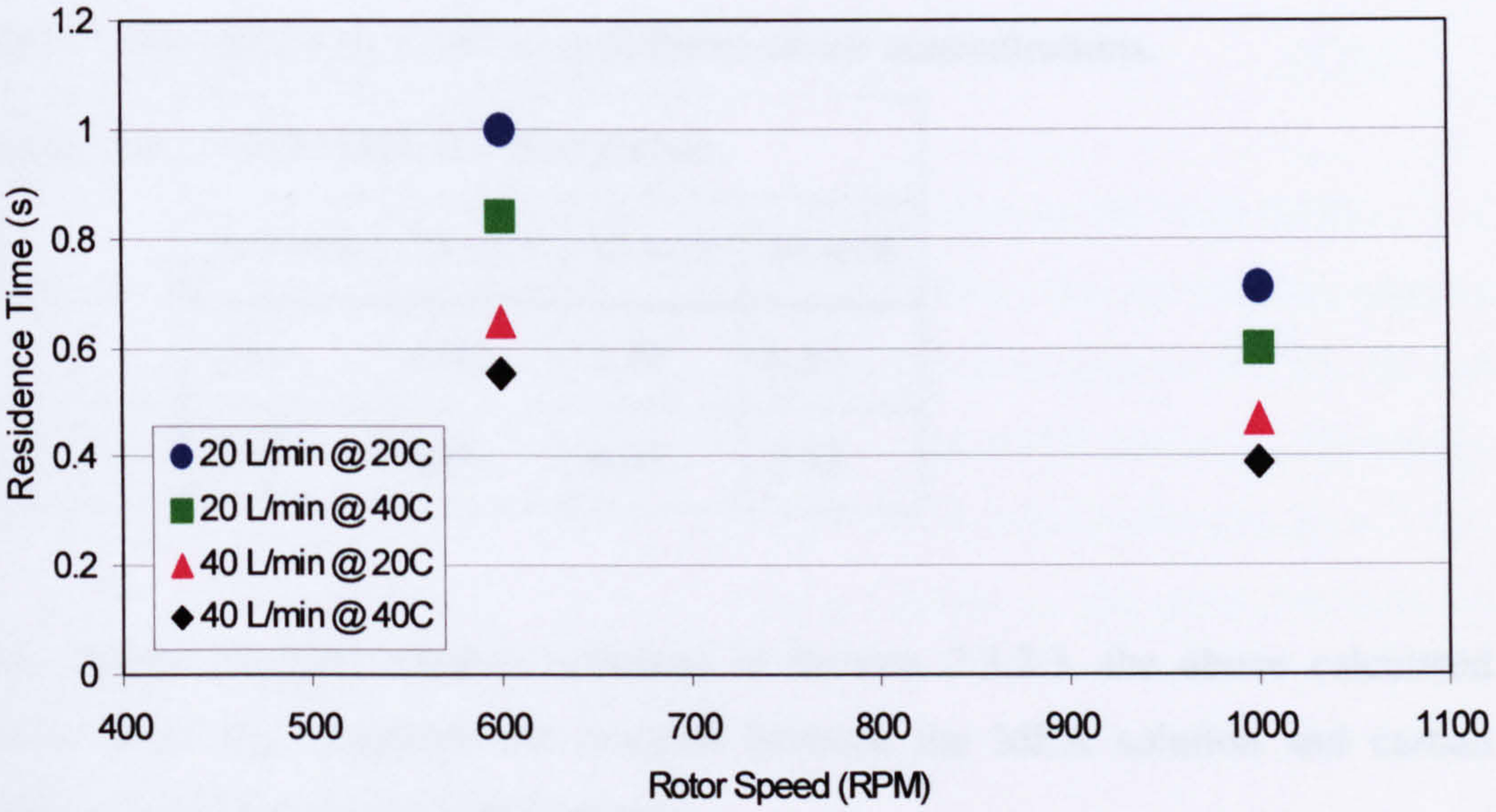

Figure 7.3: Variation of liquid flowrate and temperature on the Residence time at 30 wt%.

7.3.2 Reaction Time

The reaction time (t_r) could be calculated as follows (Astarita et al., 1983):

$$t_r = \frac{1}{k_{CF}\, m_o\, (1-2\, y_o)} \tag{7.16}$$

where k_{CF} is the second order reaction rate constant defined in Equation (2.19); and m_0, and y_0 are respectively the solution molarity and the loading at the bulk liquid composition.

The molarities of the solution at different concentrations are: 4,920 mol/m^3 (30wt%), 9,020 mol/m^3 (55wt%), 12,300 mol/m^3 (75wt%), and 16,395 mol/m^3 (100wt%). The average experimental lean loadings of the solution are 0.02, 0.05, 0.10, and 0.33 mol CO_2/mol MEA at 100, 75, 55, and 30wt% respectively. In addition, the rate constant

(k_{CF}) is sensitive to the temperature of the solution and equals 4.42 and 13.02 m^3/mol/s at 20° and 40°C respectively.

Based on the above, it is possible to calculate the reaction time (t_r) for a matrix of temperatures and concentrations as shown in Table 7.3. It is apparent that the decrease of the MEA concentration solution causes slower reaction time. In addition, doubling the temperature causes 66% faster reaction time.

Table 7.3: Reaction time x 10^5 (s) at different amine concentrations.

Temperature (°C)	MEA solution concentration			
	100 wt%	75 wt%	55 wt%	30 wt%
20	1.41	1.94	2.79	6.87
40	0.48	0.66	0.95	2.33

Based on the reaction regimes reviewed in Section 2.3.2.3, the above calculated reaction times (t_r) categories the reaction between the MEA solution and carbon dioxide as very fast but not instantaneous.

7.3.3 Diffusion Time and Film Thickness

According to the film theory model for the physical absorption, the mass transfer flux is defined as:

$$N = \frac{D}{h}(C_{ai} - C_a) \tag{7.17}$$

The liquid phase mass transfer coefficient is then defined as:

$$k^0_L = \frac{D}{h} \tag{7.18}$$

The "diffusion time" (t_D) concept is defined by (Astarita et al., 1983) from the following equation:

$$k^0_L = \sqrt{\frac{D}{t_D}} \tag{7.19}$$

Thus, combining Equations (6.18) and (6.19) yields:

$$t_D = \frac{h^2}{D} \tag{7.20}$$

The film thickness in the RPB could be calculated by integrating Equation (7.12):

$$h = \left(\frac{3\nu Q_L}{(2\pi Z a_w)(\omega^2)} \right)^{1/3} \int_{r_1}^{r_2} \frac{dr}{r^{2/3}} \tag{7.21}$$

$$h = 3\left(\frac{3\nu Q_L}{(2\pi Z a_w)(\omega^2)} \right)^{1/3} \left(r_2^{1/3} - r_1^{1/3} \right) \tag{7.22}$$

The diffusion time (t_D) in industrial mass transfer units' lies in the range ($0.004 < t_D < 0.04$ sec.). Tables P1, P2, P3, and P4 shows the diffusion time for the experimental runs at different operating conditions. The average diffusion time for 30, 55, 75, and 100 wt.% MEA solutions are 0.012, 0.036, 0.073, and 0.086 seconds respectively. The average film thickness for 30, 55, 75, and 100 wt.% MEA solutions are 4.7, 8.2, 11.3, 12.3 μm. Therefore, the diffusion time is highest at the more concentrated amine solutions due to larger film thickness.

7.3.4 The Enhancement Factor

In mass transfer coupled with a chemical reaction, the enhancement factor (I) is defined as the square root of the relative rates of reaction and diffusion (Astarita et al., 1983).

$$I = \sqrt{\frac{t_D}{t_r}} \tag{7.23}$$

Table 7.4 shows that average enhancement factors at different amine concentrations and operating temperatures. The enhancement factors are highest at strong amine concentrations and higher operating temperatures, which indicates a combination of longer diffusion time and shorter reaction time.

In addition, the mass transfer data shows that the magnitude of the enhancement factor increases with slower rotor speed at constant concentration, temperature and liquid flowrate. The rotor speed influences only the diffusion time but not the reaction time. The higher rotor speed results in thinner film thickness and hence shorter diffusion time and subsequently lower enhancement factors.

Table 7.4: Average enhancement factors (I) for RPB.

Temperature (°C)	MEA solution concentration			
	100 wt%	75 wt%	55 wt%	30 wt%
20	90.7	72.7	38.3	11.7
40	101.3	76.2	55.3	14.4

Table 7.5 shows the enhancement factors for the conventional columns. The calculation of the enhancement factor is based upon Equation 7.23. The diffusion time range for the conventional column (i.e. 1 g) is 0.04-0.004 s (Astarita et al., 1983). The reaction time calculated in Section 7.3.2 remains unchanged, as it is only dependent on the solution characteristics. Thus, it is possible to calculate the higher and lower bounds of the enhancement factors at 20° and 40°C. It is clear that the Higee enhancement factors are higher than those of the conventional columns at 50, 75 and 100 wt% amine solutions.

Table 7.5: High/Low enhancement factors (I) for conventional columns.

Temperature (°C)	MEA solution concentration			
	100 wt%	75 wt%	55 wt%	30 wt%
20	53.3/16.8	45.4/14.4	37.9/12.0	24.1/7.6
40	91.3/28.9	77.8/24.6	64.9/20.5	41.4/13.1

7.4 Absorption Runs

7.4.1 Calculation of HTU

The difficulty of separation is expressed as the number of transfer units (NTU). The number of overall transfer units based upon the change in gas concentration is defined as follows for equi-molar counter diffusion (Colburn, 1939):

$$NTU_{OG} = \int_{y_1}^{y_2} \frac{dy}{y - y^*} \qquad (7.24)$$

Assuming that the continuous counter-current fluids pass through the Higee rotor in plug flow, both the operating and the equilibrium lines are straight (dilute solutions), Henry's law is valid, and the absorption heat effects are negligible. In addition, the process is liquid film limited (Section 7.2.1) and the reaction between the amine and the carbon dioxide is very fast especially with higher amine concentrations (Section 7.3.2) then the interfacial carbon dioxide concentration is negligible. Furthermore, assuming that the reaction is irreversible then the equilibrium partial pressure is zero ($y^*=0$) (McCabe et al., 1993). Hence, the integral term can be simplified to:

$$NTU_{OG} = \int_{y_1}^{y_2} \frac{dy}{y - y^*} = \ln\left(\frac{y_2}{y_1}\right) \tag{7.25}$$

The terminology used to express the efficiency of the Higee is the Height of the Transfer Unit (HTU). Section 2.4.3 derives the equation to calculate the total height of bed from the mass balance across the RPB.

$$H = NTU_{OG}. \times HTU_{OG}. \tag{7.26}$$

Hence, the height of the transfer unit HTU_{OG} could be calculated by:

$$HTU_{OG} = \frac{\Delta r}{NTU_{OG}} = \frac{R_o - R_i}{NTU_{OG}} \tag{7.27}$$

where R_o and R_i are the outside and the inside radii of the RPB. (Note: The abbreviation of the Height of the Transfer Unit (HTU) for the absorption runs refers to HTU_{OG}).

7.4.2 Effect of Varying the RPM

The Higee was operated between 600 and 1000 RPM and thus the mean centrifugal acceleration was 597 and 1657 $m.s^{-2}$ or a gravitational acceleration of 31 and 87 g (based upon the inside diameter) or angular acceleration of 62.8 and 104.7 rad/s. Unfortunately, the speed of the Higee rotor was limited to 1000 RPM due to mechanical and safety worries.

Figures 7.4, 7.5, 7.6, and 7.7 show the effect of increasing the rotational speed of the rotor from 600 to 1000 RPM on the HTU at a constant flow of ethanolamine solution (20, and 40 L/min.) and temperature (20°, and 40°C) for 30wt.%, 50wt.%, 80wt% and 100wt% of ethanolamine solution concentration respectively.

It is evident from these plots that the rise in the rotational speed of the rotor leads to a reduction in the HTU value. On increasing the speed from 600 to 1000 RPM, the average HTU decrease is 5, 9, 10, and 13 % for 30wt%, 55wt.%, 75wt%, and 100wt% strength ethanolamine solutions respectively.

The above experimental results are consistent with the theory and the work of other researchers. The more efficient operation of the Higee at higher rotor speeds may be due to the fact that the rise in the rotor speed causes the reduction of the angular ethanolamine solution maldistribution in the packed bed (Burns, 1996).

The visual analysis carried out in this department by (Burns, 1996) using water and emulsion paint solution showed that the speed of the rotor is solely influencing the type of the flow in the RPBs. There are three types of flow:

a) Pore flow: the liquid travel as rivulets. The angular maldistribution is the highest and hence minimum gas/liquid interfacial area.

b) Droplet flow: droplets of the liquid travels through the packing voids.

c) Film flow: the liquid travels as a thin film over the packing surface area.

Pore flow was observed at low rotor speeds (<90 rad/s) and film and droplet flow at high rotational speeds (>130 rad/s). (Jamil, 1997) performed similar visual analysis but using more viscous solutions: water and propylene glycol solutions (11.5 and 21 cP). The pore flow occurred at low rotor speeds (<63.5 rad/s) and droplet and film flow occurred at high rotational speed (>125 rad/s). Thus, it could be concluded that the low rotational speeds of the experiments carried out at 600 RPM has much higher level of maldistribution than the experiments carried out at 1000 RPM due to different type of liquid flow behaviour inside the RPB.

Furthermore, the flooding exercise in Chapter 4 proved that the increase in the acceleration of the Higee causes a subsequent rise to the interphase velocity throughout the packed bed. This fact in conjunction with a large specific area causes the creation of thin films and small droplets and hence the overall result is a better mass transfer operation as shown by the small HTU values.

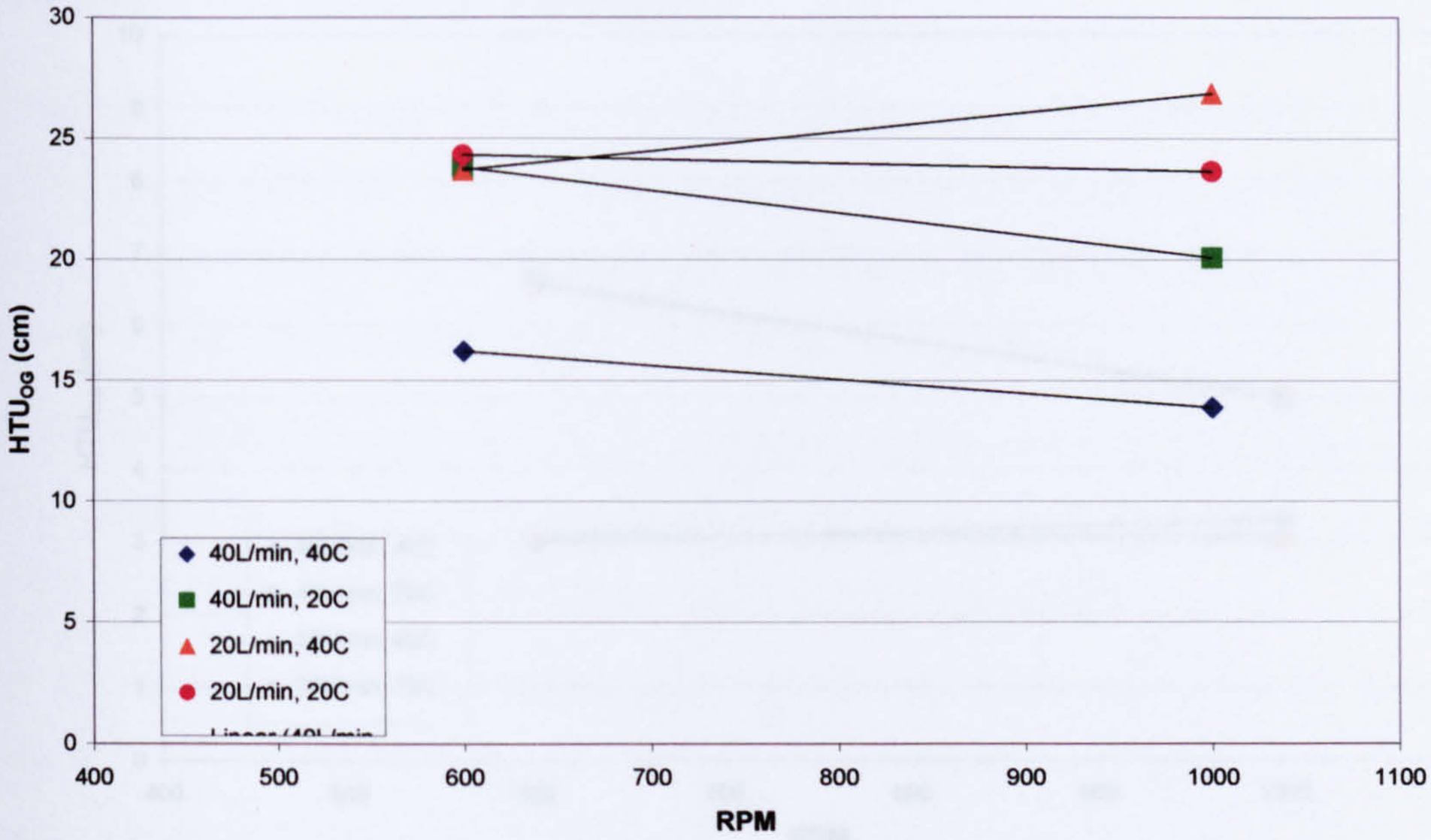

Figure 7.4: Variation of HTU with rotor speed at constant temperature and liquid flowrate for 30wt% solution.

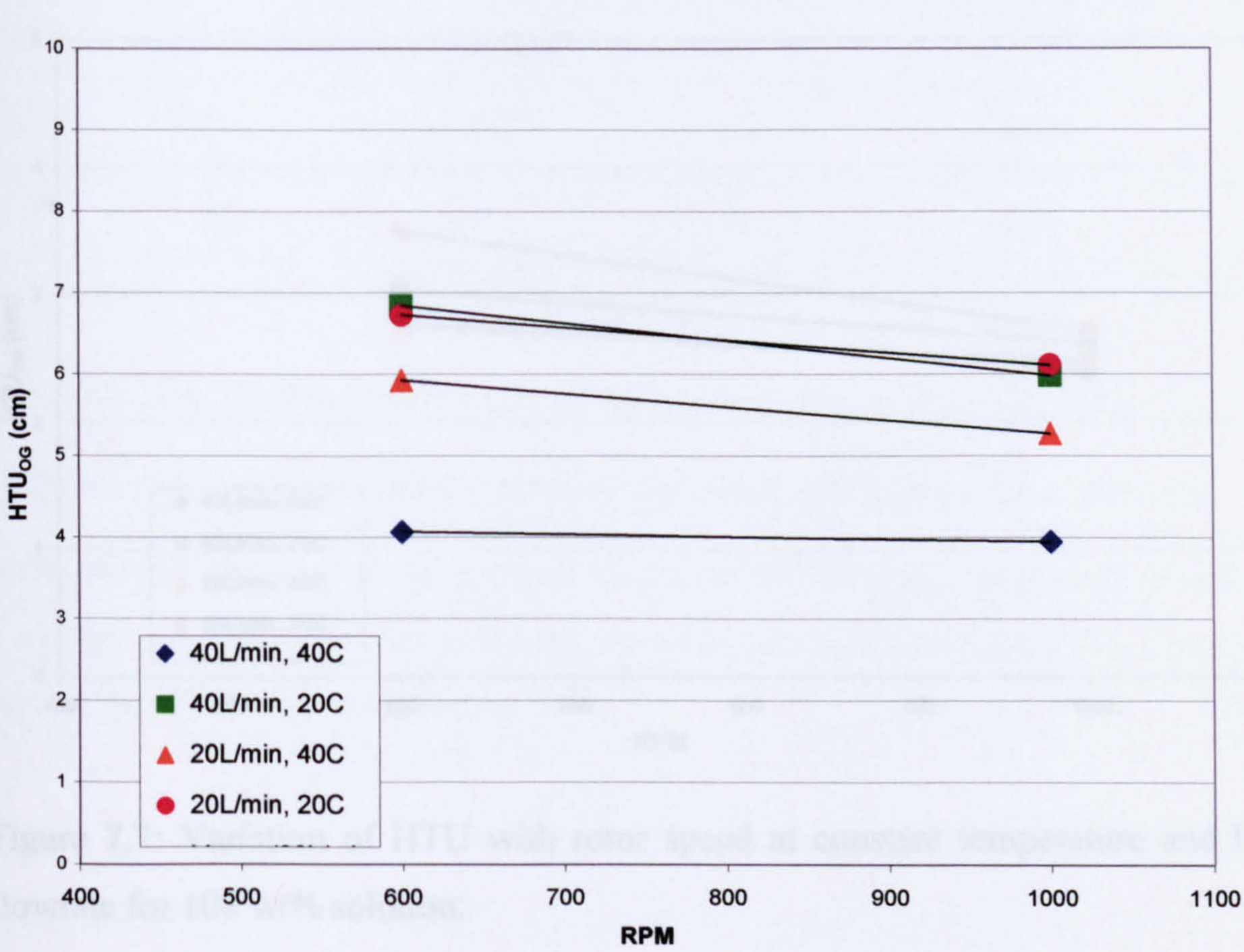

Figure 7.5: Variation of HTU with rotor speed at constant temperature and liquid flowrate for 55wt% solution.

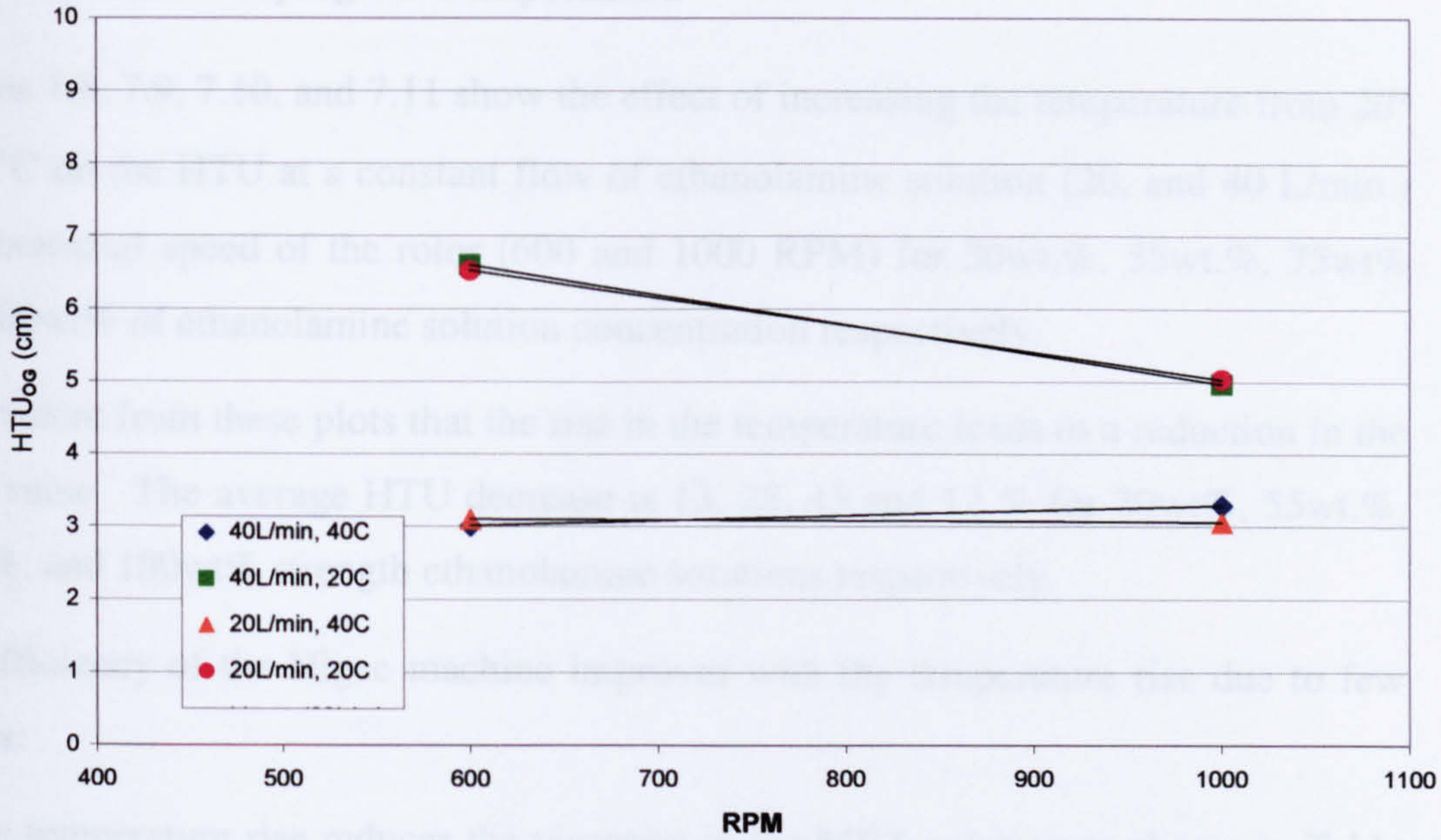

Figure 7.6: Variation of HTU with rotor speed at constant temperature and liquid flowrate for 75wt% solution.

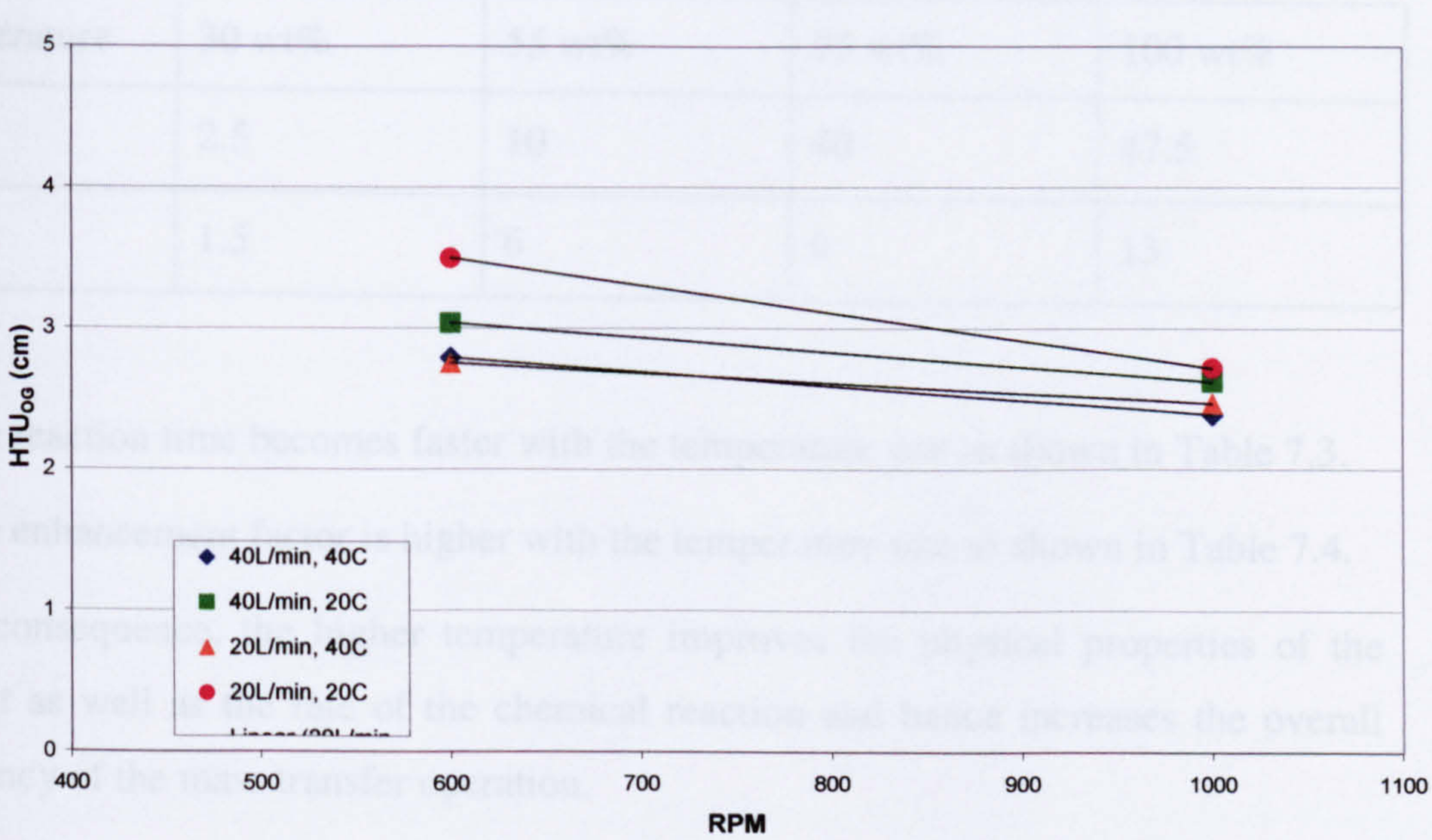

Figure 7.7: Variation of HTU with rotor speed at constant temperature and liquid flowrate for 100 wt% solution.

7.4.3 Effect of Varying the Temperature

Figures 7.8, 7.9, 7.10, and 7.11 show the effect of increasing the temperature from 20° to 40°C on the HTU at a constant flow of ethanolamine solution (20, and 40 L/min.) and rotational speed of the rotor (600 and 1000 RPM) for 30wt.%, 55wt.%, 75wt% and 100wt% of ethanolamine solution concentration respectively.

It is evident from these plots that the rise in the temperature leads to a reduction in the HTU value. The average HTU decrease is 13, 25, 45 and 12 % for 30wt%, 55wt.%, 75wt%, and 100wt% strength ethanolamine solutions respectively.

The efficiency of the Higee machine improves with the temperature rise due to few factors:

1- The temperature rise reduces the viscosity of the MEA solution as shown in Table 7.6. As a consequence, the residence time of the mass transfer operation decreases. In addition, the film thickness becomes thinner and hence the diffusion time is reduced.

Table 7.6: Kinematic viscosities (centistokes) of the MEA solutions at 20° and 40°C.

Temperature	30 wt%	55 wt%	75 wt%	100 wt%
20°C	2.5	10	40	47.5
40°C	1.5	6	9	13

2- The reaction time becomes faster with the temperature rise as shown in Table 7.3.

3- The enhancement factor is higher with the temperature rise as shown in Table 7.4.

As a consequence, the higher temperature improves the physical properties of the solvent as well as the rate of the chemical reaction and hence increases the overall efficiency of the mass transfer operation.

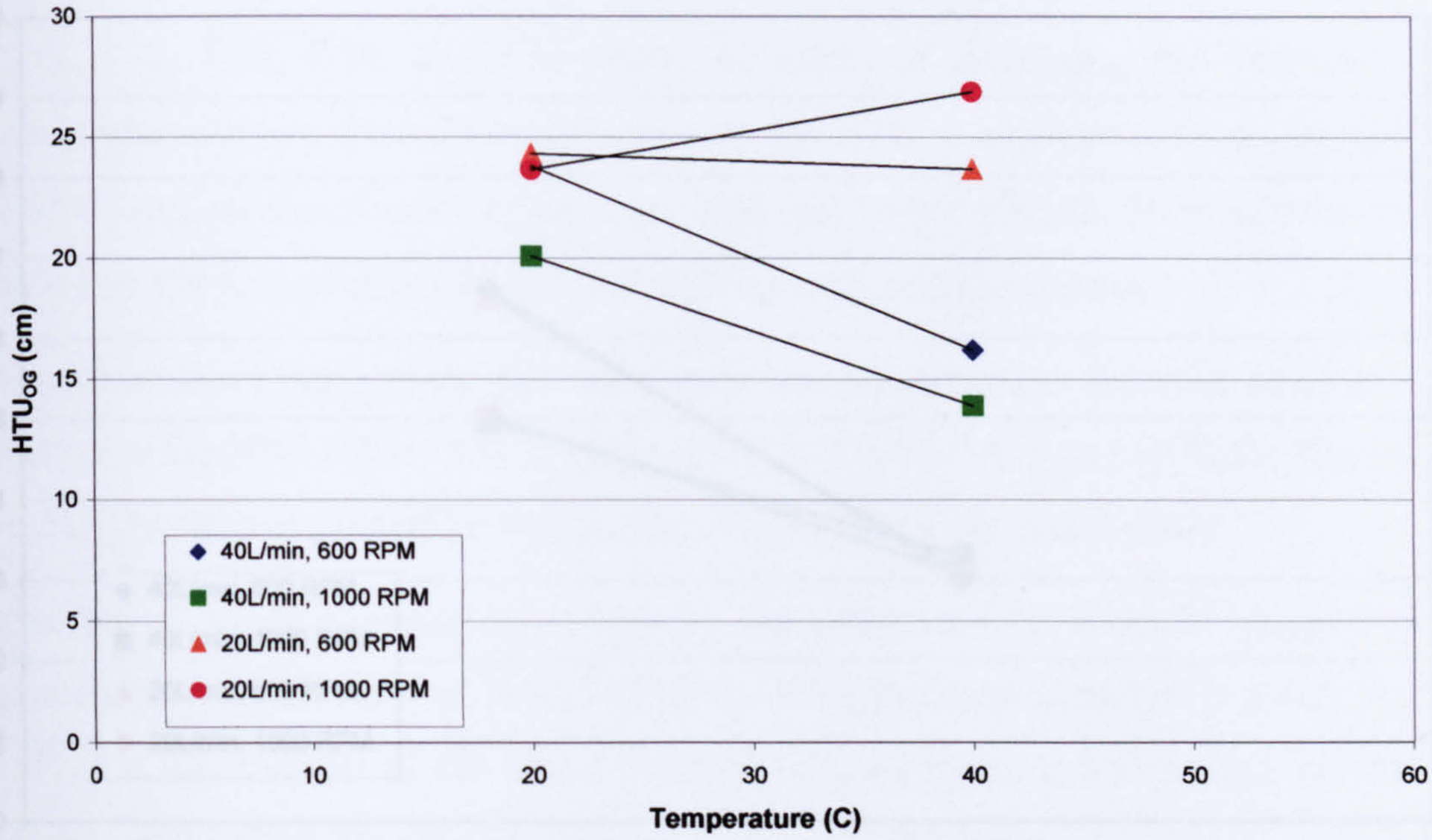

Figure 7.8: Variation of HTU with temperature at constant liquid flowrate and rotor speed for 30wt% solution

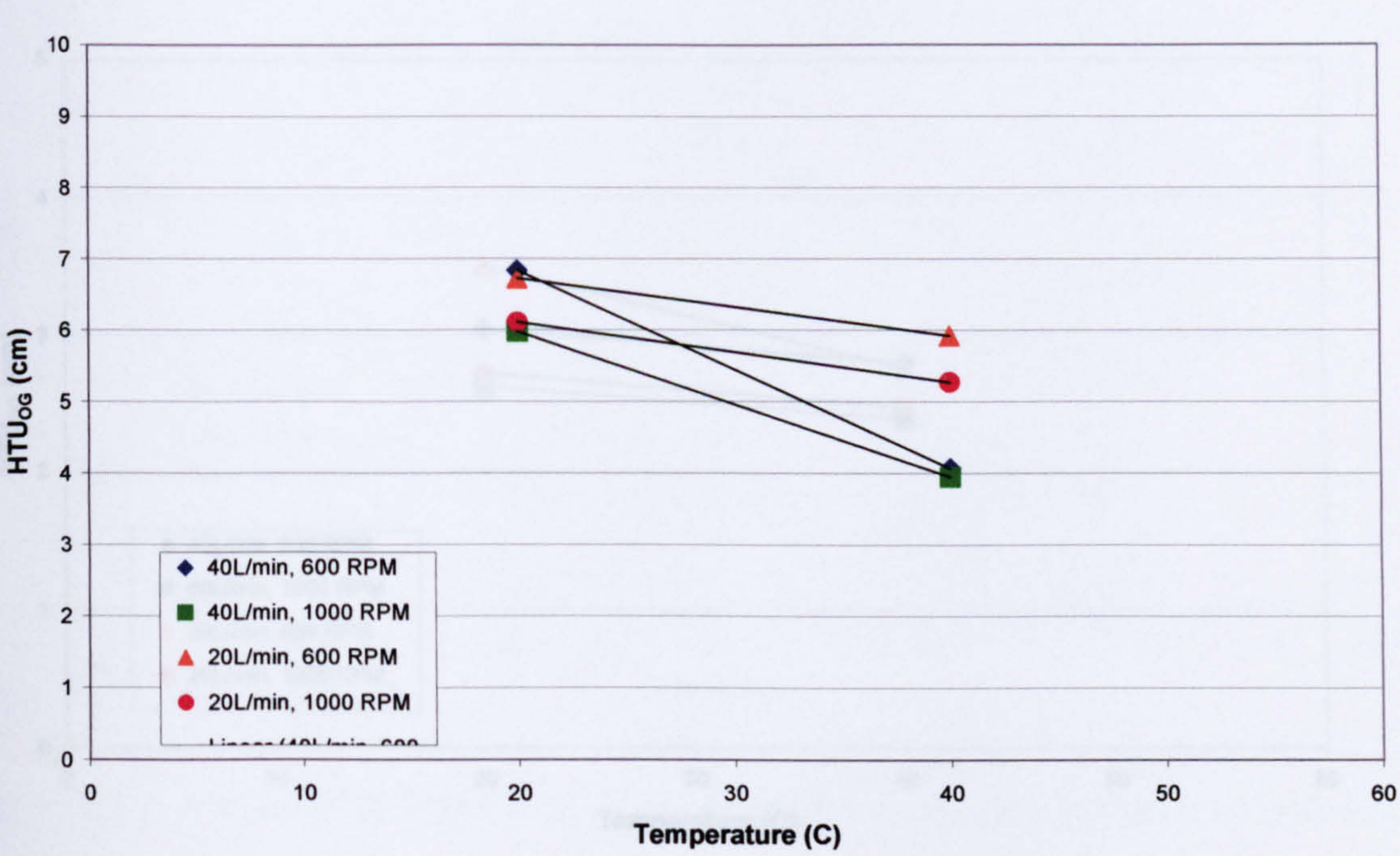

Figure 7.9: Variation of HTU with temperature at constant liquid flowrate and rotor speed for 55wt% solution.

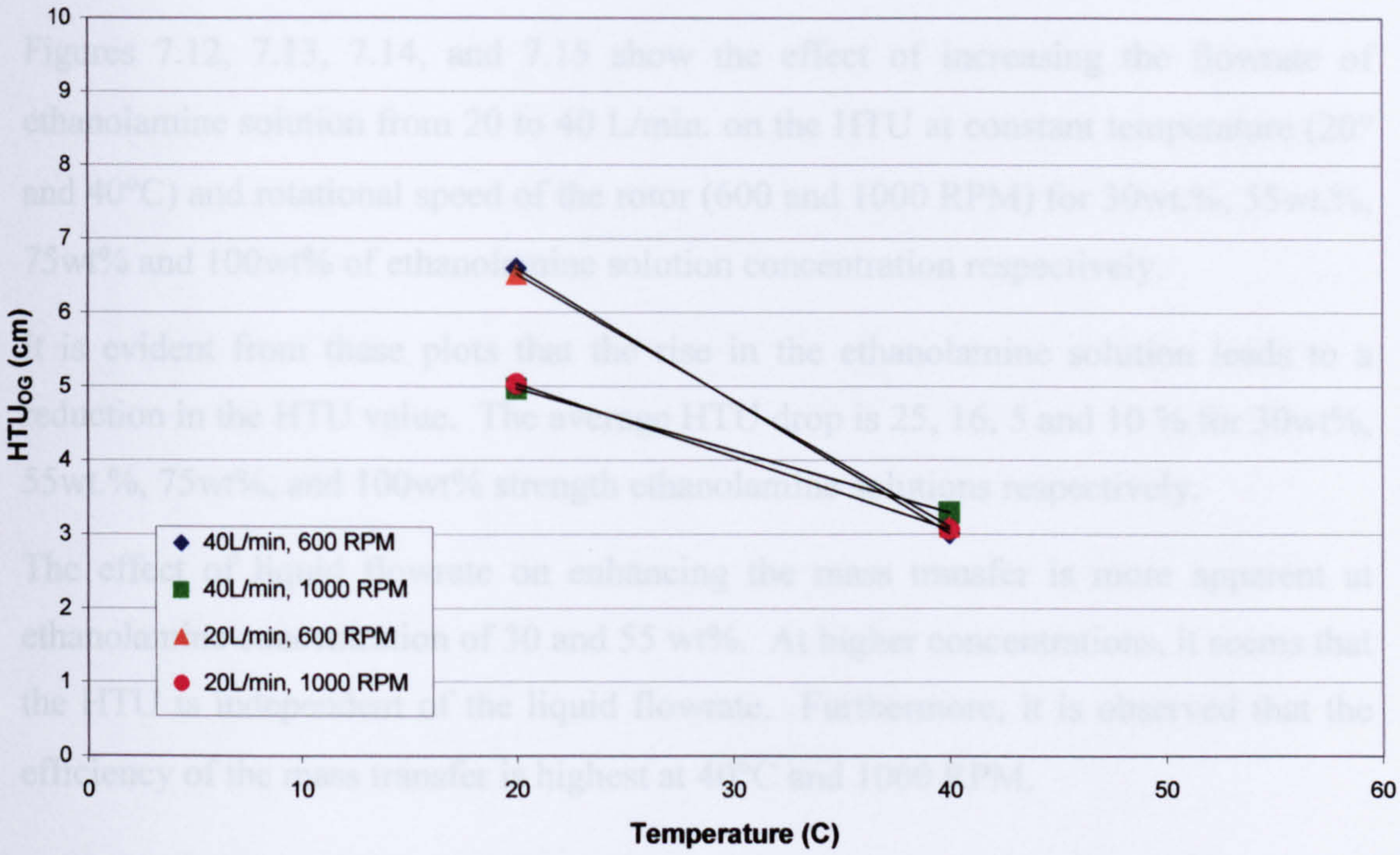

Figure 7.10: Variation of HTU with temperature at constant liquid flowrate and rotor speed for 75wt% solution.

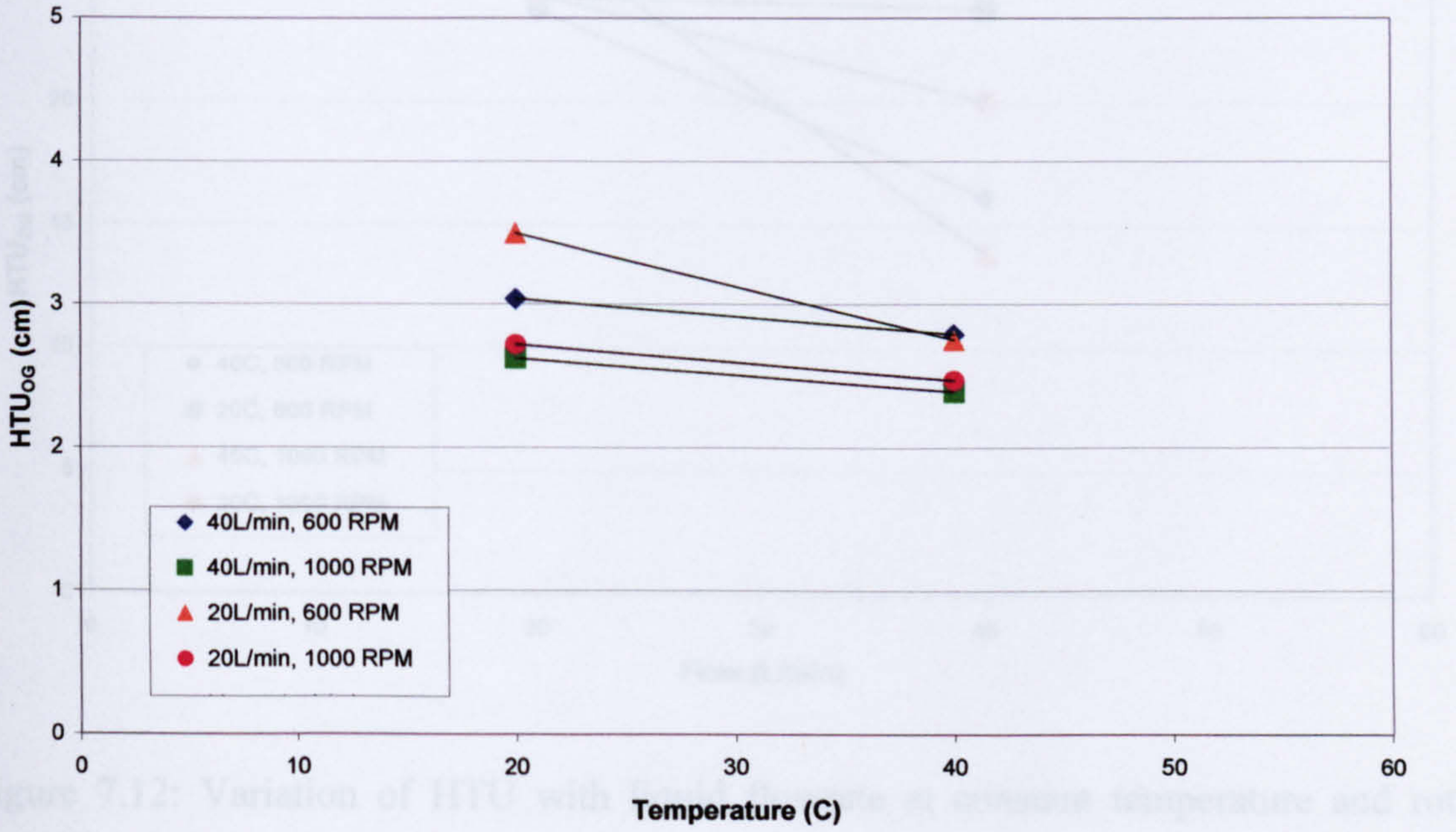

Figure 7.11: Variation of HTU with temperature at constant liquid flowrate and rotor speed for 100wt% solution

7.4.4 Effect of Varying the Liquid Flow

Figures 7.12, 7.13, 7.14, and 7.15 show the effect of increasing the flowrate of ethanolamine solution from 20 to 40 L/min. on the HTU at constant temperature (20° and 40°C) and rotational speed of the rotor (600 and 1000 RPM) for 30wt.%, 55wt.%, 75wt% and 100wt% of ethanolamine solution concentration respectively.

It is evident from these plots that the rise in the ethanolamine solution leads to a reduction in the HTU value. The average HTU drop is 25, 16, 5 and 10 % for 30wt%, 55wt.%, 75wt%, and 100wt% strength ethanolamine solutions respectively.

The effect of liquid flowrate on enhancing the mass transfer is more apparent at ethanolamine concentration of 30 and 55 wt%. At higher concentrations, it seems that the HTU is independent of the liquid flowrate. Furthermore, it is observed that the efficiency of the mass transfer is highest at 40°C and 1000 RPM.

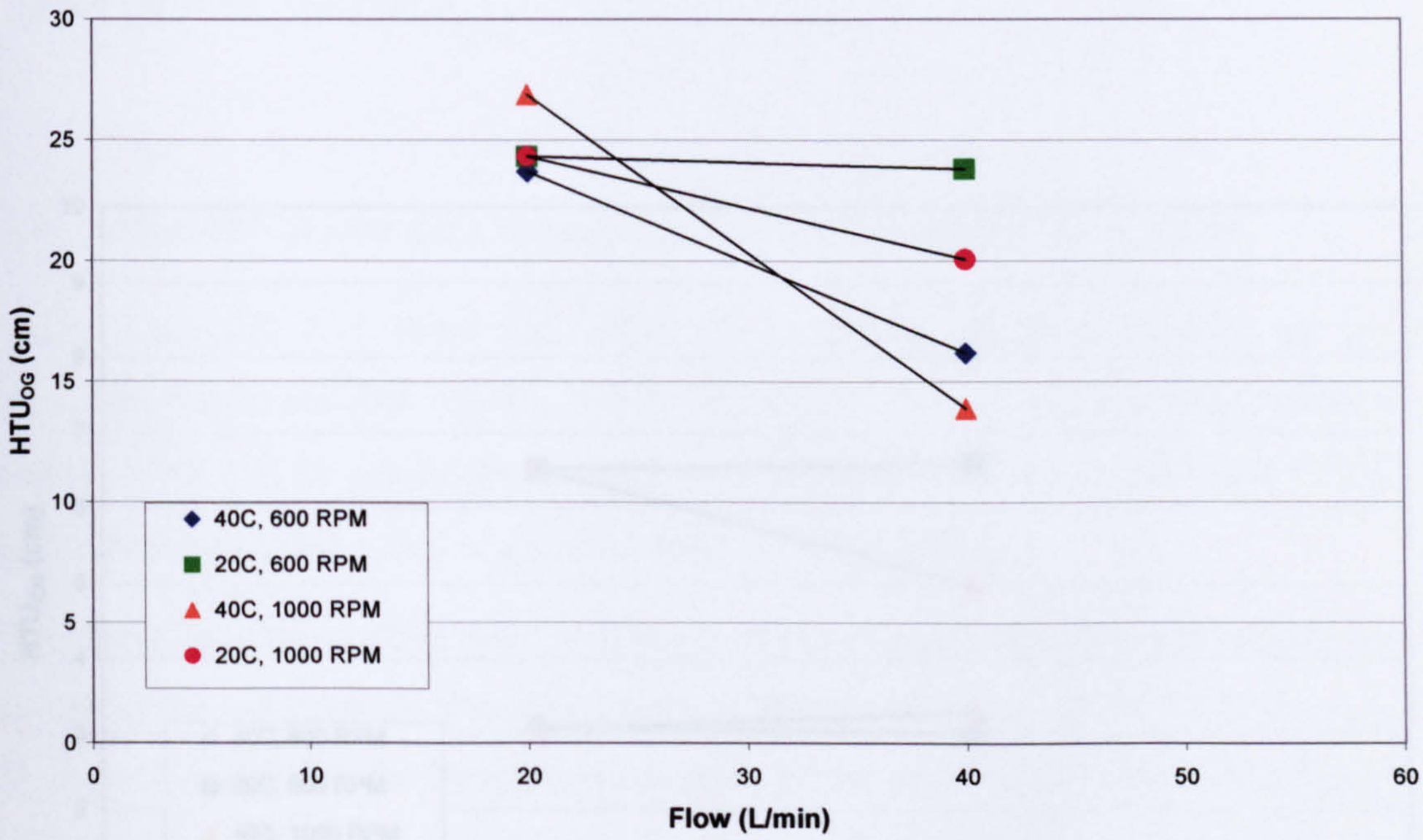

Figure 7.12: Variation of HTU with liquid flowrate at constant temperature and rotor speed for 30wt% solution.

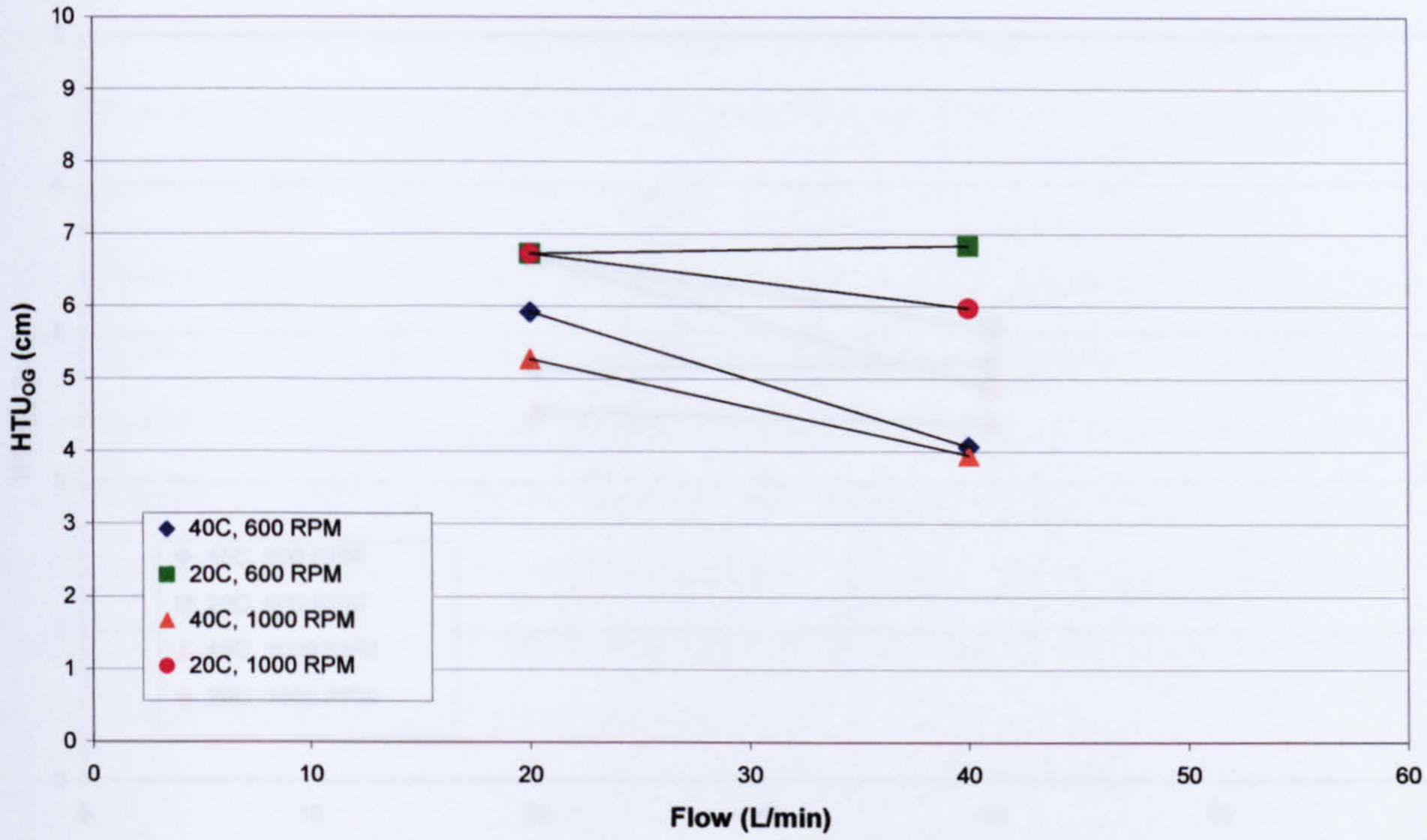

Figure 7.13: Variation of HTU with liquid flowrate at constant temperature and rotor speed for 55wt% solution

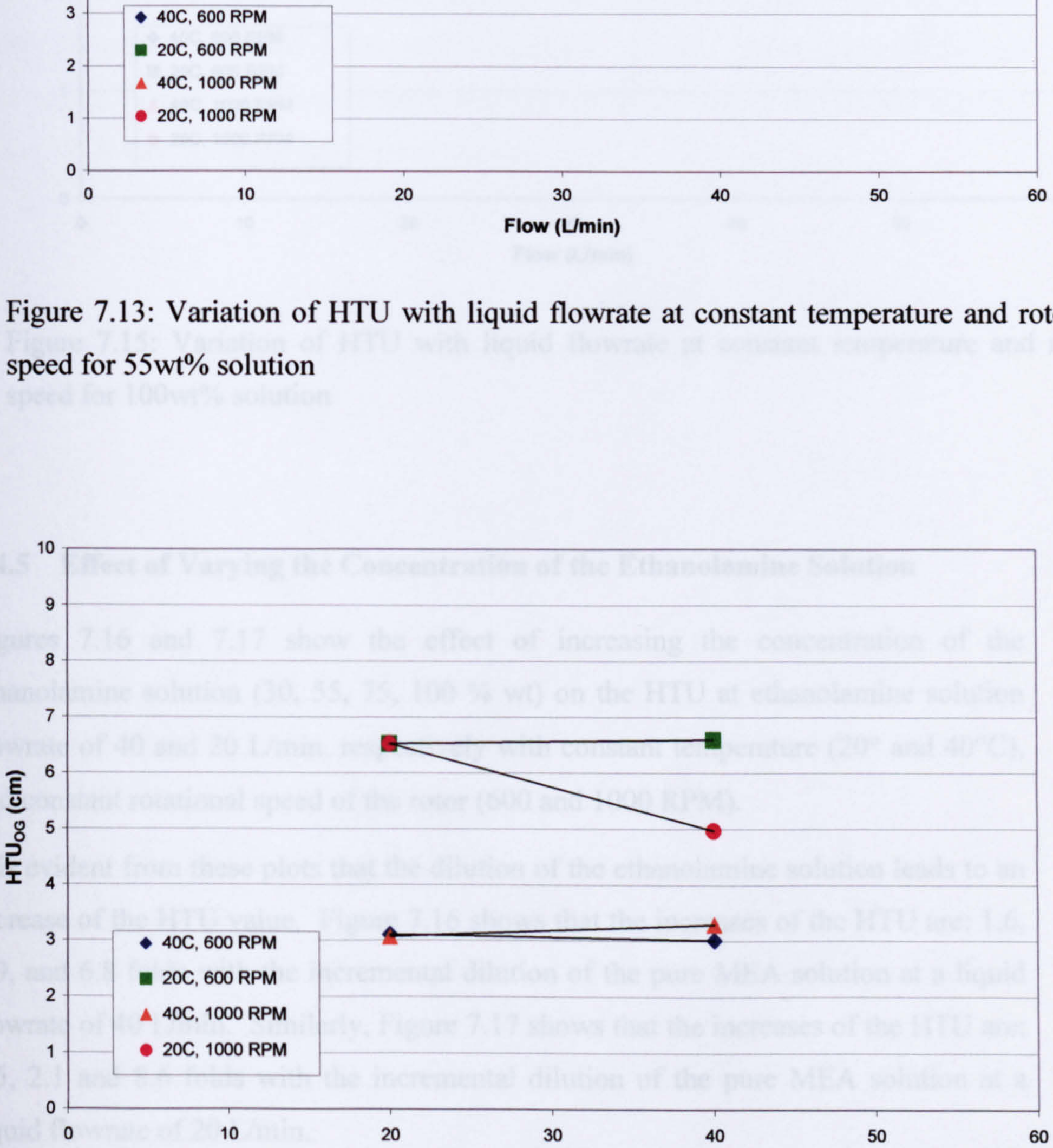

Figure 7.14: Variation of HTU with liquid flowrate at constant temperature and rotor speed for 75wt% solution

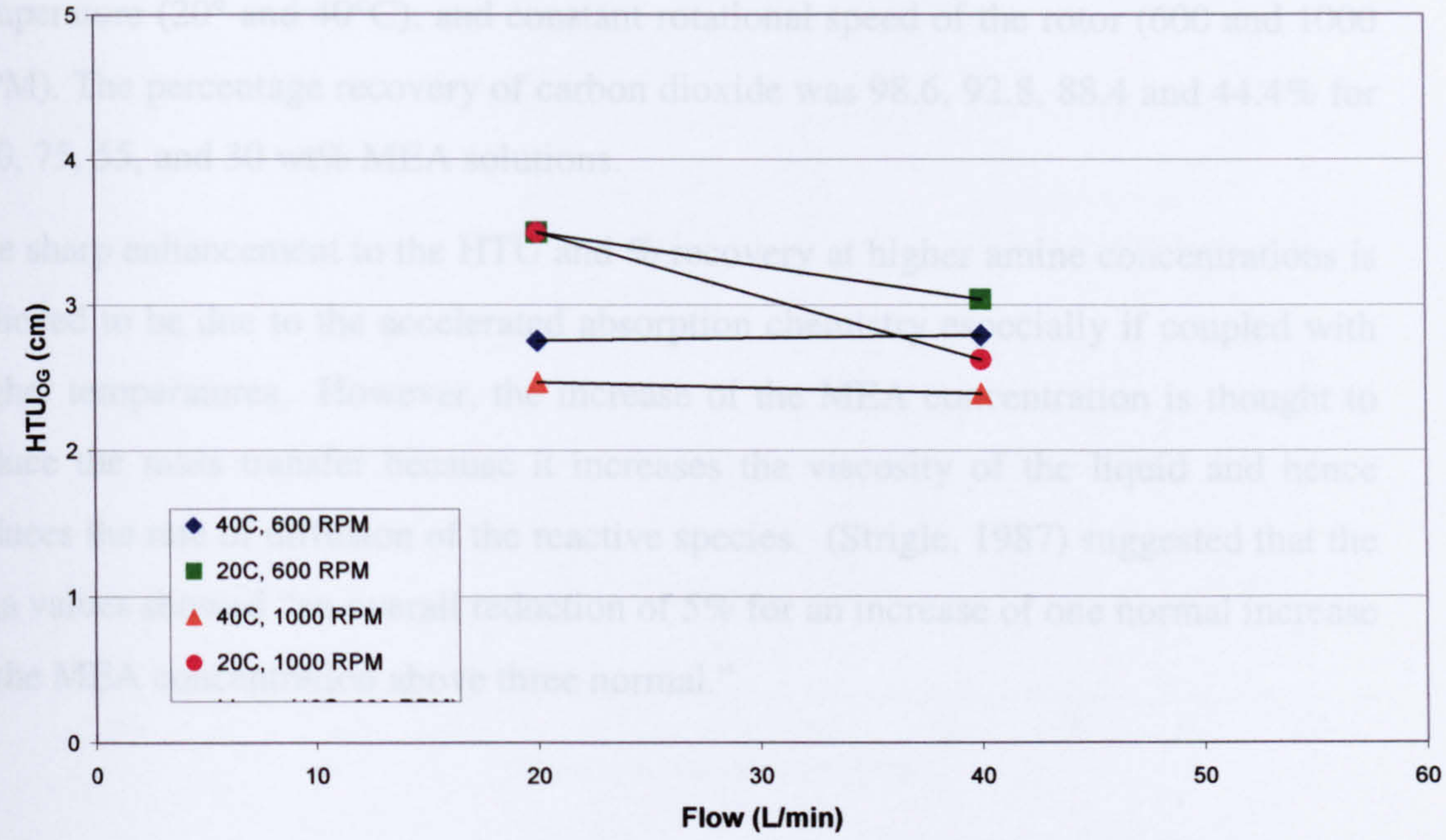

Figure 7.15: Variation of HTU with liquid flowrate at constant temperature and rotor speed for 100wt% solution

7.4.5 Effect of Varying the Concentration of the Ethanolamine Solution

Figures 7.16 and 7.17 show the effect of increasing the concentration of the ethanolamine solution (30, 55, 75, 100 % wt) on the HTU at ethanolamine solution flowrate of 40 and 20 L/min. respectively with constant temperature (20° and 40°C), and constant rotational speed of the rotor (600 and 1000 RPM).

It is evident from these plots that the dilution of the ethanolamine solution leads to an increase of the HTU value. Figure 7.16 shows that the increases of the HTU are: 1.6, 1.9, and 6.8 folds with the incremental dilution of the pure MEA solution at a liquid flowrate of 40 L/min. Similarly, Figure 7.17 shows that the increases of the HTU are: 1.5, 2.1 and 8.6 folds with the incremental dilution of the pure MEA solution at a liquid flowrate of 20 L/min.

An alternative representation of the experimental data is the % recovery variation with amine strength. Figures 7.18 and 7.19 show the effect of increasing the concentration of the ethanolamine solution (30, 55, 75, 100 % wt) on the % recovery at

ethanolamine solution flowrate of 40 and 20 L/min. respectively with constant temperature (20° and 40°C), and constant rotational speed of the rotor (600 and 1000 RPM). The percentage recovery of carbon dioxide was 98.6, 92.8, 88.4 and 44.4% for 100, 75, 55, and 30 wt% MEA solutions.

The sharp enhancement to the HTU and % recovery at higher amine concentrations is believed to be due to the accelerated absorption chemistry especially if coupled with higher temperatures. However, the increase of the MEA concentration is thought to reduce the mass transfer because it increases the viscosity of the liquid and hence reduces the rate of diffusion of the reactive species. (Strigle, 1987) suggested that the K_Ga values showed "an overall reduction of 5% for an increase of one normal increase in the MEA concentration above three normal."

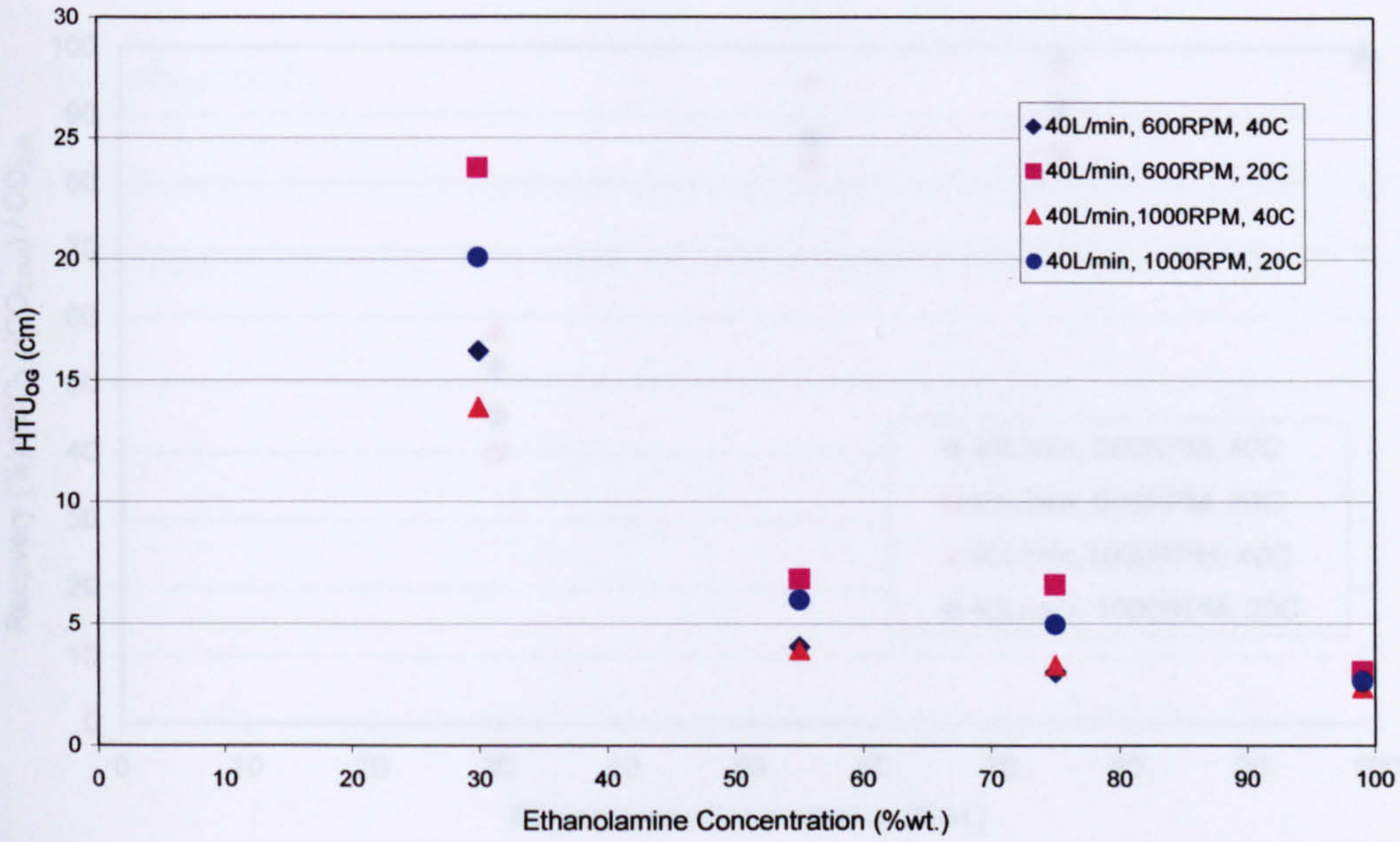

Figure 7.16: Variation of HTU with liquid concentration at constant temperature, rotor speed, and at 40 L/min liquid flowrate

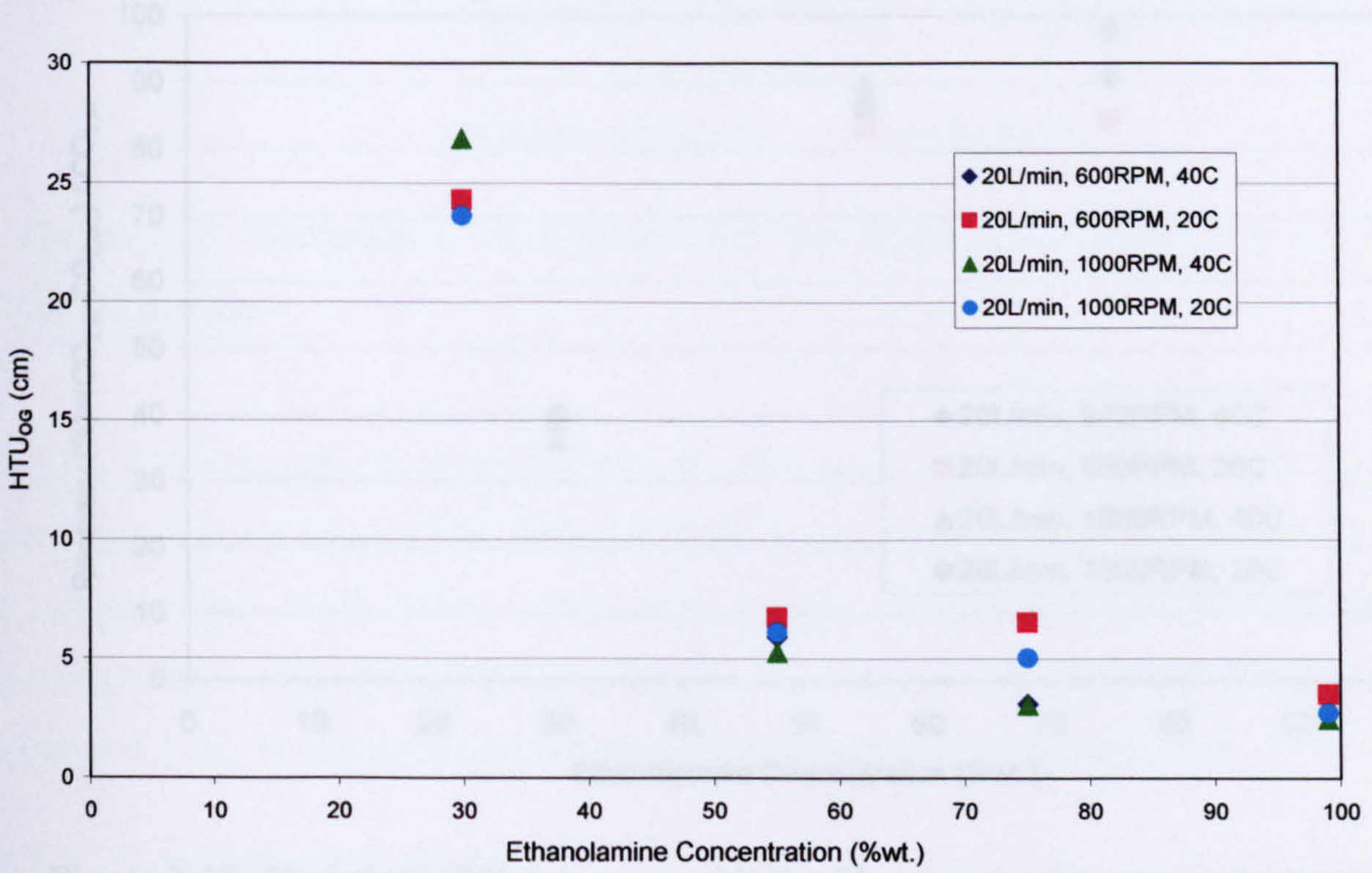

Figure 7.17: Variation of HTU with liquid concentration at constant temperature, rotor speed, and at 20 L/min. liquid flowrate.

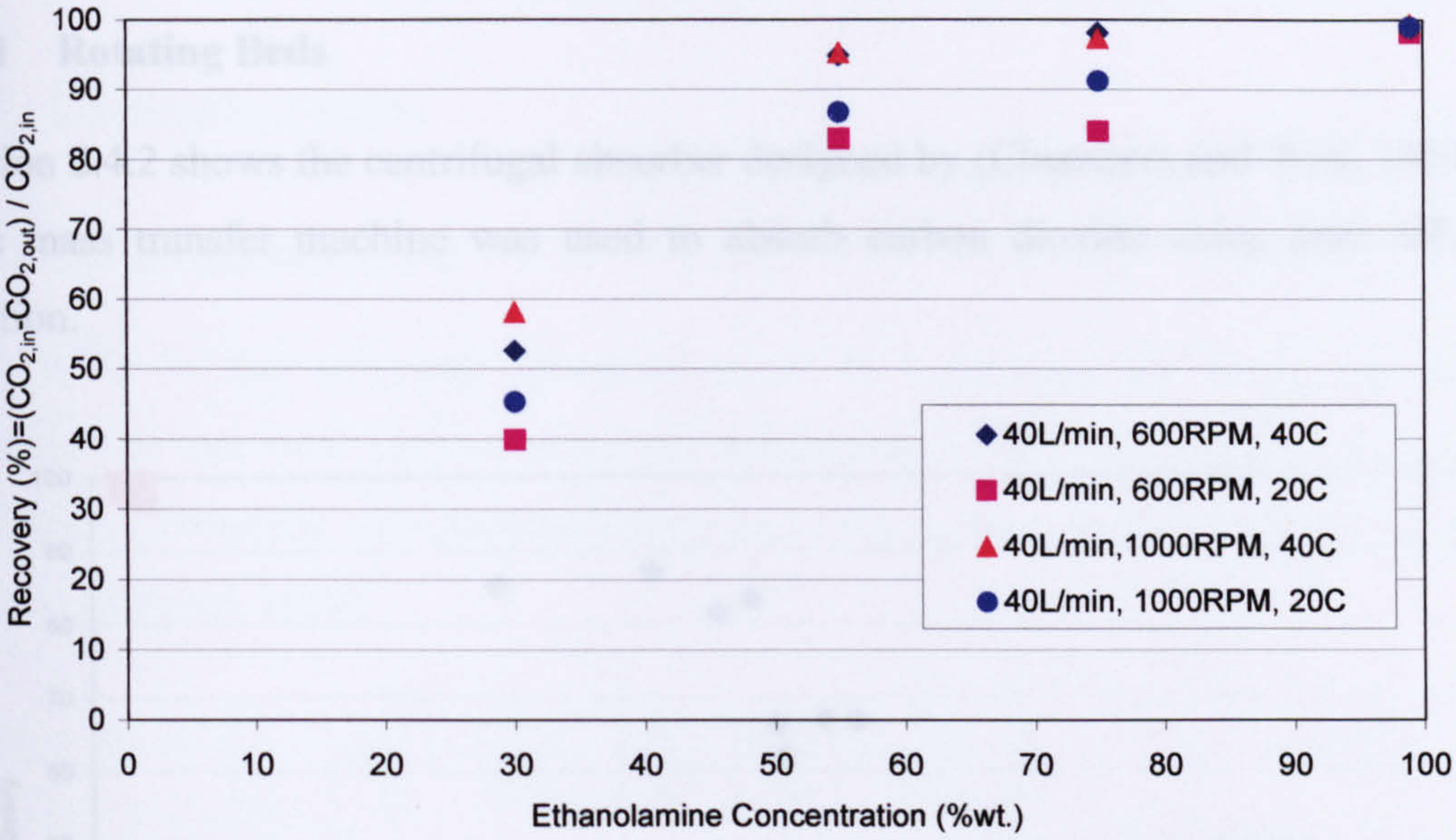

Figure 7.18: Variation of % recovery with liquid concentration at constant temperature, rotor speed, and at 40 L/min liquid flowrate.

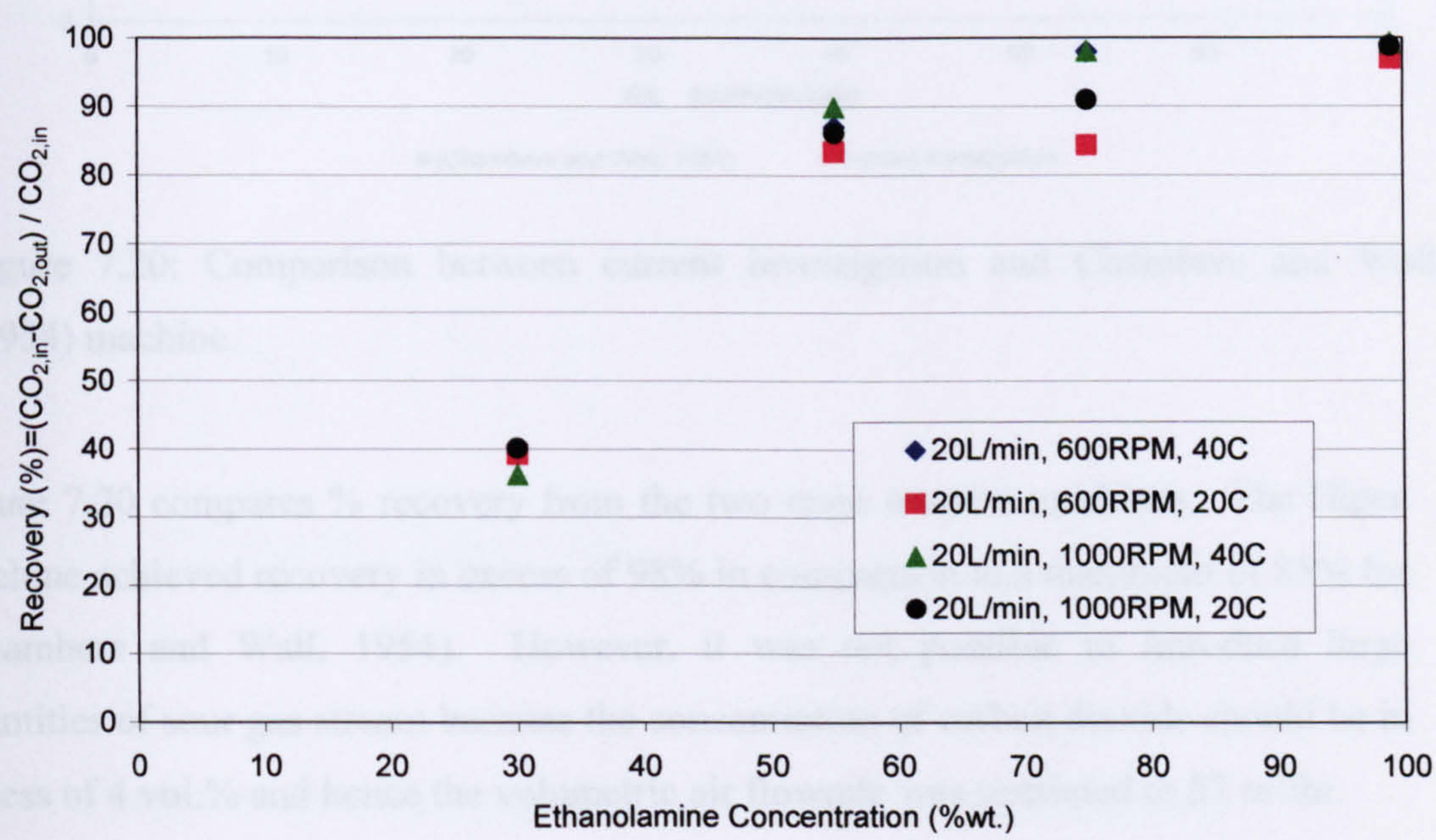

Figure 7.19: Variation of % recovery with liquid concentration at constant temperature, rotor speed, and at 20 L/min liquid flowrate.

7.5 Comparison with Other Mass Transfer Machines

7.5.1 Rotating Beds

Section 2.4.2 shows the centrifugal absorber designed by (Chambers and Wall, 1954). This mass transfer machine was used to absorb carbon dioxide using pure MEA solution.

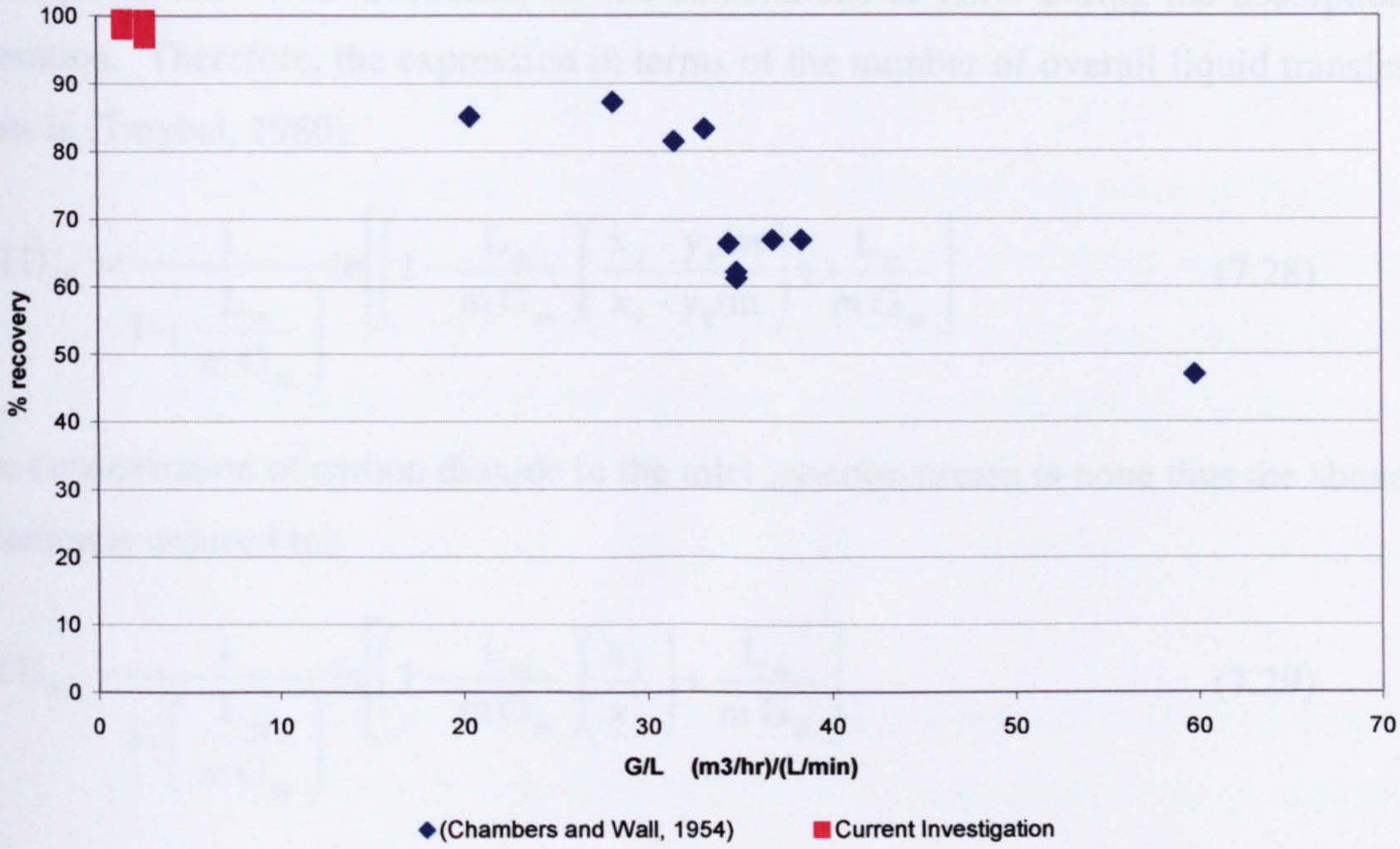

Figure 7.20: Comparison between current investigation and Chambers and Wall (1954) machine.

Figure 7.20 compares % recovery from the two mass transfer machines. The Higee machine achieved recovery in excess of 98% in comparison to a maximum of 85% for (Chambers and Wall, 1954). However, it was not possible to introduce large quantities of sour gas stream because the concentration of carbon dioxide should be in excess of 4 vol.% and hence the volumetric air flowrate was restricted to 57 m^3/hr.

7.5.2 Conventional Column

Table 2.1 shows typical engineering dimensions of a conventional gas sweetening plant. The absorber consists of two 7-m (23 ft) beds of polypropylene saddles. The number of transfer units for the absorber is 4.1 (for simplification purposes NTU =

$\ln(CO_{2,in}/CO_{2,out})$. Therefore, the HTU_{OG} is computed to be 3.4 m. In comparison, the average HTU_{OG} for the Higee machine using 30wt% MEA solution is only 21 cm.

7.6 Desorption Runs

7.6.1 Calculation of HTU

The HTU in the stripping operation could be calculated by using the same assumptions that were mentioned for the calculations of HTU during the absorption operation. Therefore, the expression in terms of the number of overall liquid transfer units is (Treybal, 1980):

$$NTU_{OL} = \frac{1}{1-\left(\frac{L_m}{mG_m}\right)} \ln\left[\left(1-\frac{L_m}{mG_m}\right)\left(\frac{x_2 - y_1/m}{x_1 - y_1/m}\right)+\frac{L_m}{mG_m}\right] \qquad (7.28)$$

The concentration of carbon dioxide in the inlet gaseous stream is none thus the above equation is reduced to:

$$NTU_{OL} = \frac{1}{1-\left(\frac{L_m}{mG_m}\right)} \ln\left[\left(1-\frac{L_m}{mG_m}\right)\left(\frac{x_2}{x_1}\right)+\frac{L_m}{mG_m}\right] \qquad (7.29)$$

or

$$NTU_{OL} = \frac{1}{1-\left(\frac{1}{S}\right)} \ln\left[\left(1-\frac{1}{S}\right)\left(\frac{x_2}{x_1}\right)+\frac{1}{S}\right] \qquad (7.30)$$

where S is defined as the stripping factor.

$$S = \frac{1}{A} = \frac{mG_m}{L_m} \qquad (7.31)$$

The total height of bed is calculated from the mass balance across the RPB.

$$H = NTU_{OL}. \times HTU_{OL}. \qquad (7.32)$$

Hence, the overall height of the transfer unit based on the liquid phase (HTU_{OL}) could be calculated by:

$$HTU_{OL} = \frac{\Delta r}{NTU_{OL}} = \frac{R_o - R_i}{NTU_{OL}}$$

The solubility behaviour of carbon dioxide in different amine concentrations and at different temperatures show the equilibrium line is curvature in nature and it is very steep at loadings greater than 0.1.

These difficulties in estimating the slope of the equilibrium line were overcome by assuming that the curve is linear in the operating line section.

7.6.2 Air

A desorption exercise was carried out on 30 wt.% MEA solution using air medium. This exercise was carried out after completing the initial absorption mass transfer experiments and prior to using the pure MEA solution. Air is not a potential stripping medium candidate because exposing the lean solution to air could promote the formation of degradation products (Section 2.2.7.2) and hence reduce its reactivity. Therefore, these experiments were only carried out to investigate the stripping efficiency of Higee machine.

The MEA solution was initially heated to an average temperature of 70°C then a counter-current mass transfer operation was carried out to desorb carbon dioxide using air at ambient temperature. The results of the experiments are shown in Table P-5. Figure 7.21 shows the variation of (G/L) ratio with HTU. The slope of the equilibrium line was extrapolated to be 32.2. The magnitude of the HTU is very large and hence indicates a poor performance of the Higee mass transfer machine when air at ambient temperature is the desorbing medium.

However, the results could have been improved if the air was preheated as the regeneration of the rich alkanolamine solution demands a substantial heat inflow to reverse the chemical reactions, as the carbamate formation in the absorption operation is an exothermic reaction that releases 20 kcal/gmol.

7.6.3 Steam

The desorption runs were carried out for 30wt% and 55 wt% MEA solutions at atmospheric pressure. The ethanolamine solution was preheated to 70°C for 30wt% and 60°C for 60wt% MEA solution. The flow of steam inside the rotating shaft, the

gas plenum, and the holes was subsonic as the Mach number (Ma) was approximately 0.43. In addition, the pressure drops calculated in different Higee compartments were not significant as shown in Appendix N. The results of the runs are presented in Tables P-6.

The concentration of carbon dioxide, collected at the centre of the rotor, was less than 10% (Run 1). These gas samples were analysed and it appeared that the remaining of the sample was air.

Therefore, the experimental procedure was improved by allowing the steam to be routed to the rig for a longer period (approximately 15 minutes) prior to the introduction of the rich ethanolamine solution. As a consequence, the atmospheric air which occupies the small void volume between the rotor and the outer enclosure was completely purged by the steam. Runs 2 shows that the improvement to the experimental procedure was partially successful as the carbon dioxide concentration increased to approximately 60%.

The gas samples were collected using 10 mL plastic syringes. The gaseous sample contained a mixture of carbon dioxide and steam. As the gas sample was withdrawn into the syringe, the steam condensed and hence the resulting pressure drop forced the outside atmospheric air into the syringe. Therefore, the atmospheric air contaminated the sample content and that was unavoidable because it happened very fast. (Strigle, 1987) quoted that the overhead vapours in a conventional stripper contained 27 mol% CO_2 and the balance was water vapour.

The slope of the equilibrium line for 30wt% MEA solution at 100°C is estimated to be 140 and it is 370 for 60wt% MEA solution. These high equilibrium slope values contributed to high stripping factors calculated for the desorption runs. Figure 7.22 shows the variation of (G/L) ratio with HTU for 30wt% MEA solution at 800 RPM.

Similarly, Figure 7.23 shows the variation of (G/L) ratio with HTU using 60 wt.% MEA solution at 600 and 1000 RPM. The increase of the molar (G/L) ratio reduces the HTU and it becomes less than 1.0 m when the ratio is greater than unity where the amount of steam consumed is (>0.4 kg steam/L solution). Table 2.1 shows the operating conditions and the physical dimensions of a conventional desorber. The amount of steam consumed is 0.1 kg steam/L solution. However, the column temperature and pressure are higher than the Higee machine.

The temperature of the ethanolamine solution leaving the rig was in excess of 100°C. There were no operational problems in dealing with high temperature ethanolamine solution because of the careful selection of the material of construction for the rig. However, it was noted that the fumes emitted during the air stripping were more irritating than when steam stripping.

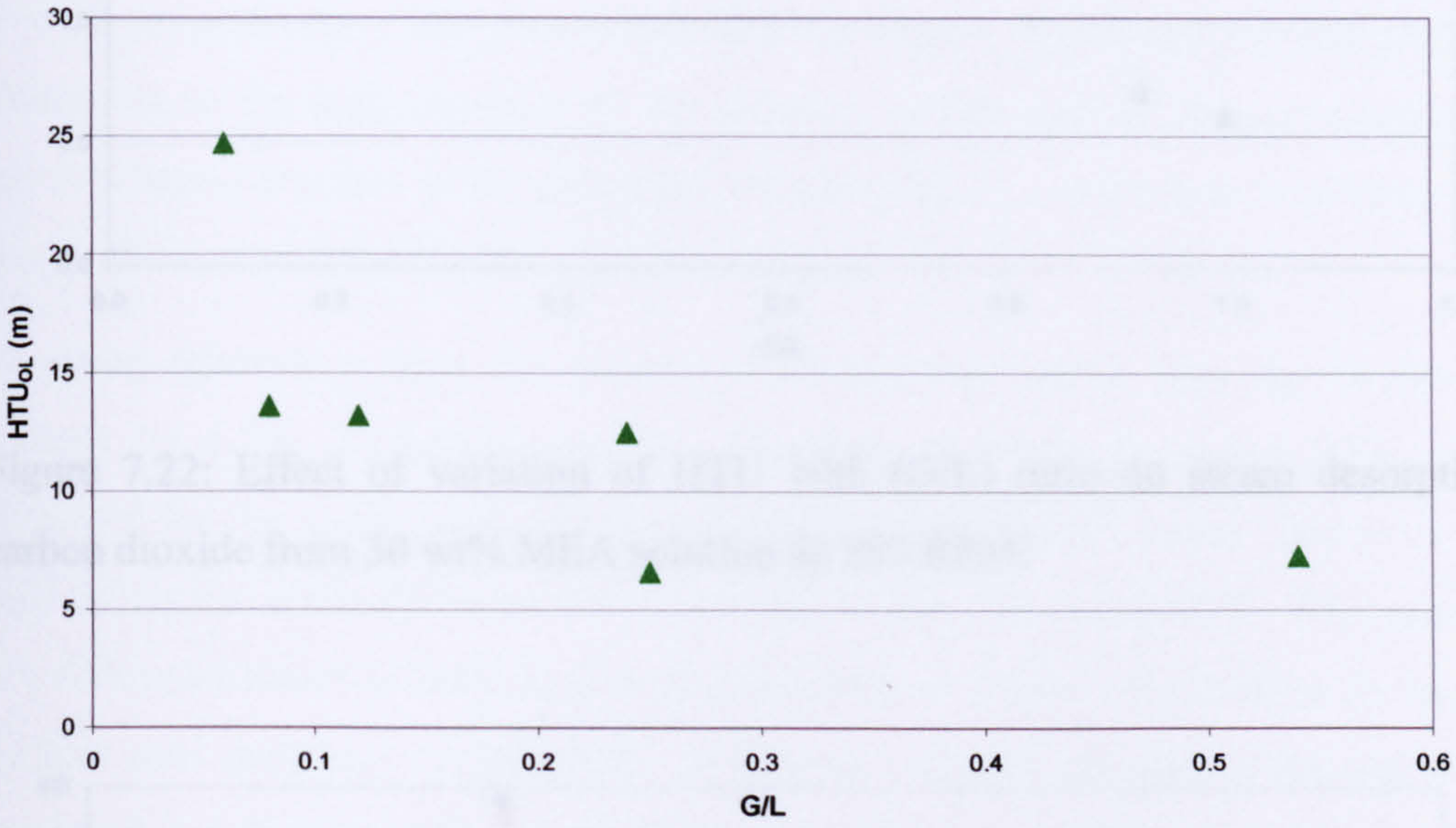

Figure 7.21: Variation of HTU with G/L on desorption of carbon dioxide from 30wt% MEA solution using air.

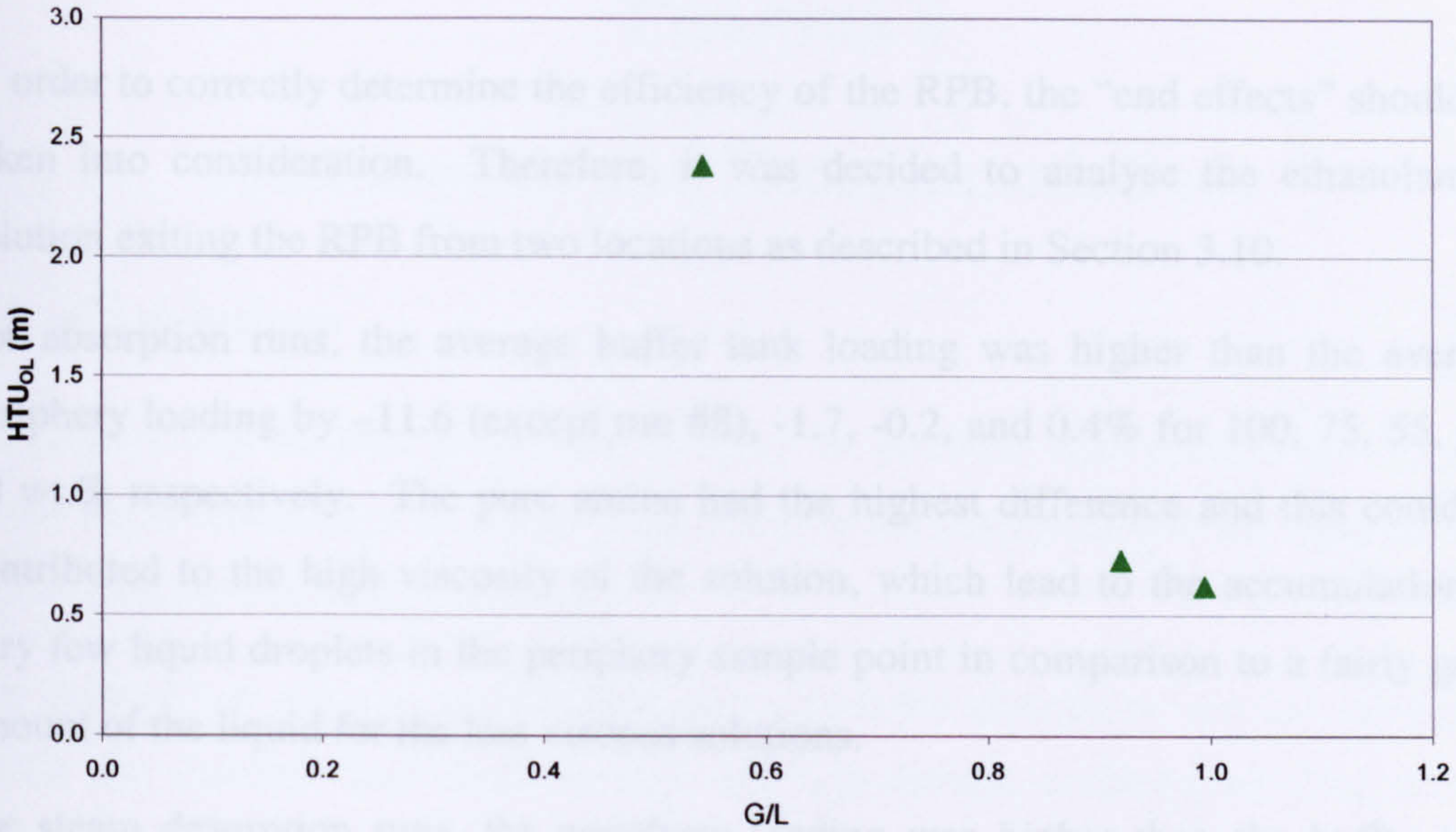

Figure 7.22: Effect of variation of HTU with (G/L) ratio on steam desorption of carbon dioxide from 30 wt% MEA solution @ 800 RPM.

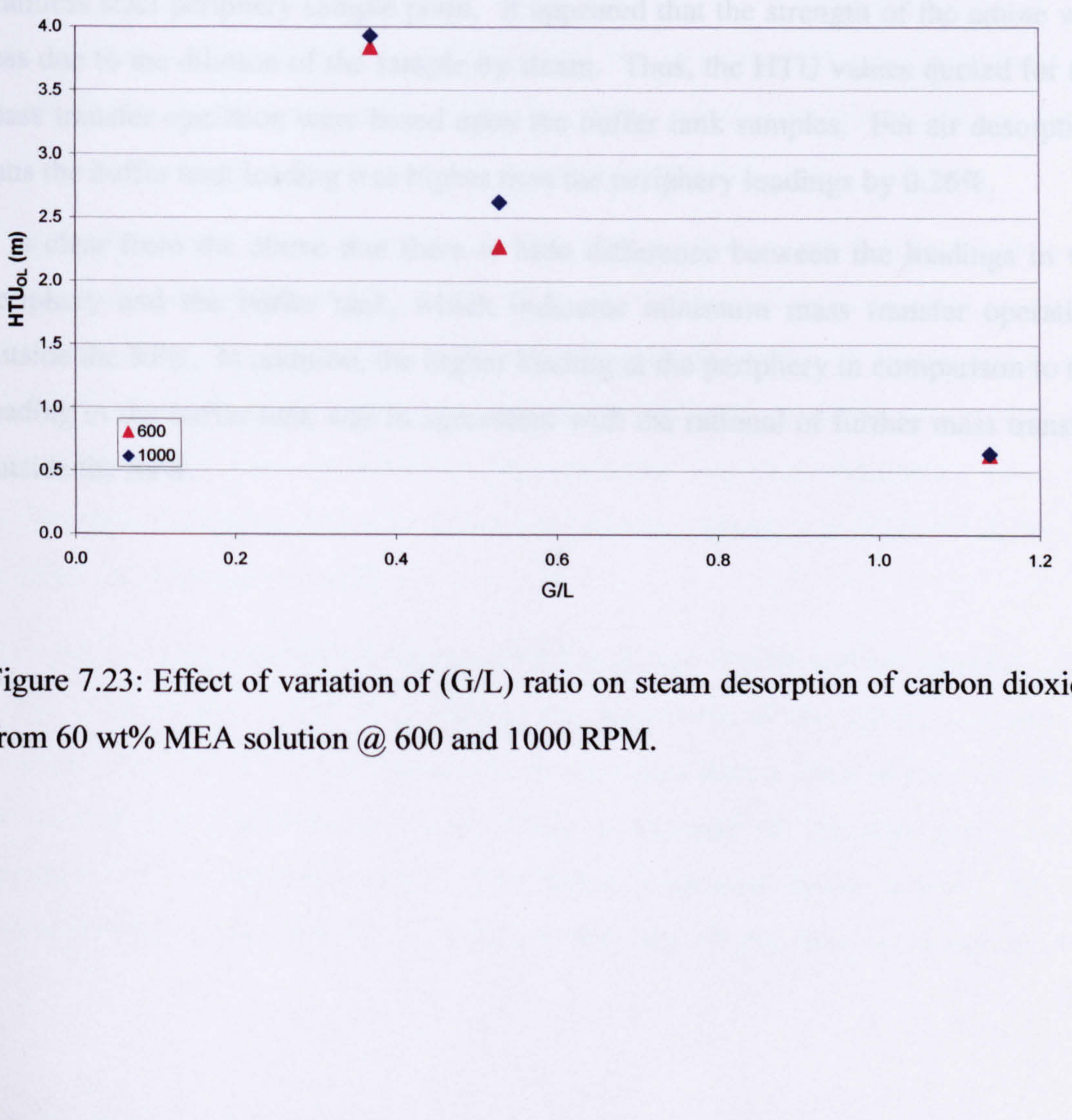

Figure 7.23: Effect of variation of (G/L) ratio on steam desorption of carbon dioxide from 60 wt% MEA solution @ 600 and 1000 RPM.

7.7 End Effects

In order to correctly determine the efficiency of the RPB, the "end effects" should be taken into consideration. Therefore, it was decided to analyse the ethanolamine solution exiting the RPB from two locations as described in Section 3.10.

For absorption runs, the average buffer tank loading was higher than the average periphery loading by –11.6 (except run #8), -1.7, -0.2, and 0.4% for 100, 75, 55, and 30 wt.% respectively. The pure amine had the highest difference and this could be contributed to the high viscosity of the solution, which lead to the accumulation of very few liquid droplets in the periphery sample point in comparison to a fairly good amount of the liquid for the less viscous solutions.

For steam desorption runs, the periphery loading was higher than the buffer tank loadings by 1.7% (excluding run 2). However, it seems from the HTU values calculated for the buffer tank and the periphery liquid sample points that even such small difference could influence the magnitude of the calculated HTU. The reason of such difference could be attributed to the possibility of steam condensation in the cold stainless steel periphery sample point. It appeared that the strength of the amine was less due to the dilution of the sample by steam. Thus, the HTU values quoted for the mass transfer operation were based upon the buffer tank samples. For air desorption runs the buffer tank loading was higher than the periphery loadings by 0.26%.

It is clear from the above that there is little difference between the loadings in the periphery and the buffer tank, which indicates minimum mass transfer operation outside the RPB. In addition, the higher loading at the periphery in comparison to the loading in the buffer tank was in agreement with the rational of further mass transfer outside the RPB.

CHAPTER 8

Conclusions and Recommendations

8.1 Conclusions

The objective of the PhD project was to study the potential mass transfer performance of the Higee technology on a pilot-plant scale for the absorption and the desorption of carbon dioxide from MEA solutions.

The packed bed material applied throughout both the absorption and the desorption cycles was stainless steel expamet with very high specific surface area (2132 m^2/m^3) and a moderate voidage (0.76).

The liquid and gas flowrates used in the mass transfer runs achieved a maximum 16% flooding at the inner radius of the RPB when operating at ethanolamine solution rate of 20-40 L/min and the gaseous Air/CO_2 rate at 57 m^3/hr and the thickness of the RPB is 25 mm. Therefore, the full hydraulic capacity of the Higee was not fully exploited.

The criterion for determining the efficiency of the mass transfer experiments was the height of the transfer units. The effects of rotor speed, temperature, ethanolamine circulation rate, and amine concentration were investigated.

These experimental runs highlighted the importance of the amine concentration in the application of the Higee technology in this particular case of gas sweetening process. The absorption cycle was most effective when the concentration of amine was at least 55wt% in which the % recovery of sour gas was 88% and the HTU value was in the region of 3.9-6.9 cm. In addition, the operation was most optimized when the ethanolamine irrigation rate was 40 L/min, the rotor speed was 1000 RPM and the solution was preheated to 40°C.

The mass transfer operation is theoretically liquid film limited and the increase of the amine concentration could have reduced the magnitude of the liquid resistance by increasing the rate of the reactive species to the liquid film in spite of the fact that the increase of the concentration would result in increase of viscosity and hence a reduction of the diffusion rates. The higher rotational speed ensures that the maldistribution in the RPB is minimum as the type of the flow is supposed to be

droplet flow instead of the pore flow in the lower rotor speeds. Furthermore, the higher irrigation rates ensured more wetting of the packed bed and the temperature rise allowed the solution to be physically less viscous and enhanced the rate of the reaction between the acid gas and the alkanolamine solution.

The HTU in the regenerative operation were more efficient at high molar (G/L) ratio. However, the amount of the ratio (kg steam/L solution) is approximately 0.43 for the lowest HTU achieved.

8.2 Recommendations

The research project was initially focused on achieving specific outlined targets. These main targets were investigated and examined throughout the three years duration of the experimental work. Nevertheless, this research outlines a number of topics that could be further investigated:

1- The effect of using different chemical solvents or a mixture of different solvents. In this research different concentrations of MEA solutions were utilized. However, the only drawback with those solutions is the energy required in the regeneration, as the carbamate formation is an exothermic reaction that releases 20 kcal/gmol. An alternative chemical solvent is a mixture of tertiary amine (MDEA) with small amount of MEA in order to accelerate the rate of reaction. The heat of the reaction of CO_2 with MDEA is 11.6 kcal/gmol thus less energy is required to reverse the reaction (Glasscock et al., 1991).

2- There is still a gap for the equilibrium solubility data bank at high MEA concentrations (50, 75, 100 wt%) at loadings less than 0.5.

3- The effect of increasing the rotor speed upto >2000 RPM. These speeds provide greater potential for enhancing the mass transfer as was proven with the experimental results. The behaviour of the liquid flow type inside the packed bed would improve from droplet to film and hence better gas/liquid contact. In addition, the film thickness is expected to reduce with higher rotations and hence less mass transfer resistance.

4- The effect of using other variations of packing material configurations with different specific surface areas and/or porosities such as stainless steel knitmesh or expamet with preferably higher porosities and lower specific surface areas. (Trent et

al., 1999) found out that it is preferable to use higher porosities packing material rather than higher specific surfaces because the impact of the liquid with the packing material leads to the formation of small liquid droplets in the voids. (Note: the current research uses stainless steel expamet with a porosity of 0.76 and a specific surface area of 2132 m^2/m^3).

5- It is necessary to devise an intensified reboiler for the desorption cycle in order to achieve a fully miniaturized chemical process.

6- The effect of using different liquid distributor arrangements. For example, the number of arms in the liquid distributor could be increased; or the number of holes or its diameter in each arm could be modified in order to manipulate the liquid injection velocities delivered to the RPB.

7- The effect of varying the gas flowrate. It is thought the RPB behaves in a similar fashion to the conventional columns i.e. a rise in the gas flowrate leads to a reduction in the HTU (Keyvani, 1989).

8- The effect of using different grades of steam such as superheated steam during the desorption runs.

Nomenclature

Latin

A	Area per unit volume	(m^2/m^3)
	Gas-liquid interfacial area (Eqn. 1.66)	(m^2/m^3)
	Axial distance between disks of rotor (Eqn. 1.71)	(m)
a_c	Centrifugal acceleration	(m/s^2)
a_e	Effective interfacial area	(m^2/m^3)
a_m	Mean acceleration	(m/s^2)
a_p	Specific surface area of packing	(m^2/m^3)
a_t	Total interfacial area of packing per unit volume of the equipment	(m^2/m^3)
a_w	Wetted surface area per unit volume	(m^2/m^3)
B	Base	
c_c	Concentration of solute in casing	(mol/m^3)
c_o	Concentration of solute at the outlet of rotor	(mol/m^3)
C_A	Molar concentration of A	$(kmol/m^3)$
C_{Ai}, C_i	Molar concentration of A at interface	$(kmol/m^3)$
C_{Ae}	Molar concentration of A in liquid phase in equilibrium with partial pressure P_{AG} in gas phase	$(kmol/m^3)$
C_{AL}, C_L	Molar concentration of A in bulk of liquid	$(kmol/m^3)$
d	Size of packing element (Eqn. 1.42)	(ft)
d_p	Diameter of the packing material	(m)
D, D_G	Diffusion coefficient of gas	(m^2/s)
D_A	Diffusion coefficient of dissolved gas A	(m^2/s)
E	Enhancement factor	-

F	Fraction of free volume in packing	(m3/m3 tower volume)
g	Gravitational acceleration	(m^2/s)
G	Superficial mass velocity of gas	(kg/s/m^2)
G'	Gas mass flux	(kg/m^2.s)
G_m	Molar flow rate of gas (Eqn. 1.67)	(mol/s)
	Molar flow rate of gas (Eqn. 1.70)	(kmol/m^2.s)
h	Height of short wetted-wall column	(m)
H	Axial bed depth	(m)
H	Henry's law constant	(N/m^2)/(kmol/m^3)
H_c	Henry's law constant (Eqn. 1.67)	(-)
H_L	Height of liquid phase transfer unit	(ft)
I	Enhancement factor	(-)
k_1	Reaction rate constant	(1/s)
K_1	First order reaction rate constant	(1/s)
K_2	Reaction rate constant	(1/s)
k_b	Rate constant	(l/mole.s)
k_G	Gas film transfer coefficient	(s/m)
$K_g a_e$	Average gas-side volumetric mass transfer coefficient	(1/s)
K_G	Overall gas phase transfer coefficient	(s/m)
$K_G a$	Overall volumetric gas-film mass transfer coefficient	(mol/atm.m^3.s)
k^o_L	Physical mass transfer coefficient in liquid phase	(m/s)
K_L	Overall liquid phase transfer coefficient	(m/s)
$K_L a$	Overall mass transfer coefficient	(1/s)
L	Superficial mass velocity of liquid	(kg/m^2/s)

L	Axial length of packing	(m)
L'	Liquid mass flux	($kg/m^2/s$)
L_m	Liquid molar flux	($kmol/m^2.s$)
m	Slope of equilibrium curve	(-)
N	Rotation speed per minute	(RPM)
N, N_A	Molar rate of absorption of A per unit	($kmol/s/m^2$)
N_{OL}	Number of overall liquid transfer units	(-)
P_{Ae}	Partial pressure of A in equilibrium with concentration C_{AL} in liquid phase	(N/m^2)
P_{AG}	Partial pressure of A in bulk of gas phase	(N/m^2)
P_{Ai}	Partial pressure of A at interface	(N/m^2)
P_t, P	Total pressure in the system	(atm)
Q_g	Volumetric flow rate of gas	(m^3/s)
Q	Volumetric flowrate of liquid	(m^3/s)
r	Rate of reaction	(mol/l.s)
r_i, r_1	Inner radius of the rotor	(m)
r_o, r_2	Outer radius of rotor	(m)
S	Stripping factor = (HG/Q)	
S	Surface area of packing (Eqn. 3.1)	(m^2/m^3)
s	Fractional rate of surface renewals	(1/s)
t_D	Diffusion time	(s)
t_r	Reaction time	(s)
t^*	Exposure time of liquid to the gas.	(s)
T	Temperature	K
u	Surface velocity of liquid	(m/s)
u_o, U_g	Superficial gas velocity	(m/s)

v	Liquid film velocity	(m/s)
X_1, x_1	Mole fraction of a gas component in inlet liquid stream	(-)
X_2, x_2	Mole fraction of a gas component in outlet liquid stream	(-)
Y_1, y_1	Mole fraction of a gas component in intlet gas stream	(-)
Y_2, y_2	Mole fraction of a gas component in outlet gas stream	(-)
z	Axial height of the packing	(m)

Dimensionless Groups

Gr	Grashof number	(gd^3/v^2)
Gr_G	Gas Grashof number	$(d_p^2 a_c/v_G^2)$
Re_l	Reynolds number for vertical surfaces (Eqn. 1.42)	$(4L/a\mu)$
Re	Reynolds number (Eqn. 1.62)	$(L/a_t\mu)$
Re_G	Gas Reynolds number of mass transfer	$(G'/a_t\mu_G)$
Re_{La}	Liquid Reynolds number for mass transfer	$(L'a_t\mu_L)$
Sc, N_{Sc}	Schmidt number	(v/D), $(\mu/\rho D)$

Greek Symbols

ε	Porosity	(-)
μ_G	Gas viscosity	(kg/m.s)
μ	Viscosity	(Pa.s)
ρ	Density	(kg/m^3)
θ	Time of exposure of liquid to gas	(s)
δ	Film thickness	(m)
φ	Ratio of diffusion and reaction times	(-)
Γ	Liquid mass flow rate per wetted perimeter	(kg/s.m)
v_G	Dynamic gas viscosity	(m^2/s)
ω	Rotational speed	(rad/s)

Subscripts

A	Soluble gas
E	Equilibrium
Eq	Equilibrium
G	Gas phase
i	Inner
	Value at interface
L	Liquid phase
o	Outer
O	Overall
*	At equilibrium

Abbreviations

ATU	Area of transfer unit	(m^2)
CO_2	Carbon dioxide	
DEA	Diethanolamine	
DGA	Diglycolamine	
DIPA	Diisoprpanolamine	
HTU	Height of transfer unit	(m)
MEA	Monoethanolamine	
MDEA	Methyldiethanolamine	
N_2O	Nitrous Oxide	
NTU	Number of transfer unit	(-)
TEA	Triethanolamine	

Bibliography

Al-Shaban, K., Balasundaram, V., Howarth, C. R., Ramshaw, C. and Peel, J. R. A., (1992), "The Hydrodynamic and Mass Transfer Characteristics of a Large Centrifugal Water Deoxygenator", In *International conference on "Energy Efficiency in Process Technology* (Ed, P. A. Pildvachi, P. A.) , Elsevier Applied Science, Athens-Greece, pp. 475-484.

Astarita, G., Savage, D. W. and Bisio, A., (1983), *Gas Treating with Chemical Solvents,* (John Wiley & Sons).

Atadan, E. M., (1955), Ph.D., "Absorption of Carbon Dioxide by Monoethanolamine Solutions", University of Tennessee, USA.

Basic, A. and Dudukovic, M., (1995), *AIChE Journal,* **41,** (2), pp 301-316, "Liquid Hold-up in Rotating Packed Beds: Examination of the Film Flow Assumption".

Bennett, H. (Ed.) (1986) *Concise Chemical and Technical Dictionary,* (Chemical Publishing Co.), New York

Blauwhoff, P. M. M., Versteeg, G. F. and VanSwaaij, W. P. M., (1984), *Chemical Engineering Science,* **39,** (2), pp 207-225, "A study on the reaction between carbon dioxide and alkanolamines in aqueous solutions".

Bucklin, R. W., Buckingham, P. A. and Smelser, S. C., (1988), "The Higee demonstration test of selective H2S removal with MDEA", In *The Laurence Reid gas conditioning conference*, The University of Oklahoma.

Burns, J. and Ramshaw, C., (1996), *Chemical Engineering Science,* **51,** (8), pp 1347-1352, "Process Intensification: visual study of Liquid Maldistribution in Rotating Packed Beds".

Burns, J. R., (1996), Ph.D., "Liquid distribution in a rotating packed bed", Newcastle upon Tyne University

Butwell, K. F., (1968), *Hydrocarbon Processing,* **47,** (4), pp 111-113, "How to maintain effective MEA solutions".

Caplow, M., (1968), *American Chemical Society,* **90,** 6795-6803, "Kinetics of carbamate formation and breakdown".

Chambers, H. H. and Wall, M. A., (1954), *Trans. Inst. Chem. Eng.,* **32,** S96-S107, "Some factors affecting the design of centrifugal gas absorbers".

Charpentier, J. C., (1982), *Trans. Inst. Chem. Eng.,* **60,** 131-156, "What's new in absorption with chemical reaction?".

Colburn, A., (1939), *Trans AIChE,* **35,** 211, "The Simplified calculation of diffusional process. General consideration of two-film resistances".

Connors, J. S., (1958), *Oil and Gas,* (3), pp 100-110, "Aqueous-amine acid removal process need not be corrosive".

Coulson, J. M., Richardson, J. F., Backhurst, J. R. and Harker, J. H., (1993), *Chemical Engineering,* **1,** 4th, (BPCC Wheatons Ltd).

Coulson, J. M., Richardson, J. F., Backhurst, J. R. and Harker, J. H., (1991), *Chemical Engineering,***2,** (Pergamon Press Ltd).

Critchfield, J. and Rochelle, G. T., (1987), "Gas absorption into aqueous MDEA and MDEA/MEA solutions", In *AICHE National Meeting*, Houston, TX.

Cross, W. T. and Ramshaw, C., (1986), *Transactions of the ASME. Series J. Journal of Pressure Vessel Technology,* **64,** (4), pp 293-301, "Process intensification: laminar flow heat transfer".

Cussler, E. L., (1997), *Diffusion - Mass Transfer in Fluid System,* 2nd, (Cambridge University Press).

Danckwerts, P. V., (1951), *Ind. Eng. Chem.,* **43,** 1460, "Significance of liquid film coefficients in gas absorption".

Danckwerts, P. V., (1979), *Chem Eng Sci,* **34,** (4), pp 443-446, "The reaction of CO2 with ethanolamines".

Danckwerts, P. V. and Sharma, M. M., (1966), *The Chemical Engineer,* (10), pp 245-281, "The absorption of carbon dioxide into solutions of alkalis and amines (with some notes on hydrogen sulphide and carbonyl sulphide".

Dankwerts, P. V., (1970), *Gas-Liquid Reactions,* (McGraw-Hill).

Davidson, J. F., (1959), *Trans. Instn. Chem. Engrs.*, **37,** 1311-136, "The Hold-up and liquid film coefficient packed towers. PartII: Statistical models of the random packing".

Deshmukh, R. D. and Mather, A. E., (1981), *Chemical Engineering Science,* **36,** (2), pp 355-362, "Mathematical model for equilibrium solubility of hydrogen sulfide and carbon dioxide in aqueous alkanolamine solutions.".

Dingman, J. C., Allen, D. L. and Moore, T. F., (1966), *Hydrocarbon processing,* **45,** (9), pp 285-290, "Minimize corrosion in MEA units".

DuPart, M. S., Bacon, T. R. and Edwards, D. J., (1993a), *Hydrocarbon Processing,* **72,** (5), pp 89-94, "Understanding corrosion in alkanolamine gas treating plants".

DuPart, M. S., Bacon, T. R. and Edwards, D. J., (1993b), *Hydrocarbon Processing,* **72,** (4), pp 75-80, "Understanding corrosion in alkanolamine gas treating plants".

Eimer, D., (1994), "Simultaneous removal of water and hydrogen sulphide from natural gas", Trondheim University, Norway

Eimer, D., (1999), Personal Communication.

Eimer, D., (2000), "Mass Transfer Control and Influence of Chemical Reaction in light of Process Intensification", Porsgrunn-Norway.

Falk-Pedersen, O., Bjerve, Y., Glittum, G. and Ronning, S., (1995), *Energy Convers. Mgmt,* **36,** (6-9), pp 393-396, "Separation of carbon dioxide from offshore gas turbine exhaust".

Furman, N. H. (Ed.) (1962) *Scott's Standard Methods of Chemical Analysis,* (D. Van Nostrand Company), New York

Geankoplis, C. J., (1983), *Transport Processes and Unit Operations,* Second, (Prentice-Hall).

Glasscock, D. A., (1990), Ph.D. thesis, "Modelling and experimental study of carbon dioxide absorption into aqueous alkanolamines", The University of Texas at Austin, USA

Glasscock, D. A., Critchfield, J. E. and Rochelle, G. T., (1991), *Chemical Engineering Science,* **46,** (11), pp 2829-2845, "CO2 absorption/desorption in mixture of methyldiethanolamine with monoethanolamine or diethanolamine".

Green, A., (1998), *Chemistry and Industry,* 168-172, "Process Intensification: the key to survival in global markets?".

Green, A., Johnson, B., and John, A., (1999), *Chemical Engineering,* (Dec.), pp 66-73, "Process Intensification Magnifies Profits".

Harris, D. C., (1991), *Quantitive Chemical Analysis,* Third, (W. H. Freeman and Company).

Hassan-beck, H. M., (1997), PhD thesis, "Process Intensification: mass transfer and pressure drop for counter-current rotating packed bed", Newcastle upon Tyne University.

Hawkes, E. N. and Mago, B. F., (1971), *Hydrocarbon Processing,* **50,** (8), pp 109-112, "Stop MEA CO2 unit corrosion".

Hendershot, D., (2000), *Chemical Engineering Progress,* **96,** (1), pp 35-40, "Process Minimization: Making Plants Safer".

Higbie, R., (1935), *Trans. Am. Inst. Chem. Engrs.,* **31,** 365-389, "The Rate of Absorption of A pure Gas into A still Liquid During Short Periods of Exposure".

Holland, F. A. and Bragg, R., (1995), *Fluid Flow for Chemical Engineers,* 2nd, (Edward Arnold).

Hutton, B. E. T., Leung, P. C., Brooks, P. C. and Nicklin, D. J., (1974), *Chemical Engineering Science,* **29,** 493-500, "On Flooding in Packed Columns".

Jamil, J. N., (1997), MPhil, "Viscous Liquid Distribution in a Rotating Packed Bed", Newcastle upon Tyne University.

Jeffery, P. G. and Kipping, P. J., (1962), *Analyst,* **87,** 594-595, "The Determination of Carbon Dioxide and Nitrous Oxide in Solutions of Monoethanolamine".

Jones, J. H., Froning, H. R. and Claytor, E. E., (1959), *Chemical Engineering Data,* **4,** (1), pp 85-92, "Solubility of Acidic Gases in Aqueous Monoethanolamine".

Jou, F. Y., Mather, A. E. and Otto, F. D., (1982), *Ind. Eng. Chem. Process Des. Dev.*, **21,** 539-544, "Solubility of H2S and CO2 in aqueous methyldiethanolamine solutions".

Jou, F.-Y., Carroll, J. J., Mather, A. E. and Otto, F. D., (1993), *Canadian Journal of Chemical Engineering,* **71,** (2), pp 264-268, "The Solubility of carbon dioxide and hydrogen sulfide in a 35 wt% aqueous solution of methyldiethanolamine".

Jou, F.-Y., Mather, A. E. and Otto, F. D., (1995), *Canadian Journal of Chemical Engineering,* **73,** (1), pp 140-147, "The solubility of CO2 in a 30 mass percent monoethanolamine solutions".

Kelleher, T. and Fair, J. R., (1996), *Industrial & Engineering Chemistry Research,* **35,** (12), pp 4646-4655, "Distillation studies in a high-gravity contactor".

Keyvani, M. and Gardner, N. C., (1989), *Chemical Engineering Progress,* **85,** (9), pp 48-52, "Operating characteristics of rotating beds".

Keyvani, M., (1989), PhD, "Operating Characteristics of Rotating Beds", Case Western Reserve Univ., Cleveland, OH.

King, C. J., (1980), *Separation Processes,* (McGraw-Hill).

Kohl, A., (1956), *A.C.Ch.E,* **2,** (2), pp 264-270, "Plate Efficiency with Chemical Reaction - Absorption of Carbon Dioxide in Monoethanolamine Solutions".

Kohl, K. and Nielsen, R., (1997), *Gas Purification,* 5, (Gulf Publishing Company).

Laddha, S. S., Diaz, J. M. and Danckwets, P. V., (1981), *Chem. Eng. Sci.,* **36,** 228

Lee, J. I., Otto, F. D. and Mather, A. E., (1974), *The Canadian Journal of Chemical Engineering,* **52,** (December), pp 803-805, "The Solubility of H2S and CO2 in Aqueous Monoethanolamine Solutions".

Leites, I. L., (1997), *Institution of Chemical Engineers Symposium Series,* **142,** 379-389, "Thermodynamics of the CO2 Solubility in mixtures of monoethanolamine with organic solvents and water and the commercial experience of energy saving gas purification technology".

Littlewood, A. B., (1970), *Gas Chromatography,* second, (Academic Press, INC).

Liu, H.-S., Lin, C.-C., Wu, S.-C. and Hsu, H.-W., (1996), *Industrial & Engineering Chemistry Research,* **35,** (10), pp 3590-3596, "Characteristics of a rotating Packed Bed".

Lobo, W. E., Friend, L., Hashmall, F. and Zenz, F., (1945), *Trans. Am. Inst. Chem. Engrs.*, **41,** 693-710, "Limiting Capacity of Dumped Tower Packings".

Lockett, M. J., (1995), *Chemical Engineering Research and Design Part A,* **73,** (A4), pp 379-384, "Flooding of rotating structured packing and its application to conventional packed columns".

McCabe, W., Smith, J. and Harriott, P., (1993), *Unit Operations of Chemical Engineering,* 5th, (McGraw-Hill).

Mallinson, R. H. and Ramshaw, C., (1982), "Mass Transfer Apparatus and Process", European Patent Office patent 0053881

Mason, J. W. and Dodge, B., (1936), *Trans. Amer. Inst. Chem. Eng.*, **32,** 27-48, "Equilibrium absorption of carbon dioxide by solutions of the ethanolamines".

Moore, S. R., (1986), PhD thesis, "Mass transfer to thin liquid films on rotating surfaces - with and without chemical reaction", Newcastle upon Tyne University.

Morris, G. and Jackson, J., (1953), *Absorption Towers,* (Butterworths Scientific Publications).

Munjal, S., Dudukovic, M. P. and Ramachandran, P., (1989), *Chemical Engineering Science,* **44,** (10), pp 2245-2256, "Mass-transfer in rotating packed beds. I. Development of gas-liquid and liquid-solid mass-transfer correlations".

Murrieta-Guevara, F., Rebolledo-Libreros, E. and Trejo, A., (1993), *Fluid Phase Equilibria,* **86,** 225-231, "Gas Solubility of Carbon Dioxide and hydrogen sulfide in mixtures of sulfolane with monoethanolamine".

Nasir, P. and Mather, A. E., (1977), *Canadian Journal of Chemical Engineering,* **55,** (6), pp 715-717, "Measurement and prediction of the solubility of acid gases in monoethanolamine solutions at low partial pressures.".

Nusselt, W. Z., (1916), *Vereines Deut. Ing.*, **60,** 541-546

Onda, K., Takeuchi, H. and Okumoto, Y., (1968), *J. Chem. Eng. Japan,* **1,** 56, "Mass transfer coefficients between Gas and Liquid phases in packed columns".

Pauley, C. R., (1991), *Chemical Engineering Progress,* **87,** (7), pp 33-38, "Face the facts about amine foaming".

Pearce, R. L., (1993), "Fundamentals of Gas Treating", In *Laurrance Reid Gas Conditioning Conference*, University of Oklahoma, Norman, Oklahoma, pp. 125-184.

Pearce, R. L., Grosso, S. and Cringle, D. C., "Amine gas treating solution analysis: a tool in problem solving", In *Proceedings of 59th annual convention gas processors association*, pp. 150-162.

Perry, R. H. and Green, D., (1984), *Perry's Chemical Engineers' Handbook,* Sixth, (McGraw-Hill Book Co).

Piche, S., Larachi, F. and Grandjean, B., (2001), *Ind. Eng. Chem. Res.,* **40,** 476-487, "Flooding Capacity in Packed Towers: Database, Correlations, and Analysis".

Pillo, C. W. and Dahlbeck, S. W., (1960), "Apparatus for intimate contacting of two fluid media having different specific weight", USA patent 2,941,872

Pilo, C. W., (1974), "Improvements in liquid-gas contact apparatus", UK patent 1,366,312

Podlbieiniak, W. J., (1966), "Continuous Centrifugal Vapour-Liquid Contactor", USA patent 3,233,880

Popovych, O. and Tomkins, R. P. T., (1981), *Non-aqueous solution chemistry,* (Wiley).

Ramshaw, C., (1983), *Chemical Engineer (London),* (389), pp 13-14, "Higee distillation - An example of process intensification".

Ramshaw, C., (1993), *Heat Recovery Systems & CHP,* **13,** (6), pp 493-513, "Opportunities for exploiting centrifugal fields".

Ramshaw, C., (2001), Personal Communication.

Ramshaw, C. and Mallinson, R. H., (1981), "Mass Transfer Process", USA patent 4,283,255

Rooney, P. C., DuPart, M. S. and Bacon, T. R., (1998), *Hydrocarbon Processing,* **77,** (7), pp 109-113, "Oxygen's role in alkanolamine degradation".

Sanilya, P., Rao, D., Sharma, A. and Biswas, G., (2001), *Industrial & Engineering Chemistry Research,* **40,** 384-392, "Gas-Phase Mass Transfer in a Centrifugal Contactor".

Sarchet, B. R., (1942), *Trans. Am. Inst. Chem. Engrs.,* **38,** 283-304, "Flooding Velocities in Packed Towers".

Shen, K. and Li, M., (1992), *J. Chem. Eng. Data,* **37,** 96-100, "Solubility of Carbon Dioxide in Aqueous Mixtures of Monoethanolamine with Methyldiethanolamine".

Sherwood, T. K., Shipley, G. H. and Holloway, F. A. L., (1938), *Industrial and engineering chemistry,* **30,** (7), pp 765-769, "Flooding Velocities in Packed Columns".

Sherwood, T., Pigford, R. and Wilke, C., (1975), *Mass Transfer,* (McGraw-Hill).

Sherwood, T. and Pigford, R., (1952), *Absorption and Extraction,* (McGraw-Hill).

Silvey, F. C. and Keller, G. J., (1966), *Chemical Engineering Progress,* **61,** (1), pp 68-74, "Testing on a Commercial Scale".

Singh, S. P., Wilson, J. H., Counce, R. M., Villiers-Fisher, J. F., Jennings, H. L., Lucero, A. J., Reed, G. D., Ashworth, R. A. and Elliott, M. G., (1992), *Industrial & Engineering Chemistry Research,* **31,** (2), pp 574-580, "Removal of volatile organic compounds from groundwater using a rotary air stripper".

Sinnott, R. K., (1993), *Chemical Engineering,***6,** (Wheatons Ltd).

Skoog, D. A., West, D. M. and Holler, F. J., (1992), *Fundamentals of Analytical Chemistry,* Sixth, (Saunders College Publishing).

Stankiewicz, A. and Moulijn, J., (2000), *Chemical Engineering Progress,* **96,** (1), pp 22-34, "Process Intensification: Transforming Chemical Engineering".

Strigle, R., (1987), *Random Packings and Packed Towers: Design and Applications,* 1st, (Gulf Publishing Company).

Szekely, J. and Mendrykowski, J., (1972), *Chemical Engineering Science,* **27,** 959-963, "On the Flooding Criteria for Liquids with High Density and High Interfacial Tension".

Tennyson, R. N. and Schaaf, R. P., (1977), *Oil and Gas,* **75,** (2), pp 78-86, "Guidelines Can Help Choose Proper Process For Gas-Treating Plants".

Trent, D., Tirtowidjojo, D. and Quarderer, G., (1999), "Reactive stripping in a rotating packed bed for production of hypochlorous acid", In *3rd International Conference on Process Intensification for Chemical Industry* (Ed, Green, A.) , London, pp. 217-231.

Treybal, R., (1980), *Mass Transfer Operations,* Third, (McGraw-Hill).

Tung, H.-H. and Mah, R. S. H., (1985), *Chemical Engineering Communications,* **39,** 147-153, "Modelling liquid mass transfer in higee separation process".

Versteeg, G. F. and Van Swaaij, W. P. M., (1988), *J. Chem. Eng. Data,* **33,** 29-34, "Solubility and Diffusivity of Acid Gases (CO2, N2O) in aqueous alkanolamine Solutions".

Vivian, J. E. and Peaceman, (1956), *AIChE.*, **2**, pp 437.

Vivian, J. E., Brian, P. L. T. and Krukonis, V. J., (1965), *AIChE,* **11,** (6), pp 1088-1091, "The influence of gravitational force on gas absorption in a packed column".

Waldie, B. and Harris, W. K., (1998), *Chemical Engineering Research & Design, Transactions of the Institute of Chemical Engineers, Part A,* **76, n A5,** 562-570, "Removal of dissolved aromatics from water - comparison of a high intensity contactor with a packed column".

Wallis, G. B., (1969), *One-Dimentional Two Phase Flow,* (McGraw-Hilll).

White, A. M., (1935), *Trans. Am. Inst. Chem. Engrs.*, **31,** 390-409, "Pressure Drop and Loading Velocities in Packed Towers".

Whitman, W. G., (1923), *Chem. Met. Eng.*, **29,** 147, "The two-film theory of absorption".

Wong, H. A., Kohler, R., Kosseim, A. J., Kubek, D. J. and McCullough, J. G., (1985), *Oil and Gas,* **83,** (45), pp 100-108, "Corrosion-inhibition system passes severest test at Chevron's Princess MEA plant".

Zarzycki ,R., and Chacuk, A., (1993), *Absorption: fundamentals and applications*, (Pergamon Press Ltd.).

Zhenh, C., Xin, Z. and Gardner, N. C., (1997), "Industrial practice of HIGRAVITEC in water deaeration", In *2nd International Conference on Process Intensification in Practice: Applications and Opportunities*(Ed, Semel, J.) , BHR Group Limited, London, pp. 273-287.

Appendix A

Properties of Monoethanolamine

Manufacture

Alkanolamines are produced by the reaction of ethylene oxide with ammonia. The products of the reactor are: mono-, di-, and tri-alkanolamines, which are separated downstream.

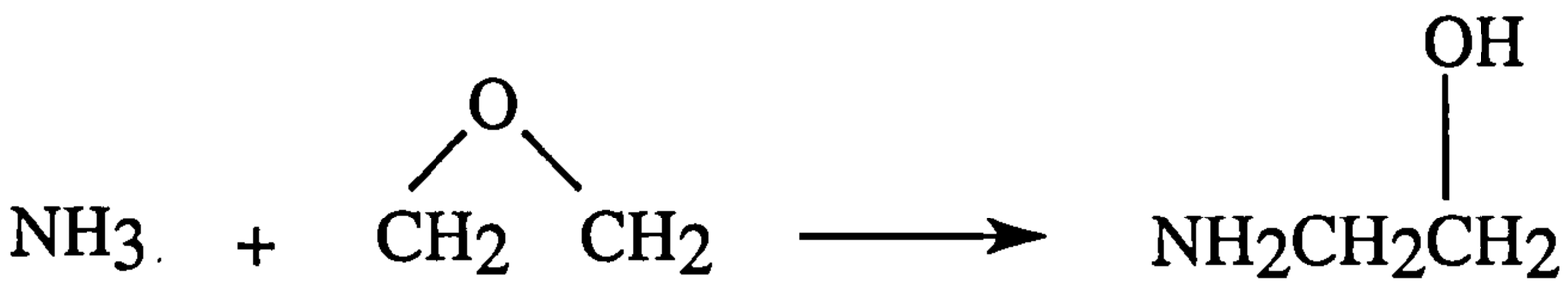

Physical Properties of MEA

Table A-1: The physical properties of MEA

Common Name	Monoethanolamine (MEA)
Molecular Formula	C_2H_7NO
CAS Registry Number	[141-43-5]
Chemical Abstracts Name	2-aminoethanol
Specific Gravity 20/20°C	1.0179
Freezing Point	10.5°C
Boiling Point	170.5°C
Flash point	95 °C
Viscosity @ 20°C	24.1 cP
Refractive Index	1.4544 n_D^{20}
Vapour Pressure @ 20°C	0.4 mmHg
Heat of Vaporization, 1 atm	355 Btu/lb
Specific Heat @ 20°C	0.648 Btu/lb/°F
Solubility in Water n-Heptane	 ∝ g/100 g 0.06 g/100 g

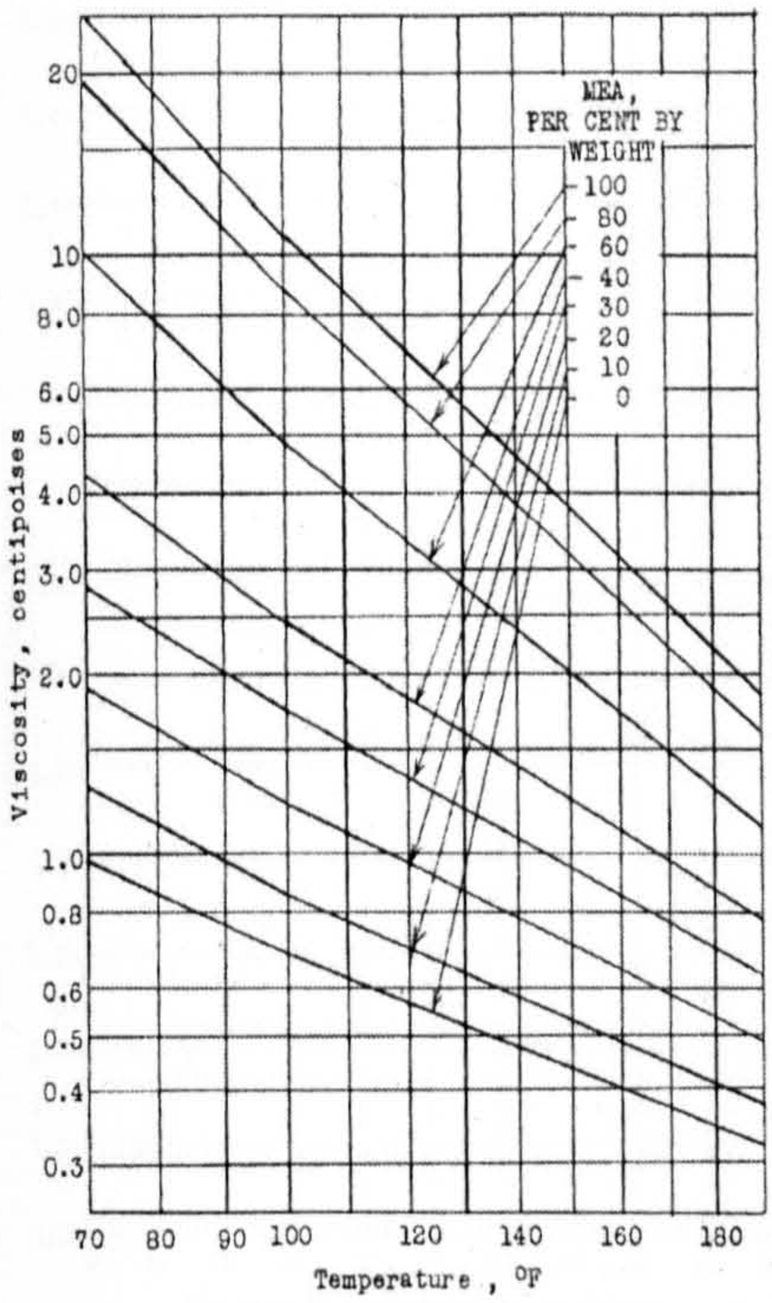

Figure A-1: Viscosity

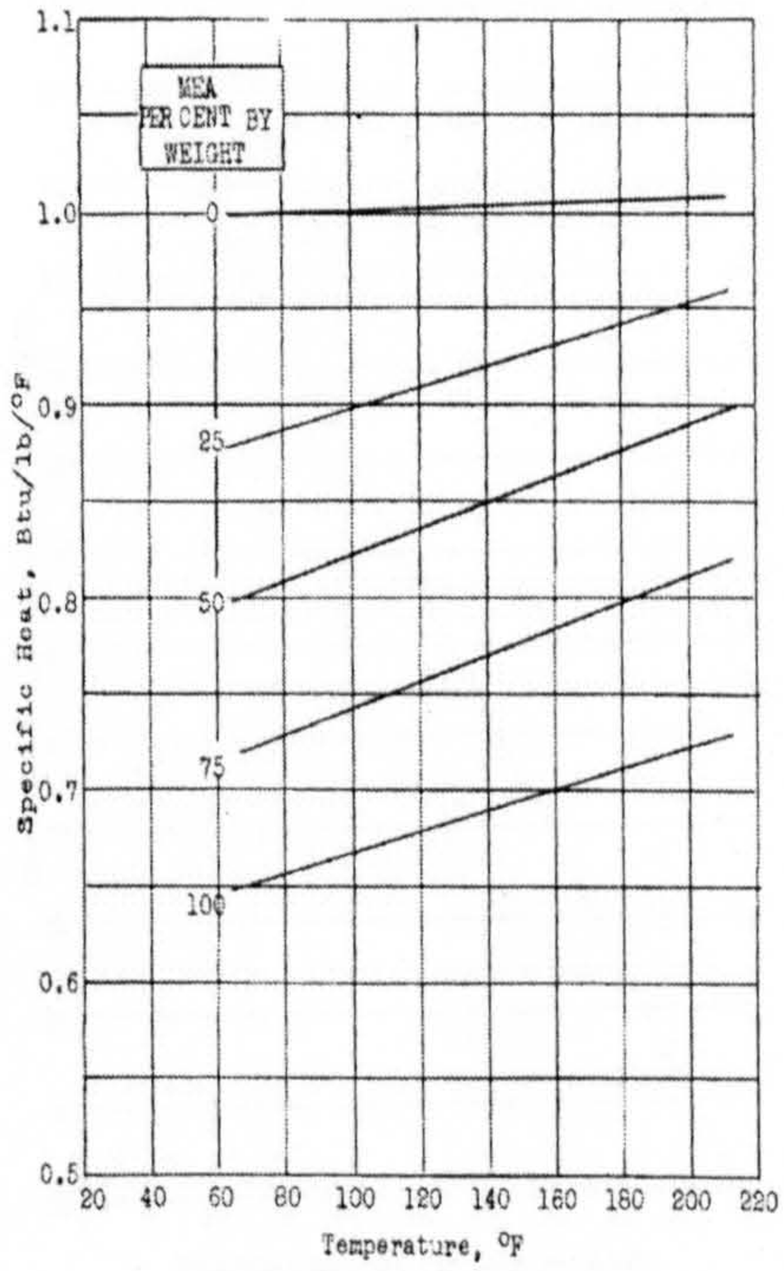

Figure A-2: Specific Heat

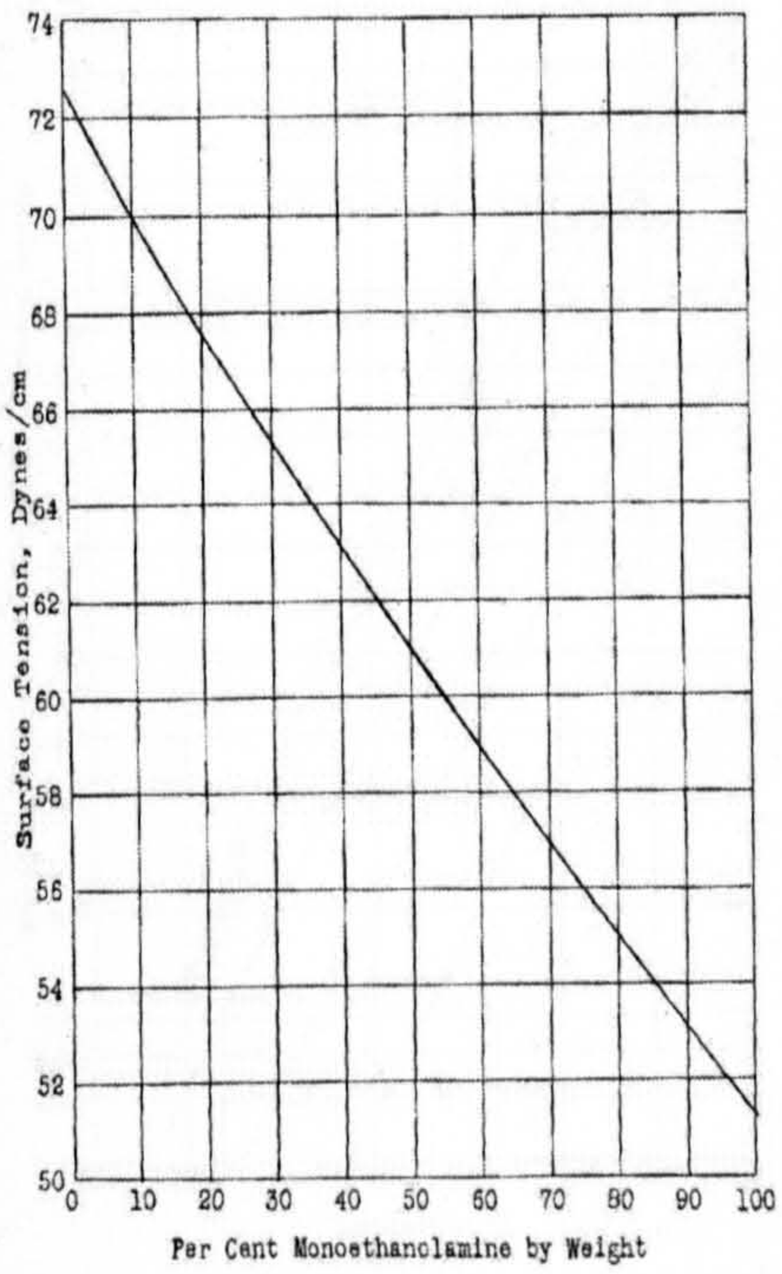

Figure A-3: Surface Tension

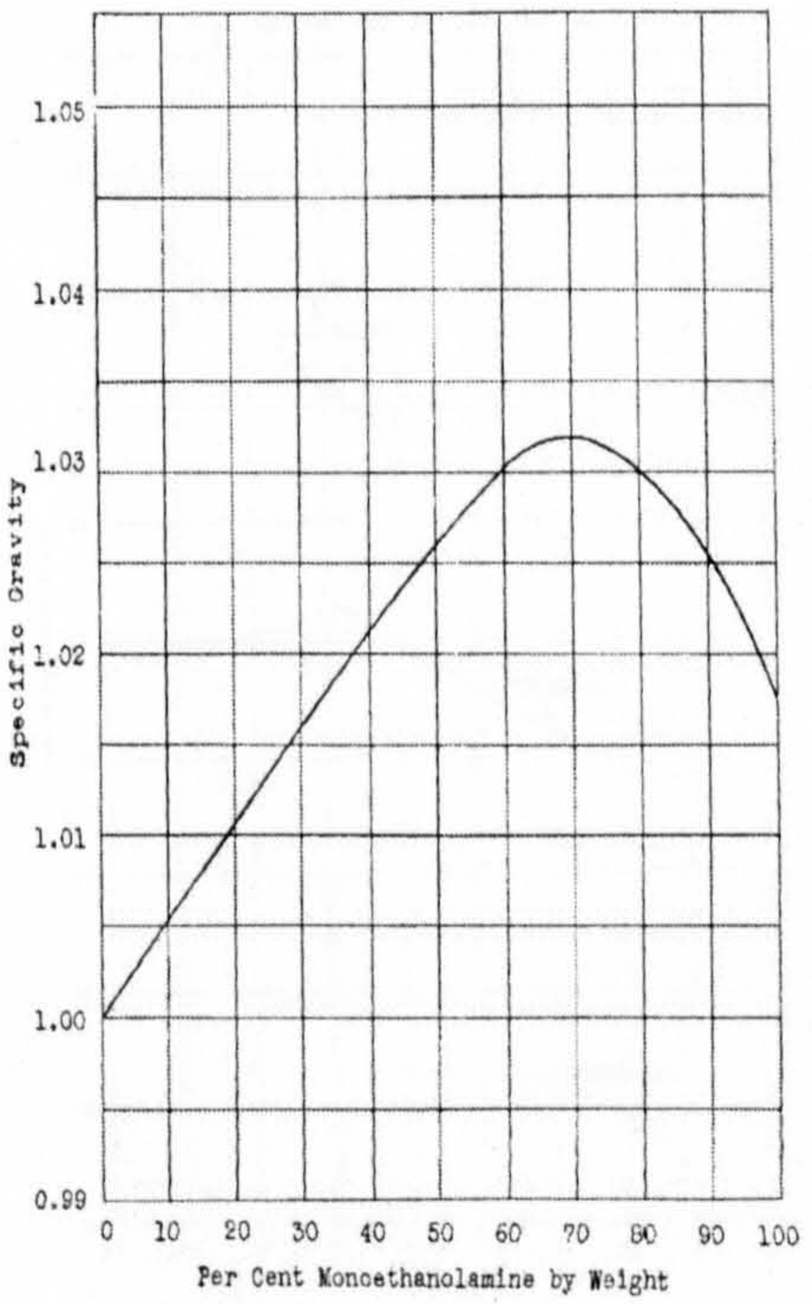

Figure A-4: Specific Gravity

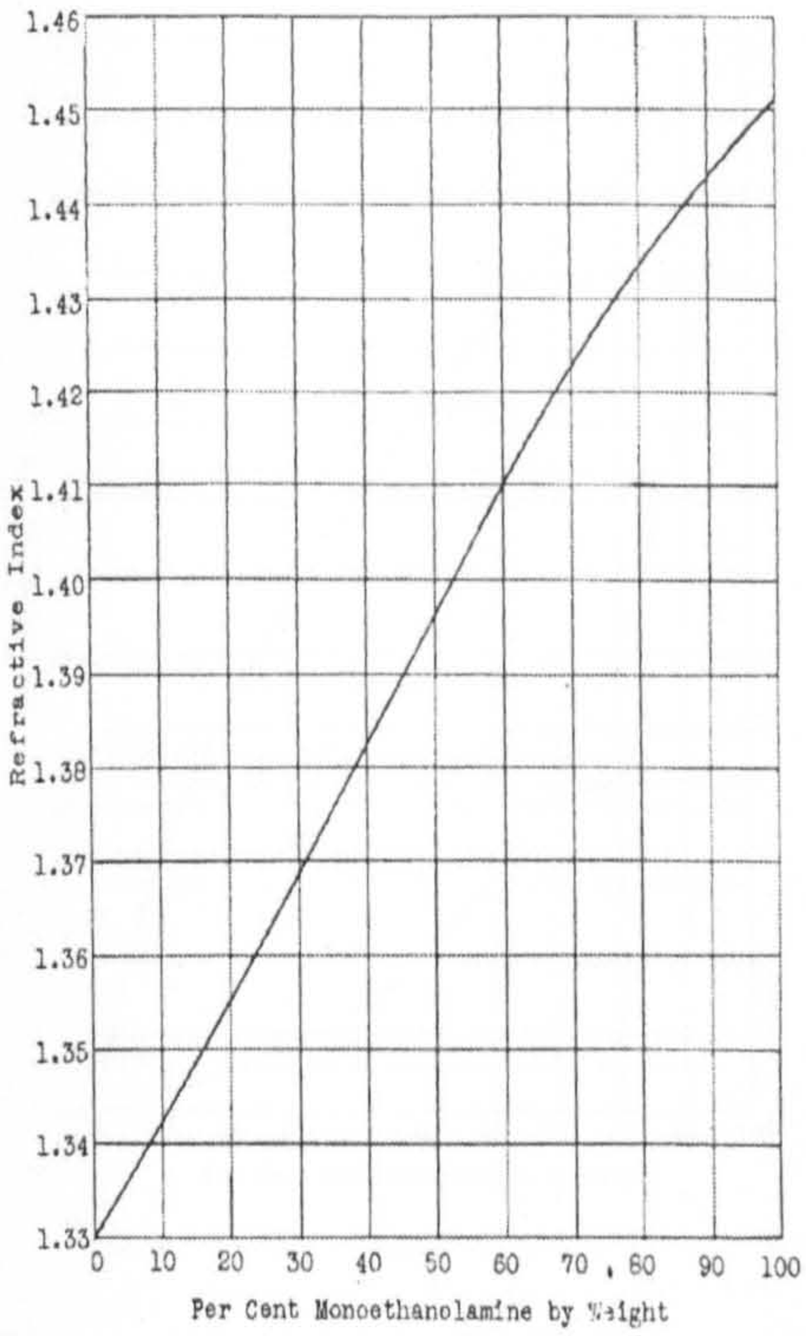

Figure A-5: Refractive indices

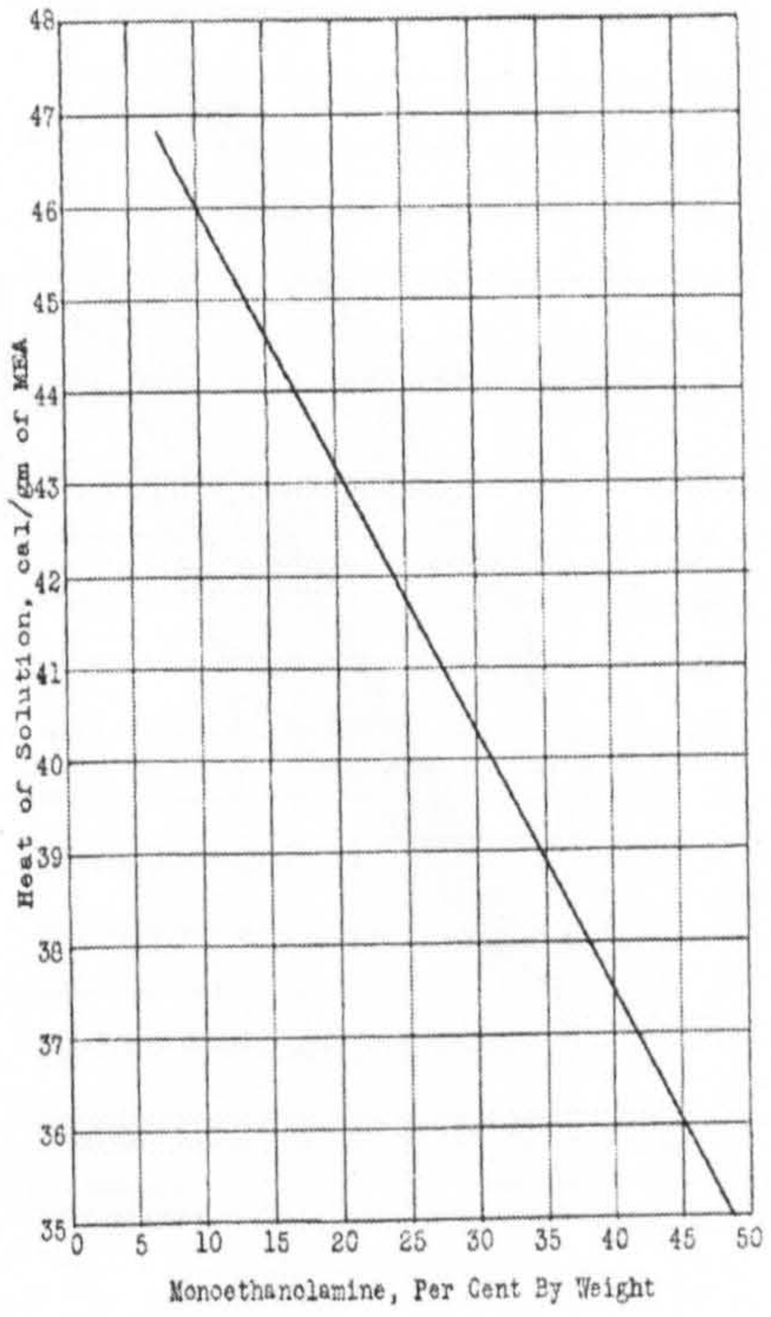

Figure A-6: Heat of solution (25°C)

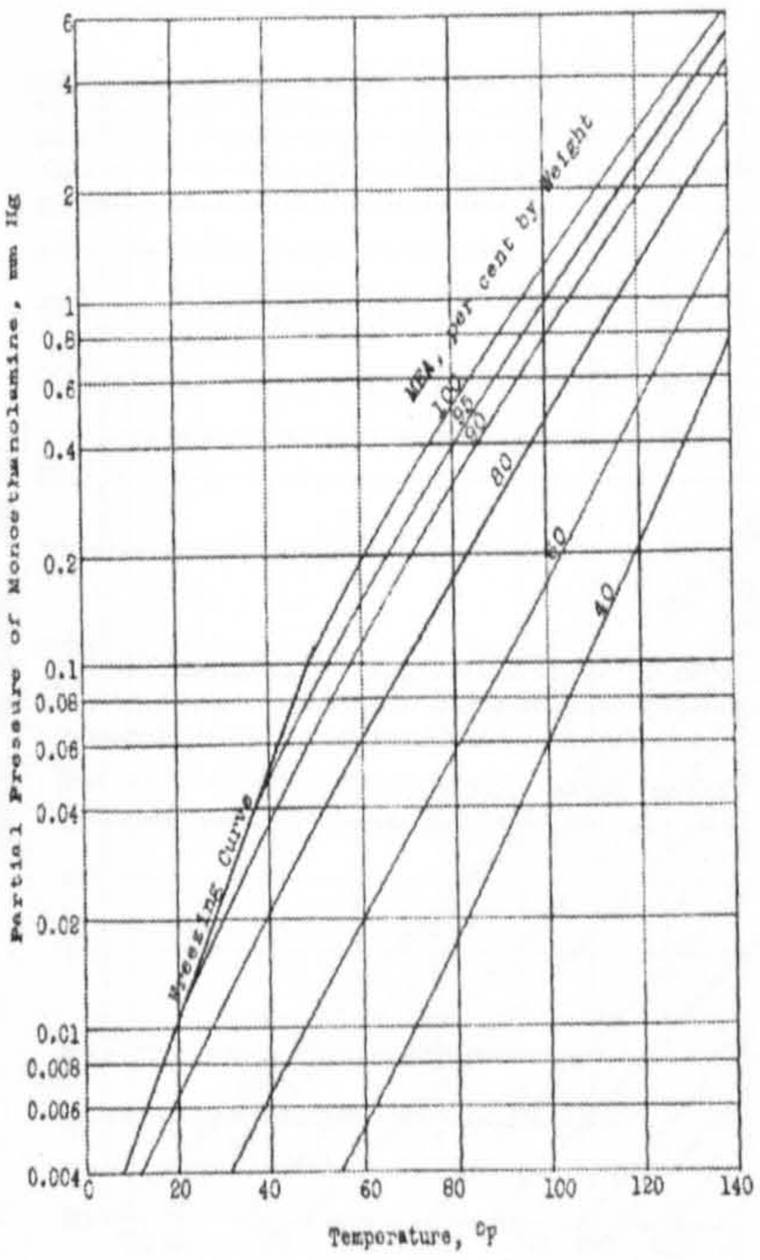

Figure A-7: Volatility

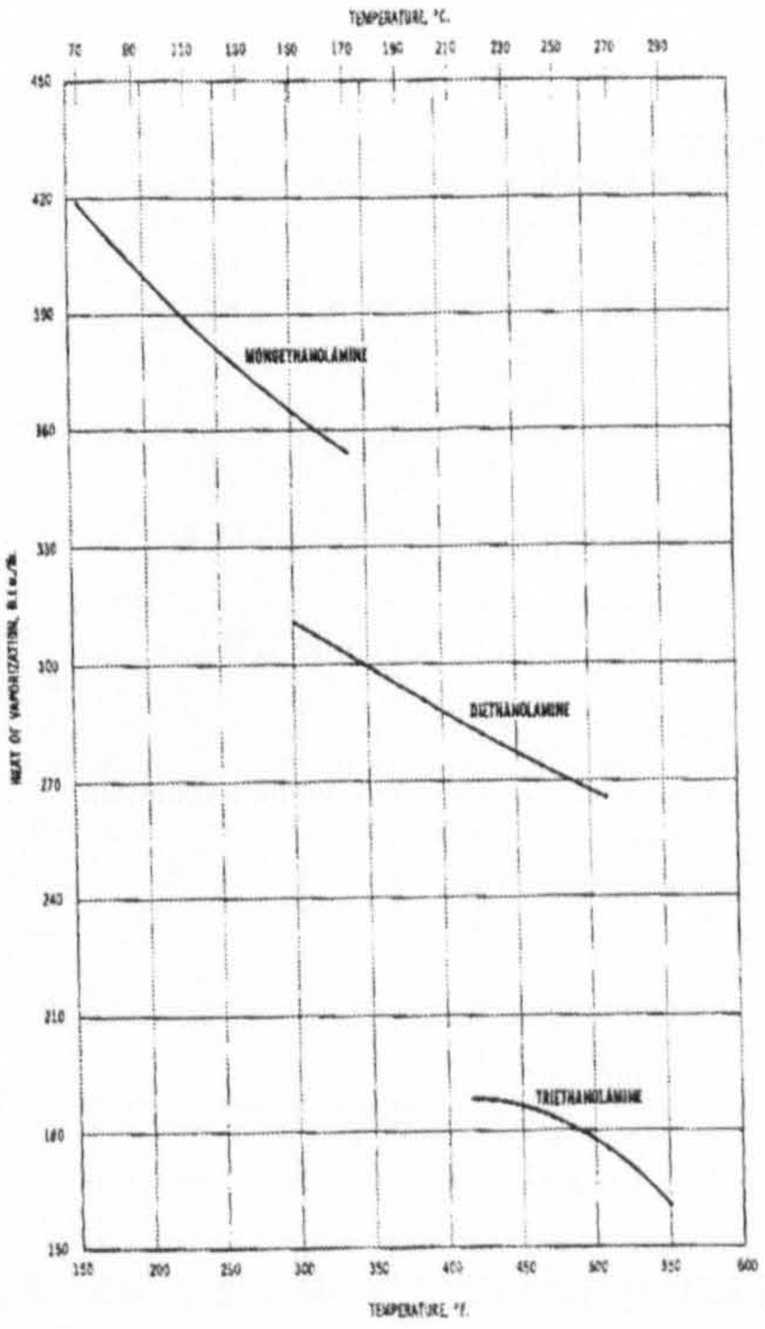

Figure A-8: Heat of vaporization.

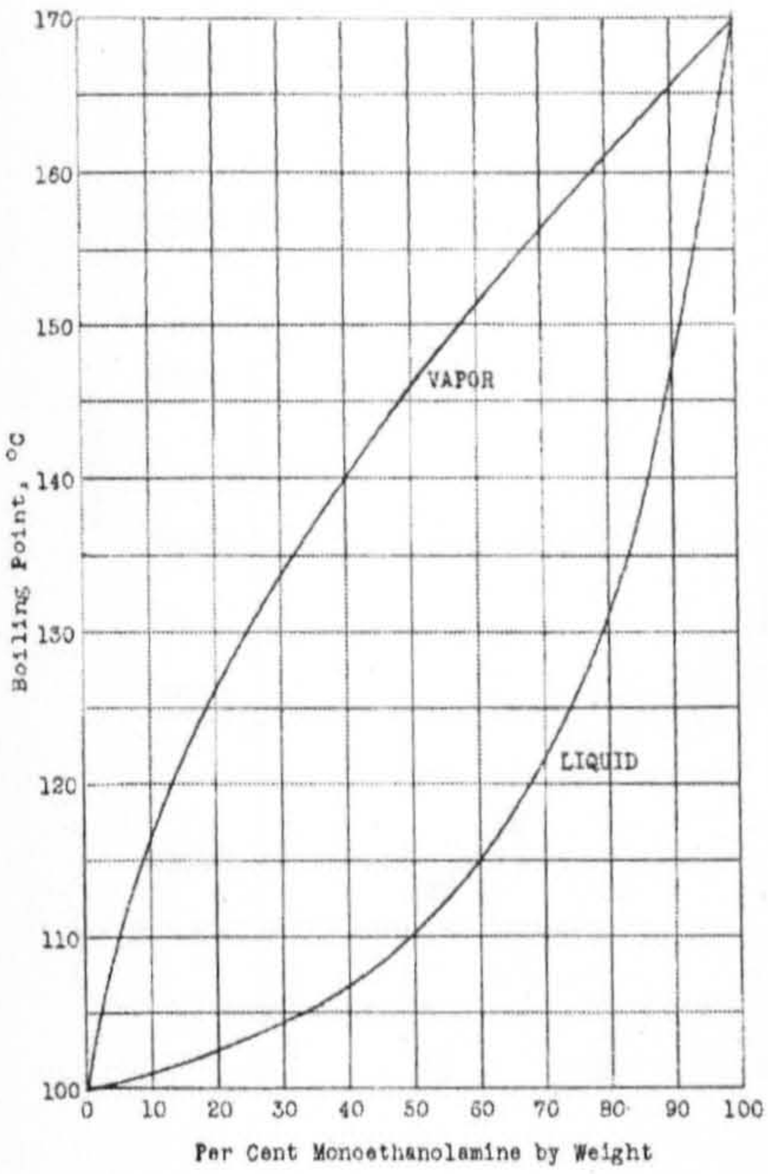

Figure A-9: Boiling point composition curve for MEA.

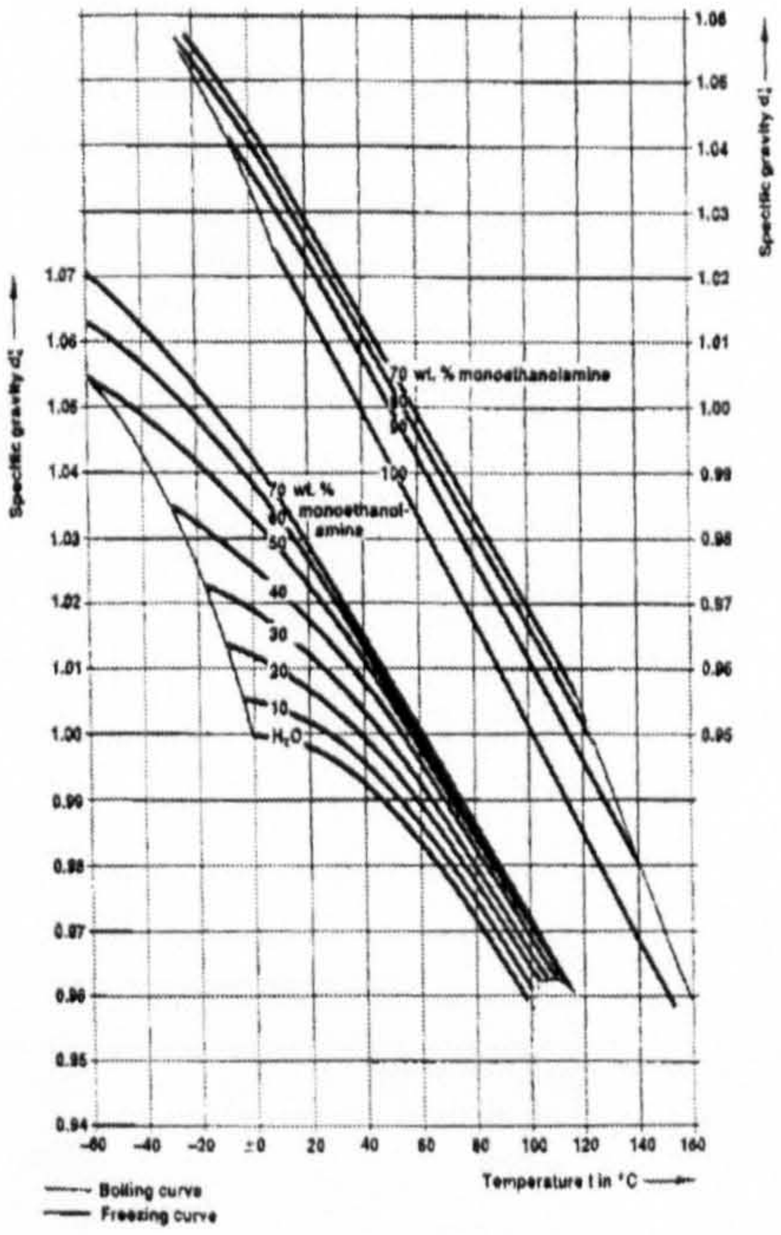

Figure A-10: Specific gravity of MEA solution.

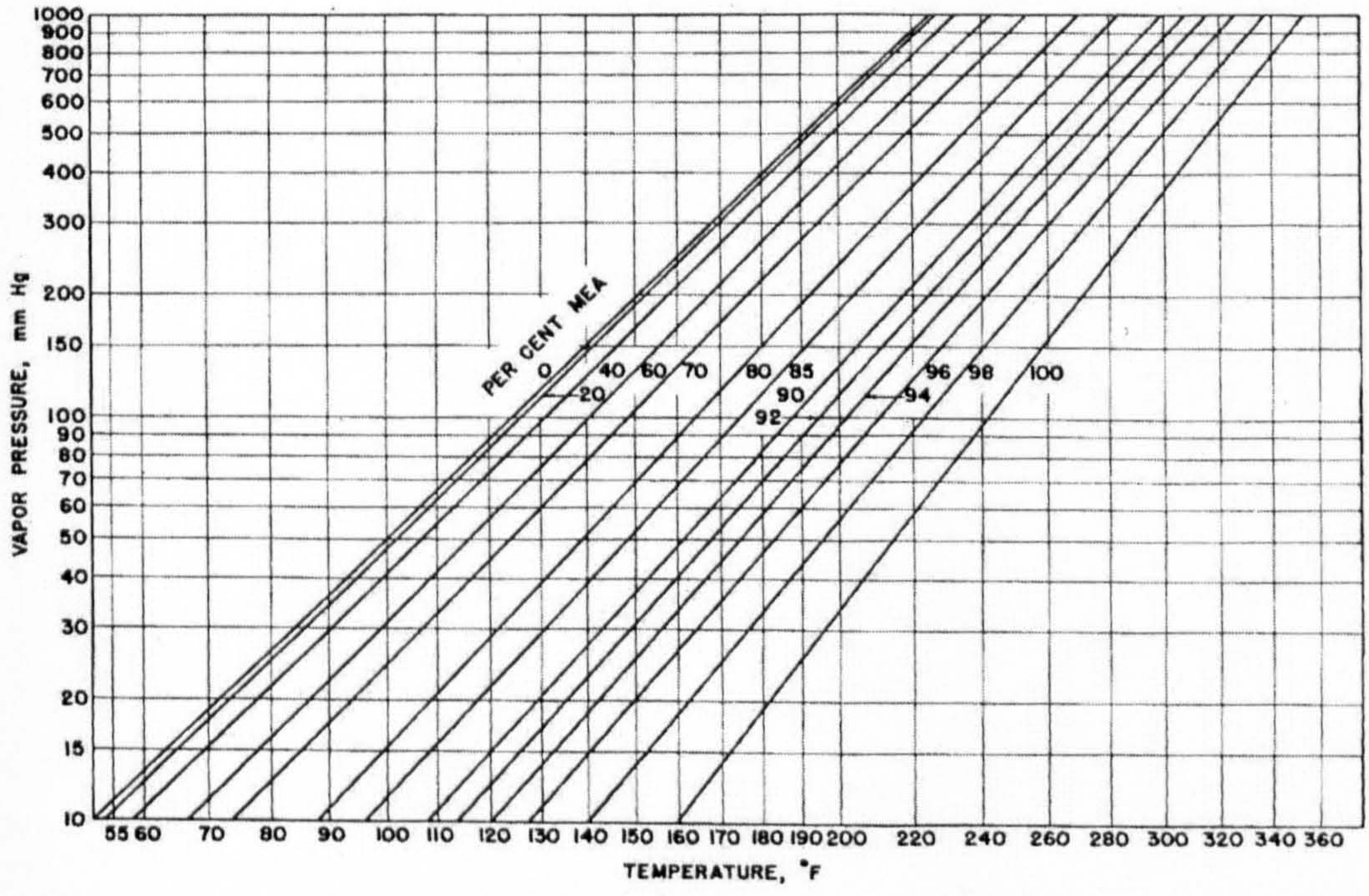

Figure A-11: Total Vapour Pressure of MEA solutions.

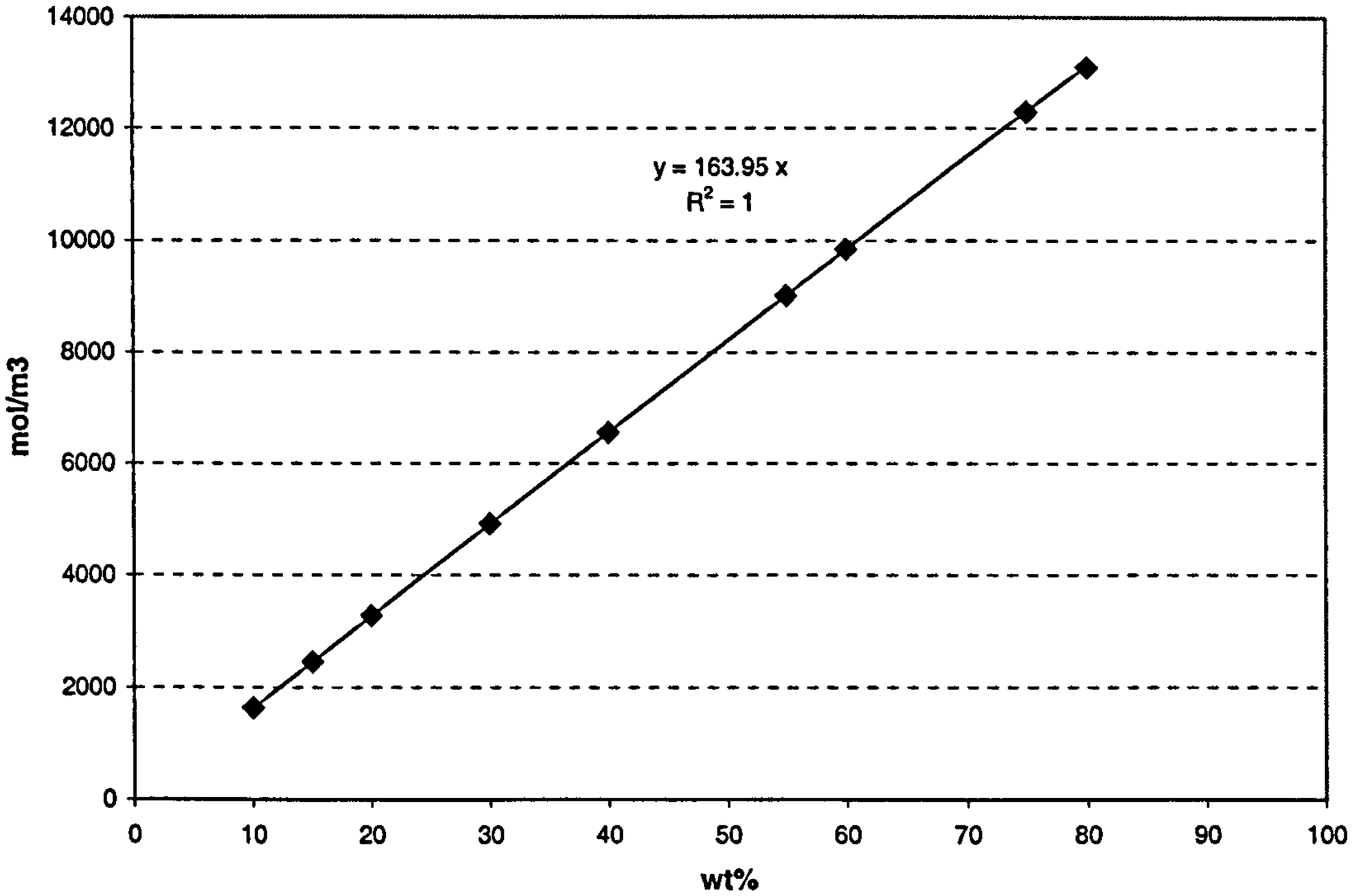

Figure A-12: Weight Percent versus Molarity for MEA solutions

Appendix B

Calibration Charts for Ethanolamine Solution and Air Flowmeters

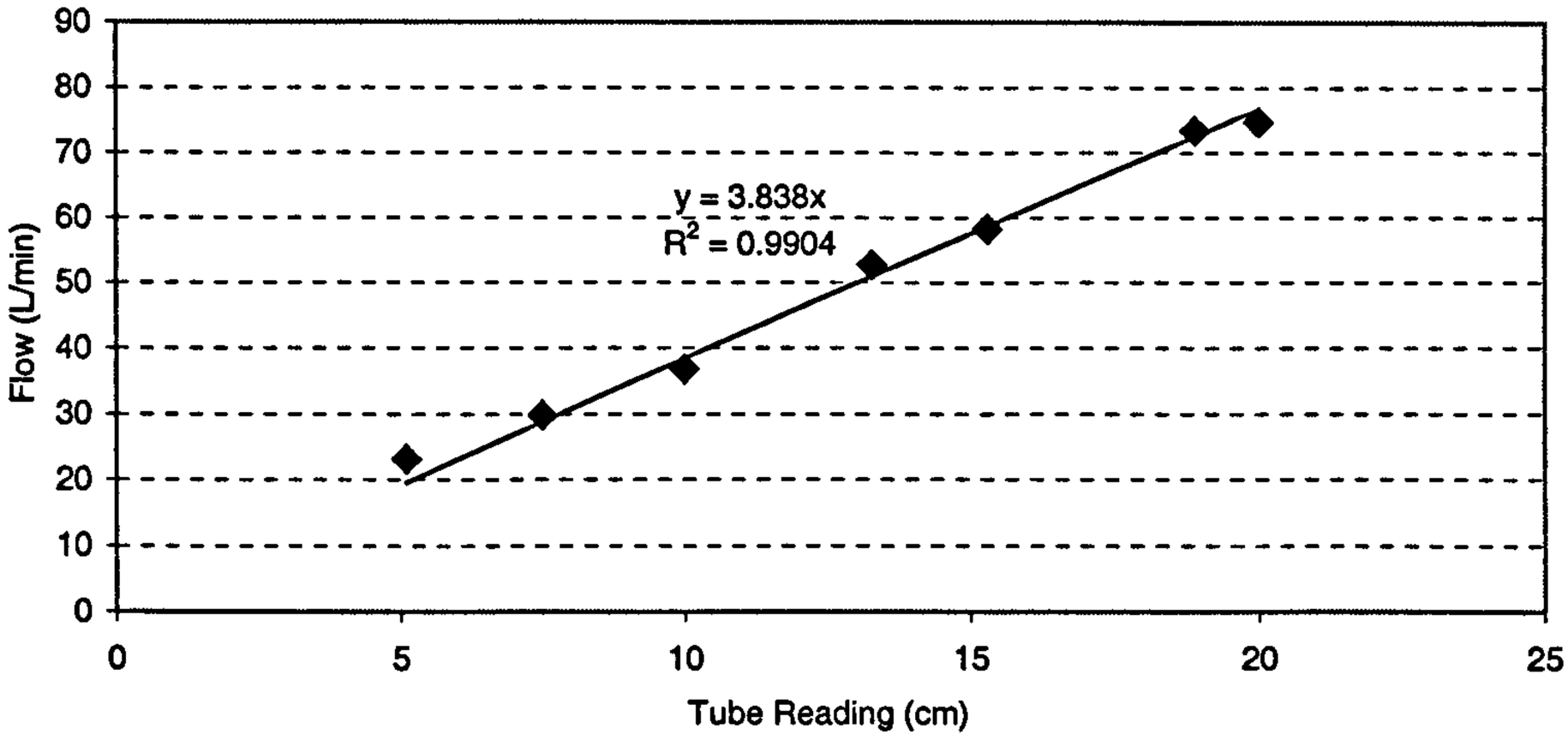

Figure B-1: Calibration chart for flowmeter (47X) at room temperature.

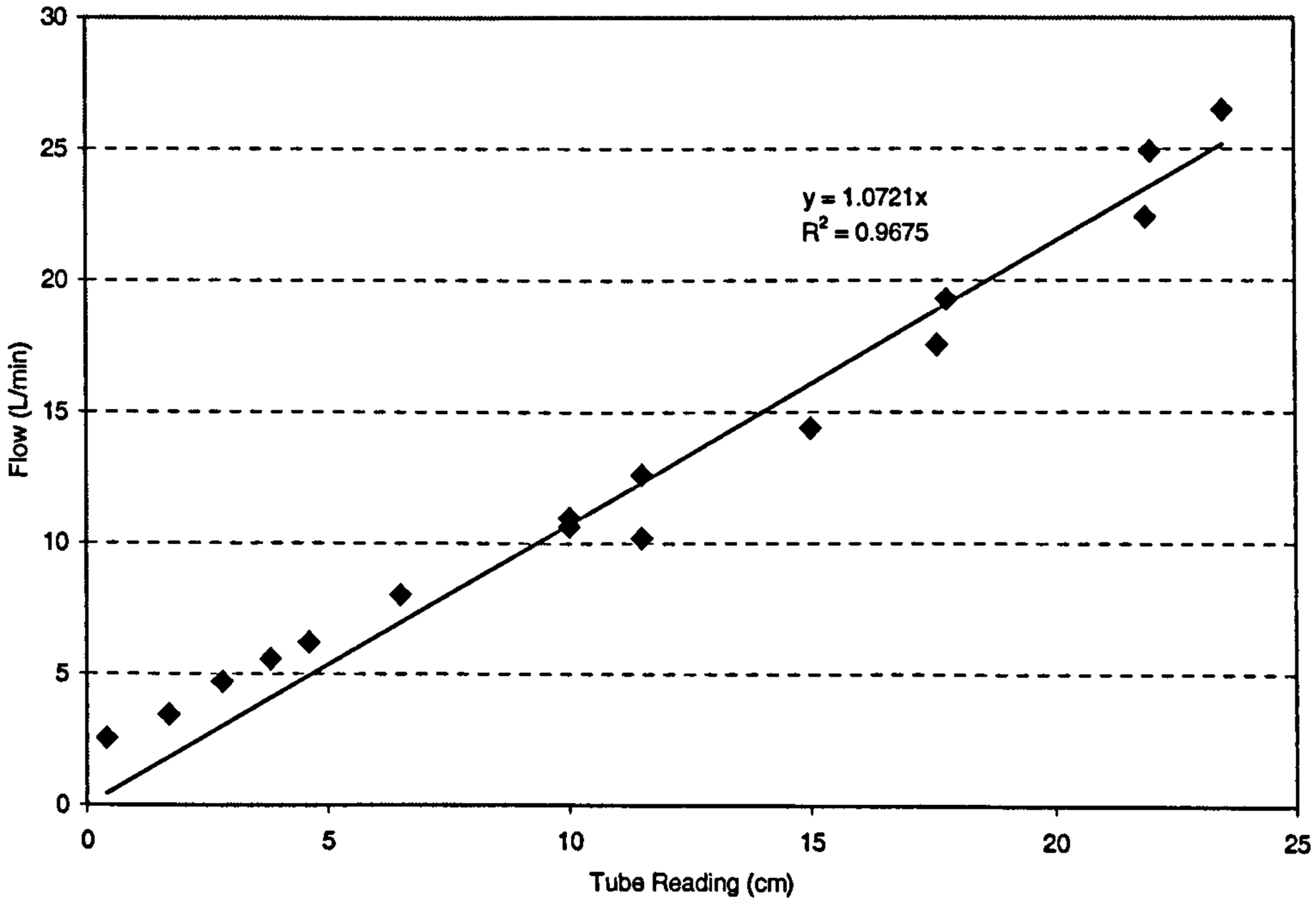

Figure B-2: Calibration chart for flowmeter (35X) at room temperature.

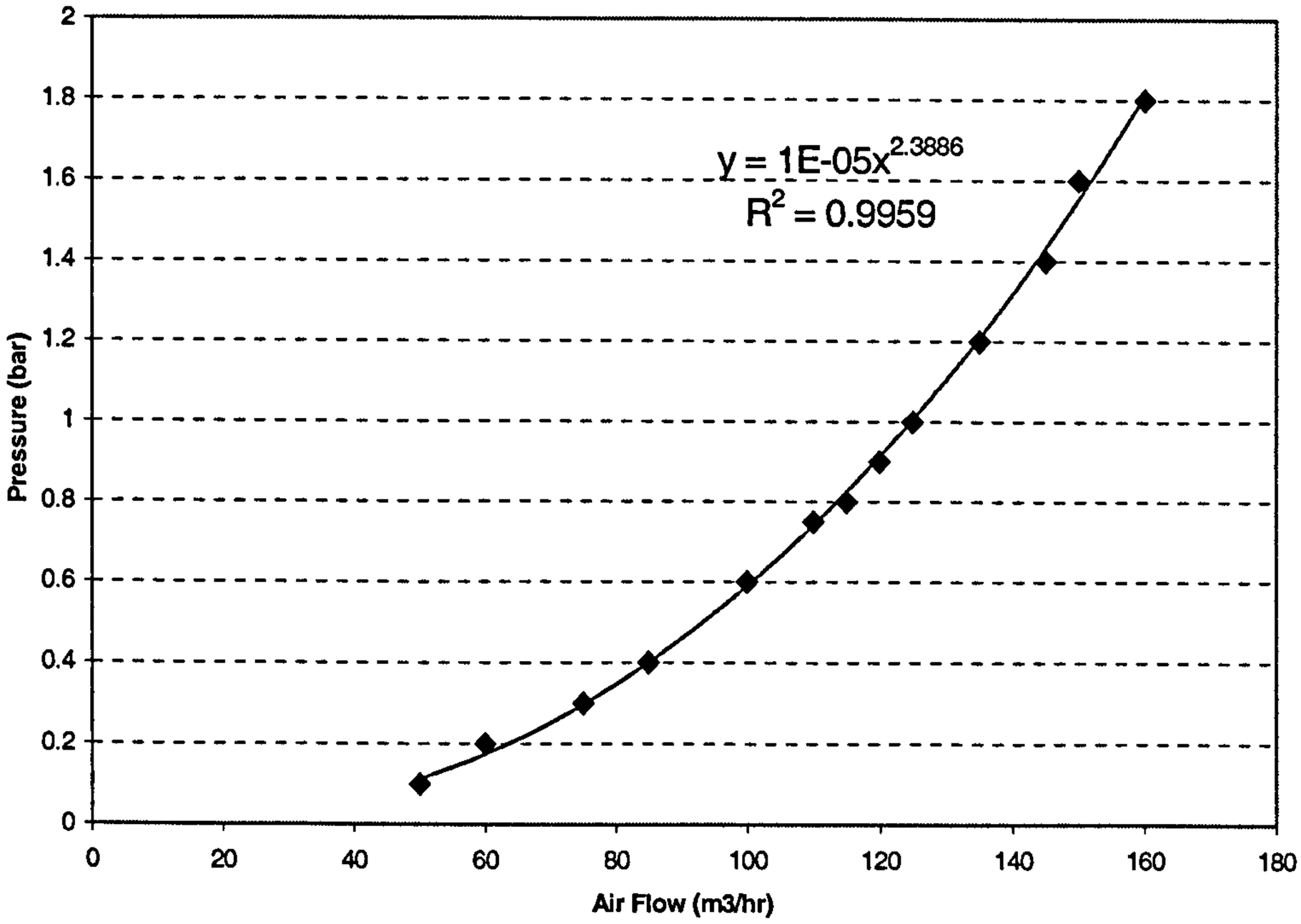

Figure B-3: Relationship between the air flowmeter and its gauge pressure.

Appendix C

Properties of the Rotating Packed Bed

Expamet Density

(Perry and Green, 1984) reported the density of steel to be in the range of 7700-7830 kg/m3. Thus, the density of steel is chosen as 7800 kg/m^3

Packed bed density

Packed bed density can be calculated using the following formula:

$$\text{Packed bed density} = \text{Weight per unit area} * \frac{\text{Number of sheets}}{\text{Axial depth}}$$

Weight per unit area = 1.69 kg/m2 (provided by manufacturer).

Number of sheets = 30.

Axial depth = 27 mm.

$$\text{Thus, packed bed density} = 1.69 * \frac{30}{0.027} = 1877.78 \text{ kg/m3}$$

Determination of expamet porosity

The relationship between packed bed density and porosity is as follows:

$$\text{Packed bed density} = \rho = \rho_{SS}(1-\varepsilon) + \varepsilon \rho_{air}$$

where ρ_{SS} is stainless steel density, ρ_{air} is air density and ε is the porosity. By neglecting air density, the above equation can be re-arranged as follows:

$$\varepsilon = 1 - \frac{\rho}{\rho_{SS}} = 1 - \frac{1877.78}{7800} = 0.76$$

Determination of Surface Area of Expamet

The dimensions of rotating packed bed (RPB) is shown in Figure A:

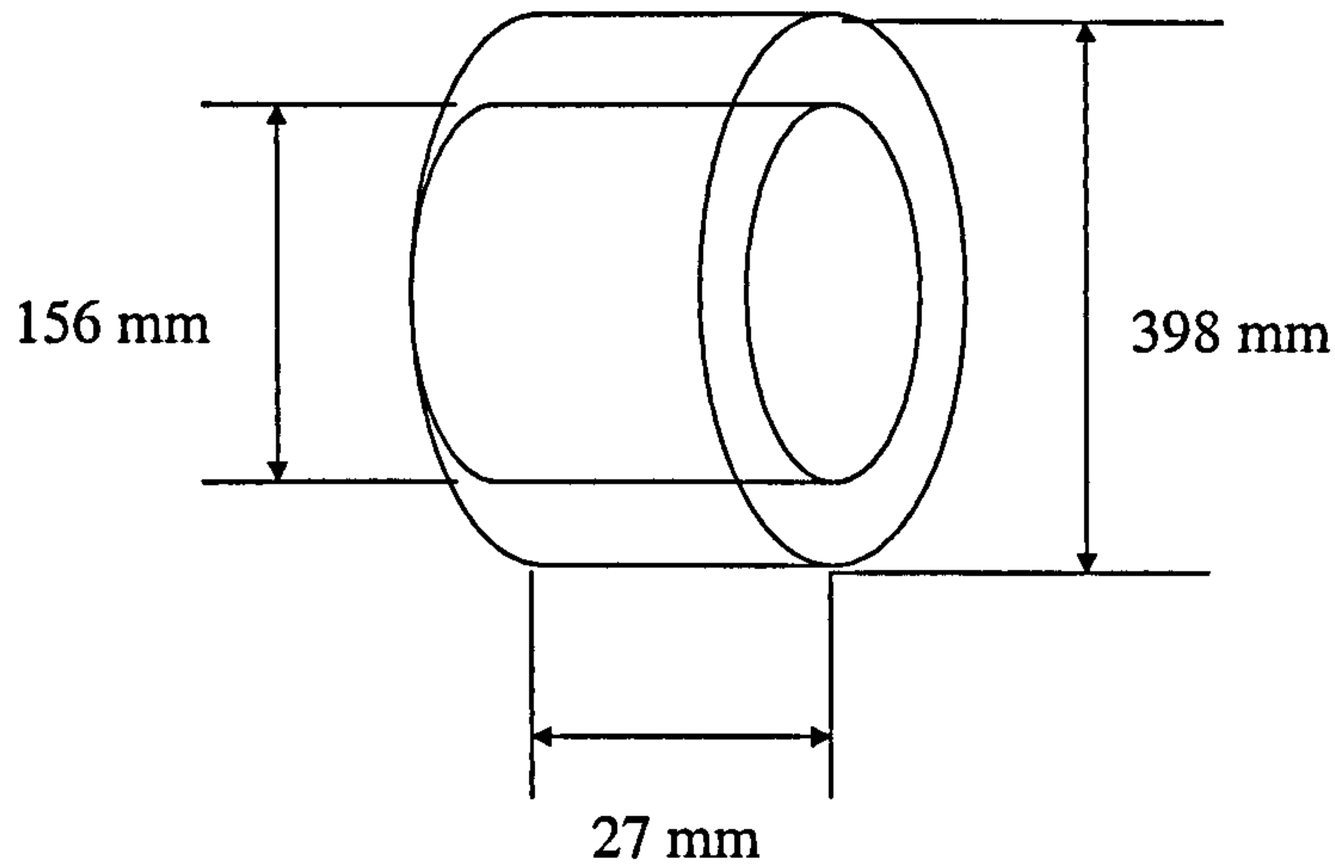

Figure C-1: Dimensions of RPB

The volume is calculated as follows:

$$\pi\left(\left(\frac{\text{OD}}{2}\right)^2-\left(\frac{\text{ID}}{2}\right)^2\right)*\text{Axial depth}=\pi\left(\left(\frac{0.398}{2}\right)^2-\left(\frac{0.156}{2}\right)^2\right)*0.027=2.843*10^{-3}m^3$$

The cross-sectional area =

$$\frac{\pi}{4}*\left(\text{OD}^2-\text{ID}^2\right)=\frac{\pi}{4}(0.398^2-0.156^2)=0.1053\,m^2.$$

Expamet Configuration

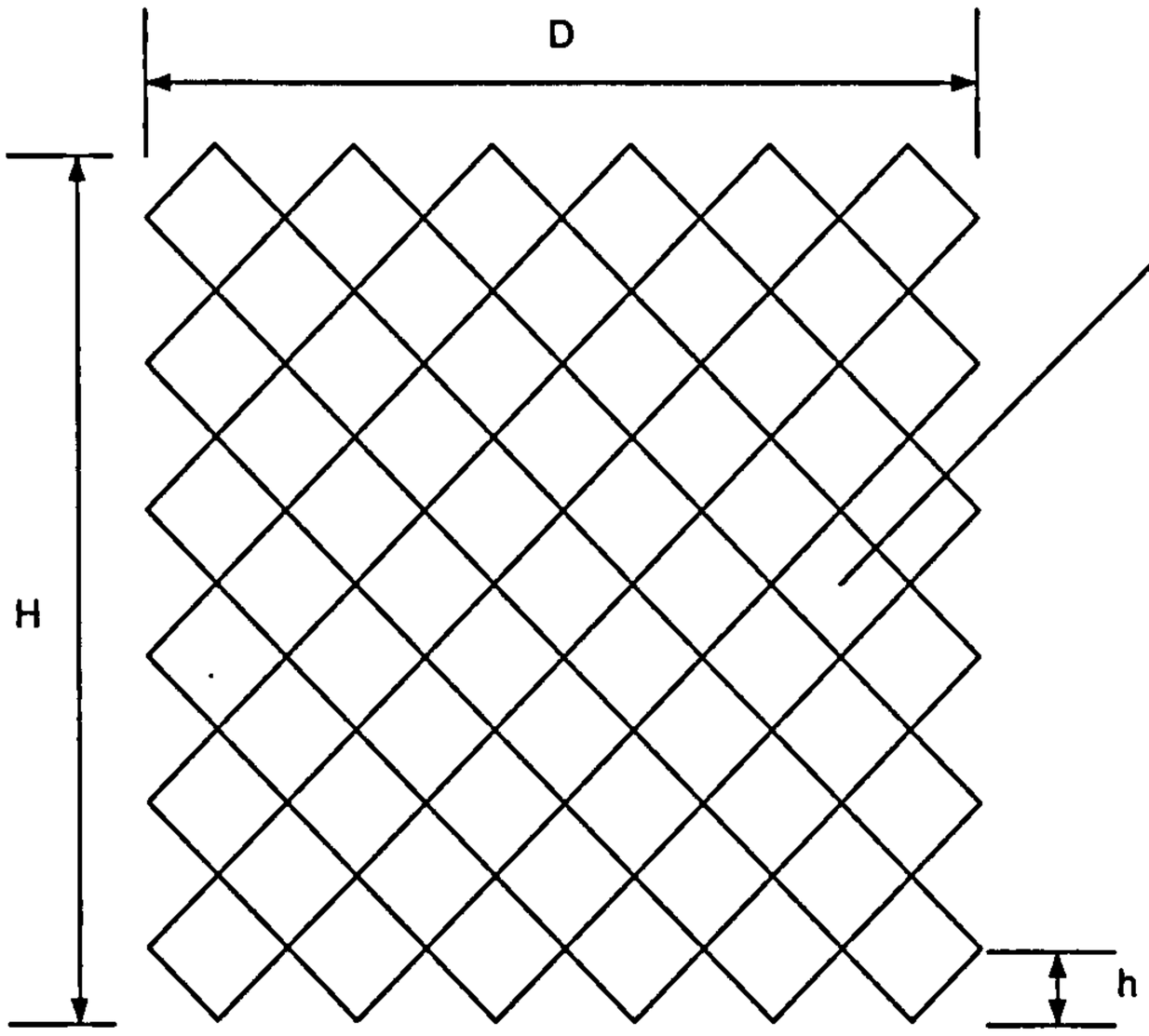

Figure (A)

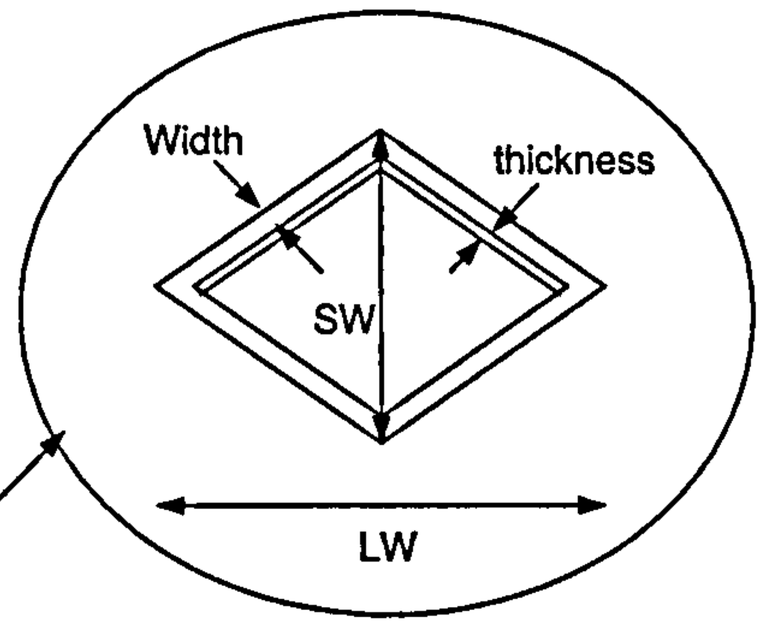

Figure (B)

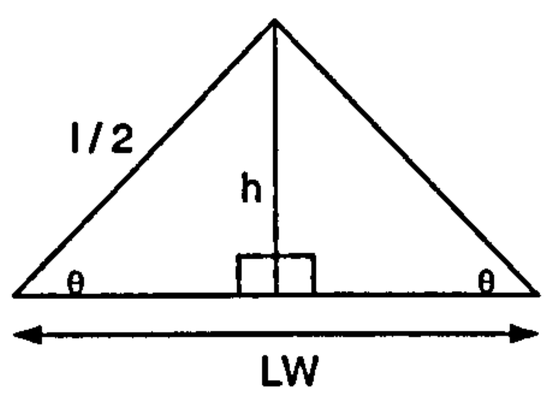

Figure (C)

Figure C-2: Expamet Configuration

Figure (A) shows a cross section area of expamet mesh with dimension of H x D. Figure (B) shows building block of mesh. Its shape can be approximated into two opposite triangles. The nomenclatures used in the above figures are:

width = w = 0.56 mm

thickness = t = 0.46 mm

LW = Long way of mesh dimension = 4.75 mm.

SW = Short way of mesh dimension = 2 h = 2.38 mm.

Thus, $\tan\theta = \frac{h}{0.5\,LW} = \frac{SW}{LW}$

$$\theta = \tan^{-1}\left(\frac{2.38}{4.75}\right) = 26.61$$

From Figure (c):

$$h = \frac{LW \,.\, \tan\theta}{2}$$

$$l = \frac{LW}{\cos\theta}$$

The formula for calculating surface area of expamet mesh can be derived as follows:

Surface area of mesh = number of strands * surface area of a single strand.

$$\text{Number of strands} = \frac{H}{h} = \frac{2H}{LW \,.\, \tan\theta}$$

$$\text{Surface area of a single sheet} = 2(w+t)\, l\, \frac{D}{LW} = 2(w+t)\frac{D}{\cos\theta}.$$

Thus, Surface area of mesh =

$$4(w+t)\frac{DH}{LW\sin\theta} = \frac{4(w+t)}{LW\sin\theta} * \text{cross sectional bed area}$$

$$\text{Thus, total surface area} = \frac{4*(0.56+0.46)}{4.75\sin(26.61)} * 0.105 * 30 = 6.06 \text{ m2.}$$

$$\text{Thus, surface area per unit volume} = \frac{6.06}{2.843*10-3} = 2132 \text{ m2/m3.}$$

Appendix D

Pressure Drop in 4-Arm Liquid Distributor

The configurations of 4-arm distributor are as follows:

Number of arms = 4

Length of each arm = 12 cm = 0.12 m.

Number of holes per arm = 8

Diameter of each hole = 2 mm = 0.002 m

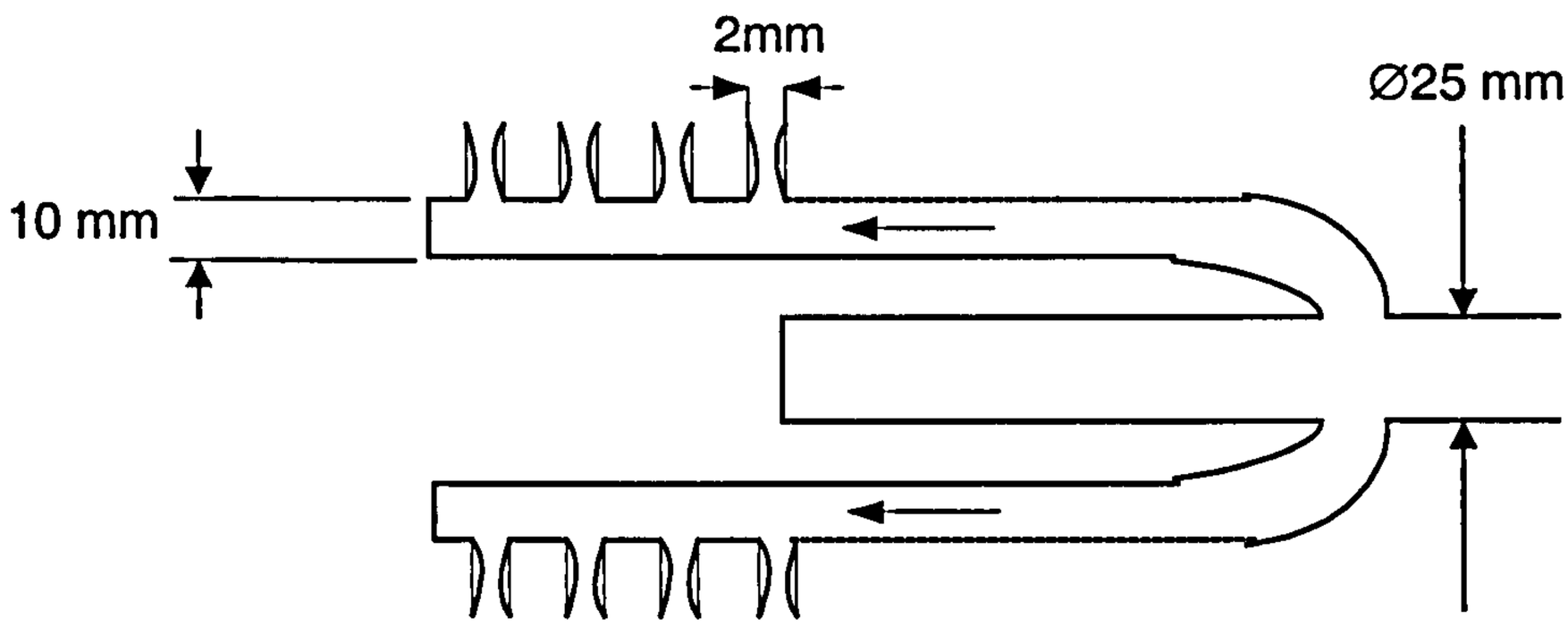

Figure D-1: Sudden contraction to the liquid flow in 4-arm distributor.

The physical properties of 30wt% ethanolamine solution @ 30°C are: density = 1013 kg/m^3, and dynamic viscosity = $2*10^{-3}$ Pa.s.

The following calculations are based upon an ethanolamine solution flowrate of 50 L/min = 0.00083 m^3/s.

$$\text{Cross sectional area of each hole} = \frac{\pi (\text{hole diameter})^2}{4}$$

$$= \pi * \frac{0.002^2}{4} = 3.141*10^{-6}\ m^2.$$

$$\text{Flowrate per hole} = \frac{\text{Total flowrate}}{\text{Number of holes}} = \frac{0.00083}{8*4} = 25.9*10^{-6}\ m^3/s.$$

$$\text{Velocity of solution for each hole} = \frac{Q}{A} = \frac{25.9*10^{-6}}{3.141*10^{-6}} = 8.24 \text{ m/s}$$

$$\text{Re} = \frac{\rho u d}{\mu} = \frac{1013*8.24*0.002}{2*10^{-3}} = 8{,}347 .$$

The pressure drop for a sudden contraction to the effective area of the flow could be calculated as follows (Coulson et al., 1993):

$$\Delta P_f = -\frac{\rho u^2}{2}\left[\frac{1}{C_c} - 1\right]^2$$

where C_c is the contraction coefficient and it varies between 0.6 and 1.0 as the ratio of the pipe diameters varies from 0 to 1 (the ratio is 0.2 in our case). Assuming a common value for C_c of 0.67. The velocity of fluid (u) refers to the smaller pipe.

Thus, the pressure drop is:

$$\Delta P_f = -\frac{1013*8.24^2}{2}\left[\frac{1}{0.67} - 1\right]^2 = -8.34 \text{ kPa}.$$

Thus, the total pressure drop in each arm due to the sudden contraction is 66.72 kPa.

The pressure drop in each arm due to frictional loss can be calculated as follows:

$$\text{Mean velocity} = \frac{Q}{\pi d_i^{\,2}/4}$$

$$Q = \frac{0.00083}{4} = 0.0002075 \text{ m}^3/\text{s}.$$

$$\frac{\pi d_i^{\,2}}{4} = \frac{\pi(0.01)^2}{4} = 0.0000785 \text{ m}^2.$$

Thus, the mean velocity = 2.64 m/s.

$$\text{The Reynolds number} = \text{Re} = \frac{\rho u d}{\mu} = \frac{1013*2.64*0.01}{2*10^{-3}} = 1.3*10^4$$

The pipe roughness = 0.000045 m (commercial steel)

$$\text{Thus, the relative roughness} = \frac{e}{d} = \frac{0.000045}{0.01} = 0.0045$$

Accordingly, the fanning friction factor = 0.009 (Holland and Bragg, 1995).

The frictional pressure drop per unit length is given by:

$$\Delta P_f = 4f\left(\frac{L}{d_i}\right)\frac{\rho u^2}{2} = 4*0.009*\left(\frac{1}{0.01}\right)\frac{1013*2.64^2}{2} = 12.7 \text{ kPa / m.}$$

The distance between the holes in each arm is approximately 0.5 cm. Thus, the frictional pressure drop is only 0.06 kPa between the two holes distance. This loss is negligible in comparison to the total pressure drop due to the sudden contraction in the holes. The length of each arm is 0.12 m thus the frictional pressure drop per arm is 1.52 kPa.

The total pressure drop in each arm = 66.72+1.52 = 68.24 kPa.

Appendix E

Heat Transfer Rate in CO_2 Heating System

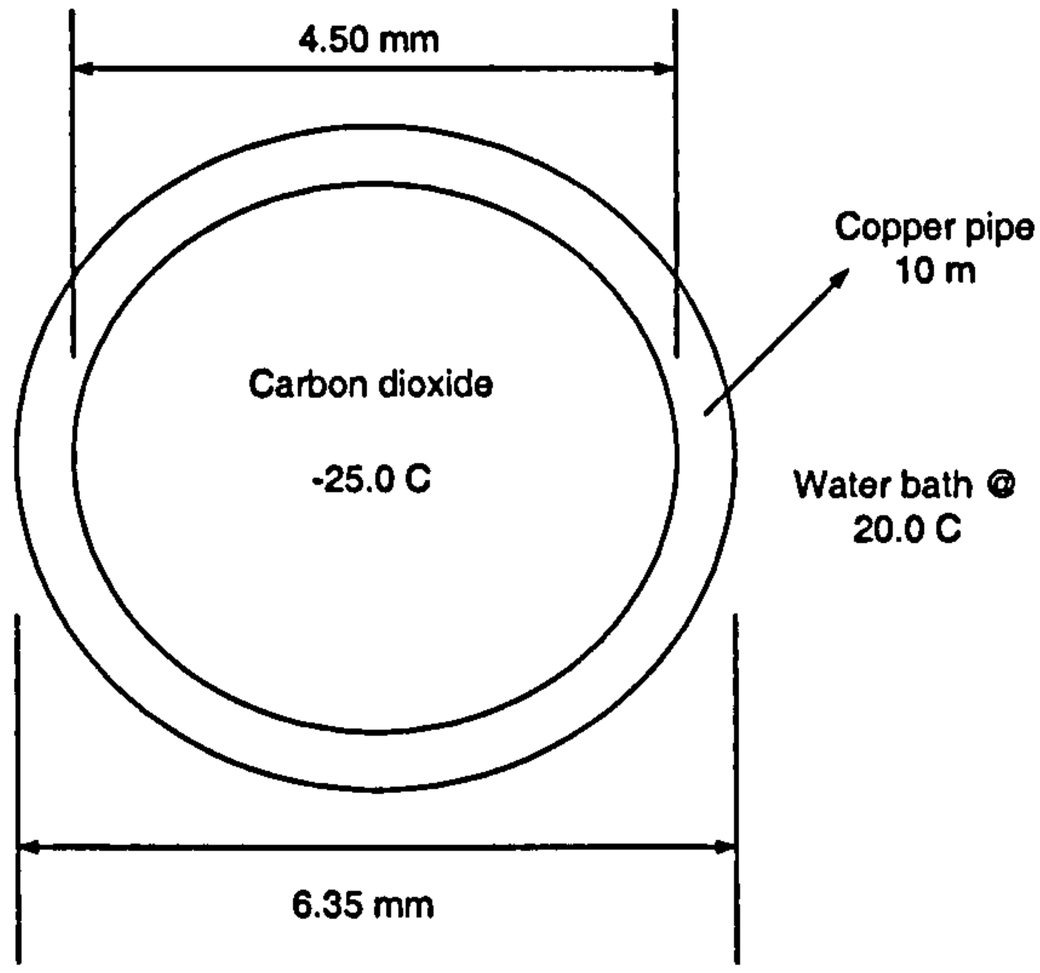

Figure E-1: Dimensions of the Copper Pipe

The specifications of copper pipe in water bath are shown in the above schematic diagram. Properties of carbon dioxide at 255 K are: Prandtl Number = N_{pr} = 0.775, ρ = 1.978 kg/m^3, thermal conductivity = k = 0.0132 W/m.K, μ = 0.0128 * 10^{-3} Pa.s., and water viscosity @ 20C= μ_w = 1*10^{-3} Pa.s.

Typical carbon dioxide flowrate = 45 L/min= 750*10^{-6} m^3/s = 47.15 m/s.

Reynolds number of pure carbon dioxide flow inside pipe is:

$$N_{Re} = \frac{D_i\, u\, \rho}{\mu} = \frac{(0.0045)(47.15)(1.978)}{(0.0128*10^{-3})} = 32{,}787.7$$

The correlation for heat transfer coefficient for turbulent flow inside a pipe under the following conditions ($N_{Re}>10^4$, $0.7<N_{Pr}<700$, $L/D>60$) is:

$$\text{Nusselt Number} = N_{Nu} = \frac{h\,D}{k} = 0.023\, N_{Re}^{0.8} N_{Pr}^{1/3} \left(\frac{\mu}{\mu_w}\right)^{0.14}$$

$$\frac{h\,(0.0045)}{(0.0132)} = 0.023\,(32787.7)^{0.8}\,(0.775)^{1/3}\left[\frac{0.0128*10^{-3}}{1.0*10^{-3}}\right]^{0.14}$$

Solving for h = 137.96 W/m^2.K.

Assume a typical value for water side heat transfer coefficient = 10,000 W/m^2.K.

The areas can be calculated as follows:

$A_i = \pi D_i L = \pi (0.0045)(10) = 0.141$ m^2.

$A_o = \pi D_o L = \pi (0.00635)(10) = 0.2$ m^2.

$$A_{LM} = \frac{A_o - A_i}{\ln(A_o/A_i)} = \frac{0.2-0.141}{\ln(0.2/0.141)} = 0.169 \text{ m}^2.$$

The resistances can be calculated as follows:

$$R_i = \frac{1}{h_i A_i} = \frac{1}{0.141*137.96} = 0.051$$

$$R_o = \frac{1}{h_o A_o} = \frac{1}{0.2*10000} = 0.5*10^{-3}$$

Thermal conductivity for copper is 380 W/m.K.

$$R_m = \frac{r_o - r_i}{k A_{LM}} = \frac{((0.00635-0.0045)/2)}{380*0.169} = 14.4*10^{-6}$$

$$\sum R = 0.051 + 0.5*10^{-3} + 14.4*10^{-6} = 0.0515$$

Overall heat transfer coefficient is:

$$q = U_i A_i (T_o - T_i) = \frac{T_o - T_i}{\sum R}$$

$$\text{Thus, } U_i = \frac{1}{A_i \sum R} = \frac{1}{0.141*0.0515} = 137.7 \text{ W/m}^2.\text{K}$$

Thus, heat transfer rate = $q = U_i A_i (T_o - T_i) = 137.7 * 0.141*45 = 873.7$ W = **0.87 kW**

Appendix F

Determination of the Flooding Point in RPB

In order to locate the flooding point of RPB in the Sherwood Plot, the following calculations should be carried out:

Determination of abscissa:

Liquid: 30wt% MEA solution

Flowrate of Liquid = L = 21.06 L/min

Density of 30wt% MEA solution = 1000 kg/m^3.

Molecular weight of 30wt% MEA solution = 48.1

$$\text{Thus, } L = 21.06\frac{L}{min}\frac{60\,min}{hr}\frac{1000\,kg}{m^3}\frac{m^3}{1000\,L} = 1263.62\frac{kg}{hr}$$

$$L = \frac{1263.62}{\text{molecular weight}} = \frac{1263.62}{48.1} = 26.27\frac{kmol}{hr}$$

Gas: Air is routed from the departmental compressed air.

Flowrate of Gas = G = 120 m^3/hr.

Density of air = 1.2 kg/m^3.

Molecular weight of air = 29 kmol / kg.

Atmospheric pressure = 749.025 mmHg.

Gauge pressure = 0.93 barg.

$$\text{Corrected air flowrate } (m^3/hr) = 120\frac{m^3}{hr}\left[\frac{\left[\left[0.93+\left(\frac{749.025}{760}\right)\right]\right]}{\left(\frac{749.025}{760}\right)}\right]^{0.5} = 167.1\,m^3/hr$$

$$\text{Corrected air flowrate} = 167.1\frac{m^3}{hr} * 1.2\frac{kg}{m^3} = 200.5\frac{kg}{hr} = 6.9\frac{kmol}{hr}$$

Therefore, the abscissa can be calculated as follows:

$$X = \frac{L}{G}\sqrt{\frac{\rho_G}{\rho_L}} = \frac{26.27}{6.9}\sqrt{\frac{1.2}{1000}} = 0.131617$$

Determination of ordinate

Packing density = a_p = 2132 m^2/m^3 (Refer to Appendix C).

Packing porosity = ε = 0.76 (Refer to Appendix C).

Inside diameter = d_i = 156 mm = 0.156 m.

Therefore, the hydraulic performance of packed bed =

$$\frac{\text{Packing density}}{(\text{Packing porosity})^3} = \frac{a_p}{\varepsilon^3} = \frac{2132}{0.76^3} = 4856.8\,\frac{m^2}{m^3}.$$

Rotational speed = 500 RPM.

$$\omega = \frac{RPM}{60} * 2\pi = 52.36\ s^{-1}.$$

$$\text{Area of packed bed} = 2\pi * r_i * \text{Axial Thickness} = 2 * \frac{0.156}{2} * 0.025 = 0.0123\ m^2$$

The flooding occurs in the eye of rotor.

$$\text{Thus, the flooding velocity} = \frac{\text{Air Flowrate}}{\text{Area of Packed Bed}} = \frac{167.1\,m^3}{3600\,hr}\frac{1}{0.0123\,m^2} = 3.79\ \text{m/s}.$$

The gravitational acceleration is defined as follows in RPB:

$$g = \left(\frac{d_i}{2}\right)\omega^2 = \left(\frac{0.156}{2}\right) * 52.36^2 = 213.8\,\frac{m}{s^2}.$$

The ordinate is defined as follows: $Y = \left(\frac{U_g^{\,2}}{g}\right)\left(\frac{.a_p}{\varepsilon^3}\right)\left(\frac{\rho_G}{\rho_L}\right)$

$$\text{Thus, } Y = \frac{3.79^2}{213.8} * 4856.8 * \left(\frac{1.2}{1000}\right) = 0.3911$$

Table F-1: Experimental Flooding Data

RPM	L (L/min.)	Corrected Q_g (m^3/hr)	Flooding Velocity U_g (m/s)	X	Y
300	16.26	101.0	2.29	0.168	0.397
400		167.1	3.79	0.102	0.611
500		214.9	4.87	0.079	0.647
300	21.06	93.2	2.11	0.236	0.338
400		136.2	3.09	0.161	0.406
500		167.1	3.79	0.132	0.391
600		202.2	4.58	0.108	0.398
700		318.5	7.22	0.069	0.725
300	39.34	25.3	0.57	1.625	0.025
400		71.7	1.63	0.573	0.113
500		117.8	2.67	0.349	0.194
600		156.3	3.54	0.263	0.238
700		190.0	4.31	0.216	0.258
800		241.9	5.48	0.169	0.320
400	50.3	30.5	0.69	1.722	0.020
500		71.7	1.63	0.732	0.072
600		126.8	2.87	0.414	0.156
700		156.3	3.54	0.336	0.175
800		190.0	4.31	0.276	0.197

Effective Wetted Area of the Packing (Onda's Method)

Onda's equation (Sinnott, 1993) for effective wetted area of packing is:

$$\frac{a_w}{a} = 1 - \exp\left[-1.45\left(\frac{\sigma_c}{\sigma_L}\right)^{0.75}\left(\frac{L^*_w}{a\,\mu_L}\right)^{0.1}\left(\frac{L^{*2}_w\,a}{\rho^2_L\,g}\right)^{-0.05}\left(\frac{L^{*2}_w}{\rho_L\mu_L\,a}\right)^{0.2}\right]$$

where:

a_w = effective interfacial area of packing per unit volume, m^2/m^3

a = actual area of packing per unit volume = 2132 m^2/m^3

σ_c = critical surface tension for steel = $75*10^{-3}$ N/m.

σ_L = 30 wt% Ethanolamine solution surface tension = $65.3*10^{-3}$ N/m.

μ_L = 30 wt% Ethanolamine solution viscosity = $2.5*10^{-3}$ N.s/m^2.

ρ_L = 30 wt% Ethanolamine solution density = 1000 kg/m^3.

g = Acceleration due to gravity = $\omega^2.r_i$

Rotor Speed = 1000 RPM = 104.7 rad./s

Bed radius = 78 mm.

Thus, $g = \omega^2.r = (104.7)^2 * \left(\frac{78}{1000}\right) = 855.4\ m/s^2$

Maximum liquid volumetric flowrate = 50 L/min.

$$\text{Liquid mass flowrate} = 50\frac{L}{min} * \frac{min}{60\,sec} * \frac{1m^3}{1000L} * 1000\frac{kg}{m^3} = 0.83\frac{kg}{s}$$

r = radius = 78 mm.

Bed thickness = Δ = 0.025 m.

$$\text{Cross sectional area} = 2\pi.r.\Delta = \pi(2*0.078)*0.025 = 0.0123\ m^2$$

L^*_w = Liquid mass flowrate per unit cross-sectional area = $\frac{0.83}{0.0123} = 67.5\ kg/m^2/s$.

Applying the above equation = $\frac{a_w}{a} = 0.73$

Thus, a_w = 1556 m^2/m^3.

Appendix G

Calibration of the Ethanolamine Solution

Measurement of S.G. of MEA: @ 22.5°C (Room temperature).

Weight of 50 ml flask = 31.7665 g.

Weight of flask + distilled water = 82.2913 g.

Weight of flask + MEA solution = 86.0171 g.

Weight of water = 50.5206 g.

Weight of MEA = 54.2506 g.

Thus, S.G. of 30 wt.% MEA = 54.2506 / 50.5206 = 1.073742.

The quoted literature value of SG_4^{20} is 1.014. Thus, the error is 5.6%, which can be mainly attributed to difference in base water temperature.

Determination of Amine Strength by Weight

30 wt% MEA/water solution was prepared by weighing in 500 ml flask using PM4800 DeltaRange balance (± 0.02g).

An example is given:

Weight of water = 49.54 g.

Weight of MEA = 21.20 g.

Thus, % wt MEA = 30%

Weight of pure CO_2 injected = 2.94 g.

Thus, %CO_2 = 3.99, %MEA = 28.77, % water = 67.23.

mol CO_2 / mol MEA = (2.94/44) / (21.20/61.09) = 0.193

Determination of Amine Strength by Titration

A titrimetric method was applied in order to determine strength of amine solution. A 1 ml sample was measured with a 1 ml syringe and placed into a flask then few drops of bromophenol blue indicator were added in order to get an observable physical

change in appearance from blue to white when 0.1 M HCl was added from 50 mL burette. The pH change was from 4.5 to 5.0 (Skoog et al., 1992).

$$\text{Amine concentration \%} = \frac{(\text{ml of HCl})\,(\text{Molarity of HCl})\,(\text{milliequivalent weight of Amine})}{(\text{sample size in ml})\,(\text{S.G. of approx. amine})}$$

Milliequivalent weight of: MEA is 0.061, DEA is 0.105, MDEA is 0.119, and DIPA is 0.133.

Comparison between Determination of Amine Strength by Weight and Titration.

Table G-1: Comparison between weight technique and titration to calculate MEA strength.

Exp.	MEA wt %	CO_2 wt %	$\frac{\text{mol } CO_2}{\text{mol MEA}}$	MEA Strength by titration	% error in MEA determination
1	29.81	0.65	0.030	29.69	0.4
2	29.34	1.15	0.054	27.60	5.93
3	29.62	1.22	0.057	29.08	1.82
4	29.60	1.38	0.065	30.86	-4.26
5	29.39	2.08	0.098	29.94	-1.87
6	29.23	2.57	0.123	31.01	-6.09
7	29.09	3.01	0.144	27.30	6.15
8	29.97	3.89	0.180	31.21	-4.14
9	28.77	3.99	0.193	29.23	-1.60
10	29.44	5.30	0.259	26.4	7.03
11	28.29	5.68	0.279	26.4	6.68
12	27.95	6.85	0.340	28.69	-2.65
14	27.78	7.43	0.370	28.15	-1.33
Average	**29.02**			**28.89**	**3.56**

The average error between titration and weight experiments is 3.56%. For calibration purpose, the set of data obtained by weight experiments will be supplied to the gas chromatograph software.

Preparing a Calibration Chart

The concentrations of aqueous ethanolamine solutions used in this research are: 30, 50, 80, and 100wt%. Hence, four calibration charts were prepared and then used according to the solution strength in operation.

The procedure of calibration is as follows: Different concentrations of carbon dioxide in ethanolamine solution were prepared. Then, 0.2 μL sample was injected into the liquid port in the gas chromatograph via a syringe. The sensitivity of the FID was set to LOW and METHOD 3 was used to store the calibration file.

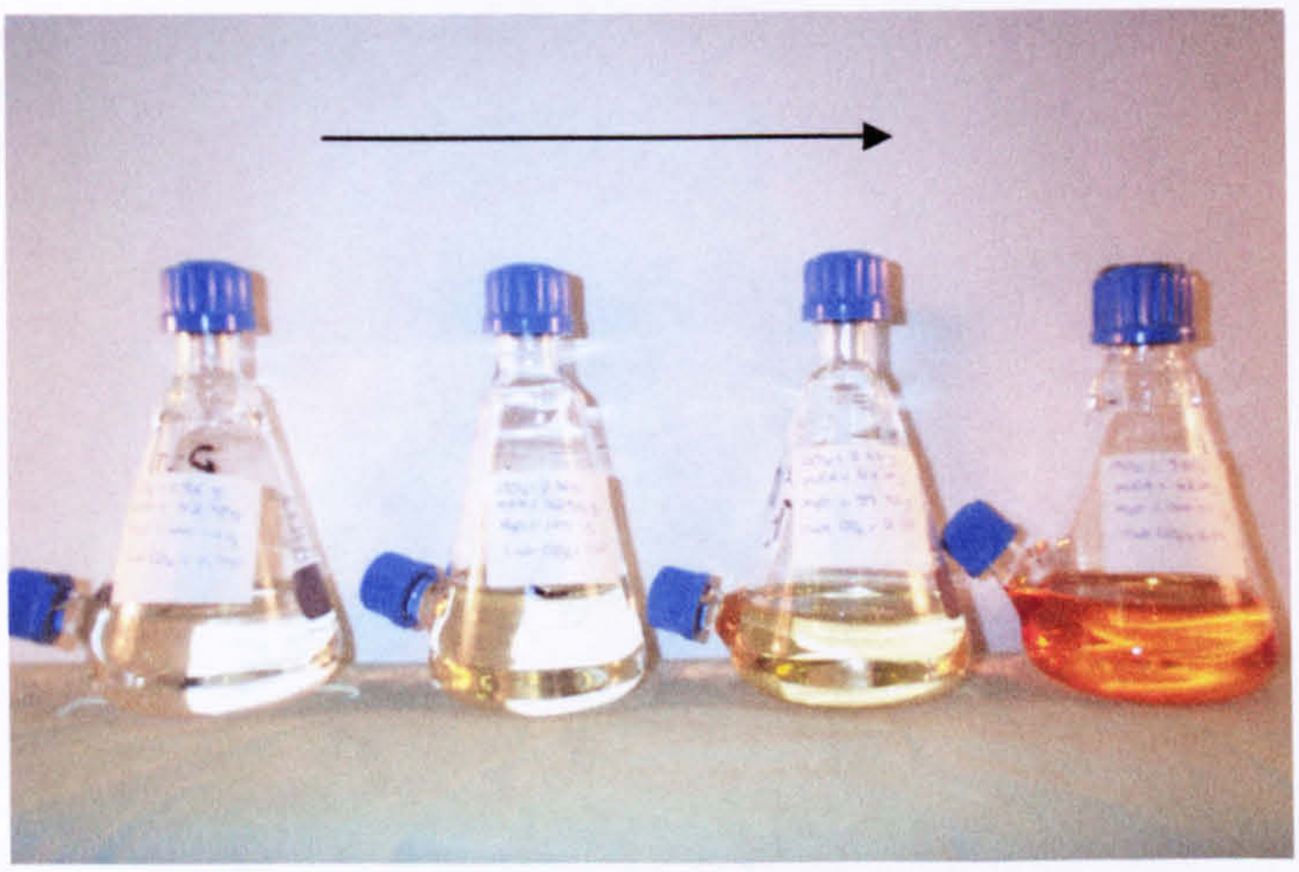

Figure G-1: The increase in CO_2 concentration in 30wt% MEA solution leads to colour change.

The peak areas of carbon dioxide and ethanolamine were then plotted against its corresponding concentrations and hence a calibration chart was feasible.

For example: The calibration chart for 30wt% MEA solution is:

(a) Linear equation for absorbed carbon dioxide and forcing line through origin:

Area = 9.196726 Concentration

Coefficient of determination = 0.99431

Retention time = 4.188 min.

(b) Linear equation for MEA and forcing line through origin:

Area = 6.008881 Concentration.

Coefficient of determination = 0.95194

Retention time = 7.655 min.

Appendix H

Calibration of Carbon Dioxide/ Air

This section outlines the experimental procedure necessary to prepare CO_2/air sampling standards. The samples were then analysed by the gas chromatograph, which generates an invariable peak area for a specific CO_2/air mixture.

Experimental Procedure

The following steps are used to prepare a calibration gas sample:

A glass cylinder is purged with compressed air for 5 minutes at moderate flowrate as shown in Figure A.

Flow of compressed air is stopped then the inlet and the outlet valves are closed and hence the air at atmospheric pressure occupies the cylinder.

Pure CO_2 is injected into the cylinder via a 1 mL syringe as shown in Figure B. The cylinder is then shaken for 10 minutes with the aid of small glass balls in order to enhance the mixing.

A well-mixed sample is taken with a 10 mL syringe in order to be analysed by the gas chromatograph.

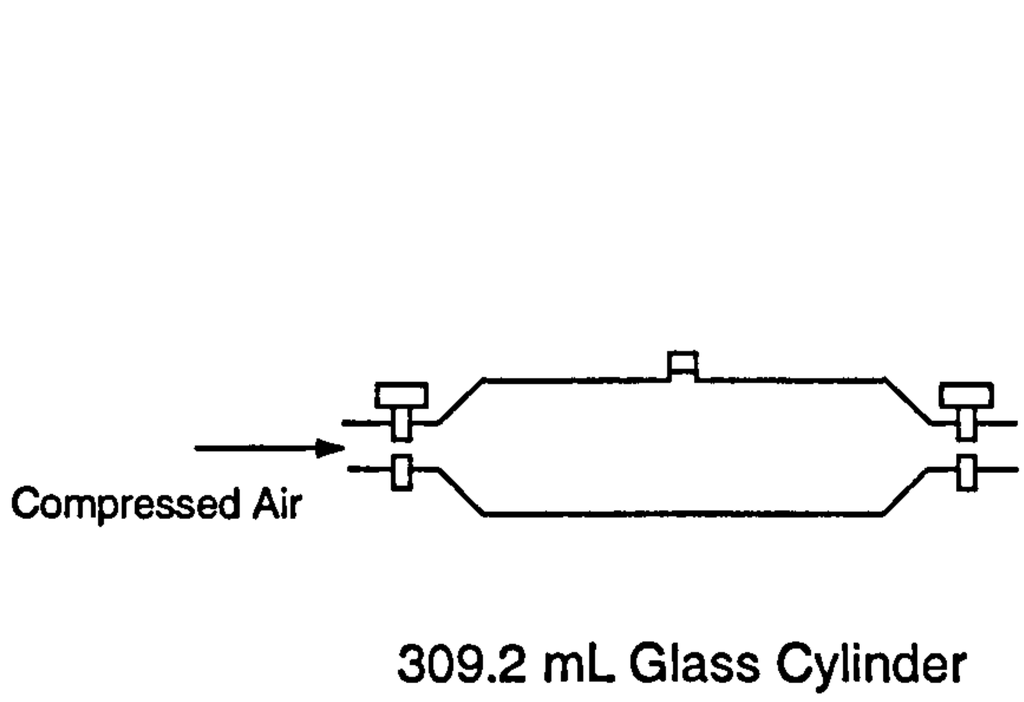

Figure A

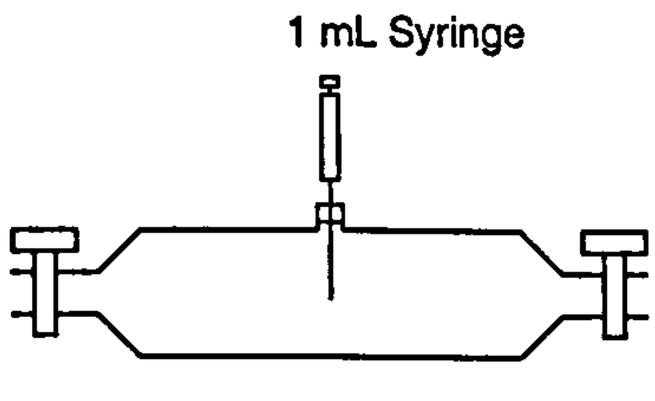

Figure B

Figure H-1: Procedure for Gas Calibration.

Determination of Cylinder Volume

Weight of cylinder = 179.38 g.

Weight of cylinder and water = 486.73 g.

Thus, weight of water = 308.35 g.

Temperature of water = 24.5°C.

Density of water @ 24.5C = 997.172 kg/m3. (Perry and Green, 1984)

Thus, volume of cylinder = $\frac{308.35}{0.997172} = 309.2245$ mL.

Determination of Air/CO_2 Composition

Volume of cylinder = 309.2245 ml.

Typical composition of CO_2 in air = 0.03 vol% (300 ppmv).

Thus, amount of initial CO_2 inside the cylinder = 0.0003 * 309.2245 = 0.09276 mL.

CO_2 introduced by the syringe = 1 mL.

Thus, total CO_2 = 1 + 0.09276 = 1.09276 mL.

$$\text{ppmv } CO_2 = \frac{\text{quantity of component}}{\text{total quantity}} * 10^6 = \frac{1.09276}{309.2245 + 1} * 10^6 = 3522.48$$

Similarly, two other amounts of CO_2/air mixtures were prepared and analysed by the gas chromatograph, which produced specific peak area for each concentration. Therefore, three levels of concentrations were used to calibrate carbon dioxide peak as shown in the print out of gas calibration file. The linear regression of the calibration data was good with 0.99817 coefficient of determination.

Appendix I

Gas Chromatography Calibration Charts

The following calibration charts were prepared:

Gas Phase: Calibration charts for absorption runs (low CO_2%) and desorption runs (high CO_2%):

I-1: Low concentration of CO_2 in air.

I-2: High concentration of CO_2 in air.

Liquid Phase: Calibration charts were prepared for different amine strengths for CO_2-MEA-H_2O system:

I-3: 100 wt%.

I-4: 80 wt%.

I-5: 50 wt%.

I-6: 30 wt%

TEXT BOUND INTO THE SPINE

Calibration | Calibration File | 13:08 Tue Feb 19 2002 | I-1

METHOD2 | Last changed 12:51 Mon Jun 19 2000

RF Calc Method :
Polynomial order 1, forcing line through origin

Peak : **Carbon Dioxide**
RT(Mins) : 4.207
Area = 0.000000 * C^2 + 0.120868 * C + 0.000000
Residual Std Dev : 5.057
Residual Mean : -0.073
Coefficient of Determination : 0.99817

	Use	Area	Samples	Max	Min	Conc	Residual
	Y	42.929	1	-	-	352.2480	0.353
	Y	42.996	1	-	-	352.2480	0.420
	Y	44.353	1	-	-	352.2480	1.777
	Y	42.769	1	-	-	352.2480	0.193
	Y	43.456	1	-	-	352.2480	0.880
	Y	190.090	1	-	-	1620.739	-5.807
	Y	190.959	1	-	-	1620.739	-4.938
	Y	196.348	1	-	-	1620.739	0.451
	Y	194.854	1	-	-	1620.739	-1.043
10	Y	195.452	1	-	-	1620.739	-0.445
11	Y	320.393	1	-	-	2551.114	12.043
12	Y	314.095	1	-	-	2551.114	5.745
13	Y	311.834	1	-	-	2551.114	3.483
14	Y	304.926	1	-	-	2551.114	-3.424
15	Y	297.488	1	-	-	2551.114	-10.862

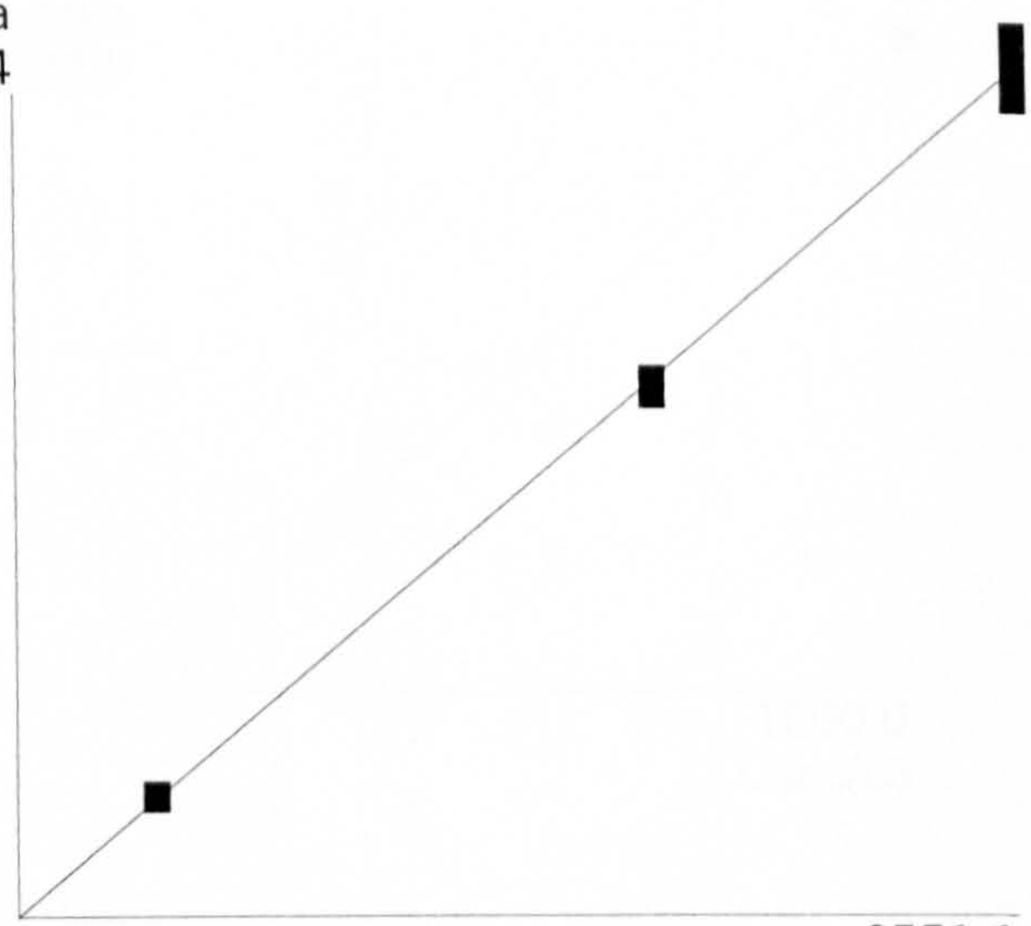

Peak : **MEA**
RT(Mins) : 7.025
Area = 0.000000 * C^2 + 0.109602 * C + 0.000000

ADDED PEAK

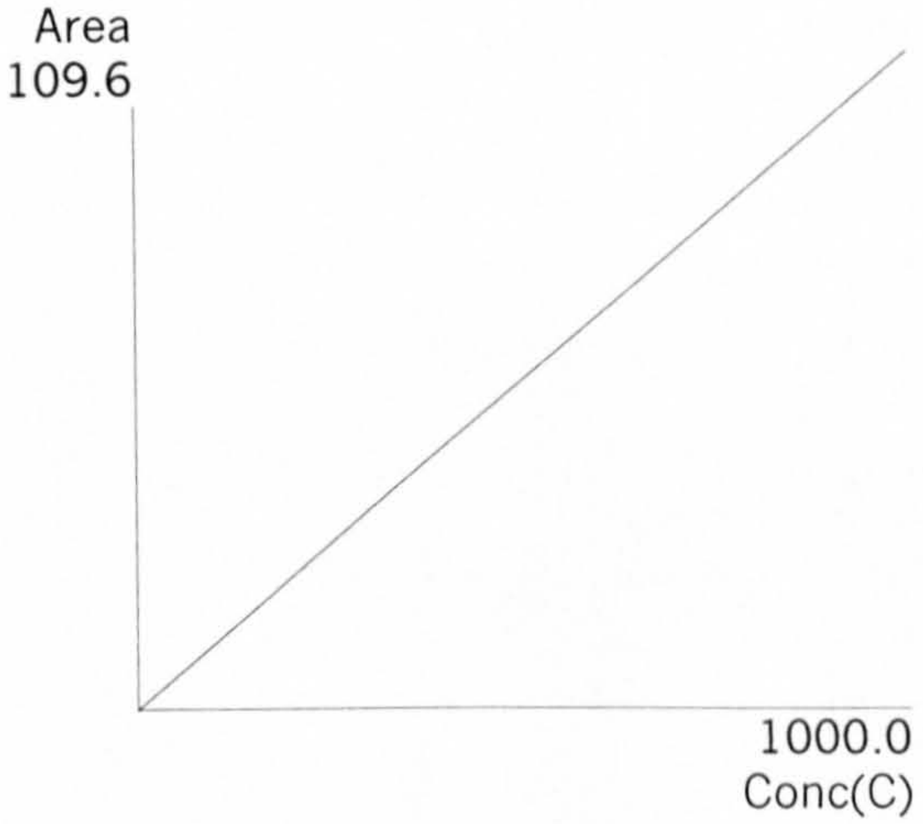

Calibration | Calibration File | 13:11 Tue Feb 19 2002 | I-2

METHOD2 | Last changed 13:07 Tue Jan 30 2001

RF Calc Method :
Polynomial order 1, forcing line through origin

Peak : **Carbon Dioxide**
RT(Mins) : 4.042
Area = $0.000000 * C^2 + 1.232046 * C + 0.000000$
Residual Std Dev : 0.000
Residual Mean : 0.000
Coefficient of Determination : 1.00000

	Use	Area	Samples	Max	Min	Conc	Residual
1	Y	1232.046	2	1235.172	1228.920	1000.000	0.000

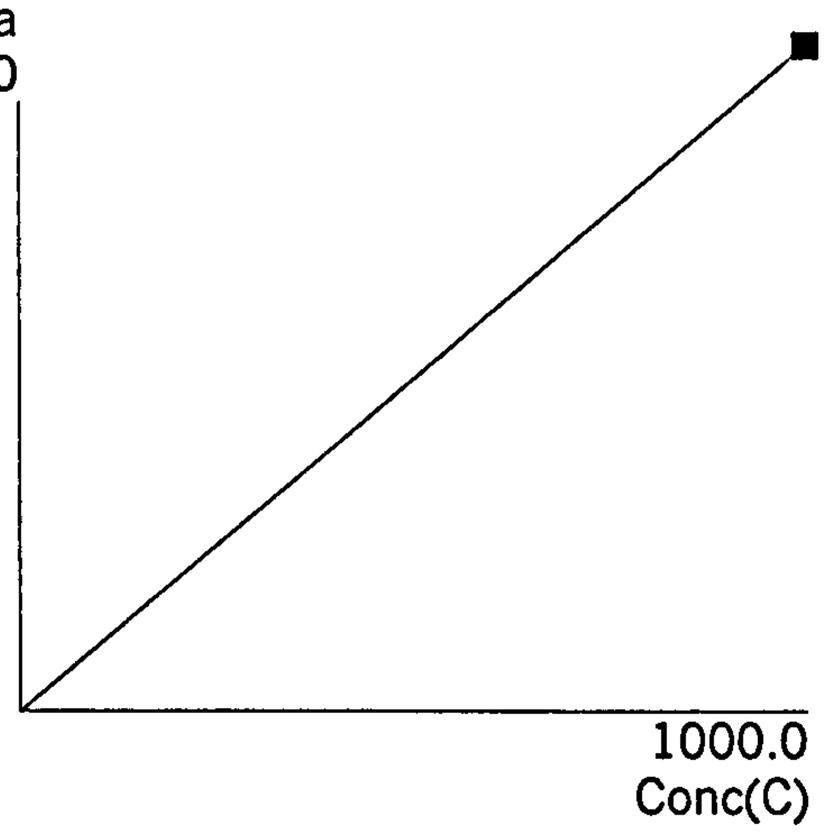

Calibration | Calibration File | 13:14 Tue Feb 19 2002 | I-3

METHOD3 | Last changed 16:27 Thu Mar 08 2001

RF Calc Method :
Polynomial order 1, forcing line through origin

Peak : **Carbon Dioxide**
RT(Mins) : 4.005
Area = 0.000000 * C^2 + 10.18371 * C + 0.000000
Residual Std Dev : 2.480
Residual Mean : -0.650
Coefficient of Determination : 0.99400

	Use	Area	Samples	Max	Min	Conc	Residual
1	Y	68.248	6	71.736	65.715	6.560123	1.441
2	Y	25.012	5	25.384	24.670	2.788951	-3.390

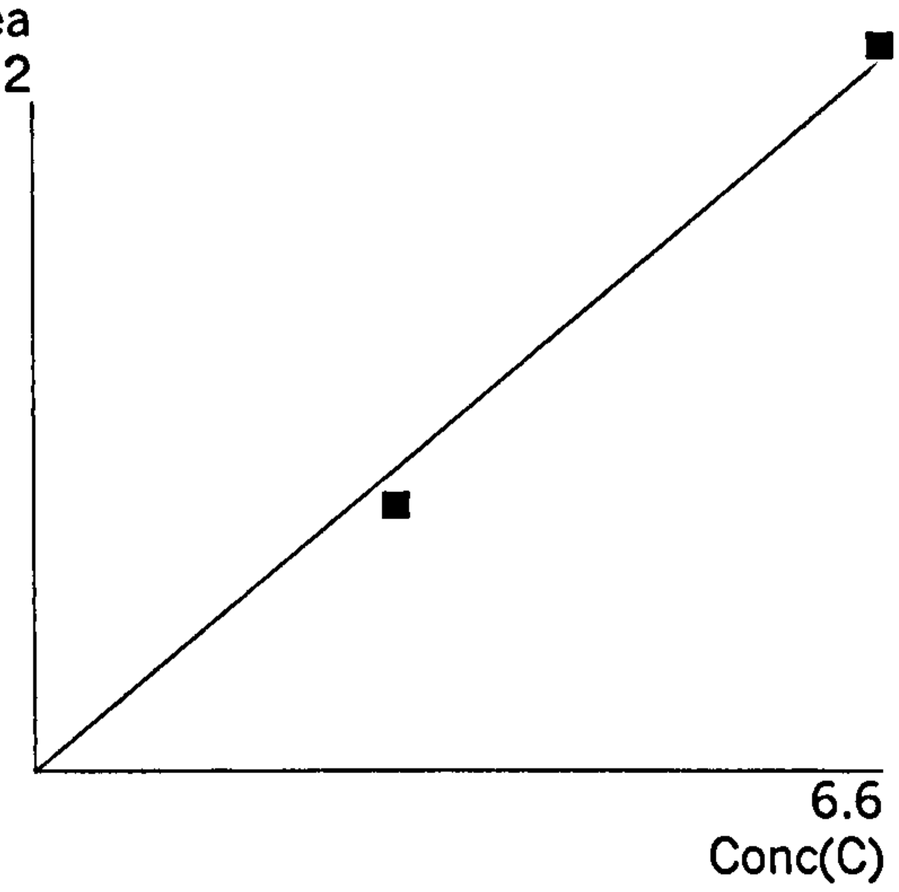

Peak : **MEA**
RT(Mins) : 7.031
Area = 0.000000 * C^2 + 7.798319 * C + 0.000000
Residual Std Dev : 2.407
Residual Mean : 0.000
Coefficient of Determination : 0.99997

	Use	Area	Samples	Max	Min	Conc	Residual
1	Y	774.440	6	783.433	765.603	99.00000	2.407
2	Y	769.627	5	774.744	765.329	99.00000	-2.407

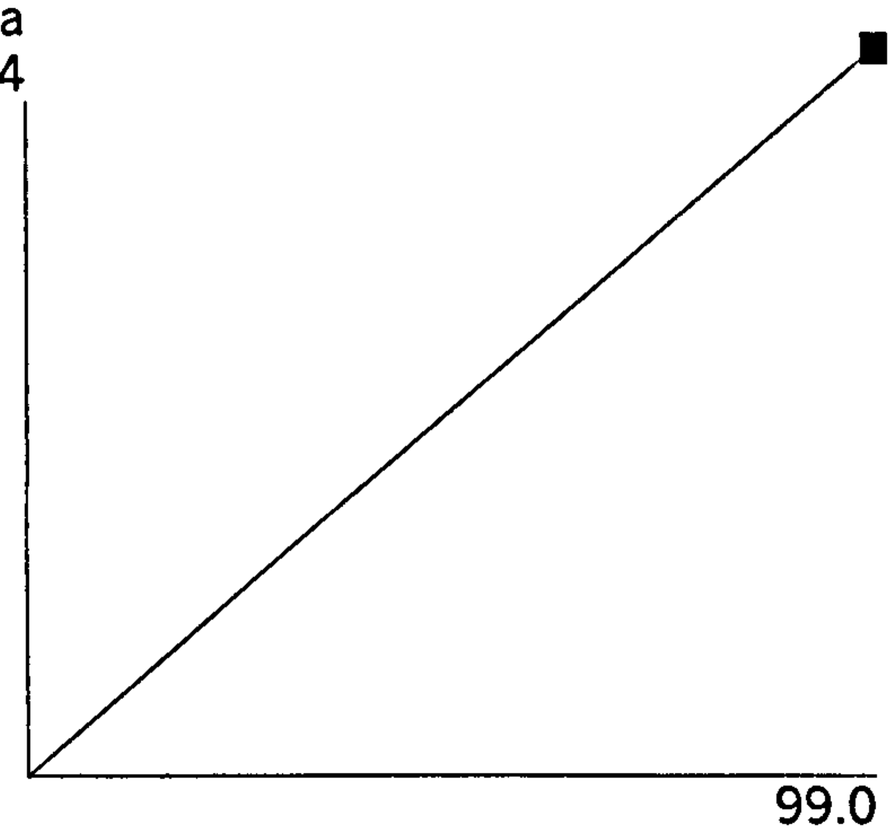

Calibration | Calibration File | 13:17 Tue Feb 19 2002 | I-4

METHOD3 | Last changed 10:27 Tue May 15 2001

RF Calc Method :
Polynomial order 1, forcing line through origin

Peak : **Carbon Dioxide**
RT(Mins) : 3.986
Area = 0.000000 * C^2 + 11.44648 * C + 0.000000
Residual Std Dev : 0.276
Residual Mean : 0.029
Coefficient of Determination : 0.99985

Use	Area	Samples	Max	Min	Conc	Residual
Y	31.924	8	34.616	28.712	2.761140	0.318
Y	43.225	6	45.655	40.696	3.796495	-0.231

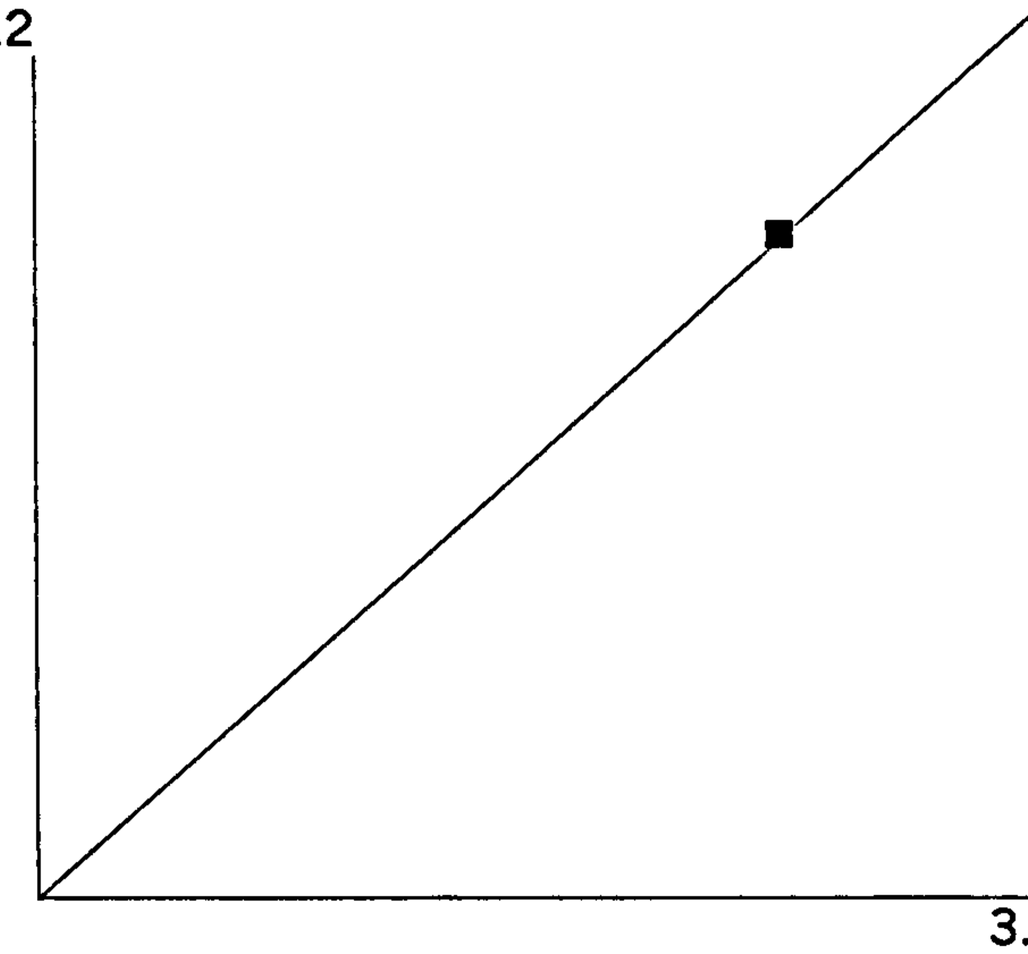

Peak : **MEA**
RT(Mins) : 6.479
Area = 0.000000 * C^2 + 8.086693 * C + 0.000000
Residual Std Dev : 0.126
Residual Mean : -2.5E-14
Coefficient of Determination : 1.00000

Use	Area	Samples	Max	Min	Conc	Residual
Y	647.062	8	660.380	637.881	80.00000	0.126
Y	646.809	6	652.332	636.097	80.00000	-0.126

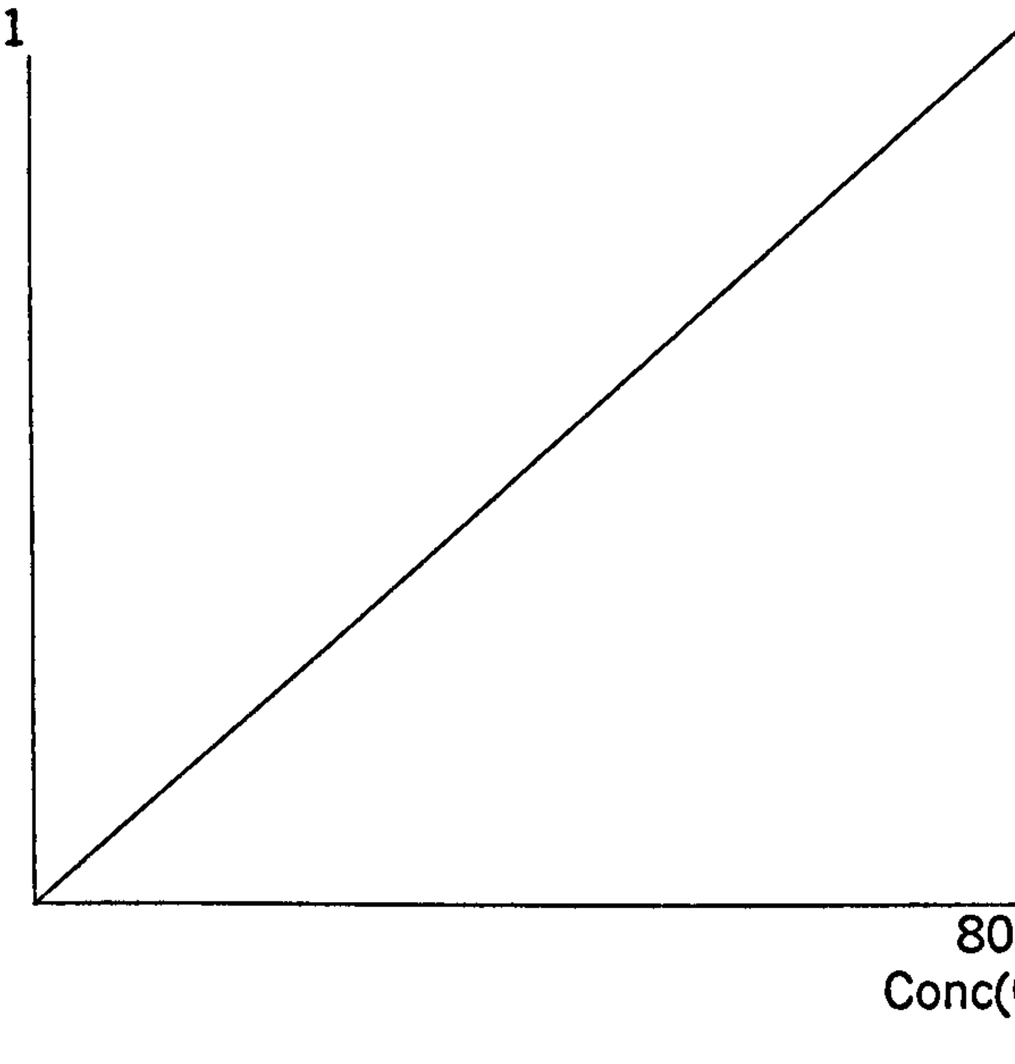

Calibration | Calibration File | 13:19 Tue Feb 19 2002 | 1-5

METHOD3 | Last changed 18:59 Tue May 29 2001

RF Calc Method :
Polynomial order 1, forcing line through origin

Peak : **Carbon Dioxide**
RT(Mins) : 3.970
Area = 0.000000 * C^2 + 7.756038 * C + 0.000000
Residual Std Dev : 0.347
Residual Mean : -0.036
Coefficient of Determination : 0.99917

	Use	Area	Samples	Max	Min	Conc	Residual
1	Y	16.742	4	17.804	15.727	2.210053	-0.399
2	Y	23.686	4	24.367	23.298	3.016196	0.292

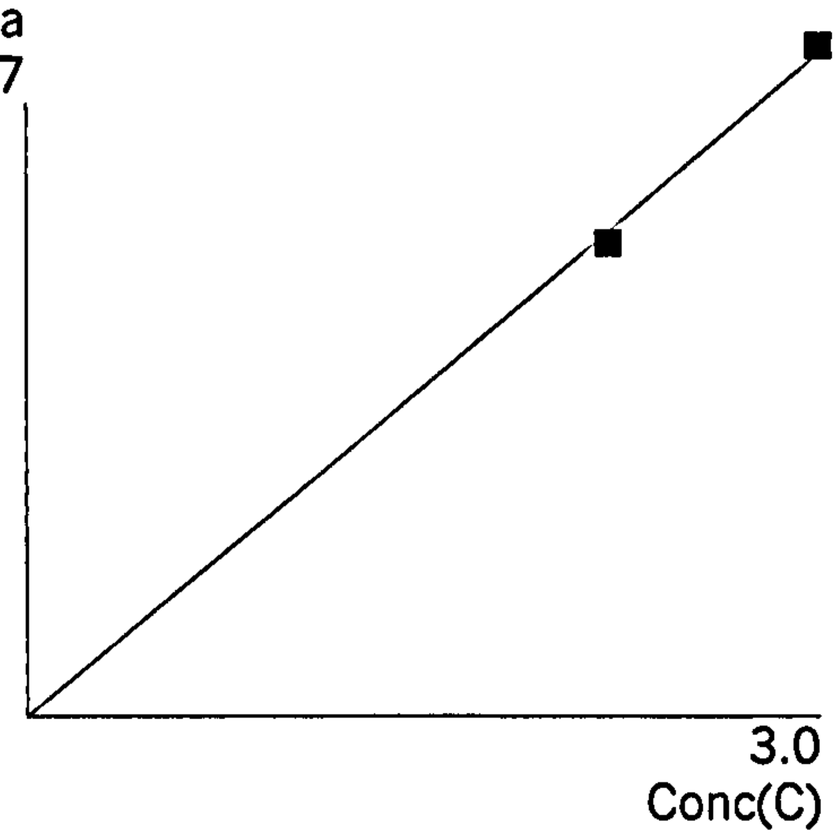

Peak : **MEA**
RT(Mins) : 6.011
Area = 0.000000 * C^2 + 7.407646 * C + 0.000000
Residual Std Dev : 13.039
Residual Mean : 0.000
Coefficient of Determination : 0.99630

	Use	Area	Samples	Max	Min	Conc	Residual
1	Y	357.343	4	387.014	334.647	50.00000	-13.039
2	Y	383.421	4	390.513	377.188	50.00000	13.039

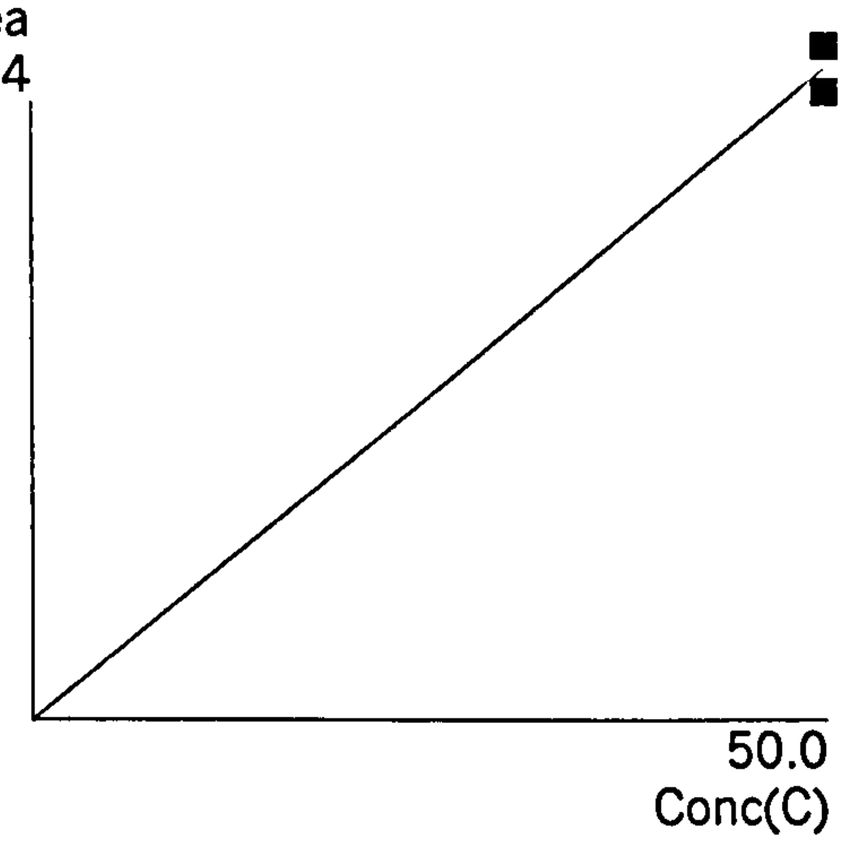

---

alibration | Calibration File | 13:21 Tue Feb 19 2002 | Σ-6(A)

METHOD3 | Last changed 13:08 Mon Jan 22 2001

F Calc Method :
olynomial order 1, forcing line through origin

eak : **Carbon Dioxide**
T(Mins) : 4.004
rea = 0.000000 * C^2 + 83.09149 * C + 0.000000
esidual Std Dev : 6.855
esidual Mean : -2.337
oefficient of Determination : 0.99861

Use	Area	Samples	Max	Min	Conc	Residual
Y	121.582	6	124.837	118.154	1.623555	-13.322
Y	209.309	6	215.536	199.677	2.481593	3.110
Y	73.789	7	76.743	71.306	0.941176	-4.414
Y	513.291	12	546.654	390.429	6.142022	2.941

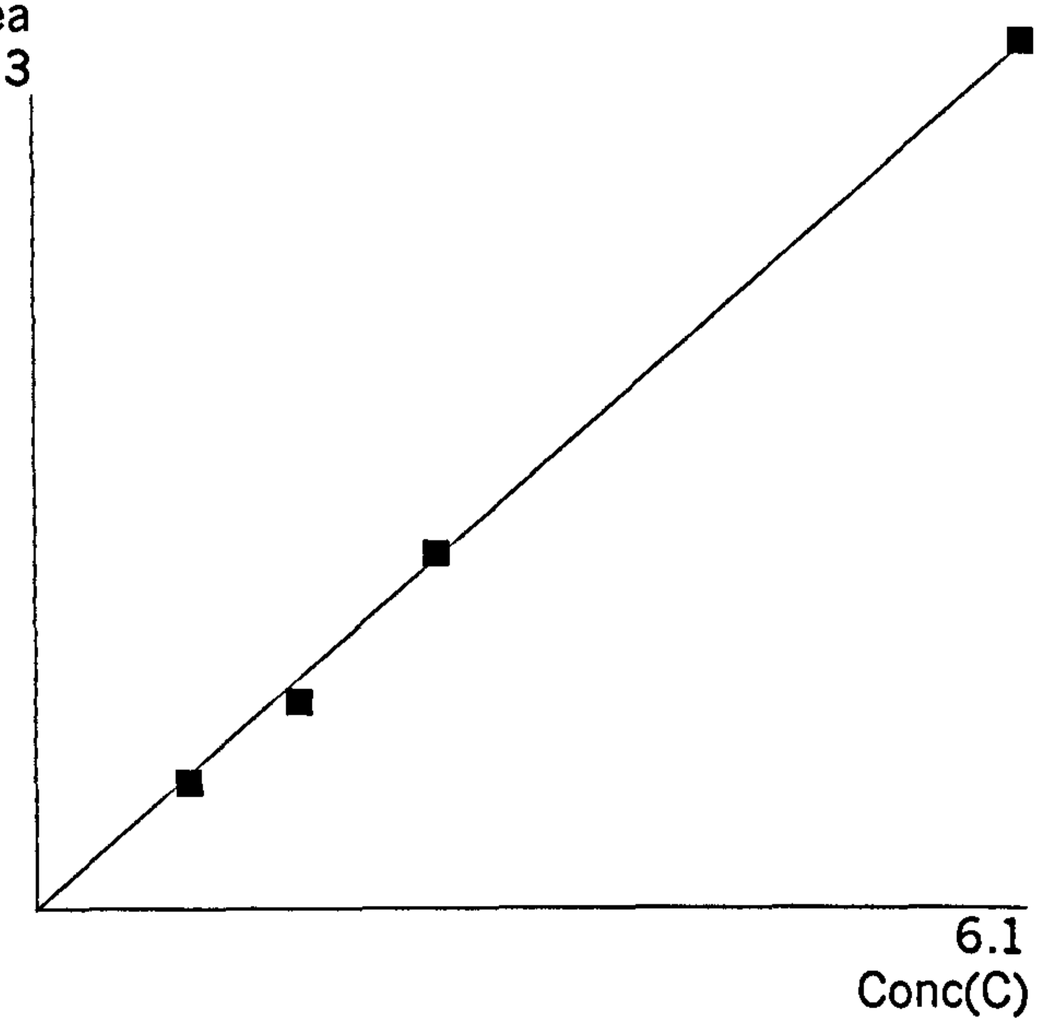

alibration | Calibration File | 13:21 Tue Feb 19 2002 | I-6 (B)

METHOD3 | Last changed 13:08 Mon Jan 22 2001

F Calc Method :
olynomial order 1, forcing line through origin

eak : **MEA**
T(Mins) : 6.594
rea = 0.000000 * C^2 + 71.04056 * C + 0.000000 Area
esidual Std Dev : 25.683 2103.6
esidual Mean : 0.355
oefficient of Determination : 0.99924

Use	Area	Samples	Max	Min	Conc	Residual
Y	2068.609	6	2121.106	2033.098	29.51293	-28.006
Y	2103.573	6	2142.083	2056.034	29.35642	18.076
Y	2091.864	7	2117.634	2068.649	29.74394	-21.162
Y	2032.997	12	2143.443	1552.946	28.15477	32.867

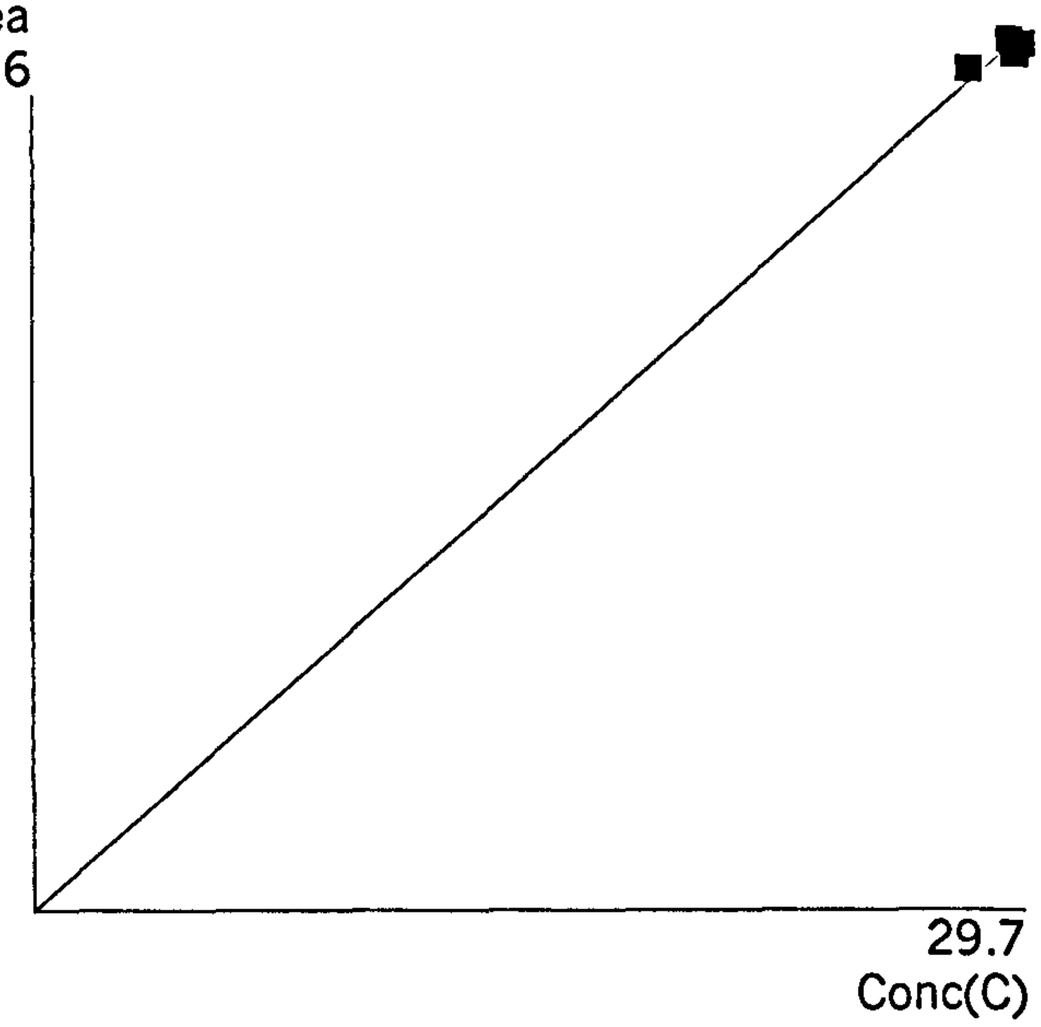

Appendix J

Literature Solubility Data

Table J-1: (Mason and Dodge, 1936) Solubility Data.

MEA Concentration % wt.	Temperature (°C)	Partial Pressure CO_2 (kPa)	mol. CO_2/mol MEA
30	25	99.02	0.657
		33.97	0.601
		13.15	0.563
		5.94	0.539
		1.41	0.507
	50	90.23	0.574
		32.69	0.527
		9.58	0.525
		9.53	0.505
		1.38	0.453
	75	69.06	0.493
		19.00	0.460
		7.30	0.418
56	25	98.08	0.588
		33.61	0.554
		13.19	0.532
		5.97	0.519
		1.48	0.495
	50	93.47	0.538
		34.03	0.522
		9.90	0.492
		1.43	0.443
	75	74.60	0.468
		20.41	0.458
		7.56	0.424

MEA Concentration % wt.	Temperature (°C)	Partial Pressure CO_2 (kPa)	mol. CO_2/mol MEA
74	25	99.85	0.548
		34.16	0.518
		6.05	0.521
	50	95.46	0.525
		94.59	0.525
		34.58	0.501
		26.12	0.495
		10.07	0.483
		10.06	0.503
		10.05	0.496
		10.05	0.508
		1.45	0.467
	75	83.96	0.479
		22.40	0.453
		8.56	0.395

Table J-2: (Jou et al., 1995)Solubility Data.

MEA Concentration % wt.	Temperature (°C)	Partial Pressure CO_2 (kPa)	mol. CO_2/mol MEA
30	25	97.2	0.694
		55.1	0.648
		11.8	0.583
		2.80	0.540
		0.392	0.494
		0.0600	0.439
		0.00927	0.323
		0.00213	0.211
40		103	0.646
		36.1	0.609
		8.09	0.557
		2.57	0.513
		0.604	0.461
		0.0677	0.365
		0.00896	0.203
		0.00147	0.0888

MEA Concentration % wt.	Temperature (°C)	Partial Pressure CO_2 (kPa)	mol. CO_2/mol MEA
30	60	82.0	0.527
		34.1	0.565
		11.0	0.504
		2.01	0.438
		0.528	0.389
		0.0579	0.206
		0.0193	0.119
		0.00428	0.0564
	80	56.0	0.517
		16.0	0.460
		2.67	0.348
		0.278	0.187
		0.0992	0.118
		0.0465	0.0781
		0.00484	0.0236
		0.00296	0.0174
	100	109.0	0.481
		69.0	0.477
		39.0	0.422
		19.0	0.381
		1.43	0.188
		0.136	0.0566
		0.00724	0.0117

Appendix K

Experimental Solubility Results

Table K-1: Experimental Solubility Data.

Temperature (°C)	Partial Pressure CO_2 (kPa)	Average Partial Pressure CO_2 (kPa)	Loading $\frac{\text{mol } CO_2}{\text{mol MEA}}$	Average Loading $\frac{\text{mol } CO_2}{\text{mol MEA}}$	Deviation from (Jou et al., 1995) data, %
25	0.006901 0.006130 0.006295	0.006442	0.2092 0.2100 0.2134	0.2109	66.54
	0.007404	0.007404	0.2345	0.2345	50.55
	0.007849	0.007849	0.2360	0.2360	52.13
	0.01198 0.01266	0.012319	0.2526	0.2526	60.90
	0.011148	0.011148	0.2557 0.2514 0.2515	0.2528	56.68
	0.020902	0.020902	0.2842 0.2858	0.2850	67.07
	0.022159	0.022159	0.2853	0.2853	68.85
	Average deviation				60.38
40	0.020717 0.021759	0.021239	0.2097 0.2113	0.2105	44.78
	0.039907 0.039672	0.039789	0.2531 0.2515	0.2523	32.43
	0.099898 0.114349 0.110576	0.093658	0.2991 0.2977	0.2946	54.92

Temperature (°C)	Partial Pressure CO_2 (kPa)	Average Partial Pressure CO_2 (kPa)	Loading $\frac{\text{mol } CO_2}{\text{mol MEA}}$	Average Loading $\frac{\text{mol } CO_2}{\text{mol MEA}}$	Deviation from (Jou et al., 1995) data, %
40	0.097163	0.108274	0.2910	0.2984	59.73
	0.087986		0.2917		
	0.095826		0.3010		
	Average deviation				47.96
60	0.131752	0.139170	0.2207	0.2209	30.89
	0.144210		0.2212		
	0.141548				
	0.334923	0.341922	0.2600	0.2597	42.72
	0.348922		0.2595		
	0.588104	0.630519	0.2945	0.2933	55.25
	0.644472		0.2922		
	0.658980				
	Average deviation				42.95
80	0.664316	0.6506553	0.2010	0.2036	19.37
	0.641920		0.2063		
	0.645730				
	0.805934	0.8103565	0.2141	0.2146	15.09
	0.814779		0.2151		
	2.101058	2.1048705	0.2687	0.2664	30.74
	2.108683		0.2640		
	2.360338	2.3912560	0.2708	0.2718	35.68
	2.422174		0.2727		
	Average deviation				25.22

Table K-2: Linear relationships between 0.2-0.3 loading data for (Jou et al., 1995)

Temperature	CO_2 partial pressure = A (Loading) + B
25	A = 0.0638, B = - 0.0113
40	A = 0.3626, B = - 0.0646
60	A = 2.5689, B = - 0.4713
80	A = 14.857, B = - 2.5003

Appendix L

Dry Runs Results

A typical dry run calculations

RPM = 500

CO_2 flowrate

CO_2 flowmeter reading: 40 L/min.

CO_2 pressure gauge: 0.6 bar.

$$\text{Corrected } CO_2 \text{ flowrate} = 40\frac{L}{min.} * \left(\frac{0.6+1.013}{1.013}\right)^{0.5} = 50.5\frac{L}{min.}$$

Air flowrate

Air flowmeter reading: 110 m^3/hr = 1833.3 L/min.

CO_2 pressure gauge: 0.7 bar.

$$\text{Corrected air flowrate} = 1833.3\frac{L}{min.} * \left(\frac{0.7+1.013}{1.013}\right)^{0.5} = 2384\frac{L}{min.}$$

Theoretical CO_2 composition

$$\%\ CO_2 = \frac{50.5}{50.5+2384} * 100 = 2.073$$

Actual CO_2 composition

The Gas Chromatograph (GC|) recorded the inlet CO_2 = 2.065%.

% Error between GC and theory

$$\%\ \text{Error} = \frac{2.073-2.065}{2.073} * 100 = 0.4$$

Outlet CO_2 compositions

A) Composition of CO_2 at the 'eye' = 2.007

Error between the inlet and outlet CO_2 compositions = 2.8%

B) Composition of CO_2 at the 'periphery' = 2.029

Error between the inlet and outlet CO_2 compositions = 2.5%.

Table L1: Dry Runs Results

	RPM	CO2 Flowmeter (L/min)	CO2 Pressure Gauge (bar)	Air Flowmeter (m3/hr)	Air Pressure Gauge (bar)	Corrected CO2 Flowmeter (L/min)	Corrected air Flowmeter (m3/hr)	Theoretical CO2%	GC inlet (% vol)	% error	GC outlet (eye)	GC outlet (periphery)	% error
1	0	40	0.6	110	0.8	50.5	147.2	2.016	1.911	5.2	1.966	0	-2.9
	0	40	0.6	110	0.7	50.5	143.0	2.073	1.942	6.3	0	2.022	-4.1
	500	40	0.6	110	0.7	50.5	143.0	2.073	1.978	4.6	1.558	0	21.2
	500	40	0.6	110	0.7	50.5	143.0	2.073	1.993	3.9	0	2.002	-0.5
	800	40	0.6	110	0.7	50.5	143.0	2.073	1.979	4.5	1.065	0	46.2
	800	40	0.6	110	0.7	50.5	143.0	2.073	1.944	6.2	0	2.034	-4.6
	1000	40	0.6	110	0.7	50.5	143.0	2.073	2.034	1.9	0.759	0	62.7
	1000	40	0.6	110	0.7	50.5	143.0	2.073	2.079	-0.3	0	1.735	16.5
2	0	40	0.6	110	0.7	50.5	143.0	2.073	2.031	2.0	2.032	0	0.0
	0	40	0.6	110	0.7	50.5	143.0	2.073	1.967	5.1	0	1.963	0.2
	500	40	0.6	110	0.7	50.5	143.0	2.073	2.065	0.4	2.007	0	2.8
	500	40	0.6	110	0.7	50.5	143.0	2.073	2.081	-0.4	0	2.029	2.5
	800	40	0.6	110	0.7	50.5	143.0	2.073	2.048	1.2	1.554	0	24.1
	800	40	0.6	110	0.7	50.5	143.0	2.073	1.971	4.9	0	1.965	0.3
	1000	40	0.6	110	0.7	50.5	143.0	2.073	2.1	-1.3	1.466	0	30.2
	1000	40	0.6	110	0.7	50.5	143.0	2.073	2.029	2.1	0	1.836	9.5
3	1000	40	0.6	110	0.7	50.5	143.0	2.073	2.071	0.1	0	2.089	-0.9
	1000	55	1.55	155	1.7	87.5	253.7	2.027	1.926	5.0	1.912	0	0.7

Appendix M

Typical Mass Balance Calculation

A typical mass balance calculation across the Higee is shown below for Run #4:

Rotor Speed = 1000 RPM.

SOUR GAS

A) Carbon Dioxide Flowrate

The flowrate of the fluid is proportional to the square root of its density in variable area meters (Coulson et al., 1993). In addition, the ideal gas law shows that the density is a function of its temperature and pressure. Hence, the flowmeters readings were corrected as shown:

Pressure of CO_2 stream = 0.6 barg.

Temperature of CO_2 stream = 19°C.

Reading of CO_2 flowmeter = 40 L/min.

Room Temperature = 22 °C.

$$\text{Corrected } CO_2 \text{ flowrate} = 40 * \left(\frac{0.6+1.013}{1.013}\right)^{0.5} \left(\frac{295}{292}\right)^{0.5} = 50.73 \text{ L/min.} = 3.04 \text{m}^3\text{/hr.}$$

B) Air Flowrate

Pressure of air stream = 0.75 barg.

Reading of air flowmeter = 110 m^3/hr.

Temperature of air stream = 20°C.

$$\text{Corrected air flowrate} = 110 * \left(\frac{0.75+1.013}{1.013}\right)^{0.5} \left(\frac{295}{293}\right)^{0.5} = 145.9 \text{ m}^3\text{/hr.}$$

C) Combined Air/CO_2 mixture

Total Flowrate = 3.04 + 145.9 = 148.9 m^3/hr.

Temperature = 10 °C = 283 K.

Pressure = 2.5 psia = 118.52 kPa.

$$\text{Molar Flowrate @ STP} = \frac{273.15}{283} * \frac{118.52}{101.3} * \frac{148.9}{22.414} = 7.50 \text{ kmol / hr}$$

Measured concentration of CO_2 in the sour stream = 18294 ppmv = 1.8294 vol %.

$$\text{Calculated concentration of } CO_2 \text{ in the sour stream } = \frac{2.93}{139.5} * 100 = 2.08 \text{ vol\%}.$$

Thus, the error between the calculated and the measured carbon dioxide concentration is 12%.

SWEET GAS

Measured concentration of CO_2 in the sweet stream = 11140 ppmv = 1.114 vol%.

Therefore, the amount of carbon dioxide absorbed =

$$7.50 * \frac{(1.8294 - 1.114)}{100} = 0.054 \text{ kmol } CO_2 \text{ / hr } = 2.36 \text{ kg } CO_2 \text{ / hr.}$$

LEAN ETHANOLAMINE

MEA solution density = 1000 kg/m3.

Molecular weight, MEA = 61.

Molecular Weight, CO_2 = 44.

Flowrate of aqueous MEA Solution = 20.32 L/min. = 0.34 kg/s.

The lean ethanolamine sample was analysed by the gas chromatograph twice:

% wt., CO_2 = 2.277, 2.269

% wt., MEA = 31.773, 31.736

The loading of the solution could be computed as follows:

$$\alpha = \frac{(2.277/44)}{(31.773/61)} = 0.0994 \text{ mol } CO_2\text{/mol MEA}$$

The loading of the second sample is 0.0991 mol CO_2/mol MEA. Thus, the average loading is 0.0993 mol CO_2/mol MEA. Also, the average MEA concentration is 31.755 wt%.

$$\text{Mass rate of MEA} = \frac{31.755}{100} * 0.34 = 0.11 \text{ kg MEA/s}$$

$$\text{Molar rate of MEA} = \frac{0.11}{61} * 3600 = 6.34 \text{ kmol MEA/hr.}$$

RICH ETHANOLAMINE

There are two sampling points for rich ethanolamine:

The periphery where the concentration is likely to represent that of the exit solution from the rotor most accurately; and

The buffer tank where there will have been an opportunity for further mass transfer (end effect) in the machine enclosure.

Periphery

% wt, CO_2 = 2.400, 2.444

% wt, MEA = 31.354, 31.701

Similarly the loadings = 0.1061, 0.1069 mol CO_2/mol MEA.

The average loading = 0.1065.

$$\text{Thus, } \frac{\text{kmol CO}_2}{\text{hr}} = (\alpha_1 - \alpha_2) * \frac{\text{kmol MEA}}{\text{hr}} = (0.1065 - 0.0993) * 6.34 = 0.05$$

$$\frac{\text{kg CO}_2}{\text{hr}} = 0.05 * 44 = 2.02$$

Thus, % mass balance error using the periphery sample =

$$\frac{\left[\frac{\text{kg CO}_2}{\text{hr}}\right]_{liquid} - \left[\frac{\text{kg CO}_2}{\text{hr}}\right]_{gas}}{\left[\frac{\text{kg CO}_2}{\text{hr}}\right]_{gas}} * 100 = \frac{2.02 - 2.36}{2.36} * 100 = 14.4\%$$

Similarly, the % mass balance error using the buffer tank sample = 0.6%

Appendix N

Steam Desorption Runs

Mach Number

The Mach number (Ma) is defined as:

$$\text{Ma} = \frac{\text{Speed of gas}}{\text{Speed of sound}} = \frac{u}{c}$$

The speed of sound can be calculated as follows:

$$c = \sqrt{\gamma PV} = \sqrt{\frac{\gamma RT}{M}}$$

where γ is the ratio of the heat capacities = c_p/c_v = 1.2 (Steam Tables in Perry)

Thus, the speed of the sound = c = $\sqrt{\frac{1.2*8314*373.15}{18}}$ = 455 m/s

The diameter of the shaft is 33 mm. Thus, the cross sectional area = 8.55 cm^2.

The maximum steam flowrate = 0.1 kg/s = 0.167 m^3/s. (steam density = 0.6 kg/m^3)

Thus, the velocity of the gas = 0.167/ ($8.55*10^{-4}$)=**195.3** m/s.

Thus, Mach number = 195.3/455 = 0.43.

Pressure Drop Calculations

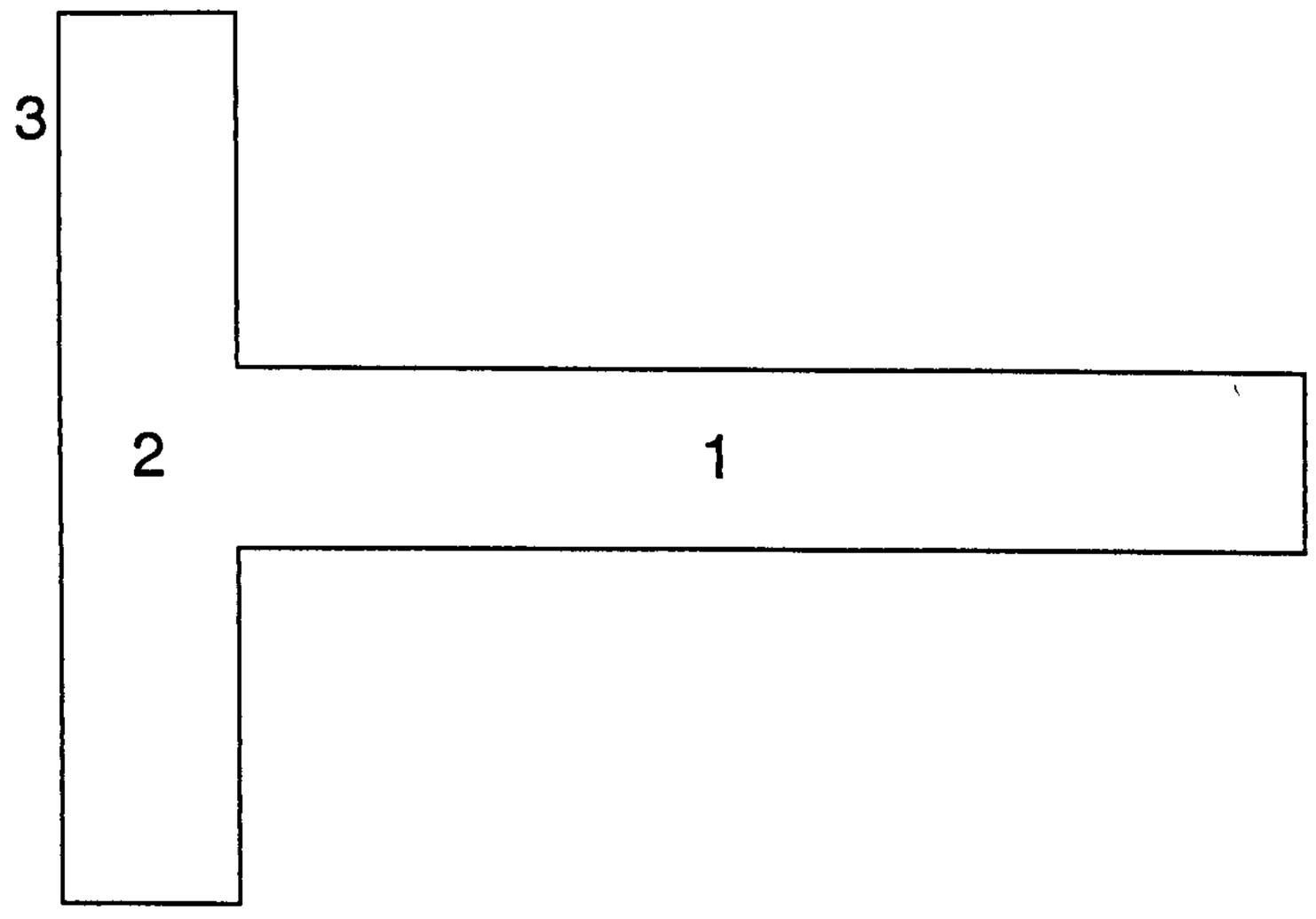

Figure N-1: Different flow compartments in the Higee

Figure N-1 shows different flow compartments in the Higee: (1) shaft, (2) gas plenum; and (3) holes in the stainless steel disc.

(1) Shaft

Diameter of the horizontal pipe = 33 mm = 0.033 m.

Length of the horizontal pipe = 305 mm = 0.305 m.

Cross sectional area = 8.55 cm^2.

Flowrate of steam = 0.1 kg/s = 0.167 m3/s.

Thus, the velocity = $0.167/(8.55*10^{-4})$=195.3 m/s.

Pressure drop = $0.5 \rho u^2 = 0.5*0.6*195.3^2 = 11.4$ kPa

(2) Gas Plenum

It comprises of two areas:

A)

Length = 20 mm.

Diameter = 455 mm.

Area = π D L = 0.028 m^2.

Velocity = 0.167 / 0.028 = 5.8 m/s.

Similarly, the pressure drop = 10.2 Pa.

B)

Length = 20 mm.

Diameter = 33 mm.

Area = π D L = 0.00207 m^2.

Velocity = 0.167 / 0.00207 = 80.4 m/s.

Similarly, the pressure drop = 1.9 kPa.

(3) Holes in the Stainless Steel Disc

For each hole:

Length = 12.5mm.

Diameter = 8 mm.

Area = π D L = 0.000314 m^2.

Number of holes = 72.

Thus, the total area = 0.02262 m^2.

Velocity = 0.167 / 0.02262 = 7.37 m/s.

Similarly, the pressure drop = 16.3 Pa.

Appendix O

Mass Balance Results

Table O-1: Results of Mass Balance Runs for MEA Solution(30 wt%)

	Lean MEA Solution											Rich MEA - Periphery							Rich MEA - Tank						
			Temperature (C)																						
Run	Flowrate, L/min	Flowrate, kg/s	Before Higee	After Higee	CO2, %wt/wt	MEA, %wt/wt	Average MEA, %wt/wt	α (kmol CO2/kmol MEA)	Average α	kg MEA/s	kmol MEA/hr	CO2, %wt/wt	MEA, %wt/wt	α (kmol CO2/kmol MEA)	Average α	kmol CO2 / hr	kg CO2/hr	%error	CO2, %wt/wt	MEA, %wt/wt	α (kmol CO2/kmol MEA)	Average α	kmol CO2 / hr	kg CO2/hr	%error
1	12.97	0.22	room temperature (20 C)		2.094, 2.053, 2.060	30.890, 31.414, 31.420	31	0.0940, 0.0906, 0.0909	0.0918	0.07	3.98	-	-	-	-	-	-	-	2..277, 2.257, 2.286	31.619, 31.484, 31.650	0.0998, 0.0994, 0.1001	0.0998	0.032	1.390	-47.6
2	12.41	0.21	room temperature (20 C)		2.188	30.942	31	0.0980	0.0980	0.06	3.77	2.301	30.34	0.1051	0.1051	0.03	1.18	-57.2	2.408	30.830	0.1083	0.1083	0.039	1.702	-38.3
3	18.29	0.30	room temperature (20 C)		2.276, 2.332, 2.321	30.628, 31.795, 32.05	31	0.1030, 0.1017, 0.1004	0.1017	0.10	5.66	2.448, 2.503, 2.498, 2.398	31.993, 31.866, 32.221, 30.851	0.1061, 0.1089, 0.1075, 0.1078	0.1076	0.03	1.46	-42.0	2.458, 2.403, 2.478	31.265, 31.017, 31.547	0.1090, 0.1074, 0.1089	0.1084	0.038	1.676	-33.5
4	20.32	0.34	room temperature (20 C)		2.277, 2.269	31.773, 31.736	32	0.0994, 0.0991	0.0993	0.11	6.34	2.400, 2.444	31.354, 31.701	0.1061, 0.1069	0.1065	0.05	2.02	-14.3	2.413, 2.472	31.504, 31.623	0.1062, 0.1084	0.1073	0.051	2.245	-4.8
5	23.36	0.39	room temperature (20 C)		2.373, 2.398, 2.452, 2.375, 2.361	31.104, 31.449, 31.867, 31.184, 30.971	31	0.1058, 0.1057, 0.1067, 0.1056, 0.1057	0.1059	0.12	7.18	2.532, 2.574, 2.513	31.358, 31, 850, 31.137	0.1119, 0.1120, 0.1119	0.1119	0.04	1.91	-30.5	2.525, 2.554	31.211, 31.084	0.1122, 0.1139	0.1131	0.051	2.260	-17.6
6	20.42	0.34	room temperature (20 C)		2.473, 2.478	31.069, 31.019	31	0.1104, 0.1108	0.1106	0.11	6.23	2.600, 2.595	31.423, 31.641	0.1147, 0.1137	0.1142	0.02	0.99	-59.2	2.621, 2.599	32.015, 31.447	0.1135, 0.1146	0.1141	0.021	0.945	-60.9
7	23.36	0.39	room temperature (20 C)		2.478, 2.471	32.108, 32.087	32	0.1070, 0.1068	0.1069	0.12	7.36	2.611, 2.637	31.901, 32.264	0.1135, 0.1133	0.1134	0.05	2.11	-17.6	2.569, 2.598	31.812, 31.958	0.1120, 0.1127	0.1124	0.040	1.766	-30.9
8	50.30	0.84	28.0	35.0	2.757, 2.759, 2.746	32.554, 32.303, 32.657	33	0.1174, 0.1184, 0.1166	0.1175	0.27	16.06	2.806, 2.822, 2.826	31.836, 32.600, 32.285	0.1222, 0.1200, 0.1214	0.1212	0.06	2.64	15.8	2.841, 2.829, 2.922, 2.829	32.328, 31.955, 32.403, 32.437	0.1218, 0.1227, 0.1250, 0.1209	0.1226	0.082	3.628	59.2
9	51.03	0.85	23.1	27.1	2.818, 2.898, 2.872, 2.889	31.720, 32.949, 32.783, 32.991	33	0.1232, 0.1219, 0.1215, 0.1214	0.1220	0.28	16.35	2.885, 2.960, 2.917, 2.908	32.072, 33.287, 33.088, 32.793	0.1247, 0.1233, 0.1222, 0.1229	0.1233	0.02	0.92	-56.5	2.952, 2.999, 2.954	32.881, 33.133, 33.087	0.1245, 0.1255, 0.1238	0.1246	0.043	1.870	-11.3
10	51.03	0.85	23.1	27.1	2.843, 2.844	32.222, 32.265	32	0.1212, 0.1222	0.1217	0.27	16.16	3.001, 2.942	33.010, 32.534	0.1260, 0.1254	0.1257	0.06	2.84	34.4	2.936, 2.923	32.682, 32.313	0.1245, 0.1254	0.12495	0.053	2.311	9.2
11	51.40	0.86	22.3	25.3	3.107, 3.022, 3.063, 3.063, 3.049	32.531, 32.392, 32.777, 33.222, 33.104	33	0.1324, 0.1293, 0.1296, 0.1278, 0.1277	0.1294	0.28	16.56	3.244, 3.288, 3.249, 3.262, 3.237, 3.193, 3.245, 3.200	33.131, 33.571, 33.385, 33.854, 33.450, 33.153, 33.146, 32.886	0.1357, 0.1358, 0.1349, 0.1336, 0.1342, 0.1335, 0.1357, 0.1349	0.1348	0.09	3.96	-16.1	3.275, 3.291, 3.267, 3.291, 3.262, 3.146, 3.221	33.524, 33.215, 33.185, 34.490, 33.548, 32.711, 33.391	0.1354, 0.1374, 0.1365, 0.1323, 0.1348, 0.1333, 0.1337	0.134771	0.090	3.944	-16.4
12	52.13	0.87	23.2	26.2	3.254, 3.126, 3.271, 3.311, 3.199, 3.385, 3.385, 3.217, 3.290, 3.243, 3.327, 3.213, 3.297, 3.240	32.667, 32.470, 33.470, 33.675, 33.133, 34.839, 35.048, 33.525, 34.318, 33.821, 33.940, 33.622, 34.107, 33.615	34	0.1381, 0.1335, 0.1355, 0.1363, 0.1339, 0.1347, 0.1339, 0.1330, 0.1329, 0.1329, 0.1359, 0.1325, 0.1340, 0.1336	0.1343	0.29	17.27	3.408, 3.463, 3.287, 3.346, 3.416, 3.418	33.577, 33.785, 32.860, 33.523, 33.668, 34.052	0.1407, 0.1421, 0.1387, 0.1384, 0.1407, 0.1392	0.1400	0.10	4.28	1.8	3.401, 3.372, 3.387, 3.432	34.040, 33.616, 33.633, 33.664	0.1385, 0.1391, 0.1396, 0.1413	0.139625	0.091	4.020	-4.3

	Sour Gas									Sweet Gas					
Run	Corrected CO2 Flowmeter (L/min)	Corrected CO2 Flowmeter (m3/hr)	Corrected Air Flowmeter (m3/hr)	Temperature (C)	Pressure (psig)	Total Flowrate kmol/hr	Re	CO2 vol%	Average CO2 (vol%)	CO2 vol%	Average CO2 (vol%)	kmol CO2 Absorbed / hr	kg CO2 Absorbed/ hr	NTU	HTU (cm)
1	50.7	2.9	143.8	10	2.5	7.39	1.31E+05	1.826, 1.806	1.817	1.000	1.000	0.060	2.653	0.6	20.3
2	50.7	2.9	145.9	10	2.5	7.49	1.33E+05	1.848	1.848	0.990, 1.031	1.011	0.063	2.760	0.6	20.1
3	50.7	2.9	145.9	10	2.5	7.49	1.33E+05	1.829	1.829	1.093, 1.064, 1.036	1.065	0.057	2.521	0.5	22.4
4	50.7	2.9	145.9	10	2.5	7.49	1.33E+05	1.829	1.829	1.126, 1.111, 1.106	1.114	0.054	2.358	0.5	24.4
5	51.0	3.0	147.5	10	2.5	7.58	1.34E+05	1.829	1.829	1.102, 0.965, 0.953	1.007	0.062	2.743	0.6	20.3
6	51.5	3.0	147.5	10	2.5	7.58	1.34E+05	1.826	1.826	1.110, 1.092	1.101	0.055	2.416	0.5	23.9
7	51.5	3.0	147.5	10	2.5	7.58	1.34E+05	1.826	1.826	1.053, 1.067	1.060	0.058	2.556	0.5	22.2
8	21.8	1.3	52.9	10	2.5	2.73	4.84E+04	2.171	2.171	0.273	0.273	0.052	2.279	2.1	5.8
9	21.8	1.3	52.9	10	2.5	2.73	4.84E+04	2.065	2.065	0.338, 0.314, 0.273	0.308	0.048	2.108	1.9	6.4
10	21.8	1.3	52.9	10	2.5	2.73	4.84E+04	2.065	2.065	0.292, 0.304, 0.307	0.301	0.048	2.117	1.9	6.3
11	49.0	2.8	52.9	10	2.5	2.81	4.98E+04	4.720, 4.800	4.760	0.986, 0.956, 0.942, 0.930, 0.906	0.944	0.107	4.714	1.6	7.5
12	43.5	2.5	52.9	10	2.5	2.79	4.95E+04	4.130	4.130	0.745, 0.725, 0.701, 0.704, 0.692, 0.688	0.709	0.095	4.202	1.8	6.9

Appendix P

Absorption/desorption Results

Table P-1: Results of Absorption Runs for MEA Solution (100 wt%)

		Lean										Rich - Tank								Rich - Periphery								Sour Gas			Sweet Gas			NTU	HTU (cm)	Recovery (%)	End effect (%)	Residence time (s)	Film thickness (m)	Diffusion Time (s)	Enhancement Factor
				Temperature (C)																																					
Run	RPM	Flowrate, L/min	Flowrate, kg/s	Before Higee	After Higee	CO2, %wt./wt.	MEA, %wt./wt.	Average MEA, %wt./wt.	α (kmol CO2/kmol MEA)	Average α	kg MEA/s	kmol MEA/hr	CO2, %wt./wt.	MEA, %wt./wt.	Average MEA, %wt./wt.	α (kmol CO2/kmol MEA)	Average α	kmol CO2/hr	kg CO2/hr	% Mass Balance error	CO2, %wt./wt.	MEA, %wt./wt.	Average MEA, %wt./wt.	α (kmol CO2/kmol MEA)	Average α	kmol CO2/hr	kg CO2/hr	% Mass Balance error	Total Flowrate (m3/hr)	kmol/hr	Average CO2 (vol%)	CO2 (vol%)	Average CO2 (vol%)	kg CO2/hr							
1	600	39.3	0.66	40.7	45.1	0.667 0.526 0.656 0.633	99.421 97.592 101.103 103.403	100	0.0093 0.0075 0.0090 0.0085	0.0086	0.66	38.84	0.762 0.739 0.656 0.679	99.983 101.520 100.877 100.071	101	0.0106 0.0101 0.0090 0.0094	0.0098	0.05	2.05	-52	0.801 0871 0.717 0.680	100.097 99.801 99.797 100.303	100	0.0111 0.0121 0.0100 0.0094	0.0107	0.08	3.55	-17	57	2.87	3.445	3.4847 3.5883 3.2395 3.4660	0.0489	0.045	4.30	4.34	2.79	98.7	-9	1.14	1.25E-05	0.082	130.7
2	600	39.3	0.66	20.6	25.1	2.238 2.329	100.750 103.063	102	0.0308 0.0313	0.0311	0.67	39.43	2.766 2.690 2.833 2.732 2.757	101.869 101.521 98.434 97.626 96.818	99	0.0376 0.0367 0.0399 0.0388 0.0395	0.0385	0.29	12.87	129	3.054 2.969 2.975	99.121 95.023 93.940	96	0.0427 0.0433 0.0439	0.0433	0.48	21.23	277	57	2.87	4.535	4.5981 4.5164 4.4904	0.0894	0.084	5.62	3.98	3.04	98.1	-12	1.77	1.93E-05	0.193	117.0
3	1000	39.3	0.66	40.5	44.8	0.341 0.319 0.313	93.287 99.019 98.815	97	0.0051 0.0045 0.0044	0.0047	0.64	37.55	0.503 0.515	100.372 101.724	101	0.0069 0.0070	0.0070	0.09	3.80	-33	0.497 0.469 0.487	99.559 101.195 101.570	101	0.0069 0.0064 0.0066	0.0067	0.07	3.25	-43	57	2.87	4.531	4.6623 4.5410 4.5408 4.3787	0.0272	0.029	5.69	5.07	2.39	99.4	-5	0.81	8.92E-06	0.041	92.9
4	1000	39.3	0.66	24.3	29.6	1.395 1.386 1.356 1.332 1.316	101.385 104.001 99.894 102.357 102.202	102	0.0191 0.0185 0.0188 0.0180 0.0179	0.0185	0.67	39.46	1.574 1.585 1.648 1.597	98.746 99.135 100.477 101.432	100	0.0221 0.0222 0.0227 0.0218	0.0222	0.15	6.50	25	2.364 2.259	105.273 105.444	105	0.0311 0.0297	0.0305	0.47	20.78	300	57	2.87	4.156	4.2840 4.2665 4.1832 4.1321 3.9116	0.0385	0.041	5.20	4.62	2.62	99.0	-37	1.26	1.37E-05	0.098	83.3
5	600	21.1	0.35	41.1	45.8	0.566 0.582 0.548	99.789 102.550 99.660	101	0.0079 0.0079 0.0076	0.0078	0.35	20.85	0.927 0.907	101.312 100.068	101	0.0127 0.0126	0.0127	0.10	4.42	-22	1.097 1.095	102.686 101.159	102	0.0148 0.0149	0.0149	0.15	6.48	15	57	2.87	4.526	4.6882 4.4178 4.5730 4.4239	0.0400	0.054	5.65	4.42	2.74	98.8	-18	1.73	1.02E-05	0.054	106.1
6	600	21.1	0.35	20.4	28.5	2.615 2.624 2.582 2.648 2.586 2.637	100.993 101.671 101.788 102.245 103.702 102.139	102	0.0359 0.0358 0.0352 0.0359 0.0346 0.0357	0.0355	0.36	21.15	3.176 3.101 3.250	102.364 101.173 102.364	102	0.0430 0.0425 0.0440	0.0432	0.16	7.14	33								57	2.87	4.222	4.6157 4.5228 4.0040 4.0613 3.9049	0.1050	0.133	5.17	3.46	3.50	96.9	-	2.68	1.56E-05	0.127	95.0
7	1000	21.1	0.35	40.9	45.1	0.000 0.000 0.000	97.871 97.910 98.509	98	0 - -	0.0000	0.34	20.32	0.302 0.293 0.330 0.347 0.298 0.343 0.298	97.557 98.234 97.918 99.449 97.058 98.014 98.254	98	0.0043 0.0041 0.0047 0.0048 0.0043 0.0049 0.0042	0.0045	0.09	4.01	-25	0.341 0.334 0.267 0.274	97.452 97.256 95.733 97.155	97	0.0049 0.0048 0.0039 0.0039	0.0044	0.09	3.93	-27	57	2.87	4.273	4.4949 4.3945 4.2748 4.1796 4.0216	0.0315	0.032	5.36	4.90	2.47	99.3	-2	1.23	7.25E-06	0.027	75.5
8	1000	21.1	0.35	20.3	27.1	1.873 1.822 1.639 1.657	102.914 103.622 103.902 102.803	103	0.0252 0.0244 0.0219 0.0223	0.0235	0.36	21.40	2.264 2.240 2.128	102.124 102.715 102.126	102	0.0307 0.0302 0.0289	0.0300	0.14	6.11	12	3.401 3.648 3.367	96.216 98.798 104.874	100	0.0490 0.0512 0.0445	0.0483	0.53	23.34	329	57	2.87	4.356	4.5143 4.4240 4.2843 4.2025	0.0503	0.051	5.44	4.45	2.72	98.8	-61	1.91	1.11E-05	0.064	67.6

Table P-2: Results of Absorption Runs for MEA Solution (75 wt%)

		Lean										Rich - Tank								Rich - Periphery								Sour Gas			Sweet Gas			NTU	HTU (cm)	Recovery (%)	End effect (%)	Residence time (s)	Film thickness (m)	Diffusion Time (s)	Enhancement Factor
				Temperature (C)																																					
Run	RPM	Flowrate, L/min	Flowrate, kg/s	Before Higee	After Higee	CO2, %wt./wt.	MEA, %wt./wt.	Average MEA, %wt./wt.	α (kmol CO2/kmol MEA)	Average α	kg MEA/s	kmol MEA/hr	CO2, %wt./wt.	MEA, %wt./wt.	Average MEA, %wt./wt.	α (kmol CO2/kmol MEA)	Average α	kmol CO2/hr	kg CO2/hr	% Mass Balance error	CO2, %wt./wt.	MEA, %wt./wt.	Average MEA, %wt./wt.	α (kmol CO2/kmol MEA)	Average α	kmol CO2/hr	kg CO2/hr	% Mass Balance error	Total Flowrate (m3/hr)	kmol/hr	Average CO2 (vol%)	CO2 (vol%)	Average CO2 (vol%)	kg CO2/hr							
1	600	39.3	0.66	41.0	48.3	2.671 2.694 2.759 2.583	75.965 74.854 76.698 74.181	75	0.0487 0.0499 0.0499 0.0483	0.0492	0.49	29.19	2.837 2.837 2.932 2.893	74.925 78.110 75.598 74.358	76	0.0525 0.0528 0.0531 0.0539	0.0531	0.11	4.98	-6	2.931 2.774 2.810 2.923	77.142 75.111 74.189 75.115	75	0.0527 0.0512 0.0525 0.0539	0.0526	0.10	4.33	-20	57	2.87	4.396	4.6625 4.3821 4.2726 4.2283	0.0718	0.08	5.44	4.06	3.03	98.2	0.9	1.02	1.11E-05	0.064	98.3
2	600	39.3	0.66	21.4	26.7	2.271 2.101 2.150 2.140	78.714 76.959 77.269 76.093	77	0.0400 0.0378 0.0388 0.0390	0.0389	0.51	29.90	2.367 2.317 2.367 2.426	78.561 77.269 77.250 77.819	78	0.0418 0.0416 0.0425 0.0432	0.0423	0.10	4.44	-4	57	2.87	4.396	4.4759 4.3654 4.3387 4.2650	0.0709	0.069	4.64	1.81	6.66	84.2	-0.7	1.68	1.81E-05	0.171	93.9
3	1000	39.3	0.66	40.2	49.6	2.583 2.603	73.969 75.014	74	0.0484 0.0481	0.0483	0.49	28.82	2.738 2.818	73.303 76.787	75	0.0518 0.0509	0.0514	0.09	3.87	-28	57	2.87	4.340	4.3670 4.3559 4.2820	0.0892	0.11	5.34	3.7	3.3	97.5	-1.7	0.72	7.87E-06	0.032	69.9
4	1000	39.3	0.66	21.0	25.9	1.936 1.902 1.925	74.902 75.041 75.248	75	0.0358 0.0351 0.0355	0.0355	0.49	29.05	2.194 2.226 2.151 2.257 2.238	74.292 77.017 75.570 77.439 77.113	76	0.0409 0.0401 0.0395 0.0404 0.0402	0.0402	0.14	6.06	22	2.236 2.267 2.282 2.332	76.864 76.437 75.748 76.975	77	0.0403 0.0411 0.0418 0.0420	0.0413	0.17	7.44	50	57	2.87	4.299	4.4086 4.3227 4.2149 4.2198	0.0704	0.088	4.95	2.4	5.0	91.2	-2.7	1.20	1.29E-05	0.087	66.8
5	600	21.1	0.35	40.8	48.8	3.078 3.056 2.977	73.503 72.703 71.119	72	0.0581 0.0583 0.0580	0.0582	0.25	15.01	3.262 3.220 3.298 3.315	71.503 70.795 73.201 70.705	72	0.0632 0.0631 0.0625 0.0650	0.0635	0.08	3.50	-20	3.337 3.365 3.392 3.440	70.077 71.814 74.575 73.995	73	0.0660 0.0650 0.0631 0.0645	0.0647	0.10	4.30	-2	57	2.87	3.555	3.6643 3.6501 3.4316 3.4358	0.0703	0.07	4.39	3.9	3.1	98.0	-1.9	1.54	8.98E-06	0.042	79.8
6	600	21.1	0.35	22.1	29.2	2.356 2.502 2.412 2.461	75.794 75.009 76.125 77.863	76	0.0431 0.0462 0.0439 0.0438	0.0443	0.27	15.78	2.747 2.746 2.822 2.709	77.518 75.923 78.101 76.892	77	0.0484 0.0506 0.0501 0.0488	0.0495	0.08	3.63	-23	2.878 2.803 2.876 2.875	78.264 77.177 77.661 76.040	77	0.0510 0.0504 0.0513 0.0524	0.0513	0.11	4.88	4	57	2.87	4.396	4.4860 4.4275 4.3630 4.3014	0.0759	0.069	4.68	1.9	6.5	84.3	-3.6	2.55	1.47E-05	0.113	76.3
7	1000	21.1	0.35	39.4	48.5	2.810 2.863 2.857	74.732 75.122 76.535	75	0.0521 0.0528 0.0518	0.0523	0.26	15.44	3.238 3.241 3.215 3.117 3.212	76.996 75.582 76.494 75.550 74.361	76	0.0583 0.0594 0.0583 0.0572 0.0599	0.0586	0.10	4.33	-20	3.245 3.201 3.252 3.290	74.079 74.310 75.439 77.085	75	0.0607 0.0597 0.0598 0.0592	0.0599	0.12	5.17	-5	57	2.87	4.358	4.4488 4.3797 4.3082	0.0848	0.08	5.43	3.9	3.1	98.1	-2.1	1.10	6.39E-06	0.021	56.8
8	1000	21.1	0.35	20.6	28.3	2.284 2.307 2.294 2.284	77.629 78.391 78.211 78.555	78	0.0408 0.0408 0.0407 0.0403	0.0407	0.27	16.20	2.707 2.708 2.638 2.730	78.642 79.256 77.219 78.851	78	0.0477 0.0474 0.0474 0.0480	0.0477	0.11	4.99	-4	2.727 2.758 2.665 2.727	78.084 77.742 76.087 78.249	78	0.0484 0.0492 0.0486 0.0483	0.0487	0.13	5.70	10	57	2.87	4.353	4.6495 4.5536 4.4853 4.4126	0.0701	0.041	5.20	2.4	5.0	91.0	-2.1	1.82	1.05E-05	0.057	54.2

Table P-3: Results of Absorption Runs for MEA Solution (55 wt%)

		Lean										Rich - Tank								Rich - Periphery								Sour Gas				Sweet Gas							
				Temperature (C)																																					
Run	RPM	Flowrate, L/min	Flowrate, kg/s	Before Higee	After Higee	CO2, %wt./wt.	MEA, %wt./wt.	Average MEA, %wt./wt.	α (kmol CO2/kmol MEA)	Average α	kg MEA/s	kmol MEA/hr	CO2, %wt./wt.	MEA, %wt./wt.	Average MEA, %wt./wt.	α (kmol CO2/kmol MEA)	Average α	kmol CO2/hr	kg CO2/hr	% Mass Balance error	CO2, %wt./wt.	MEA, %wt./wt.	Average MEA, %wt./wt.	α (kmol CO2/kmol MEA)	Average α	kmol CO2/hr	kg CO2/hr	% Mass Balance error	Total Flowrate (m3/hr)	kmol/hr	CO2 (vol%)	Average CO2 (vol%)	CO2 (vol%)	Average CO2 (vol%)	kg CO2/hr	NTU	HTU (cm)	Recovery (%)	End effect (%)	Residence time (s)	Film thickness (m)	Diffusion Time (s)	Enhancement Factor
1	600	38.2	0.64	39.6	43.8	3.179, 3.043, 3.072, 3.085	56.745, 54.906, 55.252, 55.521	56	0.0777, 0.0768, 0.0771, 0.0770	0.0772	0.35	20.92	3.321, 3.261, 3.248, 3.216	55.592, 55.077, 55.119, 54.367	55	0.0828, 0.0821, 0.0817, 0.0820	0.0822	0.10	4.60	-19	3.353, 3.310, 3.202	55.866, 54.876, 53.413	55	0.0832, 0.0836, 0.0831	0.0833	0.13	5.64	0	57	2.87	4.7110, 4.7404, 4.6908	4.71	0.24440, 0.23667	0.24	5.65	3.0	4.1	94.9	-1.4	0.90	9.59E-06	0.048	71.0
2	600	39.3	0.66	20.7	28.7	3.462, 3.452, 3.449	53.289, 53.251, 53.732	53	0.0901, 0.0899, 0.0890	0.0897	0.35	20.67	3.647, 3.896, 3.709, 3.679	53.168, 56.106, 54.317, 54.287	54	0.0951, 0.0963, 0.0947, 0.0940	0.0951	0.11	4.87	1	3.695, 3.625, 3.786, 3.844	53.595, 52.930, 55.038, 55.667	54	0.0956, 0.0949, 0.0954, 0.0957	0.0954	0.12	5.21	8	57	2.87	4.5965, 4.6718, 4.6777, 4.4390	4.60	0.8609, 0.7280, 0.7543, 0.7909	0.78	4.82	1.8	6.8	83.0	-0.4	1.06	1.14E-05	0.068	49.4
3	1000	38.2	0.64	40.1	44.1	3.143, 3.048, 3.113, 3.061	56.406, 55.157, 56.104, 54.812	56	0.0772, 0.0766, 0.0769, 0.0774	0.0771	0.35	20.92	3.322, 3.276, 3.299, 3.365	55.586, 54.827, 55.830, 56.348	56	0.0829, 0.0828, 0.0819, 0.0828	0.0826	0.12	5.13	-5	3.346, 3.269, 3.216, 3.403	55.669, 55.556, 55.122, 56.257	56	0.0833, 0.0816, 0.0809, 0.0839	0.0825	0.11	4.97	-8	57	2.87	4.4872, 4.4795, 4.4613	4.48	0.2060, 0.2069, 0.2065	0.21	5.39	3.1	3.9	95.4	0.2	0.64	6.82E-06	0.024	90.5
4	1000	39.3	0.66	20.9	25.6	3.527, 3.454, 3.732, 3.740	52.811, 51.934, 56.240, 56.015	54	0.0926, 0.0922, 0.0920, 0.0926	0.0924	0.36	20.99	3.874, 3.898, 3.807, 3.819	56.228, 56.539, 55.154, 55.359	56	0.0949, 0.0956, 0.0957, 0.0956	0.0955	0.07	2.86	-41	3.815, 3.971, 3.907, 3.812	55.312, 56.937, 56.452, 55.544	56	0.0956, 0.0967, 0.0959, 0.0951	0.0959	0.07	3.21	-34	57	2.87	4.4469, 4.4532, 4.4367	4.45	0.5681, 0.5872, 0.5815	0.58	4.89	2.0	5.9	87.0	-0.4	0.75	8.14E-06	0.034	35.2
5	600	21.1	0.35	39.5	38.4	3.948, 3.947, 4.097, 3.957	53.858, 55.302, 56.413, 55.533	55	0.1016, 0.0989, 0.1007, 0.0988	0.1000	0.19	11.45	4.490, 4.488, 4.529, 4.439	56.072, 56.557, 56.791, 55.838	56	0.1110, 0.1100, 0.1106, 0.1102	0.1105	0.12	5.26	8	4.520, 4.374, 4.426, 4.244	57.214, 56.175, 56.554, 54.537	56	0.1095, 0.1079, 0.1085, 0.1079	0.1085	0.10	4.26	-13	57	2.87	4.4715, 4.5058, 4.3524, 4.4078	4.43	0.5782, 0.5705, 0.5783, 0.5722	0.57	4.88	2.0	5.9	87.0	1.8	1.34	7.86E-06	0.032	58.2
6	600	21.1	0.35	22.3	25.9	3.863, 3.954, 3.884, 3.855	55.748, 57.003, 56.732, 56.507	56	0.0961, 0.0962, 0.0949, 0.0946	0.0955	0.20	11.70	4.297, 4.129, 4.252	57.049, 55.066, 56.344	56	0.1044, 0.1040, 0.1046	0.1044	0.10	4.58	-4	4.215, 4.215, 4.299	56.927, 56.705, 57.588	57	0.1026, 0.1031, 0.1035	0.1031	0.09	3.93	-17	57	2.87	4.5244, 4.4781, 4.4802, 4.4069	4.47	0.7520, 0.6315, 0.7043, 0.7639	0.71	4.75	1.8	6.6	84.1	1.2	1.60	9.29E-06	0.045	40.1
7	1000	21.1	0.35	39.6	36.9	4.118, 3.878, 3.979, 3.887	56.565, 54.493, 55.261, 54.406	55	0.1009, 0.0987, 0.0998, 0.0990	0.0996	0.19	11.43	4.374, 4.198, 4.345, 4.258	55.853, 54.442, 55.923, 55.718	55	0.1086, 0.1069, 0.1077, 0.1059	0.1073	0.09	3.86	-22	4.123, 4.193, 4.346	55.070, 54.641, 56.384	55	0.1090, 0.1065, 0.1064, 0.1069	0.1072	0.09	3.82	-23	57	2.87	4.4465, 4.3646, 4.2414	4.35	0.4788, 0.3997, 0.4277, 0.4461	0.44	4.94	2.3	5.3	89.9	0.1	0.95	5.59E-06	0.016	41.4
8	1000	21.1	0.35	22.6	24.9	3.878, 3.876, 3.872, 3.979	57.377, 56.928, 56.736, 58.042	57	0.0937, 0.0944, 0.0946, 0.0950	0.0945	0.20	11.86	4.093, 4.130, 4.173, 4.249	55.523, 56.295, 56.920, 57.310	57	0.1022, 0.1017, 0.1016, 0.1028	0.1021	0.09	3.99	-10	4.354, 4.318, 4.330, 4.460	57.918, 57.299, 57.361, 58.847	58	0.1042, 0.1045, 0.1047, 0.1051	0.1047	0.12	5.32	20	57	2.87	4.6075, 4.5479, 4.5371, 4.5649	4.09	0.5479, 0.5371, 0.5649	0.56	4.45	2.0	6.1	86.2	-2.5	1.14	6.61E-06	0.023	28.5

Table P-4: Results of Absorption Runs for MEA Solution (30 wt%)

		Lean										Rich - Buffer Tank								Rich - Periphery								Sour Gas				Sweet Gas							
				Temperature (C)																																					
Run	RPM	Flowrate, L/min	Flowrate, kg/s	Before Higee	After Higee	CO2, %wt./wt.	MEA, %wt./wt.	Average MEA, %wt./wt.	α (kmol CO2/kmol MEA)	Average α	kg MEA/s	kmol MEA/hr	CO2, %wt./wt.	MEA, %wt./wt.	Average MEA, %wt./wt.	α (kmol CO2/kmol MEA)	Average α	kmol CO2/hr	kg CO2/hr	% Mass Balance error	CO2, %wt./wt.	MEA, %wt./wt.	Average MEA, %wt./wt.	α (kmol CO2/kmol MEA)	Average α	kmol CO2/hr	kg CO2/hr	% Mass Balance error	Total Flowrate (m3/hr)	kmol/hr	CO2 (vol%)	Average CO2 (vol%)	CO2 (vol%)	Average CO2 (vol%)	kg CO2/hr	NTU	HTU (cm)	Recovery (%)	End effect (%)	Residence time (s)	Film thickness (m)	Diffusion Time (s)	Enhancement Factor
1	600	39.3	0.66	40.5	37	7.859, 7.465	31.996, 31.450	32	0.3405, 0.3291	0.3349	0.21	12.28	7.824, 7.777, 7.533	32.065, 32.049, 30.840	32	0.3383, 0.3364, 0.3386	0.3378	0.04	1.59	-47	7.890, 7.521, 7.827	32.034, 30.619, 32.571	32	0.3415, 0.3405, 0.3332	0.3384	0.04	1.94	-35	57	2.87	4.5631, 4.5168, 4.4009	4.49	2.2435, 2.0865, 2.0805, 2.1088	2.13	2.99	0.7	16.2	52.6	-0.2	0.55	5.12E-06	0.0195	16.8
2	600	40.4	0.67	22.5	24	7.510, 7.492, 7.556	32.360, 32.455, 32.074	32	0.3217, 0.3200, 0.3266	0.3228	0.22	12.84	7.483, 7.590, 7.745	31.853, 32.534, 33.244	33	0.3257, 0.3234, 0.3230	0.3241	0.02	0.72	-68	7.785, 7.618, 7.562	32.928, 32.202, 32.387	33	0.3278, 0.3280, 0.3280	0.3280	0.07	2.92	31	57	2.87	4.4767, 4.4428, 4.4042	4.44	2.7282, 2.6577, 2.5472, 2.7495	2.67	2.24	0.5	23.8	39.9	1.2	0.65	5.15E-06	0.0197	16.9
3	1000	39.3	0.66	40.6	37.3	7.545, 7.623, 7.032	30.625, 31.103, 29.468	30	0.3416, 0.3398, 0.3308	0.3374	0.20	11.76	7.806, 6.576, 7.914, 7.905	31.738, 26.792, 31.896, 32.336	31	0.3410, 0.3403, 0.3440, 0.3389	0.3411	0.04	1.88	-41	7.726, 7.968, 7.871	31.546, 32.576, 31.808	32	0.3395, 0.3391, 0.3431	0.3406	0.04	1.64	-49	57	2.87	4.3465, 4.3575, 4.2992	4.33	1.8708, 1.8470, 1.7277, 1.7678, 1.8550	1.81	3.19	0.9	13.9	58.2	0.1	0.39	4.35E-06	0.0099	12.0
4	1000	39.3	0.66	22.8	24.3	7.370, 7.543	31.404, 32.105	32	0.3254, 0.3257	0.3256	0.21	12.29	7.671, 7.683, 7.617	32.154, 32.166, 31.906	32	0.3307, 0.3311, 0.3310	0.3310	0.07	2.90	26	7.398, 7.758	31.435, 32.849	32	0.3263, 0.3274	0.3269	0.02	0.70	-69	57	2.87	4.3269, 4.2586, 4.1763	4.25	2.4979, 2.4558, 2.3606, 2.4541, 2.3850	2.43	2.30	0.6	21.6	42.9	1.2	0.47	4.34E-06	0.0098	11.9
5	600	21.1	0.35	39.9	46.1	7.266, 7.401, 7.420	31.024, 31.545, 31.552	31	0.3247, 0.3253, 0.3260	0.3254	0.11	6.50	7.676, 7.076, 7.679	31.867, 29.387, 31.800	31	0.3339, 0.3338, 0.3348	0.3342	0.06	2.53	5	7.436, 7.715, 7.673	30.943, 31.516, 32.057	32	0.3332, 0.3394, 0.3318	0.3348	0.06	2.71	13	57	2.87	4.4070, 4.3466	4.38	2.4740, 2.5272, 2.4363	2.48	2.40	0.6	21.3	43.4	-0.2	0.84	4.97E-06	0.0128	13.7
6	600	21.1	0.35	23.1	22.4	7.265, 7.365	31.288, 31.982	32	0.3219, 0.3192	0.3206	0.11	6.55	7.393, 7.418, 7.896	31.244, 31.482, 33.064	32	0.3280, 0.3267, 0.3311	0.3286	0.05	2.32	0	7.497, 7.590, 7.487	31.551, 32.196, 31.733	32	0.3294, 0.3268, 0.3271	0.3278	0.05	2.08	-10	57	2.87	4.3889, 4.3409	4.36	2.5528, 2.6864, 2.7211, 2.4791, 2.2341	2.53	2.31	0.5	22.3	41.9	0.3	1.00	4.95E-06	0.0128	13.6
7	1000	21.1	0.35	39.3	44.3	7.370, 7.480, 7.377	31.031, 31.424, 31.452	31	0.3293, 0.3300, 0.3252	0.3282	0.11	6.48	7.518, 7.793	30.805, 32.075	31	0.3383, 0.3368	0.3376	0.06	2.67	60	7.580, 7.556, 7.879	31.507, 31.505, 32.414	32	0.3330, 0.3325, 0.3370	0.3342	0.04	1.71	3	57	2.87	3.6441, 3.5817, 3.6004	3.61	2.3087, 2.2383, 2.2289, 2.3652, 2.3001	2.29	1.67	0.5	26.6	36.6	1.0	0.60	3.53E-06	0.0065	9.7
8	1000	21.1	0.35	23.8	21.7	7.054, 7.524, 6.689	30.768, 32.668, 29.722	31	0.3178, 0.3193, 0.3120	0.3164	0.11	6.43	7.415, 7.616, 7.485	31.586, 32.880, 32.074	32	0.3255, 0.3211, 0.3235	0.3234	0.05	1.98	-6	7.597, 6.795, 7.444	32.352, 29.511, 31.867	31	0.3256, 0.3192, 0.3238	0.3229	0.04	1.84	-12	57	2.87	4.1929, 4.1061, 4.1364	4.15	2.4523, 2.5455, 2.5032, 2.4358	2.48	2.10	0.5	23.6	40.1	0.2	0.71	3.52E-06	0.0065	9.7

Table P5: Regeneration by Air

Run	1	2	3	4	5	6
Date	11-Dec	16-Jan	17-Jan	18-Jan	23-Jan	23-Jan
Speed (RPM)	600	600	1000	800	800	800
CO2 - inlet	441.1	683.2	645.8	554.5	548.7	674.0
CO2 - outlet	1166.5	1306.8	1969.2	2883.3	3997.8	5384.5
Ratio	2.6	1.9	3.0	5.2	7.3	8.0
Liquid rate						
L/min	20.3	11.0	19.3	35.3	37.1	37.1
kg/hr	1219.8	659.7	1158.2	2118.9	2228.5	2228.5
Kmol/h	25.4	13.7	24.1	44.1	46.3	46.3
Gas rate						
m3/hr	146.0	177.5	145.5	126.4	65.3	86.0
kg/hr	175.3	213.0	174.6	151.7	78.3	103.1
kmol/hr	6.0	7.3	6.0	5.2	2.7	3.6
G/L	0.24	0.54	0.25	0.12	0.06	0.08
Temperature (C)						
Feed Tank	57.6	70.0	72.0	74.5	69.5	70.5
Buffer Tank	52.0	52.5	55.0	64.5	62.0	64.0
Difference	5.6	17.5	17.0	10.0	7.5	6.5
Loading (mol CO2 / mol MEA)						
Feed	0.4087	0.4336	0.4141	0.4115	0.4067	0.4112
Product Liquid						
A) Side	0.3957	0.4295	0.4073	0.4080	0.4043	0.4056
B) Buffer Tank	0.3981	0.4289	0.4066	0.4077	0.4048	0.4075

Stripping Factor	7.2	16.2	7.6	3.6	1.8	2.3
NTU - Side	0.032	0.010	0.017	0.008	0.006	0.014
HTU (m) - Side	3.7	12.5	7.3	14.4	20.4	8.9

End Effect(%)	0.58	0.14	0.18	0.07	0.10	0.47

		Ethanolamine Solution Rate		Steam Rate						Temperature		
Run	RPM	L/min	kg/hr	kg/s	kmol/hr	kg/hr	kg/s	kmol/hr	G/L	kg Steam / L solution	Feed Tank	Buffer Tank	Difference
1	800	36.8	2206.8	0.6	45.9	200	0.056	11.1	0.2	0.091	68.0	94.0	26.0
2	800	11.2	672.0	0.2	14.0	250	0.069	13.9	1.0	0.372	69.0	108.5	39.5
3	800	12.6	756.0	0.2	15.7	260	0.072	14.4	0.9	0.344	67.1	114.0	46.9
4	800	21.3	1278.0	0.4	26.6	260	0.072	14.4	0.5	0.203	70.0	104.0	34.0
5	600	30.2	1812.0	0.5	37.7	250	0.069	13.9	0.4	0.138	58.9	118.0	59.1
6	1000	30.2	1812.0	0.5	37.7	250	0.069	13.9	0.4	0.138	59.3	137.6	78.3
7	600	21.1	1263.6	0.4	26.3	250	0.069	13.9	0.5	0.198	56.9	95.6	38.7
8	1000	21.1	1263.6	0.4	26.3	250	0.069	13.9	0.5	0.198	57.2	130.6	73.4
9	600	37.5	2250.6	0.6	46.8	260	0.072	14.4	0.3	0.116	58.2	96.7	38.5
10	1000	37.5	2250.6	0.6	46.8	260	0.072	14.4	0.3	0.116	59.7	103.0	43.3
11	600	10.2	610.8	0.2	12.7	260	0.072	14.4	1.1	0.426	58.8	140.0	81.2
12	1000	10.2	610.8	0.2	12.7	260	0.072	14.4	1.1	0.426	58.4	113.0	54.6

		Loading (mol CO2/mol MEA)																			
CO2 outlet		Feed					Tank								Periphery						
Tests	Average	CO2, %wt/wt	MEA, %wt/wt	Average MEA, %wt./wt.	α (kmol CO2/kmol MEA)	Average α	CO2, %wt/wt	MEA, %wt/wt	Average MEA, %wt./wt.	α (kmol CO2/kmol MEA)	Average α	Stripping Factor	NTU	HTU (m)	CO2, %wt/wt	MEA, %wt/wt	Average MEA, %wt./wt.	α (kmol CO2/kmol MEA)	Average α	NTU	HTU (m)	End Effect
74699, 65590, 58500, 54524, 56063, 55096, 57003, 52643	59.265	10.128, 10.472, 10.549	34.540, 35.870, 36.186	35.5	0.4065, 0.4047, 0.4042	0.4052	9.436, 10.321, 10.115	32.937, 35.749, 35.297	34.7	0.3972, 0.4002, 0.3973	0.3983	34	0.02	7.04	10.011, 10.229, 9.853	34.612, 35.360, 34.169	34.7	0.4010, 0.4010, 0.3998	0.4006	0.01	10.75	0.6
652875, 466674, 346096, 441975, 472226, 288839, 398669, 367397	429.344	10.282, 10.292	35.574, 35.770	35.7	0.4007, 0.3989	0.3999	7.441, 7.504, 7.294, 7.511	30.538, 31.749, 31.159, 31.875	31.3	0.3378, 0.3277, 0.3245, 0.3267	0.3292	139	0.19	0.62	8.625, 8.777, 8.779	30.536, 30.938, 30.826	30.8	0.3916, 0.3933, 0.3948	0.3933	0.02	7.29	16.3
856730, 638732, 571458, 598630, 631567, 490296, 530368, 676257	624.255	8.944, 9.248, 8.901, 8.843	32.175, 33.892, 32.881, 32.594	32.9	0.3854, 0.3783, 0.3753, 0.3761	0.3788	6.916, 7.035, 7.204, 6.802	29.958, 30.560, 30.972, 29.243	30.2	0.3201, 0.3191, 0.3225, 0.3225	0.3211	129	0.17	0.73	7.146, 7.441, 7.454, 7.646	29.060, 30.182, 30.230, 30.919	30.1	0.3409, 0.3418, 0.3418, 0.3428	0.3419	0.10	1.18	6.1
731864, 699227, 561747, 594910, 612461, 535528, 618660, 545721	612.515	7.578, 7.654, 7.760	30.349, 30.753, 31.148	30.8	0.3462, 0.3450, 0.3454	0.3456	7.046, 6.965, 7.087	29.689, 29.651, 29.717	29.7	0.3290, 0.3257, 0.3306	0.3285	76	0.05	2.38	6.857, 6.914, 7.148	29.007, 29.040, 29.806	29.3	0.3277, 0.3301, 0.3325	0.3301	0.05	2.65	0.5
126525, 116682	121.604	18.618, 18.861, 18.848, 18.848	57.693, 59.568, 60.169, 61.043	59.6	0.4474, 0.4390, 0.4343, 0.4281	0.4372	17.797, 17.383, 17.686	57.793, 56.829, 58.398	57.7	0.4269, 0.4241, 0.4199	0.4237	136	0.03	3.84	17.649, 17.658, 17.669	58.002, 58.176, 58.313	58.2	0.4218, 0.4208, 0.4201	0.4209	0.04	3.19	-0.6
120240	120.241	19.177, 19.116	61.563, 61.284	61.4	0.4319, 0.4324	0.4322	17.695, 17.482, 17.391	58.113, 58.244, 57.545	58.0	0.4221, 0.4161, 0.4190	0.4191	136	0.03	3.93	17.361, 17.955, 16.755, 16.755, 17.955	57.238, 58.356, 54.988, 54.185, 58.508	56.7	0.4205, 0.4266, 0.4224, 0.4287, 0.4254	0.4247	0.02	6.95	1.3
240902, 168780, 149152, 128643, 122120	161.920	17.187, 17.407, 17.633	54.072, 56.736, 57.479	56.1	0.4407, 0.4253, 0.4253	0.4305	15.874, 15.936, 15.930	54.328, 53.885, 53.963	54.1	0.4051, 0.4100, 0.4093	0.4082	196	0.05	2.27	16.169, 16.152, 16.122	53.650, 54.441, 53.888	54.0	0.4178, 0.4113, 0.4148	0.4147	0.04	3.24	1.6
418605, 385054, 337351, 375610	379.155	17.211, 17.633, 17.530	56.229, 58.176, 57.779	57.4	0.4243, 0.4202, 0.4206	0.4217	15.793, 15.540, 15.702	54.502, 53.526, 53.897	54.0	0.4017, 0.4025, 0.4039	0.4027	196	0.05	2.62	15.921, 15.371, 15.375	53.683, 51.706, 51.772	52.4	0.4112, 0.4121, 0.4117	0.4117	0.02	5.02	2.2
57778, 55015, 51741	54.845	15.938, 15.813, 15.885	52.902, 53.568, 53.110	53.2	0.4177, 0.4092, 0.4147	0.4139	15.213, 15.158, 15.118	52.149, 51.810, 51.977	52.0	0.4044, 0.4056, 0.4032	0.4044	114	0.02	5.23	14.937, 14.995, 13.888	50.855, 51.557, 48.116	50.2	0.4072, 0.4032, 0.4002	0.4036	0.03	4.79	-0.2
80461, 82627, 86297, 82763	83.037	15.984, 15.986	54.821, 54.368	54.6	0.4059, 0.4076	0.4068	14.782, 13.952, 15.186	51.662, 48.255, 52.672	50.9	0.3967, 0.4008, 0.3997	0.3991	114	0.02	6.33	15.365, 14.369, 14.633	52.517, 48.787, 49.101	50.1	0.4056, 0.4083, 0.4132	0.4091	-0.01	-21.78	2.4
478643, 453766, 420671, 408759, 380966	428.561	14.726, 14.776, 14.833	51.106, 50.695, 51.019	50.9	0.3995, 0.4041, 0.4031	0.4023	11.032, 11.060, 10.812	46.190, 45.904, 45.225	45.8	0.3311, 0.3340, 0.3314	0.3322	421	0.19	0.63	11.086, 11.151, 11.182	45.272, 45.012, 45.248	45.2	0.3395, 0.3434, 0.3426	0.3419	0.16	0.74	2.8
510511, 433709, 433475, 371371, 369621, 381759	416.741	15.105, 15.119, 15.090	51.676, 52.268, 52.026	52.0	0.4052, 0.4010, 0.4021	0.4028	11.426, 11.472	47.587, 47.584	47.6	0.3329, 0.3342	0.3336	421	0.19	0.64	11.023, 11.401, 11.352	45.319, 46.361, 46.357	46.0	0.3372, 0.3409, 0.3395	0.3392	0.17	0.70	1.7